THREE DIMENSIONAL ANALYTICAL SOLUTIONS FOR STATIC AND MODAL ANALYSIS OF PIEZOLAMINATED CYLINDRICAL SHELLS USING EXTENDED KANTOROVICH METHOD

A Thesis Submitted in

Partial Fulfillment of the Requirements

for the Degree of

DOCTOR OF PHILOSOPHY

By

SHRANISH KAR

(Roll No.156103008)

DEPARTMENT OF MECHANICAL ENGINEERING

INDIAN INSTITUTE OF TECHNOLOGY GUWAHATI

GUWAHATI (ASSAM)-781039

FEBRUARY, 2022

Dedicated to my
beloved father Mr. Nishit Chandra Kar,
&
mother Mrs. Shrabani Kar.

Certificate

This is to certify that the thesis entitled "**Three-Dimensional analytical solutions for static and Modal Analysis of Piezolaminated Cylindrical Shells using Extended Kantorovich Method**" being submitted by **Mr. Shranish Kar** to the Indian Institute of Technology, Guwahati, for the award of the degree of Doctor of Philosophy in Mechanical Engineering is a record of original bonafide research work carried out by him under my supervision and guidance. The thesis work, in my opinion, has reached the requisite standard fulfilling the requirements for the degree of Doctor of Philosophy.

The results contained in this thesis have not been submitted in part or full to any other University or Institute for the award of any degree or diploma.

Poonam
06-04-2022

Dr. Poonam Kumari

Associate Professor

Department of Mechanical Engineering

Indian Institute of Technology Guwahati

Guwahati - 781039

Declaration

I, Shranish Kar (Roll no: 156103008) declare that the present written submission is my thoughts in my own words. I have adequately cited and referenced the original sources, where other's ideas have been involved. I also declare that I have adhered to all principles of academic honesty and integrity and have neither fabricated nor falsified any idea/data/fact/source in my submission. I understand that any violation of the above will be cause for disciplinary action by the Institute and can also evoke penal action from the sources which have thus not been properly cited or from whom proper permission has not been taken when needed.

(Shranish Kar)

Date: Roll No. 156103008

Acknowledgements

First and foremost, I want to express my sincere gratitude toward my Ph.D. supervisor, Dr. Poonam Kumari, for providing me an opportunity to work under her supervision. I am grateful to her for her consistent guidance, motivation, patience, and inducting her intellectuality, over these years. She has always made available herself for discussions besides her busy schedules. Her enthusiasm, sublime work ethics, analytical abilities, and never-say-die attitude toward research and life as well, has nurtured my scientific skills and also inspired me immensely to work hard. And, a hearty thanks for the greatest support which helped me get through some unprecedented times. I am proud and blessed to have her as my Ph.D. supervisor. Thank you, Ma'am, for all your help, advice, and support.

I want to thank my doctoral committee members, Prof., Santosha Kumar Dwivedy, Dr. Satyajit Panda, and Dr. Hrishikesh Sharma, for their encouragement, insightful comments, and suggestions which has helped me to refine and widen my research from various perspectives. My sincere gratitude also goes to the Head of Department of Mechanical Engineering, Prof. K. S. R. Krishna Murthy, for providing all the resources needed for my research. I am also thankful to all the faculty and staff members of the Mechanical Engineering department who helped me whenever I needed. Without their help, it would not have been possible to conduct my research. It is an honor for me to thank the Indian Institute of Technology Guwahati for giving me such an excellent opportunity for undergoing my research.

I am also thankful to the Ministry of Human Resource and Development (MHRD), Government of India for providing me financial support during my Ph.D. at IIT Guwahati. In this regard, I

should thank Dr. Poonam Kumari for offering opportunities where I could assist as a resource person and learn from the exposure offered during the online MOOCs courses.

I want to thank my seniors, Dr. Agyapal Singh, Dr. Susanta Behera, and Dr. Sathish Kumar R. for their mentorship related to make things done and hand-holding whenever I got stuck during the research. I should also mention about Mr. Viwek Kumar, Mr. Dhirendra K. Verma, Mr. Mukesh Kumar, Ms. Mridusmita Bora, Mr. Abir Saha and Mr. Nikhil Kulkarni for their timely help, suggestions, and encouragements. It was fun to work with the PG students whose contributions showed new dimension to this research. I am indebted to my colleagues and friends, Dr. Ramesh Kumar, Dr. Avinish Tiwari, Mr. Abhay Gupta and Dr. Vikas Kumar who made this journey along with me creating a memorable campus life.

My special gratitude goes to my family for their role in my life. I offer my regards to my loving parents, Mr. Nishit Chandra Kar and Mrs. Shrabani Kar, whose love, teachings, sacrifices, and blessings brought me this far. I am thankful to my younger sister Shalini Kar and brother-in-law, Kunal Roy for supporting my parents and at instances taking my share of responsibilities.

I extend my sincere thanks to my friends Ashirbad, Sankalp and Mr. Abhilash Purohit who helped me emotionally, financially, socially during the tough times of my life. Thanks for being what you are.

Last but not least, I am immensely grateful to my best friend and life partner, Sukanya Borkataki who has been a constant inspiration, understanding, and had faith in me which has been my greatest strength. I am truly blessed for having you in my life. My parents are the backbone of my happiness, and I dedicate my thesis to them.

Finally, I thank God for always being with me.

Shranish Kar

Abstract

The recent smart structures have extensive applications and has facilitated structural health monitoring, integrated control mechanisms, distributed sensing and actuating capabilities and various other precision, automation engineering applications. The mechanics of such smart composite structures is dependent on coupling of two or more forcing fields which has to be integrated in the multi-physics based governing theory. Moreover, geometric parameters of the structures such as curvature of shells, thickness, layer wise inhomogeneity in laminates, adhesion and material heterogeneity which cause generation of localised stresses needs to be addressed. This indicates that multi-field response of structures are truly three-dimensional (3D) in nature. 3D theories can accurately predict the stress concentration zones and variation of other variables in smart structures as the field variables take no prior assumptions and full constitutive relations are considered. However, there is inherent complexity in solving the problem analytically. Very recently, analytical solutions are being developed by thoughtful incorporation of the numerical techniques to achieve dual advantage of avoiding the complexity and reduced computational cost which would have been otherwise incurred in case of a full numerical solution. These solutions are termed as semi-analytical solutions.

The extended Kantorovich method (EKM) is an efficient semi-analytical technique. In the past decade, the method has been employed to deliver reliable and accurate 3D solutions for beams and plates, and has constantly developed to be more powerful with significantly fast convergence and has exhibited other advantages of being an analytical solution. Here, for the first time, the method has been extended to obtain 3D elasticity/ piezoelasticity based solution for the static

and free vibration analysis of hybrid laminated composite cylindrical shells. Its ability to solve for cylindrical shells with any/ arbitrary combinations of support conditions such as simply supported, clamped and free edges is a notable feature. Derivation of the weak form of governing equations from a Reissner's-type mixed variational principle, inclusion of fully coupled constitutive relation, shear-slip phenomena, multi-term and multi-field variable incorporation in the formulation are some of the novelty in the presently developed solution.

Initially, a 3D elasticity based solution has been developed for analysing cylindrical bending of the cylindrical shells subjected to arbitrary boundary conditions. The coupled electro-mechanical field variables are further considered for the development of another piezoelasticity based 3D solution for the hybrid composite cylindrical shell panels. The weak form of the governing equations are obtained from the mixed type variational principle where displacements, stresses, and electrical field variables are all treated as the primary variables. Subsequently, the expression for multi-term EKM in terms of separable functions of the coordinates θ and r, is substituted in the variational equation to obtain two systems of non-homogeneous ordinary differential equations (ODE)s in θ and r. The system of ODEs in r contains variable coefficients whose solution is not straight forward as compared to standard solutions available for the system of ODEs with constant coefficients arising in the case of beams and plates. By employing the modified power series, this mathematical complexity is tackled and a closed-form solution is obtained. On the other hand, separate closed-form solution is obtained corresponding to the constant coefficient set of ODEs for θ functions. In this manner, the formulation can be applied to elastic/ piezoelastic problems involving a thickness direction along with an in-plane direction. An extensive numerical study of cross-ply, angle-ply, sandwich laminates, shallow, deep, thin, moderately thick and thick cylindrical shell panels have been conducted. The effects of these parameters and arbitrary boundary conditions has been investigated. The nature of stresses at the clamped edges, boundary effects, interfacial discontinuities and deflection extremities are accurately predicted where the inconsistencies in 3D finite element (FE) results have been observed. But, wherever available, 3D exact results are used for comparison.

Furthermore, a 3D elasticity based solution has been presented for laminated cylindrical shell panels with imperfectly bonded plies. The solution is a significant contribution in the field as such solutions realistically match the physical phenomena. Results are presented for cylindrical shells which are subjected to arbitrary boundary conditions and by varying the magnitude of bonding imperfection between the plies. The bonding between the plies is modeled as a linear-spring and is included in the mixed formulation defined over the lamina interfacial area. As a result, the interfacial conditions corresponding to displacement jumps are obtained which exists along with the continuity of the transverse stresses across the interface. Comparison with FE model analysed by employing 3D elastic and 3D cohesive elements has shown good match and further study has been done to draw physical inferences from the effective parameters.

Lastly, free vibration analysis has been done from the 3D dynamic solution. The solution is obtained from the extended Hamilton's principle of similar mixed nature. Primarily, the presented 3D solutions can be used for revisiting and development of 1D/2D theories. Moreover, the benchmark results are reported for ready design guidelines and references of other studies.

Contents

List of Figures

List of Tables

List of Symbols

L	=	Number of plies in the laminated composite
ψ	=	Circumferential span of the cylindrical shell
θ	=	Circumferential coordinate direction
h	=	Total thickness of the laminate
R	=	Mid-surface radius of the cylindrical shell
r	=	Radial coordinate direction
z	=	Axial coordinate direction
R_i	=	Radius of inner surface of cylindrical shell
R_o	=	Radius of outer surface of cylindrical shell
t	=	Thickness of a kth ply
R_1	=	Radius of inner surface of kth ply
β^o	=	Fiber angle of a kth ply
σ_{ij}	=	Normal stress components for i & j=θ, r and z; denoted as σ_i when $i = j$
τ_{ij}	=	Shear stress components for i & j=θ, r and z
ε_{ij}	=	Normal strain components; denoted as ε_i when $i = j$
γ_{ij}	=	Shear strain components
$\bar{s}_{ij}$	=	Components of transformed compliance matrix
Y_i	=	Young's modulus of elasticity
G_{ij}	=	Shear modulus of elasticity
ν_{ij}	=	Poisson's ratios
v, w and u	=	Displacement components u_i along θ, z and r
Δu_i	=	Components of displacement jump
K_i	=	Stiffness coefficient of interlaminar bonding
$\bar{\mathbf{R}}_i$	=	Interface Compliance coefficient
p_1& p_2	=	Magnitude of pressure load on inner and outer surfaces, respectively
ε_{ij}^G	=	Components of the geometrical strain

$\Delta u_i^{G(k)}$	=	Geometrical displacement jump
T_i^n	=	Surface traction vector
n_j	=	Direction cosines of outward normal $\bar{n}$ to the surface
V	=	Volume of the shell panel per unit length in the z direction
A_u	=	Boundary surfaces where displacements $\bar{u}_i$ are prescribed
A_T	=	Boundary surfaces where tractions $\bar{T}_i^n$ are prescribed
A_k	=	Area of the kth interface
ξ	=	Non-dimensionalized circumferential coordinate along θ
ζ	=	Non-dimensionalized radial coordinate along r for a kth ply
$\mathbf{X}$	=	Vector with displacement and stress field variables
$\bar{\mathbf{G}}$	=	Vector with field variables g_l^i occurring in inner/ outer boundary conditions
$\hat{\mathbf{G}}$	=	Vector with field variables g_l^i not occurring in inner/ outer boundary conditions
δX_l	=	First variation of $\mathbf{X}$
$\mathbf{C_o}$	=	Real constants for solving along ζ for kth ply
$\bar{\mathbf{F}}$	=	Vector with field variables f_l^i occurring in circumferential boundary conditions
$\hat{\mathbf{F}}$	=	Vector with field variables f_l^i not occurring in circumferential boundary conditions
$\mathbf{Y}_i, \lambda_i$	=	Eigenvalues and eigenvectors of $\mathbf{B}$ matrix
$\mathbf{C}_i$	=	Real constants for solving along ξ
l	=	Axial length of cylindrical shell
S	=	Thickness ratio R/h of the cylindrical shell
E_{nn}	=	Elastic traction stiffness in the normal direction
E_{ss} and E_{tt}	=	Elastic traction stiffness along the two local shear directions
$\bar{\sigma}_i, \bar{\tau}_{ij}$	=	Non-dimensionalized stress components
$\bar{\varepsilon}_i, \bar{\gamma}_{ij}$	=	Non-dimensionalized strain components
$\mathbf{t}$	=	Time variable

Chapter 1

INTRODUCTION

1.1 PREFACE

Advancement in material sciences has delivered multi-functional materials with characteristics of superior mechanical and certain other physical properties such as voltage, temperature sensitivity, magnetism, etc. Smart materials can not only be made in such a manner but also are resourcefully integrated with conventional structures to construct an intelligent structural system. Piezoelectric fiber reinforced composites (PFRC) have been developed aiming at high strength, conformability to curved surfaces and toughness with their wide range of piezoelectric properties. Such hybrid composite and sandwich shells with embedded or surface- mounted piezoelectric sensors and actuators form a very important part of the new generation of smart structures with potential applications in aerospace vehicles, automobiles, micro air vehicles, sport products, etc. Due to the presence of high layerwise inhomogeneity in mechanical and electric properties in the hybrid laminates, modeling of structures of such laminates requires special attention. The most accurate global laminate level as well as local layerwise response of hybrid laminated structures can be obtained by the exact analytical solution based on the three-dimensional (3D) piezoelasticity. In these solutions, no ad hoc assumptions are made on the variations of the field variables across the thickness. These solutions provide insight into the complex electromechanical behaviour of the hybrid structures and also serve as assessing benchmarks. The governing equations of 3D piezoelasticity for cylindrical shells involve variable coefficients as a function of the radial coordinate, which prevent a straight forward closed form solution unlike in case of constant coefficients (beams, plates).

Further, for large scale structural control applications such as in aerospace structures, monolithic piezoelectric actuators and sensors suffer from certain shortcomings with regard to tailorable anisotropic actuation i.e. directional actuation, robustness against damage during use and handling, ability to cover the entire structure for distributed actuation and sensing, and conformability to curved structural members such as shells and tubes. Piezoelectric fiber reinforced composites have been introduced to address these concerns.

But mathematical detailing of these structures is a hard nut to crack due to the inherent curvature of these structures. After the pioneering postulate of Love (first thin shell theory), a number of shell theories were proposed and further refined by introducing assumptions and approximation on the curvature, to provide accurate solution for shell structures under bending and vibration. Displacement field variables are assumed 'a priori' in these theories due to which accurate global laminate level as well as local layerwise response of hybrid laminated structures cannot be predicted. Three dimensional analytical/ semi-analytical solutions are required to address the above concern. Literature survey indicates the recent research interest in that direction. Although predominant development has been observed for the beams and plates, but those for shell structures are considerably sparse. Developing analytical solutions for structural problems involving material inhomogeneity, arbitrary boundary conditions, geometric discontinuities and under coupled field adds to the challenge and is equally rewarding. The presently developed 3D static and dynamic solution for composite shell structures based on piezoelasticity is able to predict singular stresses corresponding to the presence of arbitrary boundaries, weak interfaces and electro-mechanical coupled variable fields which can be utilized for the assessment of 1D/ 2D theories and other solutions obtained numerically. Initially, the solution is obtained for the angle-ply/ sandwich composite cylindrical thin, thick, shallow and deep shells. Further, the mechanics of imperfect bonding between the plies is incorporated in the formulation for obtaining the solution and some interesting physical aspects is presented. The solution is extended to piezolaminated shell structures based on electro-mechanical coupled theory for its static and free vibration analysis. An extensive review of

various 3D solution approaches is presented in the next chapter and the motive behind this work can be clearly reasoned from the following conceptual discussions.

1.2 SHELL STRUCTURES

Shells are three dimensional bodies bounded by two, relatively close, curved surfaces. Historically, introduction of shells as a basic structural element has contributed in many branches of engineering. Masonry domes and faults from the Middle Ages has led to development of architecture and more spacious building constructions in recent times which are made up of reinforced concrete. Separate stones or voussoir sub-units are arranged in Masonry dome structures which may or may not be cemented to each other. Design of boilers which was crucial for the industrial revolution are shells which were initially built from suitably formed and riveted plates. Thus pressure vessels with associated pipelines is crucial for power and chemical industries. Designing steel as a member under compression against buckling was a structural engineering problem which was solved in the building of the Forth railway bridge in 1889 by riveting steel plates into reinforced tubes. In the automobile and vehicle body structures of modern day, skins which are preformed into thin doubly-curved shells by power press machines are the structural members which has replaced earlier day's system of structural ribs and non-structural panelling and sheeting. Similar is the case for the aircraft and boat making where thin yet strong skin design is of importance. Introduction of shell structures has also developed cooling towers, silos and arch dams. In addition to that list, shells are primary structural components in instruments and engineering structures such as cartridge shells, mediaeval armour, petroleum containers & pipelines, hulls of submarine & ships, housing of nuclear power plant, body of missiles and chimney. Abundant examples also do exist in nature in the form of shells, such as mushroom, eggs, vegetables (like tomato, pumpkin), tree leaves, shapes of bones at the joints and skull, biological and geological formations. Mostly man made structures in the form of domes and missionaries are also classified as spherical shells.

Certain shell structures require higher external energy to collapse into plane form than the others.

These shells are termed as nondevelopable and developable shells, respectively. Technically, those shells with positive and negative Gaussian curvatures can be developable and those with zero valued Gaussian curvature are nondevelopable. Shells are classified through the Gaussian curvature κ of the surface defined at a point. It is mathematically expressed as:

$$\kappa = \kappa_1 \times \kappa_2 \tag{1.1}$$

κ_1 & κ_2 are the maximum and minimum principal curvatures of the surface which are defined for those curves which are obtained by the intersection of normal principal planes sections with the shell at the point. Further, the shells are categorized based on the translational surfaces, ruled surfaces and surfaces of revolution. When a curve is translated along a generator curve, translational surface is obtained. On the other hand, when a straight line is made to slide with its two ends over the two generator curves, a ruled surface is generated. Surfaces of revolution are obtained by revolving the meridional curve about the axis of revolution.

Many researchers have been deeply studying these structures over the years mainly for their high load carrying capacity. This phenomenon is due to shell curvature that couples the membrane and flexural behaviors of doubly and singly curved structures. These have high degree of reserved strength and structural integrity, high stiffness, containment of space and high strength : weight ratio (larger is this ratio, the more optimal is a structure). According to these criteria, shell structures are much superior to other structural systems having the same span and overall dimensions. The shell structure can make a fast transition between the initial state and the bending state when it is subjected to a bending movement [1]. Few interesting work of researchers who derived energy from shell structures due to its inherent curvature are also discussed. An experiment by Yang and Yun [2] demonstrated that shell structures with various curvatures produce high output potential and consequently offer high output power in comparison to a simple flat structure. Being structurally continuous is another essential factor for imparting its structural benefits. In that sense, shells can transmit forces in its surface in a number of different directions, as required. This mode

of action is different from the skeletal structures which transmit load only through its discrete structural members [3].

Hence the development of the theory of electroelasticity is strongly motivated and influenced by its applications in shell structures.

1.3 SMART MATERIALS AND STRUCTURES

The emergence of synergistically integrating active and functional materials as in situ actuators, sensors and control components in the structures has originated the concept of adaptive, intelligent, and smart materials and structures. The discipline for the study of such structures has been very recently known by a concept *adaptronics*, coined as a generic term. Its origin is merely around 1980, from the early efforts of vibration suppression and interests in the development of aviation and space technologies. Technologically, smart structures integrate sensors, actuators and controls within a material or with a parent structural component. Hence, the conventional passive elastic definition of the structures has been enhanced to active *structronic* (structure + electronic) system, as these structures are multi-functional and life-like adaptive [4]. Functional materials are the prime components of a smart structure. Functional material responds to a stimuli and its functional property is intact even after subdividing its volume. The stimuli can be temperature, light, moisture, mechanical strain, electric, magnetic fields, etc. Commonly known functional/ smart materials are piezoelectrics, electrostrictive materials, pyroelectrics, flexoelectrics, shape memory materials, magnetostrictive materials, light-actuated shape memory polymers (LaSMP), magneto-optical materials, photostrictive materials, photoferroelectric materials, electrorheological & magnetorheological fluids, polyelectrolyte gels, etc.

The structures are 'distributed' in nature which means that its structural behaviour is function of two components, time and space. Therefore, distributed control functionality is crucial requirement for developing smart material based structures. The control can be at various levels such as local, global or at higher cognitive levels. For example, augmenting damping and minimization

of residual displacements require local control capabilities. Further, shape control and stabilization of structural response are global control and cognitive control refers to instances of failure diagnosis, further reconfiguration and adapting after that failure. The smart structures can be made by synthesizing nano-structured materials with smart functionality at the molecular level. Alternatively, these can be made as composites with active and non-active plies. A more mature methodology is by attaching or embedding the smart components onto the conventional structures. The piezoelectric elements should have force-locked coupling with the structures and there should be a safe contacting/ insulation method. The Young's modulus of the integrated sensors must be comparable with that of base structure or should be isolated from the load path mechanically.

1.3.1 Piezoelectric Structures

The electromechanical phenomena which couples the elastic and electric fields is called piezoelectricity. It occurs by virtue of geometry of the crystals where its geometric center does not coincide with charge center. Twenty out of 32 classes of crystals (classified based on its symmetry with respect to a point) can exhibit piezoelectricity due to asymmetry in them which separates the positive and negative charges resulting in electrical dipole moments. However, centrosymmetric (symmetric with respect to a single point) crystals can not possess piezoelectricity. After original quantitative measurements of piezoelectricity in quartz and tourmaline, other natural crystals like cane sugar, tartaric acid, ammonium phosphate, and Rochelle's salt were discovered to exhibit piezoelectric effect. Other examples of piezoelectric materials are glass rubber and paraffin which are non-crystalline materials, bone and wood are textures and piezoceramics are synthetic piezoelectric materials. Lead zirconate titanate (PZT), lead lanthinum zirconate titanate (PLZT), lead niobrate, etc. are examples of piezoceramics with general compositional formulae $Pb[Zr_xTi_{(1-x)}]O_3$. Being environmentally concerned, lead-free piezoelectric materials are developed such as barium titanate, potassium sodium niobate (KNN), Bismuth sodium titanate (BNT), crystallines such as lithium sulfate, ammonium dihydrogen phosphate, etc. and polyvinylidene fluoride (PVDF or

PVF2) is a synthetic piezoelectric polymer material. Recently developed lead magnesium niobate (PMN) which shows superior properties are termed as relaxor materials. Piezoelectricity properties has also been achieved in certain materials through processes other than chemical doping. $Pb(Zn_{1/3}Nb_{2/3})O_3 - PbTiO_3$ (PZN-PT) and $Pb(Mg_{1/3}Nb_{2/3})O_3 - PbTiO_3$ (PMN-PT) have been developed by poling along a non-polar axis which physically creates disorder in the ordered system. These materials possess very large value of $d_{33} > 2000$ pC/N and electromechanical coupling coefficient (k_{33}) of 90%. Piezoelectric-piezomagnetic composite, magnetoelectric-piezoelectric composite, etc. are other multifunctional materials which enhance the functionality of individual constituting materials employed together as a composite. Originally, in unprocessed form piezoceramics are isotropic and macroscopically non-polar which acquire piezoelectricity properties and attain anisotropy after polarization through a strong electric field. Specifically, when the electric field strength E crosses the electric coercivity (E_c) of the piezoceramic material, its domains start changing their structure until a maximum electric field strength (E_{max}) where saturation of change in domain orientation is reached. At the mesoscopic level, domain wall motion is affected by presence of dopants and defects in the material. This influences the magnitude of piezoelectric coefficients (d) which subsequently quantifies the piezoelectric properties. When the motion of the domain wall is inhibited, it is called as hard piezoelectric material which has a small d value. Alternatively, soft piezoelectric material has larger strain which are mostly used as actuators. After manufacturing through a powder metallurgy process, the piezoceramics are available as semi-finished products in form of fibers, powder or foils as shown in the Fig. 1.1, to be integrated with the base structures. As the piezoceramics possess unfavourable mechanical properties for load carrying capacity alone, these are combined into composites with polymer materials. Further, this allows configuration of directional functionality by spatial arrangement of the constituents/ phases which is characterised by *connectivity*. For example, if the active piezoelectric phase (usually considered as phase 1) and passive polymer matrix phase (considered 2) extends in m-direction and n-directions, respectively, it is called m-n-connectivity two-phase composite material. 0, 1 and 2- connectivity are denoted

corresponding to particle, fiber and foil shaped piezoelectric phases, respectively, which counts the number of orthogonal directions along which the phase extends continuously. The directional piezoelectric coefficients and permittivity of these composites do not follow the rule of mixture which a different for different series or parallel phase connectivity.

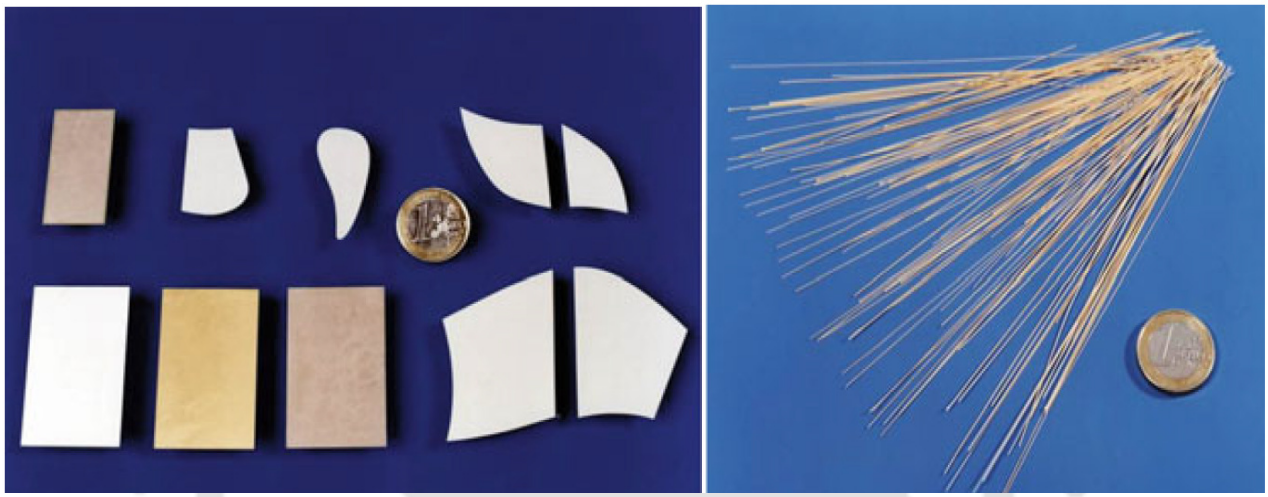

Fig. 1.1: Shapes and forms of available semi-finished piezoelectric ceramics. (Sinapius [5])

The reciprocal piezoelectric effect is utilized for development of piezoelectric actuators. Conversion of a input energy into mechanical displacement is performed by an actuator. In order to gain a mechanical strain **S**, under the mechanical stress **T** and applied electric field **E**, actuator equation based on linear piezoelectricity is expressed in the following manner:

$$\mathbf{S} = s^E\mathbf{T} + d^T\mathbf{E} \tag{1.2}$$

In this equation, s^E is the elastic compliance of the piezo material under a constant **E** and d^T is the transpose of d. The actuation can happen from three effects of electromechanical behaviour of the piezoceramics depending on the direction of applied electric field and direction of strain obtained. Considering that an external electric field is applied along the polarization direction of the piezoceramic, a strain obtained along the same direction defines the piezoelectric coefficient d_{33} according to the longitudinal effect and a strain in transverse direction defines d_{31} under the transverse effect. Again, applying the external electric field orthogonally to the polarization, causes

the shear effect quantified as d_{15}. According to these effects, piezoelectric actuators are designed in the following ways:

1. Stacked transducer: Piezoceramic discs of size 0.3 - 1mm of opposing polarization are stacked and glued with outer nickel or copper electrodes. This employs the d_{33} effect.

2. Laminar transducer: Piezoceramic strips are stacked into laminate as they have higher geometric aspect ratio (i.e., ratio of in-plane/thickness dimension). This employs the d_{31} effect.

3. Bending element: When a piezoceramic is mounted on a spring metal substrate it is termed as a monomorph and when two piezoceramic strips of which one shortens and the other elongates is a bimorph. This design also utilizes the d_{31} effect.

4. Shear element: This is used to design a x-y positioner by utilizing the d_{15} effect. When used along with the d_{33} piezoceramic, a 3-axis positioning system can be designed.

5. Thin films: Through sputtering on a substrate the thin film of AlN, ZnO or ZnS is deposited which can be also multilayered for optimum piezo properties.

Few of the applications where the piezoelectric actuators have been used are the auto focus zoom facilitated by a piezoelectric ultrasonic motor (USM) in the cameras, active damping of ski with piezo actuator mounted in front of the shoe and accelerometer on top of the ski.

The piezoelectric ceramics through the direct effect show sensory applicability. The following is the sensor equation to express charge displacement $\mathbf{D}$ as:

$$\mathbf{D} = d\mathbf{T} + \epsilon^{T}\mathbf{E} \tag{1.3}$$

where, d is the piezoelectric coefficient and ϵ_T is the electrical permittivity. The key factor which define the sensor properties is sensitivity which is the drop in the open-circuit voltage across the contact to the applied stress. Coupling coefficient is another sensor property which quantifies the conversion of mechanical energy into electrical energy. Also, temperature dependent properties such

as temperature drift and pyroelectricity need to be considered along with embeddibility and repeatability. Hence, the sensors are designed in the shapes of plates, globe, disks, cylinders, bending (unimorph and bimorph arrangements), piezoelectric composites (AFC, MFC and PFC), ceramic metal composites (flextensional type) and piezoelectric MEMS. An illustration of piezo fiber composites (PFC) is shown in the Fig. 1.2. Piezoelectric sensors possess higher signal-to-noise ratio and

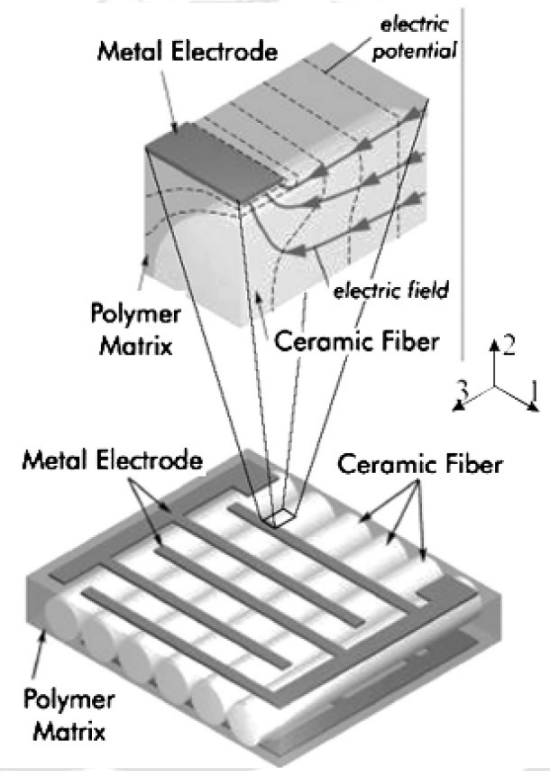

Fig. 1.2: Schematic of the cross section of a 1–3 piezo fiber composite. (Janocha [6])

high-frequency noise suppression as compared to conventional strain gauges. Those sensors operate in either of the two working principles i.e. passive and active mode. Physically, passive sensors do not influence the structure and just measure the deformation by direct piezoelectricity effect. On the contrary, active sensors work by scanning (done by sending defined wave for deformation) the structure where ever required and detect the location and magnitude of a damage by recording the reaction of the structure to that applied deformation. Novel 1-3 piezo fiber composite is ideally adapted for both passive and active structural health monitoring (SHM) applications [6].

When ever these piezoelectric sensors or actuators are employed, they require an additional signal conditioning system. Piezoelectric materials posses a large internal resistance. Due to which, they behave like a capacitor and develop large voltage across its electrodes which can leakoff very slowly when subjected to static strain. There is further issue in measuring dynamic strain. Hence, a signal conditioning system is required to provide the signal with a low output impedance and very high input impedance is presented to the piezoelectric sensor, simultaneously.

1.3.1.1 Applications of piezoelectric smart structures

The First World War saw the development of piezoelectric devices such as ultrasonic emitters, receivers, resonators, transformers and oscillators from the interest of underwater and ocean floor object explorations. Sensor applications are found in pressure transducers, microphones, force transducers, accelerometers, etc. and precision manipulators, ultrasonic motors, robot manipulators and driving mechanisms in microscopes are examples of actuator applications. Since the last decade, energy harvesting devices are being constantly invented and patented. Piezoelectric devices with thin-layers are applied in helicopter rotor blades, precision trusses, airplane wings, vibration control and isolation systems, and micro-sensors/ actuators. Few very recent technological advancement in application of piezoelectric shell structures has been seen in diverse fields of medicines, communication, flight control, sports utilities, new age manufacturing and food processing industries. In an experimental study, ultrasonic field was produced for drying foodstuff for which an aluminum cylindrical chamber was designed that was driven by a piezoelectric transducer [7].

Typical applications in specific domain of engineering are as follows:

Space systems: Space organizations have tried piezoelectric layer for actuation of shell membrane during space imaging. A kind of space imaging instrument called as Lenticular membrane reflector (Fig. 1.3a) has piezoelectric layer on its shell structure for focal length adjustment when placed in the orbit. Another instrument called as an adaptive elastic shell (Fig. 1.3b) can be rolled after manufacturing and unfolded after placing in the orbit. This causes surface modulations which are

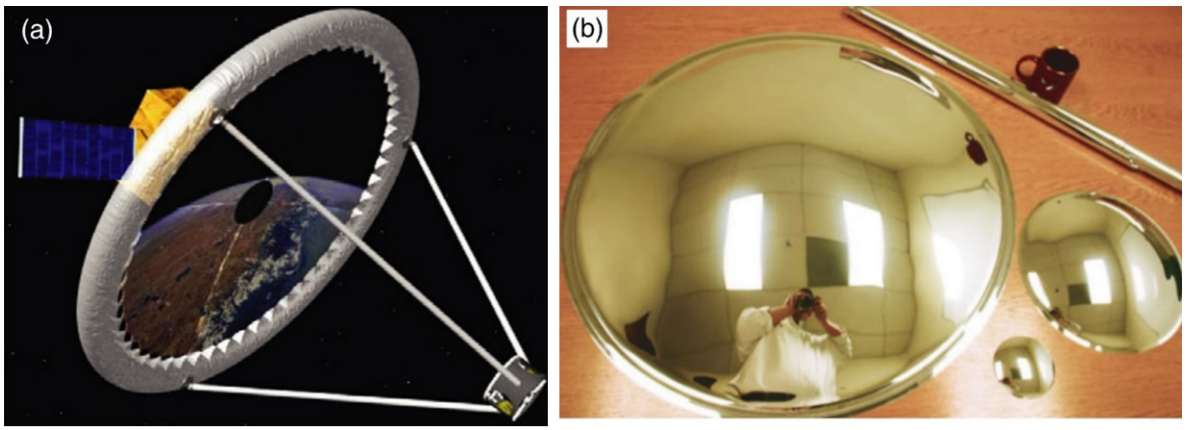

Fig. 1.3: Application of piezoelectric shell structures in space imaging. (a) Lenticular membrane reflectors, (b) Adaptive elastic shells (Bastaits et al. [8])

again corrected by surface mounted piezoelectric actuators.

$Fixed-wing\ aircraft$: The aeroelastic effects such as lift, roll effectiveness and divergence are controlled by piezoelectric actuators as embedded sheets in laminated-composite wing structure. Active control of panel flutter has been analysed after embedding piezoelectric sheet actuators along with passive utilization of shape memory alloy actuator by recovery forces and stiffness variation [9]. Application of smart structures in fixed wings aircrafts aim at reliability by condition-based maintenance, reduced noise in cabin and its vibration to enhance crew comfort.

$Rotary-wing\ aircraft$: The rotor confronts to transonic flow, stalled reverse flow and blade-vortex interactions. Piezo-stack actuators integrated in the flap can enhance its vibration and noise control. Composite beams with bending torsion coupling induced by piezoelectric actuator has also been designed to actuate the rotor [10].

$Jet-engines$: For a wide range of flight conditions, the inlet of the otherwise fixed-geometry engine is variably shaped such as inlet wall shaping and lip blunting. Piezoelectric material actuated-liquid-fuel modulation system has shown improved performance in active combustion control [11].

Civil structures: In service detection of loading and damage of the structure in real-time is done by using PZT transducer and propagation of guided ultrasonic-wave. Liao et al. [12] monitored the tensile load distribution (i.e. dynamic response) of the cable-stayed bridge wirelessly by using

PVDF film sensors on the stayed cables.

Machine tools: Active vibration control for reducing chatter during high speed machining has been analysed by using piezoelectric actuators. In another study, O'Neal et al. [13] employed a micropositioner which consisted of piezo-actuator and photosensitive detectors and acted as an intelligent boring bar and actively control the cutting by extending its range of cutting depth by 40 %.

Medical systems: To assist in the surgery, active grasping tool has been designed which has localised force sensing and actuation capability through a small PZT inchworm actuator. A PVDF piezopolymer based sensor has been developed by researchers which are placed at the thorax region below the bed sheet to pick the pressure fluctuation and monitors the respiration and heart rate during the unconstrained in-sleep condition.

Robotics: Robotics find the largest application of the smart materials and structures. Uchino [14, 15] presented a comprehensive review on the development of piezoelectric ultrasonic motors of various configurations such as rotary/ linear type, variable speed/torque, standing wave and travelling wave based and of different geometries such as ring, cylindrical, etc.

1.4 MOTIVATION

Application of the shell structures in real world is obviously inevitable. Further, enlarging scope for development of the smart materials and structures in critical engineering domains has directed the evolution of theories based on coupled multi-field physical principles. Moreover, even by considering linear geometry or material properties, singularities in the mathematical form of the governing equations and stress concentration zones in the structure arise under any loading condition. These effects are due to the presence of arbitrary boundary conditions, simultaneous multi-field loading and weak structural integrity. Realizing the complexity of obtaining the solution of governing equations derived even for simplified models, available approximate numerical techniques have been employed. However, such solutions are questionable at certain critical locations and demands

analytical or semi-analytical solutions. Further motivation comes from the wide-range frequency applications, low surface potential in certain piezoelectric materials or minor imperfection in the bonding between the components whose effect on the system needs to be very accurately predicted.

Chapter 2

LITERATURE REVIEW

Precision is required in the design of an engineering structure so that it is economical and wherever straightforward geometries are concerned, employing the theory of shell structures is an efficient design tool. Whereas, long before existence of any textbook for shell structures, engineers used to build shell structures out of strongly empirical outlook. German physician and businessman, Aron was the first to discuss problems on shell theory [16]. Kirchhoff-Love shell theory is the pioneering shell theory proposed by an English mathematician, Love [17]. Subsequently, with assumptions of kinematical hypotheses, approximate shell theories were presented which can be expressed by two-dimensional partial differential equations (PDEs). These approximate theories are being constantly refined and improved by considering new hypotheses. Timoshenko, by accounting for transverse shear and rotational inertia effects in beams and another by von Kármán for nonlinear strains resulting from thinness of plates, introduced approaches for kinematic hypotheses. Later, the impetus for development of nonlinear shell theories was provided by the aircraft industry and refined theories in this regard were proposed by Donnell and Mushtari. Further, Reissner made an original contribution by obtaining 6th order PDEs for the shell (unlike 4th order PDEs in Kirchhoff theory) which allowed three boundary conditions to be satisfied on each boundary and starting from the dynamic problem, Raymond David Mindlin developed a similar theory in the finite element reference. Hence, the name "Reissner-Mindlin theory" has been used for the theory.

Electromechanical theories are rather being abundantly presented in recent times after the advent

of smart composites. The theory of piezoelectricity from phenomenological point of view was initiated by Kelvin, Duhem, Pockels and Voigt in the late 19th century. Mindlin first studied the high frequency modes of a piezoelectric plate through structural theories [18]. Tiersten proposed the two-continuum model corresponding to the lattice and an electronic charge continuum for the mechanics of a deformable and polarizable body. Toupin derived the piezoelectric equations and equations of equilibrium from the variational formulation with internal energy terms corresponding to the elastic dielectric. Later attempts towards construction of refined shell theories analogical with the Reissner's theory were made by accounting for the transverse stress in the formulation [19]. Thus, in this chapter an elaborate literature survey has been presented for various analytical, and numerical solutions to solve flexural, dynamic, and other mechanics problems of shell structure. However, focus is mostly directed towards the semi-analytical solutions which are presently of more practical interest.

2.1 LITERATURE REVIEW FOR ANALYSIS OF SHELL STRUCTURES

A number of historical papers and text books on the shells can be found in the references [17, 20–24]. Recently, mathematical modelling using the variational approach and numerical results for moderately thick shell is published in a book by Kraus [23]. After the invention of piezoelectric material in 1880, smart plates and shells (laminated/ elastic shell integrated, surface bonded piezoelectric actuator and sensor) are extensively used in present engineering and R&D field. In this direction, Tiersten [25] presented the basic piezoelectricity model for plate vibration. Tzou [26] presented piezoelectric shell theories applicable to distributed sensing and control applications. A detailed mathematical modelling of linear theory of thin piezoelectric shells with arbitrary form is presented by Rogacheva [27]. Shell theories available in the literature are classified depending upon shell thickness, deepness and magnitude of deformation (See Figure 2.1).

Review articles in the beams, plates and shells have been presented by eminent researchers across the world. These review articles provide the state of research methodology and timely update in

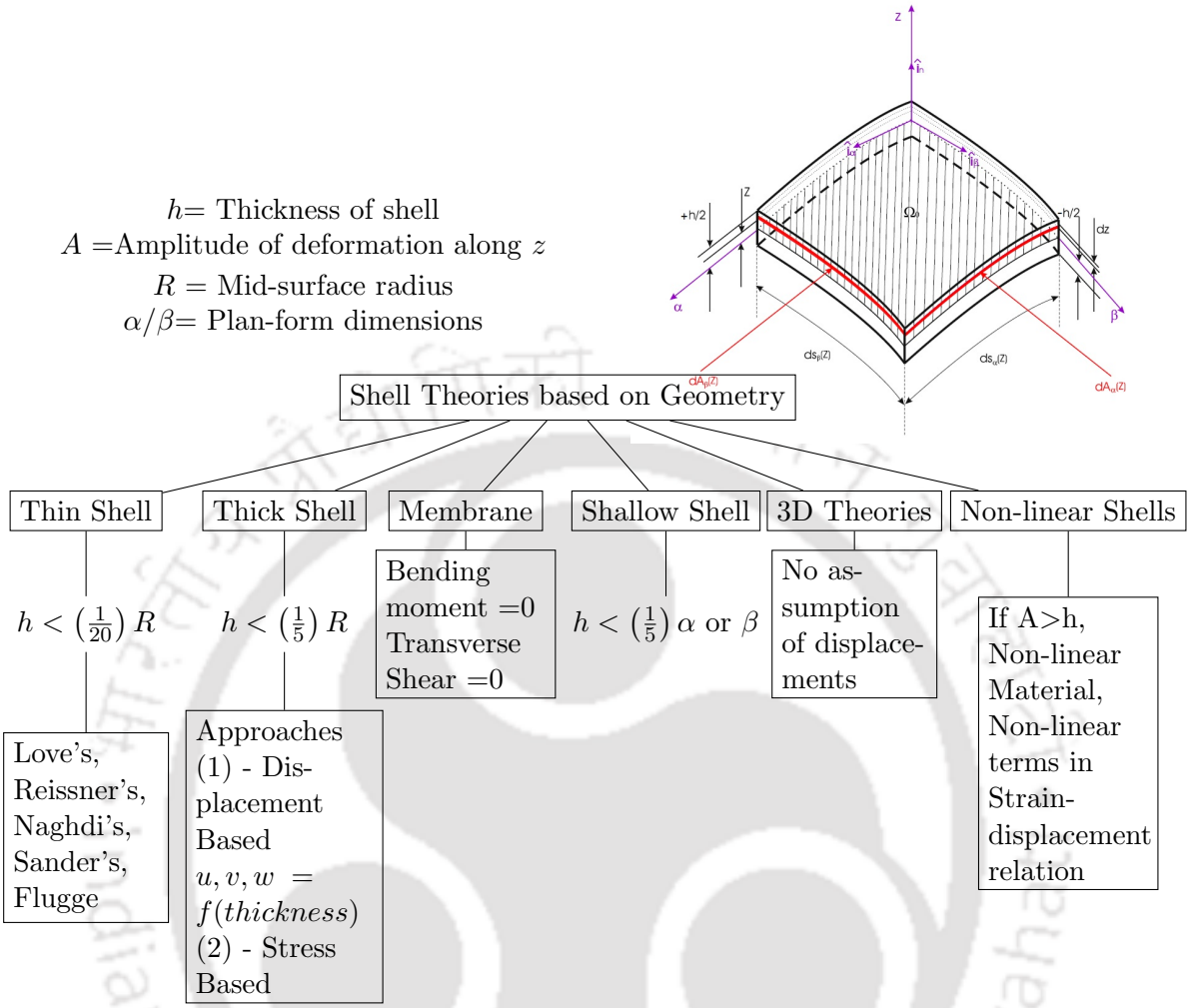

Fig. 2.1: Types of shell theories based on geometry.

this field. Some of the very relevant review articles are presented by [28–37].

A selective review and survey for interlaminar stress in the plate and shell is presented by Kant [38]. Soldatos [29] presented a literature review regarding three-dimensional dynamic analysis of cylinders and open cylindrical panel. Saravanos [30] reviewed many shell models with electro-thermo effects, non−linear effects of geometry & material. Benjeddou [39] surveyed on advances and trends in finite element (FE) modelling of adaptive structural elements like solids, shells, plates & beams specific to piezoelectric materials. Generalised 3D theories for laminates and exact piezoelectric solutions were also studied. An overview of various three dimensional (3D) analytical approaches for the analysis of multilayered and functionally graded (FG) piezoelectric plates and shells is presented by Wu et al. [40]. Liew et al. [41] reviewed the meshless methods for

laminated & functionally graded plates and shells. Thai & Kim [42] devoted a review to theoritical models which were developed to predict the global responses of functionally graded plates and shells under mechanical and thermal loadings. Very recently, a review on quasi-3D analysis of plates and shells under arbitrary boundary conditions using the semi-analytical numerical techniques has been presented by Wu and Liu [43]. They included the laminated composites, functionally graded materials and other multilayered elastic structures along with piezoelectric smart plates and shells. The experimental results usually provide the base for development and improvement of an analytical model. Experiments on the static bending of arbitrarily supported cylindrical shells do not exist as per author's knowledge, but free vibration and buckling results have been reported in the past. However, such experimental results were done for cylinders with ends supported, point loads [44], piezoelectric patch or studied under wave propagation such as the free vibration analysis by Bert and Malik [2, 45].

Due to extensive application of shell structures, numerous surveys reporting development of two dimensional static and dynamic analysis also exist. Three-dimensional solutions can provide accurate estimation of stresses and boundary effects for laminated as well as piezolaminated shells. Moreover, these solutions also act as benchmarks and are used for assessing other lower order shell theories. Since 1970, papers of 3D solutions have been published. A summary of various 3D solution approaches for static & dynamic analysis of shell structures available in the literature are shown in Fig. 2.2. As per literature, solution approaches are classified into three categories (i) Analytical, (ii) Semi-analytical and (iii) Numerical.

2.1.1 Features of a generalized 3D Exact piezoelectricity theory

Three-dimensional theories for the analysis of structural components has provided higher accuracy and is capable of predicting the actual nature of through-thickness variations. In order to develop 3D exact solution for the piezoelectric structures, the complex electro-mechanical coupling is needed to be considered along with the equations of motion for a piezoelectricity continuum.

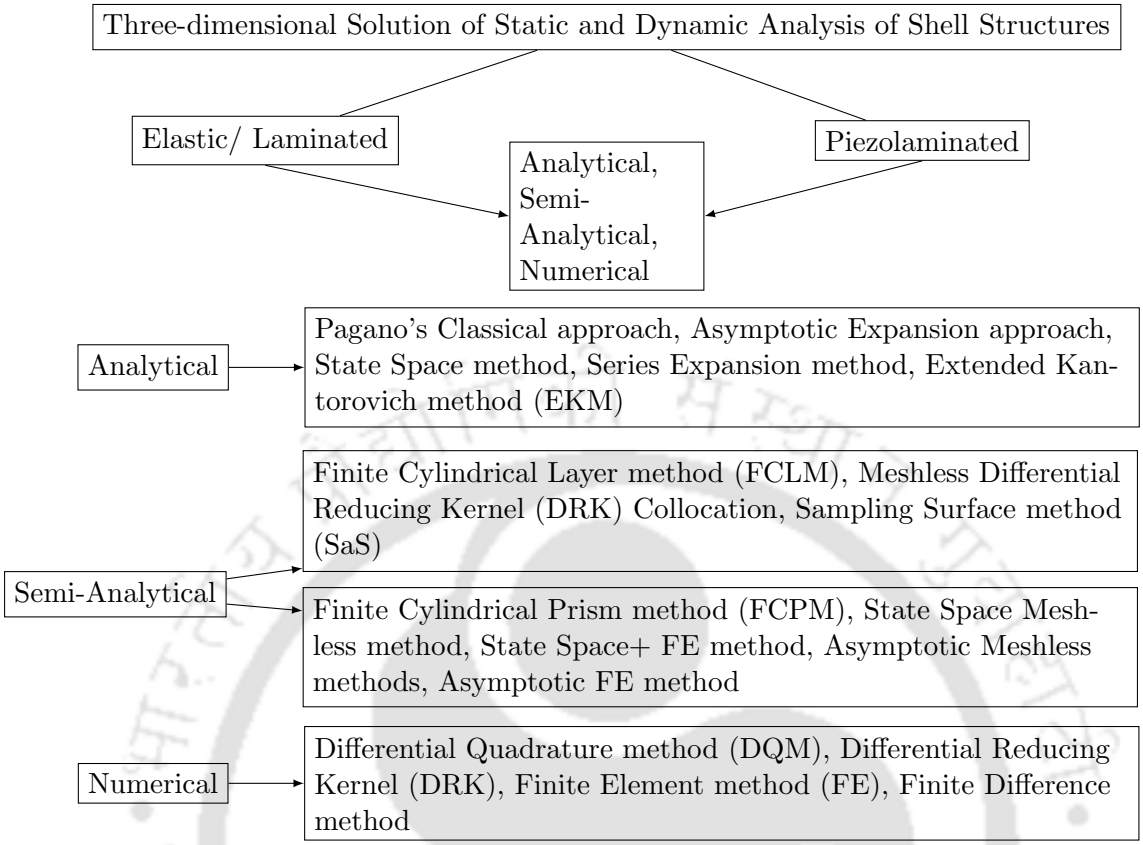

Fig. 2.2: List of solution approaches for static & dynamic analysis of Shell structures

Further, no simplifications such as displacement or stress field assumptions are required and the full 3D constitutive relations are employed. As a result, exact nature of out-of-plane displacements, stresses and electrical entities are obtained due to consideration of the effect of out-of-plane piezoelectric coefficients also. Further, the stress concentration zones such as the interlaminar transverse stresses, boundary effects, electro-mechanical coupled response and increased charge density at the surfaces can be determined. Hence, apart from providing electro-mechanical insights, the 3D exact piezoelectricity solutions serve as reference for framing kinematic hypotheses and accurate approximations for the through-thickness response of the field variables during development of refined 2D/1D theories. The necessity of such a solution increases for shell structures and more so for the hybrid composite shells. It has been observed that the electro-mechanical stress concentration is not only present at the edges but also at various other critical locations in the domain of a shell structure [46]. Yet, at the present time, such solutions are not available except for simple

geometric structures with specific electro-mechanical boundary conditions. There exists two types of piezoelectric solutions (i) Coupled, (ii) Uncoupled.

2.1.2 Three dimensional (3D) analytical shell theories

It can be observed from the literature that, various dimensionality (2D/3D) theories follow the analytical, numerical or semi-analytical approaches. In the following section, three dimensional analytical theories have been categorised depending on their applicability to obtain solutions for elastic, laminated and piezolaminated shell structures which are discussed as follows. These are presented as follows

2.1.2.1 Elasticity / laminated shell theories

As per literature, Pochhammer [47] developed one of the earliest exact solution for the infinitely extending circular cylinders made up of homogeneous isotropic material and undergoing longitudinal and torsional vibrations. Closed form solutions for those three dimensional equations were expressed in terms of Bessels function of first kind by Chree [48]. Subsequently, exact solutions were obtained using Papkovich-Neuber stress functions [49], fourier transform [50], Dougall's stress function [51]. Problems of plane strain state of stress for cylindrical panels where both edges were simply supported, was solved by Ren [52] by applying a stress function. The stress function satisfied the differential equation obtained from the equation of compatibility and the constitutive equations. Following that, developments have been reported on three dimensional elasticity theories of shell in a review article by Kapania [53]. The review dealt with following developments:

(i) Thick shell theories,

(ii) Analytical studies on the analysis of laminated shell structures,

(iii) Buckling and post-buckling analysis of laminated perfect and imperfect shells, and

(iv) Dynamic transient analysis.

This review covered the development till year 1988. In year 1989, dynamic transient solution for homogeneous isotropic cylindrical shell and panel was reported based on 3D elasticity

by Soldatos [54]. Noor and Burton [55] did an assessment of computational models for multi-layered composite shells. Developments on the three dimensional dynamic analyses of circular cylinders and cylindrical shells were critically reviewed by Soldatos [29]. They emphasized on exact three-dimensional analysis as those act as benchmark for other corresponding studies based on two dimensional and finite element modelling. Chandrashekhara and Kumar [56] assessed the accuracy of classical shell theories (CST) based on Flugge, Sanders, Love and Donnell theories, with respect to the three-dimensional elasticity solution, for cross-ply laminated circular cylindrical shells under static loads. Further, Jaunky and Knight Jr [57] checked the accuracy for buckling of circular cylindrical laminated composite panels loaded in axial compression. Soldatos [29], further categorised geometric and material complexities as two main difficulty factors involved in achieving a three dimensional analytical solution for shells (boundary value problem). In the next decade, 3D theories for free vibration utilizing ritz method [58, 59], spline prism method [60] and nonlinear vibration utilizing Galerkin method [61] were developed. All such developments on 3D solutions for dynamic and applicative problems such as fluid filled cylindrical shell [62] and non-axisymmetric problems were assessed in a series of reviews by Qatu [34, 36]. Qatu [36] had also presented a literature survey on the static 3D elasticity theory including the following topics :

(i) Nonlinear theories,

(ii) Incorporation of shell geometries,

(iii) Thermal and hygrothermal loadings, and

(iv) Failure, delamination and damage analyses.

During the previous decade, Wu [63] discussed 3D elasticity solutions of laminated annular spherical shells. Wang [64] used 3D theory to solve problems of smart laminated anisotropic circular cylindrical shells with imperfect bonding.

2.1.2.2 Piezolaminated shell theories

Much of the early work on developing exact solutions of the stress and charge equilibrium equations were concentrated on specific geometries and boundary conditions [65, 66]. Drumheller and Kalnins [67] presented one of the earliest piezoelectric shell theories based on thickness expansion of elastic and electric variables. Theoretical developments for more general laminated piezoelectric shells have been given by Dökmeci [68]. Thereafter, Tzou and co-workers worked on thin shells with piezoelectric layers [69] and went on to consider charge equation along with shear deformation theory [70]. Saravanos [71] reported a coupled mixed theory for curvilinear composite−piezolaminates combining first order shear deformation theory assumptions with a layer wise approximation of the electric potential field. Subsequently, exact solutions to laminated piezoelectric cylinders are reported in literature [72, 73]. Exact solution for a laminated piezoelectric finite panel using trigonometric functions has been developed by Nosier and Ruhi [74]. Finite element model for static and dynamic analysis of laminated shell with piezoelectric sensors and actuators are also reported [75].

Recently, Wu [40] reviewed the four different approaches for 3D analysis of piezoelectric structures. The four approaches are presented here in details

***(i)* Pagano's classical approach**

Using the Pagano's classical approach, the primary variables in displacement based formulation are assumed as exponential function of coordinate direction. Upon substitution of the assumed function for primary variable in the governing equation, polynomial functions are obtained whose roots are functions of the material and geometric properties. However, exact analysis for shell structures through this approach fails which has been overcome by artificially dividing the shell into certain small thickness layers and has been named as successive approximation (SA) method [54]. Very recently, the same procedure has been used to analyse functionally graded piezoelectric sandwich cylinders by Wu [76].

***(ii)* The state space approach**

In state space approach, the sets of state variable equations with constant coefficients for plates and with variable coefficients for shells are obtained by means of direct elimination. Using a modal matrix composed of eigenvectors, the coupled system of equation is transformed to an uncoupled system of equation. Utilizing the approach, first time Xu and Noor [77] analysed fully coupled thermoelectroelastic response of hybrid multilayered composite cylindrical shells. Chen et al. [78] obtained decoupled system equations with constant coefficient during exact static analysis of a multilayered, spherically isotropic, piezoelectric hollow sphere. As an extension of it, decoupled equations with variable coefficients (due to radial material gradient) are obtained during vibration analysis of a functionally graded (FG) piezoelectric hollow sphere [79]. Subsequently, static laminated [64], dynamic FG and radially polarized piezolaminated hollow cylinder filled with compressible fluid were presented by the researchers [80, 81].

***(iii)* The series expansion approach**

Here, the primary variables are constructed in form of a power series in the coordinate direction. Substituting this into the system differential equation and equating the various power terms, an indicial equation and a recurrence relation is obtained. The feasibility of series expansion method for exact analysis of shell has been reported by Chen et al. [82] considering an orthotropic cylindrical shell with piezoelectric layers under cylindrical bending. Fourier series expansion in the circumferential direction has been used by Dumir et al. [83] in case of piezoelectric cylindrical panels and along both axial and circumferential directions by Kapuria et al. [84]. Heyliger [73] presented solutions for simply supported piezoelectric cylindrical shells and laminated piezoelectric cylinders. Further, series expansion has also been used in case of thermal loadings on piezoelastic shell structures [84, 85]. Dynamic problems are presented for a simply-supported cross-ply cylindrical shell with a piezoelectric layer by Chen and Shen [86] and laminated cylindrical shells with distributed piezoelectric layers by Hussein [87]. Cases involving radial inhomogeneity (FG) of material property were also reported to be solved exactly by series expansion approach [88, 89]. Very recently, Kapuria et al. [90] first presented exact two-dimensional (2D) piezoelasticity solution and later a benchmark

three-dimensional (3D) solution [91] for free vibration and steady-state forced response of simply supported piezoelectric angle-ply laminated circular cylindrical panels and simply supported smart cross-ply circular cylindrical shell panels, respectively, under harmonic electromechanical load with and without damping.

***(iv)* The asymptotic approach**

The asymptotic formulation is obtained by asymptotically expanding a 3D problem into a series of 2D problems governed by the equations of 2D theories. In the asymptotic formulation, a geometric perturbation term is used. Upon substituting, the expansion into the 3D system differential equation and collecting the coefficients of equal power of perturbation factor and performing the successive integration to the resulting equations of various order problems through the thickness coordinate, a recursive set of governing equation is obtained. But regular asymptotic expansions caused nonuniform expansion terms in case of shell problems. This has been extended to various benchmark problems of static bending of piezoelectric shells [92–94], Functionally Graded shells [95] and dynamic problems of shell structures [96, 97].

2.1.3 3D Semi-analytical numerical solution methods

The numerical solutions are usually computationally costlier, and there exists inherent complexity in solving such a problem pure analytically. The semi-analytical methods are recently being developed, incorporating the numerical techniques in the analytical solution wherever necessary. Hence, such solutions incur a minimum computational cost with improved accuracy over numerical solutions. Specific semi-analytical solutions are applicable for only the simply-supported boundary conditions, and others are more robust to handle the case of arbitrary boundary conditions.

2.1.3.1 Applicable for simply supported boundary conditions

Finite rectangular/ cylindrical layer method (FRLM/ FCLM): The FCLM formulation is developed by employing the trigonometric functions along the in-plane directions, and polynomial

functions are used for finding the variations along the thickness direction for a simply-supported cylindrical shell. Such functions are applied to each of the layers, which constitutes a laminate [98]. As a result, the dependent variables reduce to be the only function of thickness which effectively causes a 3D structural problem to be solved in one-dimension (1D) in a quasi-3D manner. Usually, a 1D FE method is conveniently utilized to solve the reduced problem, and this quasi-3D solution was originally applied by Wu and Chang [99] for static analysis of hollow cylinders sandwiched by a functionally graded elastic core (FGEM). Later, in addition to laminated plates, bending, buckling, and free vibration analysis of cylindrical shells has been done by Wu et al. [100–102] based on the principle of virtual displacements (PVD).

Meshless DRK collocation and EFG methods: The differential reducing kernel (DRK) method is a technique for approximate 2D or quasi-3D analysis of multi-layered and electro-mechanical structures. Unlike the conventional reducing kernel (RK) method where the shape functions are determined directly by differentiating the RK approximations, in DRK, they are determined using a set of differential reproducing conditions. Inspite of that, the Kronecker delta property does not hold valid for those shape functions for RK approximation at any of the sampling nodes. However, while solving the weak formulation, issues arise in the implementation of DRK when the essential boundary conditions are imposed. This issue has been tackled by separating the shape function into a primitive function whose Kronecker delta property is necessarily satisfied by assigning a quartic spline function to it so that none of the neighbouring nodes of a sampling node are covered by its support size. Further, from a set of reproducing conditions, another enrichment function is determined. Such a separable shape function is a feature of the DRK interpolation proposed by Wu and Yang [103]. They also proposed its related element free Galerkin (EFG) and meshless DRK collocation methods to solve the quasi-3D or 2D problems of piezoelasticity and FG plates and shells subjected to simply suported boundary conditions [104–106].

Differential quadrature method (DQM) : In order to reduce the computational cost involved in numerical techniques like finite elements method, Chen et al. [107] developed a DQ method where elements were developed using weak form resulting in symmetric coefficient matrix. The DQM yielded accurate solutions with fewer grid points [108]. Mathematically, a linear summation of weighted function values at each of those grid points is considered as an approximation for the nth order partial derivative of a sufficiently continuous function at a point. This method has been mostly used along with any of the analytical methods such as state space DQM (SSDQM) [109, 110] or for instance, along with a Navier-type solution employed very recently by Monge et al. [111–113]. For dynamic analysis of pipe with different boundary conditions, DQM along with Laplace transform and its inverse for solution with time-variable [114]. This method has catered to cylindrical, spherical, toroidal shell structures and has been widely employed as a substitute for FE method to solve FG, nano-scale, or even non-linear problems of shell structural mechanics.

Sampling surface methods - SaS : The mathematical sampling surfaces are created along the thickness direction of a laminate which are not located at uniformly separated spaces. Rather, in order to avert any numerical instability arising at instances when larger than 21 uniformly spaced sampling surfaces are needed, the nth order Chebyshev polynomial roots are used. The values are obtained for the field variables at such sampling surfaces (SaS) located at the roots, on the basis of which Lagrange polynomials are employed to interpolate its through-thickness distribution. In consequence, rapidly converging results have been obtained by Kulikov and Plotnikova [115]. Multi-physical coupled quasi-3D analysis has been validated for hybrid composite structural elements [116–118]. Further, they have developed a formulation for deriving strong sampling surface of shell structures [119] utilized for solving simply-supported boundary conditions. This strong sampling surface formulation has been very recently used with the extended differential quadrature method to solve cases of shell structures subjected to arbitrary boundary conditions [120].

2.1.3.2 Applicable for arbitrary boundary conditions

Finite prism method (FRPM/FCPM) : As per the nomenclature a finite cylindrical prism (FCPM) and finite rectangular prism methods (FRPM) are respectively applied for plates and shell structures. In this, different mathematical operations are applied on the primary variables, where, a single Fourier series expansion is used along a in-plane coordinate and the variations in the surface domain are interpolated through Lagrange polynomials. Whereas, in the conventionally available layerwise element methods for plates (or shells), the distribution of primary variables in the thickness direction are interpolated through the power series, although in the domain of in-surface elements, Lagrange polynomials are used. In that sense, FRPM/ FCPM are the recent developments which has facilitated the analysis of plates and shells supported on various boundary conditions [121].

State space messless method : State-space has been used in interpolating the primary variables in the thickness coordinate, where differential quadrature (DQ) or DRK method may be used in the in-plane direction interpolation of primary variables which are a kind of mesh less method. State-space with DQ is one of the solutions applied by Alibeigloo and Shakeri [122, 123] for the analysis of elastic cylindrical panel. Further, they included free vibration of angle-ply cylindrical shell [124] and piezolaminated cylindrical shell [125] using this approach. Although analysis of functionally graded elastic material (FGEM) annular plates are presented by few researchers [126–128] but analysis of FGEM cylindrical shell are scarce using this approach except for the one done by Liang et al. [129]. Static and dynamic analysis of functionally graded cylindrical shell with piezoelectric layers are also recently developed by Alibeigloo and others [109, 130]. Wu and Jiang [131] studied FGM cylindrical shell through another technique where state space along with DRK (instead of DQ) method is used in the formulation of quasi-3D static analysis. Later, using the same approach quasi-3D analysis of carbon nanotube - reinforced composite hollow cylinders [132] has been done.

However, for simply-supported structures, exact solution has been reported by expanding the primary variables in form of double Fourier series which satisfy the in-plane boundary conditions and in the thickness direction, transfer matrix method determines the distribution of field variables [43].

State space FE method : Here, in-plane variations are approximated through finite element methods state-space is applied along the thickness direction. It is shown that the through-thickness distributions of transverse stress and displacement components obtained using the state space FE solutions are continuous and that very good estimations were obtained for the stress singularities in the vicinity of free edges. Sheng and Ye [133] applied it for the quasi-3D static analysis of laminated composite cylindrical shell.

Asymptotic meshless methods : A geometrical perturbation parameter, is introduced and the asymptotical expansion to the field variables is carried out, the basic 3D equations is decomposed in a series of differential equations for various orders. Upon successively integrating the resulting equations through the thickness direction, the recursive sets of governing equations for various orders can be obtained. The DQ method is adopted to solve the boundary-value problems for various orders. Because the differential operators of the governing equations remain the same for various orders and the nonhomogeneous terms at the higher-order level can be calculated from the lower order solutions, the solution procedure for the leading order problem can be repeatedly applied for the higher-order problems. The quasi-3D static behavior of laminated composite cylindrical shell [63], buckling of conical shell [134], thermo-buckling analysis of conical shells [135] and FGEM annular spherical shells [136] are reported. Later on, instead of DQ, DRK method is used by Wu and Jiang [137, 138] for static and free vibration analysis of sandwich FGEM cylinders, respectively. It takes Less time, rapid convergence occurs.

Asymptotic FE methods :By means of asymptotic expansions, the Reissner's functional of the plate is decomposed into a series of functionals, with which the system equations of finite element

models for the Kirchhoff–Love and Mindin-Reissner plate theories can be constructed as those of the leading-order problem. The stiffness matrix of the leading order problem remains unchanged from that of the higher-order problems, although with the different nonhomogeneous terms that can be obtained by using the known lower-order solutions. It was applied for the analyses of doubly curved multilayered shell using an asymptotic finite strip method by Wu et al. [139].

Very recently, the scaled boundary finite element method has been applied in solving this category of problems in semi-analytical form. Such formulations are relativey new for the analysis of beam, plate and shell analysis [140]. There is reduction of computational cost and hence simplier mesh can be generated by only discretizing the boundary of a domain, without considering the surrounding areas. This concept can be used to derive an analytical formulation in radial direction of the surrounding area. This has been only recently applied to a magneto-electro-elastic problem of cylindrical shell and had been earlier employed on piezoelastic cylindrical panels [141].

As a numerical technique solves a PDE by converting into algebraic set of equations and using polynomial shape functions, there is inherent error associated with these methods. Numerical analysis is also cost ineffective as it requires a large computer core storage with high running times. Even if the above semi-analytical numerical techniques are a class of compromise approach between time consuming full 3D numerical analysis and complex numerous variable exact 3D analytical technique, they agree approximately with the ones obtained exactly through 3D analytical technique. State space technique is not applicable directly for arbitrary boundary conditions and nonhomogeneous material properties, thus DQM or DRK methods are used for approximations along the thickness directions. Meshless DRK collocation methods (based on strong formulation) predicted transverse stress components more accurately than element free Galerkin (EFG) methods (based on weak formulation). But it was opposite during prediction of displacement and in-surface stress components when compared to benchmark 3D analytical solutions.

2.1.4 3D Analysis of laminated shells with weak interfaces

Composite laminated shell structures are preferred for their lightweight, high stiffness, high strength, corrosion resistance, etc. But delamination, cracking, adhesive bonding failure, fiber pull out and fiber breaking are some of the main reasons for failure. Delamination takes place due to the weakening of adhesive joints over time and leads to a loss in rigidity and load carrying capacity [142, 143] which further cause sudden failure of a structure [144]. Moreover, stress concentration and singularity of stress near the non-simply supported edges further accelerate the delamination phenomena. Nevertheless, adhesive joints are preferred in applications demanding uniform load transfer, weight reduction and joining at geometrical constraints. 3D elasticity based solutions can accurately determine stress fields [145] in these structures.

For the purpose, pure 3D numerical techniques such as the finite element method (FEM), differential quadrature method (DQM), discrete singular convolution method (DSC) [146], etc., are used to investigate the behaviour of shell. The versatility of the Rayleigh-Ritz procedure, FEM and DQM for solving numerous problems in structural mechanics are well established for analysing the structures [147–149]. Recently proposed DSC has been predominantly applied for analyzing the free vibration and dynamic response of shell structures by Civalek [150, 151]. Moreover, nonlinear vibration of plates resting on elastic foundations is presented in Ref. [152, 153]. Although, pure 3D numerical techniques are versatile but computational disadvantages have pushed the development of semi-analytical techniques [43]. Therefore, in last decade a large number of research articles [63, 133, 154–159] have been published based on three-dimensional solutions of arbitrarily supported, perfectly bonded laminated cylindrical shells using the semi-analytical approaches. However, incorporating imperfect bonding at the interfaces is practically intriguing.

In early 80's, Lene and Leguillon [160] gave the concept of interfacial slip to understand the damage of fiber reinforced composites. Later, Benveniste [161] developed mathematical model for a bi-laminated medium by considering the tractions and normal displacements to be continuous at

the interfaces, but a jump in the tangential displacement and shear traction there. Yan et al. [162] categorized modeling approaches for an imperfectly bonded interface for the composite material as follows:

- Spring layer model: As per this model, there is a jump considered in the displacement components in proportion to the corresponding transverse stresses. Response of laminates under static loading is independent of time.
- Viscous model: It considers the time dependent behaviour of interfaces and the viscous interface loses its ability of transferring stresses completely at time $t \to \infty$ (ideally).
- Viscoelastic model (Kelvin-Voigt model): It is recently proposed model having a combination of spring like model and viscous model.

Out of the above three models, first model is very popular because of relatively less complications than other two models. Various other strategies which are considered are the elastic interface model, the shear lag model [163] and the general interface model. An elaborate list of articles with their reviews can be found in the literature [164]. However, present survey is focused only on three-dimensional solution cases. Wang and Zhong [142] presented the three-dimensional static bending solution for a simply-supported and laminated anisotropic cylindrical shell strip with imperfect bonding at the off-axis elastic layer interfaces. The bending and free vibration solution of a simply-supported cross-ply laminated cylindrical panel with weak interfaces based on 3D elasticity was developed by Chen et al. [165]. Later, Chen and his co-authors [166–168] expanded the solution technique for static analysis of angle-ply cylindrical shell panels, angle-ply piezo-electric laminated cylindrical shell panels and dynamic analysis of cross-ply piezo-electric laminated cylindrical shell panels. Furthermore, they presented solutions for simply-supported shell panels with viscous interface and later viscoelastic interface between the plies [162, 169]. Yan et al. [170] extended the viscoelastic model to investigate the static behaviour of simply supported angle-ply piezoelectric laminate. Alibeigloo [171] presented the three-dimensional bending and free vibration solution for

simply supported cylindrical panel having viscoelastic interfacial imperfection. Recently, Parand & Alibeigloo [172] developed three dimensional solution by employing the DQM along axial direction and state-space along radial direction for a arbitrarily supported cylindrical shell with viscoelastic interfaces.

Hence, the literature survey indicates that, 3D solutions for imperfectly bonded shell structures is comparatively less which has got the required attention very recently. Solutions for the arbitrarily supported shell structures needs to be developed as an advancement over the simply supported cases which can be extended to the analysis of smart shells.

2.2 EXTENDED KANTOROVICH METHOD

As a step towards eliminating the weakness of Ritz/Galerkin method related to necessity of satisfying the natural and essential boundary conditions initially, Russian mathematician/economist, Leonid Vitaliyevich Kantorovich proposed a method, known as the Kantorovich method [173]. In this method, an approximate solution for the function is assumed as

$$w_m(x,y) = \sum_{n=1}^{m} f_n(x) g_n(y) \tag{2.1}$$

where $f_n(x)$ are unknown functions of one of the independent variables, and g_n are a priori chosen functions of the other independent variables. Now substituting Eq. (2.1) into the variational equation for stationary functional I_m and applying variational calculus yields m ODEs for the determination of m unknowns for the $f_n(x)$. This procedure generates a solution which tends to yield the exact variation w along x direction but is dependent on the initial choice of $g_n(y)$ along y direction.

In order to eliminate this dependence and improve accuracy along y direction also, Kerr [174] proposed extended Kantorovich method (EKM), in which, after a Kantorovich solution is obtained, the obtained functions $f_n(x)$ are considered as a priori known functions and the $g_n(y)$ functions are

considered unknown to be determined through a second Kantorovich solution process. This iterative process is repeated until the result converges to any desired degree. This method thus reduce the PDEs of the 2D problem to a double set of ODEs. It was shown by Kerr [174] and separately by Kerr and Alexander [175] while solving the problem of torsion of a rectangular cross-section bar and bending of a clamped isotropic rectangular plate, respectively, that the iterative process converges very rapidly and that the final solution is independent of the initial choice of $g_n(y)$. Most importantly, the initial assumed $g_n(y)$ functions are not required to satisfy the geometric or natural boundary conditions. After a single iteration, all boundary conditions are satisfied exactly. An one term solution was found to be very accurate for the problems considered. The other advantages of the EKM in comparison with other approximate methods are its straight forward implementation procedure, excellent accuracy, less computation time, any type of distributed loading conditions and possibility of obtaining closed form solutions in most cases.

2.2.1 Applications of the extended Kantorovich method (EKM)

The method has been shown to yield accurate results for several problems of elastic single layer [176, 177] and multi-layer plates [178–183] subjected to arbitrary and simply supported boundary conditions. The detailed literature on extended Kantorovich method can be found in a recent review article presented by Singhatanadgid and Singhanart [184]. They have reviewed various bending, vibration, and buckling problems of plates and have differentiated between the 2D and 3D approaches. Also, they have highlighted the importance of 3D elasticity solutions for 3D stress analysis, interlaminar stress, or free-edge stress where the primary strategy is that, the through-thickness behaviors are not restricted to the assumptions of plate theories. The presently discussed method has also been extended to analyze shell structures [185, 186]. A very first computational comparative study by Lee [187] inferred lesser amount of computing time and stable solutions even at larger time step by applying Kantorovich method as compared to those obtained by finite differences method for a isotropic elastic plastic dynamic behaviour of simply supported

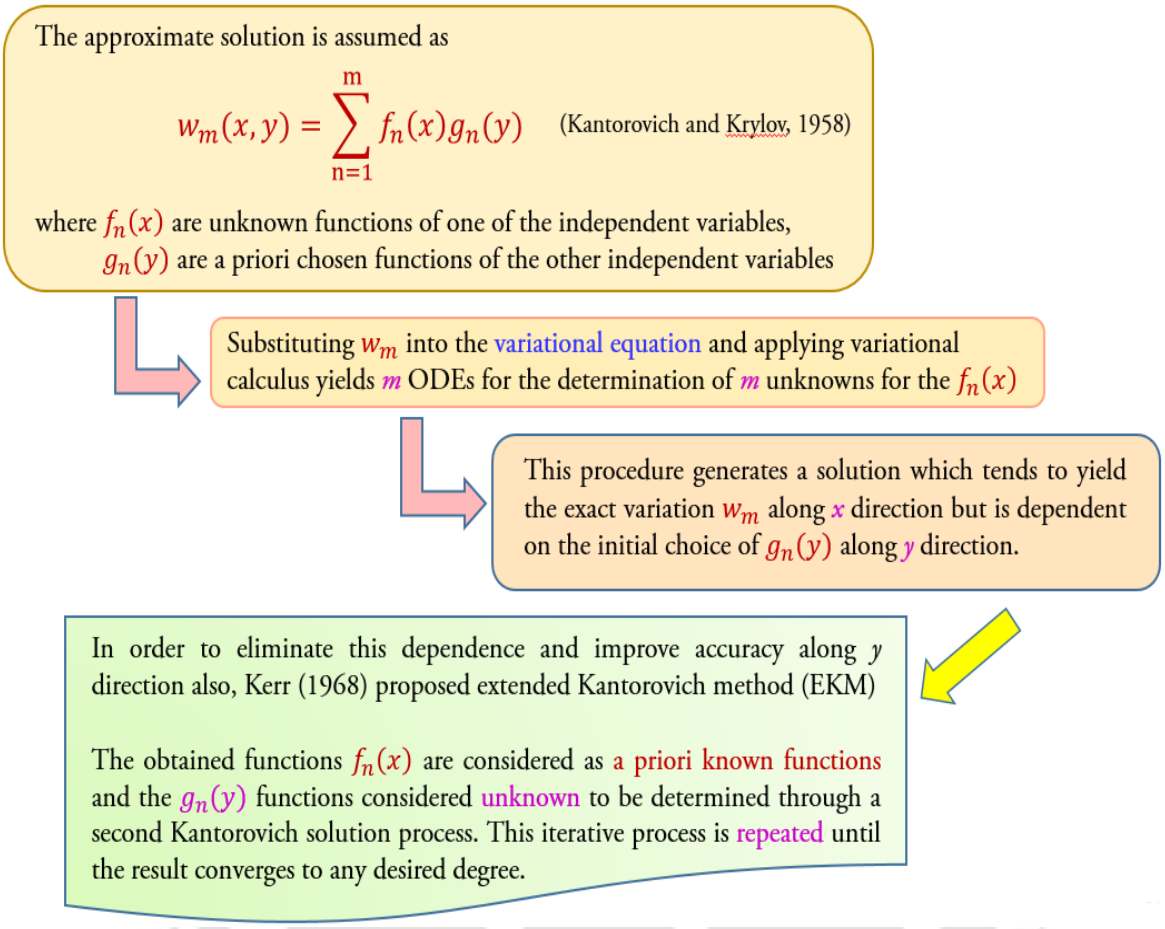

Fig. 2.3: Flowchart of iterative steps incorporated in the EKM

cylindrical shell. Strain of infinitely long cylindrical panel was solved analytically by Grigorenko and Tumashova [188] using Vlasov Kantorovich method. Subsequently, thermo elastic coupled problems [189] and dynamic problems [190, 191] for cylindrical shell were approximated as separable time and space field variables using Kantorovich method. Further, complex structural problems incorporating nonlinear theories to obtain buckling stresses [192] were handled. Recently, Moeenfard and Maleki [193] applied extended Kantorovich method to obtain the static response of micro-plates under electrostatic actuation. Similarly, using three-dimensional multi-term extended Kantorovich method (3DMTEKM), Andakhshideh el al. [194] developed analytical 3D stress solution for generally laminated piezoelectric (PZT) plates to obtain the interlaminar stresses. Motivated by its computational potentiality, the Kantorovich method has been applied for analysing field variables

such as stresses, strains, and displacements to yield the effect of orthotropy of the material, arbitrary boundary conditions [185, 195], movable and fixed hinge boundary conditions [196], structures with geometrical nonlinearity such as longitudinal/ transverse or orthogonal stiffeners [197] on the surface of a thin cylindrical shell subjected to various loading. Very recently, Tahani et al. [198] obtained analytical solutions for accurately computing interlaminar stresses at the vicinity of free edges of laminated shells. But, since a displacement formulation is adopted, all boundary and interface conditions involving stresses, including those of applied pressure on the top surface, are satisfied only in an average sense over the surface and not at all points.

Further, a partial list of literature for plates using Extended Kantorovich Method is presented in Table 2.1 and those for shells in Table 2.2. Fig. 2.3 shows few applicative problems such as plates with hole, variable thickness, nonhomogeneous material and irregular fin structures has been solved efficiently by the application of EKM.

Recently, Kapuria and Kumari's group has presented three-dimensional (3D) analytical solution for various types of composite plates [199–201] and piezoelectric laminated plates [202, 203] subjected to arbitrary support condition using the extended Kantorovich method. Further, Kumari and Behera extended this approach to develop 3D free vibration solution for a rectangular composite plate [204] and piezo-laminated plate [205] under Levy-type support conditions. The method has been extended to obtained three dimensional (3D) coupled electro-elastic solutions for piezolaminated [203] and in-plane varying FG plates [206]. Very recently, Kumari and Kar [207] have applied extended Kantorovich method to get analytical 3D elasticity solution for arbitrarily supported composite laminated cylindrical shell panels. The 3D solution for cylindrical shells with imperfectly bonded plies is the latest development by the present authors [208]. Further, some distinct features of the presently developed 3D elasticity solutions are that (1) These involve satisfaction of nonhomogeneous boundary conditions due to applied traction on top and bottom surfaces. (2) In laminated structures, the 3D solution involves satisfaction of the interfacial continuity conditions, which is not required in 2D theories. (3) Boundary conditions at the edges are

Table 2.1: Partial list of recent articles for plates using Extended Kantorovich Method

Dynamic analysis using 2D theories
[209] Transverse vibration of rectangular plates(CLT)
[210] Rectangular plate of Variable thickness elastically restrained (CLT)
[211] Piezoelectric rectangular plate all round clamped(CLT)
[212] Isotropic rectangular plate with clamped-free condition(CLT)
[213] Elastic rectangular plate with arbitrary boundary condition (TOT)
[214] In-plane vibrations of rectangular plates with rectangular cutouts
[215] Further extended to plates with variable thickness
[216] Forced vibration of rectangular orthotropic plate (FSDT)
[217] Symmetrically laminated composite rectangular plates (CLT)
[218] Free vibration of thick laminated plate (FSDT)
[219] Fully clamped skew plate based (CLT)
[220] Rectangular quartz plates with free edges using (FSDT)
[221] Moderately thick FG plates on elastic foundation (FSDT)
[222] Thickness shear vibration of rectangular quartz plate
[223] Cutouts in rectangular plates with variable thickness
Bending analysis
[224] Unidirectional variable thickness rectangular plate (CLT)
[225] Moderately thick laminated plates with clamped edges (FSDT)
[226] Thick skew plates with clamped edges
[227] Moderately thick clamped FGM conical panels (FSDT)
[228] Moderately thick FG sector plate (FSDT)
[229] Moderately thick radially FG sector plate (FSDT)
[230] Thin annular FG sector plate (CLT)
[231] Moderately thick annular sector plate (FSDT)
[232] Thin FGN skew plate on Wrinkler foundation
[233] Thick Annular Sector Plates with Variable Thickness (FSDT)
[234] Interlaminar for piezo-bonded composite laminates
[235] Composite laminates upon polynomial stress functions (FSDT)
[236] Static analysis of thin FG skew plates resting on Winkler elastic foundation
Other
[237] Laminated plates for twist actuation in subsonic projectile fin
[238] Micro-scale modeling (strain-gradient elasticity theory)
[239] Analysis of squeezed film air damping in torsional micromirrors
[240] Spectral element modeling & vibration for laminated plate
[241] Buckling and free vibration problems of CNTRC plates
[242] Static analysis of sector plates resting on Nonlinear Winkler elastic foundation with nonlinear loading

Table 2.2: Partial list of recent articles for shells using Extended Kantorovich Method

	Free vibration using 2D theories
[190]	Thermal buckling of imperfect laminated cylindrical shells (CST)
[243]	Thick Cylindrical panel with CC condition using (FSDT)
[191]	Nonlinear vibration of heated bimetallic shallow shells
[197]	Stiffened open shells with variable radii of curvature (FSDT)
	Bending analysis
[189]	Thermoelasticity of an axially symmetric cylindrical shell (CST)
[244]	Cross-ply symmetrically laminated cylindrical panels (CST)
[245]	Bending of fully clamped shallow panels (CST)
[182]	Moderately thick laminated cylindrical panels (FSDT)
[195]	Moderately thick doubly curved functionally graded panels (FSDT)
[227]	Moderately thick functionally graded conical panels (FSDT)
[185]	Laminated doubly curved or spherical panels (FSDT)
[192]	Critical behavior of flat and stiffened shell structures (CST)
[186]	Cylindrical panels with general loading & boundary conditions (CST)
[196]	Nonlinear behavior and buckling of cylindrical shells
[246]	Laminated Piezoelectric Cylindrical Panels (FSDT)
[247]	Thermal bending of doubly curved laminated shell panels (FSDT)
[198]	Thick cylindrical shell with arbitrary laminations (3D)
[248]	Thermal buckling of piezoelectric cylindrical shells (CST)
[249]	Bifurcation of nonlinear boundary problem for cyl. panel
[250]	Buckling and dynamic analysis of composite anisogrid lattice cylindrical panels (CST)
	Other
[251]	Vibration of size-dependent piezoelectric nanoshells (FSDT)

satisfied in average sense for 2D theories whereas in the present case, these are satisfied exactly.

It is apparent from the literature review on the development of extended Kantorovich method for structural problems is that, predominantly solutions are all based on 2D plate/shell theories and not on the 3D elasticity theory, and involve only homogeneous boundary conditions. Moreover, such a solution for the shell structures, piezoelectricity laminated shells, shells with imperfectly bonded plies and their corresponding static and dynamic analysis has not been reported. The challenge in development of the solution for shell structures lies in the fact that, mathematically through EKM, the final system of ODEs obtained after applying EKM has variable coefficients which are

very difficult to solve in closed-form manner. It prevents a straight forward application of existing elasticity based EKM solution for the plate structures.

2.3 OBJECTIVES OF THE PRESENT WORK

Backed by the extensive literature survey, following objectives are framed for the present work in the thesis. Broadly, the objectives involve, (i) Development of 3D elasticity analytical solution for its static and modal analysis, (ii) Extend the formulation to obtain a linear elasticity based 3D analytical solution for the laminated composites having interfacial weak interfaces and (iii) Present a 3D piezoelasticity analytical solution which incorporates the electro-mechanical coupling effects and study the response of a cylindrical shell structure under electro-mechanical loading. The objectives specifically addressed are as follows:

1. To develop a three dimensional (3D) analytical elasticity solution for cylindrical shell panel subjected to arbitrary boundary conditions which will yield benchmark results.

2. Further, extend above method to develop a three dimensional (3D) analytical elasticity solution for an angle-ply cylindrical shell panel subjected to arbitrary boundary conditions.

3. To develop an analytical solution for laminated shell panels with interlaminar weak bonding and panel being subjected to arbitrary boundary conditions and study its physical implications on the mechanics of the structure.

4. A coupled three dimensional (3D) analytical piezoelectricity solution will be developed for piezoelectric shell panel (cylindrical shell panel integrated with PZT/PFRC sensors and actuators) supported on arbitrary boundary conditions. To study the effect of PZT/PFRC parameters on the response of these smart shells.

5. To present an accurate analytical solution based on coupled three-dimensional (3D) piezoelectricity equations for free vibration analysis of the angle-ply elastic and piezoelectric laminated

shell panels under arbitrary boundary conditions.

2.4 ORGANISATION OF THE THESIS

The complete work presented in this thesis has been organized into seven chapters. Chapter 1 establishes the motivation behind the presently conducted research. An overview has been presented of smart materials and structures and the engineering characteristics of the shell structures by virtue of which they impart structural advantage and aesthetics. Their growing applications in every sphear of modern engineering has inferred the advent of intelligence in the structures. Smart materials such as piezoelectric materials have been employed for active and passive control of the intelligent structures. Various piezoelectricity materials has been discussed and the mechanics of certain important smart piezoelectricity structures has been briefed. Lured by the potentiality of the smart structures, the necessity of developing structural theories based on the coupled field mechanics can be sensed from the chapter.

In the Chapter 2 literature survey for the development and present status of piezoelasticity based shell theories has been conducted. Elasticity theories for the static and dynamic analysis of shell structures has also been reviewed emphasizing on the three-dimensional theories. Based on the extensive literature review, the proposed objectives of the present work are framed. An overview of the contents of the remaining five chapters is presented below.

Chapter 3, presents a 3D elasticity solution for static analysis of laminated composite cylindrical shell structures having arbitrary boundary conditions using the multi-term extended Kantorovich method (EKM). The cylindrical shell is considered infinitely long along its axis to undergo cylindrical bending and its span angle can be varied corresponding to those of deep and shallow shells. Benchmark numerical results are presented for different sets of boundary conditions, geometric mid-surface radius to thickness ratios and configurations of laminate scheme. For the first time from the conducted numerical study, 3D analytical solution based results are reported for such arbitrarily supported cylindrical shell panels for angle-ply, cross-ply and sandwich laminate configurations.

The numerical study reveals that the present solution converges within just two/three terms included in the general expression for multi-term EKM in case of certain boundary conditions. And, even just a single term solution gives very accurate results in presence of the simply-supported boundary conditions. It is observed that the static response of shell panel is influenced greatly by the arbitrary boundary conditions. The present analytical solution can serve as a benchmark for assessing the accuracy of the 2D or 3D numerical solutions.

In Chapter 4, the generalized 3D EKM solution is presented for the static analysis of laminated cylindrical shell panels with or without interfacial weak interfaces and subjected to arbitrary boundary conditions. Benchmark numerical results are presented for multi-layered cylindrical shell panels. The numerical results are validated thoroughly by comparing with 3D finite element (FE) results. The FE model is constructed three dimensionally to mimic the present problem exactly, with 3D elastic and cohesive elements utilized for the analysis. The influence of the interfacial weakness variation on the deflections and stresses are studied and discussed comprehensively for arbitrary sets of boundary conditions and configurations. Mathematically, the interfacial weakness is defined in terms of a coefficient which is dependent on the lamina material properties. The interface is modelled as a spring-like model. The present method provided benchmark results for the cross-ply shell panels with interfacial bonding imperfection and the physical aspects are studied which might be considered during the design of composites. The current research will also be beneficial to model cylindrical shell structures and adhesive bonded shell structures in which the interfaces or adhesives might deteriorate during its service or due to environmental effects.

In Chapter 5, a 3D piezoelectricity based analytical solution is developed for the static analysis of the angle-ply elastic and piezoelectric laminated cylindrical shell panels subjected to arbitrary boundary conditions. The present analytical solution is applicable to composite, sandwich and hybrid panels having arbitrary angle-ply lay-up, material properties and boundary conditions. The Reissner type mixed variational principle has been applied to derive the weak form of governing equations where stresses, displacements, electric potential, and electric displacement field variables

are considered as the primary variables. After that multi-term multi-field extended Kantorovich approach (MMEKM) is employed to transform the governing equation into two sets of algebraic-ordinary differential equations (ODEs), one along in-plane (θ) and other along with the thickness (r) direction, respectively. These ODEs are solved in closed-form manner which ensures the same order of accuracy for all the variables (stresses, displacements, and electric variables) by satisfying the boundary and continuity equations in exact manner. A robust algorithm is developed for obtaining the coupled response under electro-mechanical loading. The numerical results are reported for various configurations such as elastic panels and piezoelectric panels under arbitrary sets of boundary conditions. The accuracy and efficacy of the present method have been established by comparing the present numerical results with the results available in the literature and with the 3D FE results of ABAQUS. The effect of ply-angle and thickness to span ratio (s) on the static behavior of the shell panels are also investigated. The presented 3D analytical solution will be helpful in the assessment of various 1D theories and numerical methods.

In Chapter 6, the 3D piezoeleasticity based analytical solution technique is extended to obtain the free vibration solution for cylindrical shell panels integrated with piezoelectric layers and subjected to arbitrary support boundary conditions. The material properties consisted of the electro-mechanical components and its coupling effects. Further, the free vibration solution for the arbitrarily supported elastic-laminated cylindrical shell panels is also obtained as a special case of the present study. New benchmark numerical results are presented for a laminated piezoelectric cylindrical shell panels integrated with piezoelectric layers. The influence of the geometric aspects, laminate scheme and boundary conditions on the natural frequencies of the cylindrical shell panel are also investigated. Moreover, the longitudinal variation of displacements and stresses (mode shapes) for various cases are also plotted for different support conditions. These numerical results can be used for assessing other shell theories and numerical techniques.

Finally, the major conclusions of this work and suggestions for future research are summarized in Chapter 7.

Chapter 3

3D elasticity solution for static analysis of laminated cylindrical shell panel

3.1 INTRODUCTION

In this chapter, an analytical three-dimensional (3D) elasticity solution is proposed for cylindrical bending of laminated composite cylindrical shells subjected to arbitrary boundary conditions for the first time. The extended Kantorovich method (EKM) has been generalised for the 3D elasticity solution as an advancement over originally proposed solution for the two-dimensional (2D) elasticity problems. Some of the significant extensions made to the method in this study are (1) the application to the 3D elasticity problem involving an in-plane direction and a thickness direction instead of both inplane directions in 2D elasticity problems, (2) the treatment of the nonhomogeneous boundary conditions encountered in the thickness direction, (3) the use of a mixed variational principle to obtain the governing differential equations in both directions in terms of displacements as well as stresses, (4) multi-terms are included in the EKM which contribute towards accurate prediction of stress concentration zones and, (5) substantial reduction in the computational cost through this solution has been observed. The solution is taken as a sum of the products of n separable functions in the two directions, which is superimposed with a known solution that satisfies the non-homogenous boundary conditions. The Reissner's-type variational principle is used to develop a mixed formulation in terms of displacements as well as stress components as primary variables. This approach allows for exact satisfaction of boundary conditions at all points, and also ensures

the same order of accuracy for all displacements and stress variables. Applying the variational process along the inplane (θ) direction and the radial (r) directions, yields two different system of $6n$ ODEs with $2n$ algebraic equations in terms of θ and r, respectively. The system of ODEs along r has variable coefficients which is ingeniously solved through a new modified power series method whereas the set with constant coefficients along θ is solved using Pagano's approach. Exact closed form solutions are obtained for each algebraic-differential system of equations, satisfying exactly the interface continuity and/or the boundary conditions. The problem due to the occurrence of large eigenvalues for higher order terms is also addressed. In the first iteration, initial trial functions are assumed in θ-direction and functions of r are solved exactly, which are taken as known a priori in the next step to determine the functions in θ. This process is repeated till convergence is achieved.

The performance of the method is examined for cross-ply and angle-ply composite panels under various boundary conditions. It is demonstrated that the iterative procedure converges very fast irrespective of whether or not the initial guess functions satisfy the boundary conditions. It is shown, through comparison with other approximate 3D solutions (wherever available) and with the 3D finite element solution, that by considering at most three or even lesser terms in the solution ($n = 1, 2$ or 3) leads to a very accurate prediction and a drastic improvement over the single-term solution ($n = 1$) for all entities including the stress field near the boundaries when the shell panel is subjected to certain arbitrary boundary conditions. This work will facilitate development of near-exact solutions of many important unresolved problems involving 3D elasticity, such as the free edge stresses in laminated structures under bending, tension and torsion.

3.2 CYLINDRICAL SHELL PANEL CONFIGURATION

An infinitely long angle-ply cylindrical shell panel is considered for study in the frame of cylindrical coordinate system (r, θ, z) as shown in Fig. 3.1. The shell panel is supported arbitrarily on its opposite circumferential edges (i.e., at $\theta = 0, \psi$) which can be arbitrarily either of the clamped (C), free (F) or simply-supported (S) boundary conditions. Entity ψ is the circumferential span

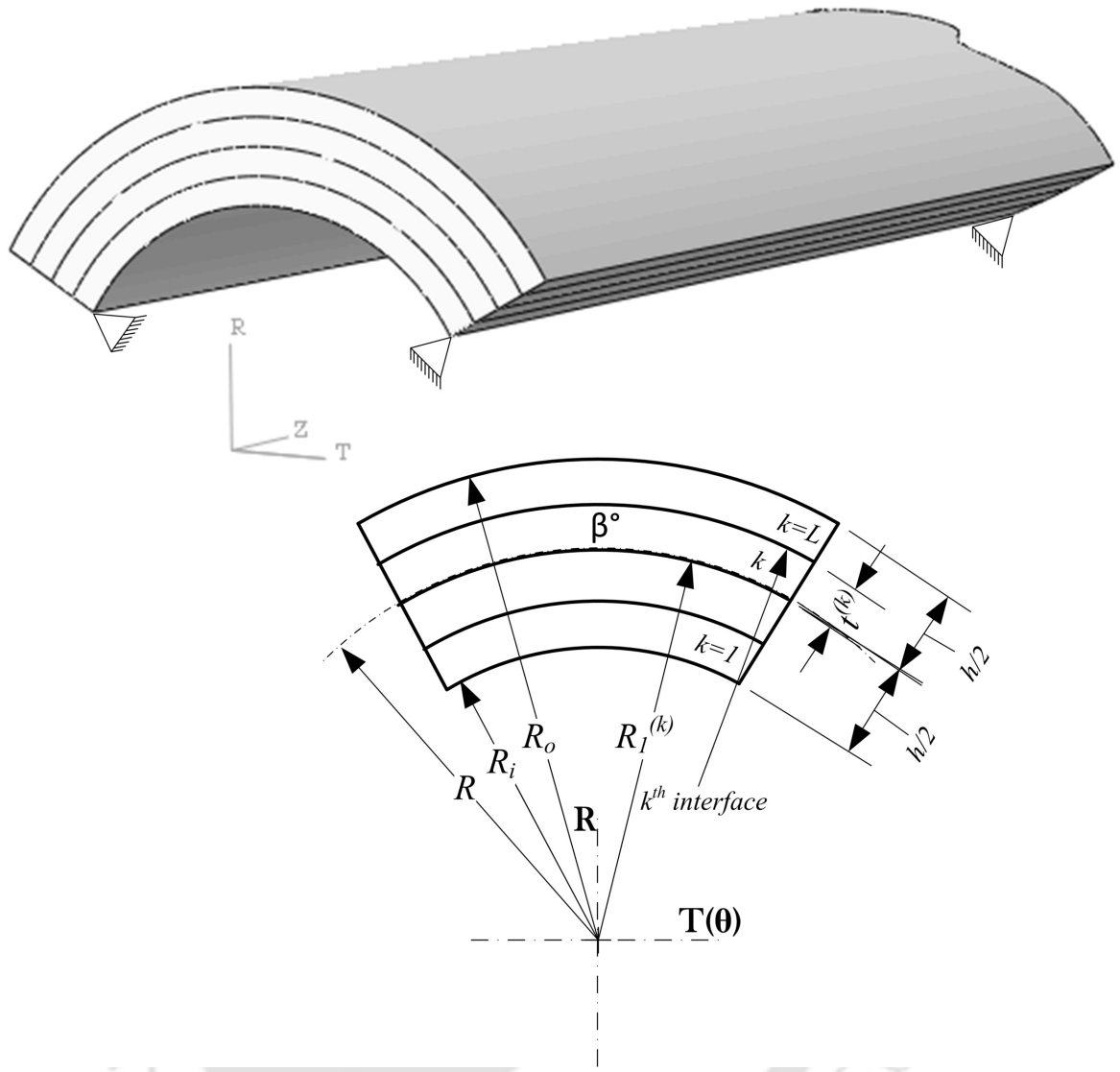

Fig. 3.1: Shell geometry and configuration of the laminate

of the shell panel along the circumferential direction θ. The shell panel is loaded with uniformly distributed pressure load (UDL) over either or both of its outer surface at $R_o = R + h/2$ and the inner surface at $R_i = R - h/2$. Here, R & h are the mean radius and total thickness along the radial direction r of the shell panel, respectively. Along r there are L perfectly bonded layers which are indexed as k (numbered from inner surface) and their corresponding ply thicknesses are denoted as t^k. The inner surface of kth layer is at $r = R_1^k$. It is assumed that the kth layer is perfectly bonded with $(k+1)$th layer at the interface which is $r = R_1^{(k+1)}$ far from the axis z of the cylinder. The layers are orthotropic elastic with one of the principal material direction oriented along the radial

r-axis. The angle made by the unidirectional fibers with the θ-axis in θz plane is denoted as $\beta^{(k)}$. A dimensionless circumferential coordinate ξ and a local thickness coordinate ζ^k for the kth layer are introduced as:

$$\xi = \theta/\psi, \qquad \zeta^{(k)} = (r - R_1^{(k)})/t^{(k)} \quad \text{with} \quad R_1^{(k)} = R - h/2 + \sum_{i=1}^{k-1} t^{(i)} \tag{3.1}$$

The coordinates ξ and $\zeta^{(k)}$ take values 0, 1 at $\theta = 0, \psi$ and $r = R_1^{(k)}, R_1^{(k)} + t^{(k)}$, respectively. In the following sections, superscript 'k' for the layers is omitted unless needed for clarity.

3.3 GOVERNING EQUATIONS

The 3D linear constitutive relation is expressed for an angle-ply composite lamina as:

$$\{\varepsilon\} = [\bar{S}]\{\sigma\} \text{ where,} \tag{3.2}$$

$$\{\varepsilon\} = [\varepsilon_\theta, \varepsilon_z, \varepsilon_r, \gamma_{zr}, \gamma_{r\theta}, \gamma_{\theta z}] \text{ are the strains,}$$

$$\{\sigma\} = [\sigma_\theta, \sigma_z, \sigma_r, \tau_{zr}, \tau_{r\theta}, \tau_{\theta z}] \text{ are the stresses,}$$

and $[\bar{S}]$ is the transformed compliance matrix for the principal material axes (x_1, x_2, x_3) oriented at an angle with the cylindrical shell axes (r, θ, z). As shown in Eq. (A.5) of Appendix A, the matrix $[\bar{S}]$ is obtained when the principal material axis x_1 makes an angle β to the θ-axis and the expressions of its components in terms of engineering properties, Young's moduli Y_i, shear moduli G_{ij} and major Poisson's ratios ν_{ij}, are also given in Appendix A. Further, UDL of magnitude p_1 on the inner surface and p_2 on the outer surface are applied on the shell panel which are independent of z. Thus, the corresponding displacements along (r, θ, z) are $(u, v \ \& \ w)$, respectively. As the panel is infinitely long and loading is invariant along z, so a plane strain assumption holds good where the field entities are independent of z. Hence, the strains are related to radial (u), circumferential (v) and axial (w) displacements by the following relations

$$\begin{aligned} \varepsilon_\theta &= (u + v_{,\theta})/r, & \gamma_{zr} &= w_{,r} \\ \varepsilon_z &= 0, & \gamma_{r\theta} &= (u_{,\theta} - v)/r + v_{,r} \\ \varepsilon_r &= u_{,r}, & \gamma_{\theta z} &= w_{,\theta}/r \end{aligned} \tag{3.3}$$

where differentiations are denoted by a comma. By imposing $\varepsilon_z = 0$ and using Eq. (3.2), the expressions of the strains for a generic kth layer are obtained as:

$$\begin{aligned}
\sigma_z &= \tilde{s}_{21}\sigma_\theta + \tilde{s}_{23}\sigma_r + \tilde{s}_{26}\tau_{\theta z} \\
\varepsilon_\theta &= \hat{s}_{11}\sigma_\theta + \hat{s}_{13}\sigma_r + \hat{s}_{16}\tau_{\theta z} \\
\varepsilon_r &= \hat{s}_{31}\sigma_\theta + \hat{s}_{33}\sigma_r + \hat{s}_{36}\tau_{\theta z} \\
\gamma_{\theta z} &= \hat{s}_{61}\sigma_\theta + \hat{s}_{63}\sigma_r + \hat{s}_{66}\tau_{\theta z} \\
\gamma_{r\theta} &= \bar{s}_{54}\tau_{zr} + \bar{s}_{55}\tau_{r\theta} \\
\gamma_{zr} &= \bar{s}_{44}\tau_{zr} + \bar{s}_{45}\tau_{r\theta}
\end{aligned} \tag{3.4}$$

where $\hat{s}_{ij} = \bar{s}_{ij} + \bar{s}_{i2}\tilde{s}_{2j},\ \tilde{s}_{2i} = -\bar{s}_{2i}/\bar{s}_{22},\ (\forall i, j = 1, 3\ \&\ 6)$ and $\bar{s}_{ij}\ (\forall i, j = 1-6)$ are the components of $[\bar{S}]$ matrix.

The equations of momentum balance without body forces for a cylindrical shell are as follows

$$\tau_{r\theta,r} + \sigma_{\theta,\theta}/r + 2\tau_{r\theta}/r = \rho\ddot{v} \tag{3.5}$$

$$\tau_{zr,r} + \tau_{\theta z,\theta}/r + \tau_{zr}/r = \rho\ddot{w} \tag{3.6}$$

$$\sigma_{r,r} + \tau_{r\theta,\theta}/r + (\sigma_r - \sigma_\theta)/r = \rho\ddot{u} \tag{3.7}$$

where an over-dot $(\dot{\cdot})$ denotes differentiation with respect to time $\mathbf{t}$. These equations are used in the Reissner's-type mixed variational principle [252] to obtain the governing equations for the cylindrical shell panel. The principle includes both the displacement and stress entities as the primary variables. It's expression for a linear elastic medium without the inertia terms is given as:

$$\begin{aligned}
&\int_V [\delta u \left(\sigma_{r,r} + \frac{\tau_{r\theta,\theta}}{r} + \frac{(\sigma_r - \sigma_\theta)}{r}\right) + \delta v \left(\tau_{r\theta,r} + \frac{\sigma_{\theta,\theta}}{r} + \frac{2\tau_{r\theta}}{r}\right) \\
&+\delta w \left(\tau_{zr,r} + \frac{\tau_{\theta z,\theta}}{r} + \frac{\tau_{zr}}{r}\right) + \delta\sigma_\theta \left(\varepsilon_\theta - \frac{(u + v_{,\theta})}{r}\right) + \delta\sigma_r(\varepsilon_r - u_{,r}) \\
&+\delta\tau_{\theta z} \left(\gamma_{\theta z} - \frac{w_{,\theta}}{r}\right) + \delta\tau_{zr}\left(\gamma_{zr} - w_{,r}\right) + \delta\tau_{r\theta}\left(\gamma_{r\theta} - \frac{(u_{,\theta} - v)}{r} - v_{,r}\right)] dV = 0, \\
&\forall\ \delta u_i,\ \delta\sigma_i,\ \delta\tau_{ij}
\end{aligned} \tag{3.8}$$

where V is the volume of the cylindrical shell panel. As implied by Eq. (3.8), the associated

variationally consistent boundary conditions which are stated below are to be exactly satisfied.

$$u_i - \bar{u}_i = 0 \quad \text{on} \quad A_u \quad \text{and} \quad \sigma_{ij} n_j - \bar{T}_i^n = 0 \quad \text{on} \quad A_T \tag{3.9}$$

where $\bar{T}_i^n$ are the components of the prescribed surface traction vector $\bar{T}^n$ on a surface with outward normal $\bar{n} = n_i \hat{e}_i$, $\hat{e}_i$ $(i = 1, 2, 3)$ being the unit vectors along θ, z, r directions. A_u and A_T are, respectively, the surface boundaries where surface tractions $\bar{T}_i^n$ and displacements $\bar{u}_i$ are prescribed. Considering unit length along z-direction and as the variables are independent of z coordinate, thus Eq. (3.8) reduces to

$$\begin{aligned}
&\int_0^r \int_0^\psi [\delta u \left(\sigma_{r,r} + \frac{\tau_{r\theta,\theta}}{r} + \frac{(\sigma_r - \sigma_\theta)}{r} \right) + \delta v \left(\tau_{r\theta,r} + \frac{\sigma_{\theta,\theta}}{r} + \frac{2\tau_{r\theta}}{r} \right) + \delta w \left(\tau_{zr,r} + \frac{\tau_{\theta z,\theta}}{r} + \frac{\tau_{zr}}{r} \right) \\
&+\delta\sigma_\theta \left(\hat{s}_{11}\sigma_\theta + \hat{s}_{13}\sigma_r + \hat{s}_{16}\tau_{\theta z} - \frac{(u + v_{,\theta})}{r} \right) + \delta\sigma_r (\hat{s}_{31}\sigma_\theta + \hat{s}_{33}\sigma_r + \hat{s}_{36}\tau_{\theta z} - u_{,r}) \\
&+\delta\tau_{\theta z} \left(\hat{s}_{61}\sigma_\theta + \hat{s}_{63}\sigma_r + \hat{s}_{66}\tau_{\theta z} - \frac{w_{,\theta}}{r} \right) + \delta\tau_{zr} \left(\bar{s}_{44}\tau_{zr} + \bar{s}_{45}\tau_{r\theta} - w_{,r} \right) \\
&+\delta\tau_{r\theta} \left(\bar{s}_{54}\tau_{zr} + \bar{s}_{55}\tau_{r\theta} - \frac{(u_{,\theta} - v)}{r} - v_{,r} \right)] r d\theta dr = 0, \ \forall \ \delta u_i, \ \delta\sigma_i, \ \delta\tau_{ij}
\end{aligned} \tag{3.10}$$

Conditions at span edges $\theta = 0$, ψ which can be assigned any arbitrary support conditions such as clamped (C), free (F) and simply-supported (S) are physically defined as:

$$\text{S}: \ u = \sigma_\theta = \tau_{\theta z} = 0; \qquad \text{C}: \ u = v = w = 0; \qquad \text{F}: \ \sigma_\theta = \tau_{r\theta} = \tau_{z\theta} = 0; \tag{3.11}$$

The transverse loads in the form of UDL of magnitude $p_1(\theta, t)$ and $p_2(\theta, t)$ are mathematically expressed at the inner and outer surfaces of the panel as:

$$\text{at } r = -\frac{h}{2} \qquad \sigma_r = -p_1, \ \tau_{r\theta} = \tau_{rz} = 0 \qquad \text{at } r = +\frac{h}{2} \qquad \sigma_r = -p_2, \ \tau_{r\theta} = \tau_{rz} = 0 \tag{3.12}$$

Furthermore, adjacent orthotropic layers are perfectly bonded therefore the following variables must be same at the interfaces between kth & $(k+1)$th layers

$$\Big[u, v, w, \sigma_r, \tau_{r\theta}, \tau_{zr}\Big]^{(k)} = \Big[u, v, w, \sigma_r, \tau_{r\theta}, \tau_{zr}\Big]^{(k+1)} \tag{3.13}$$

All entities are nondimensionalized such that the resulting dimensionless form of the governing

equations are exactly the same as the original Eqs. (3.1) to (3.13):

$$
\begin{aligned}
&S = R/h, && [r^*, h^*, R_i^*, R_o^*, t^{*(k)}, R_1^{*(k)}] = [r, h, R_i, R_o, t^{(k)}, R_1^{(k)}]/R \\
&\theta^* = \theta, && (\varepsilon_\theta^*, \varepsilon_z^*, \varepsilon_r^*, \gamma_{zr}^*, \gamma_{r\theta}^*, \gamma_{\theta z}^*) = (\varepsilon_\theta, \varepsilon_z, \varepsilon_r, \gamma_{zr}, \gamma_{r\theta}, \gamma_{\theta z})S \\
&\psi^* = \psi, && (\sigma_\theta^*, \sigma_z^*, \sigma_r^*, \tau_{zr}^*, \tau_{r\theta}^*, \tau_{\theta z,}^*, p_\alpha^*) = (\sigma_\theta, \sigma_z, \sigma_r, \tau_{zr}, \tau_{r\theta}, \tau_{\theta z}, p_\alpha)S/Y_0 \\
&\xi^* = \theta^*/\psi^* = \xi, && \zeta^{*(k)} = [r^* - R_1^{*(k)}]/t^{*(k)} = \zeta^{(k)} \\
&\bar{s}_{ij}^* = \bar{s}_{ij} Y_0, && (G_{ij}^*,\, Y_i^*) = (G_{ij},\, Y_i)/Y_0, \qquad (v^*, w^*, u^*) = (v, w, u)/h
\end{aligned}
\tag{3.14}
$$

where Y_0 is the value of the Young's modulus used for nondimensionalization. In the sequel, the dimensionless form of the equations is used, but for simplicity, the superscript * is dropped from the dimensionless entities.

3.4 GENERALISED MULTI-TERM EKM SOLUTION

The field variables comprising of displacement and stress entities which are to be solved are given in $\mathbf{X}$ which is considered as a set of primary variables where it's lth component is:

$$
\mathbf{X} = \begin{bmatrix} v & w & u & \sigma_\theta & \sigma_r & \tau_{\theta z} & \tau_{zr} & \tau_{r\theta} \end{bmatrix}^{\mathrm{T}} \tag{3.15}
$$

According to the multi-term EKM, solution of the field variables X_l are assumed in terms of a n-term series of the product of separable functions in the two independent variables (presently ξ and ζ) as:

$$
X_l(\xi, \zeta) = \sum_{i=1}^{n} f_l^i(\xi) g_l^i(\zeta) + \delta_{l5}[p_a + r p_d] \qquad \text{for} \qquad l = 1, 2, \ldots 8 \tag{3.16}
$$

where $f_l^i(\xi)$ & $g_l^i(\zeta)$ are the univariate functions of ξ and ζ, respectively for the ith term of the n-term series solution. There is no summation over l and δ is Kronecker delta. If we consider single term in the summation term ($\sum_{i=1}^{n} f_l^i(\xi) g_l^i(\zeta)$) in the above EKM expression, then it is known as single-term solution. Further, while functions $g_l^i(\zeta)$ are defined for the kth layer, functions $f_l^i(\xi)$ are valid for all layers. To take care of the nonhomogeneous boundary conditions for σ_r, an additional term satisfying the non-homogenous part is superimposed to the above solution for σ_r as given in Eq. (3.16), so that the later is required to satisfy only the homogeneous boundary conditions. Thus,

$\delta_{l5} = 1$ for $l = 5$ and else $\delta_{l5} = 0$. Furthermore, as the loading is UDL on both inner and outer surfaces, the average pressures p_a & p_d can be solved to be:

$$p_a = p_1 - \{R - (h/2)\}\{(p_2 - p_1)/h\}$$
$$p_d = (p_2 - p_1)/h \tag{3.17}$$

Constitutive equations from Eq. (3.2), strain-displacement relations from Eq. (3.3) and assumed multi-term EKM expression in Eq. (3.16) for the field variables are inserted into Eq. (3.10) iteratively to obtain separate system of ODEs in each iteration step which is discussed in the following sections.

3.4.1 Solution along radial direction (r):

In this step, functions $f_l^i(\xi)$, along the θ- direction are assumed first for the determination of $g_l^i(\zeta)$s. The first variation δX_l of X_l is given by

$$\delta X_l = \sum_{i=1}^{n} f_l^i(\xi)\delta g_l^i, \qquad l = 1, 2, \ldots 8. \tag{3.18}$$

Functions $g_l^i(\zeta)$ are partitioned into a column vector $\bar{\mathbf{G}}$ which contains those $6n$ variables that appear in the outer, inner boundary and interface continuity conditions of Eqs. (3.12) and (3.13) along r-axis and a column vector $\hat{\mathbf{G}}$ consisting of remaining $2n$ variables which are as follows:

$$\bar{\mathbf{G}} = \left[g_3^1 \ldots g_3^n \; g_1^1 \ldots g_1^n \; g_2^1 \ldots g_2^n \; g_5^1 \ldots g_5^n \; g_7^1 \ldots g_7^n \; g_8^1 \ldots g_8^n\right]^{\mathrm{T}}$$
$$\hat{\mathbf{G}} = \left[g_4^1 \ldots g_4^n \; g_6^1 \ldots g_6^n\right]^{\mathrm{T}} \tag{3.19}$$

Equations (3.16) and (3.18) are substituted in Eq. (3.10), and the integration is performed over ξ direction on the known functions of ξ. Considering that the variations δg_l^i are arbitrary, the coefficients of δg_l^i $(l = 1, ..., 8;\ i = 1, 2, ...n)$ in the resulting left hand side expression are equated to zero individually. This yields a system of $6n$ first-order ODEs for $g_l^i(\zeta)$s in $\bar{\mathbf{G}}$ and other $2n$ algebraic equations are also obtained for $\hat{\mathbf{G}}$ of a kth layer as shown below:

$$\mathbf{M}\bar{\mathbf{G}}_{,\zeta} = t[\bar{\mathbf{A}}_{\mathbf{m}}\bar{\mathbf{G}} + \hat{\mathbf{A}}_{\mathbf{m}}\hat{\mathbf{G}} + \bar{\mathbf{Q}}_{\mathbf{pm}}] \tag{3.20}$$

$$\mathbf{K}\hat{\mathbf{G}} = \tilde{\mathbf{A}}_{\mathbf{m}}\bar{\mathbf{G}} + \tilde{\mathbf{Q}}_{\mathbf{pm}} \tag{3.21}$$

$$\text{where, } \bar{\mathbf{A}}_\mathbf{m} = \bar{\mathbf{A}}_\mathbf{0} + \left(\frac{\bar{\mathbf{A}}_\mathbf{1}}{(\zeta t + R_1)}\right),\ \hat{\mathbf{A}}_\mathbf{m} = \hat{\mathbf{A}}_\mathbf{0} + \left(\frac{\hat{\mathbf{A}}_\mathbf{1}}{(\zeta t + R_1)}\right),$$
$$\tilde{\mathbf{A}}_\mathbf{m} = \tilde{\mathbf{A}}_\mathbf{0} + \left(\frac{\tilde{\mathbf{A}}_\mathbf{1}}{(\zeta t + R_1)}\right),\ \bar{\mathbf{Q}}_\mathbf{pm} = \bar{\mathbf{Q}}_\mathbf{p0} + \left(\frac{\bar{\mathbf{Q}}_\mathbf{p1}}{(\zeta t + R_1)}\right) + \bar{\mathbf{Q}}_\mathbf{p2}(\zeta t + R_1),$$
$$\tilde{\mathbf{Q}}_\mathbf{pm} = \tilde{\mathbf{Q}}_\mathbf{p0} + \tilde{\mathbf{Q}}_\mathbf{p1}(\zeta t + R_1) \tag{3.22}$$

And, $\mathbf{M}$, $\bar{\mathbf{A}}_\mathbf{0}$, $\bar{\mathbf{A}}_\mathbf{1}$ are $6n \times 6n$, $\hat{\mathbf{A}}_\mathbf{0}$, $\hat{\mathbf{A}}_\mathbf{1}$ are $6n \times 2n$, $\tilde{\mathbf{A}}_\mathbf{0}$, $\tilde{\mathbf{A}}_\mathbf{1}$ are $2n \times 6n$ and $\mathbf{K}$ is $2n \times 2n$ matrix. $\bar{\mathbf{Q}}_\mathbf{p0}$, $\bar{\mathbf{Q}}_\mathbf{p1}$, $\bar{\mathbf{Q}}_\mathbf{p2}$ are load column vectors of size $6n$ and $\tilde{\mathbf{Q}}_\mathbf{p0}$, $\tilde{\mathbf{Q}}_\mathbf{p1}$ are load column vectors of size $2n$ respectively. Using the notation $\langle \ldots \rangle_\psi = \psi \int_0^1 (\ldots) d\xi$ for integration over the span length (ψ), the non-zero elements of the matrices $\mathbf{M}$, $\bar{\mathbf{A}}_\mathbf{0}$, $\bar{\mathbf{A}}_\mathbf{1}$, $\hat{\mathbf{A}}_\mathbf{0}$, $\hat{\mathbf{A}}_\mathbf{1}$, $\tilde{\mathbf{A}}_\mathbf{0}$, $\tilde{\mathbf{A}}_\mathbf{1}$, $\mathbf{K}$ are listed below:

$$\begin{aligned}
&M_{i_1 j_1} = M_{j_4 i_4} = \langle f_5^i f_3^j \rangle_\psi, && M_{i_2 j_2} = M_{j_6 i_6} = \langle f_8^i f_1^j \rangle_\psi, && M_{i_3 j_3} = M_{j_5 i_5} = \langle f_7^i f_2^j \rangle_\psi \\
&\bar{A}_{0_{i_1 j_4}} = \hat{s}_{33} \langle f_5^i f_5^j \rangle_\psi, && \bar{A}_{0_{i_2 j_5}} = \bar{s}_{45} \langle f_8^i f_7^j \rangle_\psi, && \bar{A}_{0_{i_2 j_6}} = \bar{s}_{55} \langle f_8^i f_8^j \rangle_\psi \\
&\bar{A}_{0_{i_3 j_5}} = \bar{s}_{44} \langle f_7^i f_7^j \rangle_\psi, && \bar{A}_{0_{i_3 j_6}} = \bar{s}_{45} \langle f_7^i f_8^j \rangle_\psi, && \bar{A}_{1_{i_2 j_1}} = -\tfrac{1}{\psi} \langle f_8^i f_{3,\xi}^j \rangle_\psi, \\
&\bar{A}_{1_{i_2 j_2}} = \langle f_8^i f_1^j \rangle_\psi, && \bar{A}_{1_{i_4 j_4}} = -\langle f_3^i f_5^j \rangle_\psi, && \bar{A}_{1_{i_4 j_6}} = -\tfrac{1}{\psi} \langle f_3^i f_{8,\xi}^j \rangle_\psi \\
&\bar{A}_{1_{i_5 j_5}} = -\langle f_2^i f_7^j \rangle_\psi, && \bar{A}_{1_{i_6 j_6}} = -2\langle f_1^i f_8^j \rangle_\psi, && \hat{A}_{0_{i_1 j_1}} = \hat{s}_{31} \langle f_5^i f_4^j \rangle_\psi, \\
&\hat{A}_{0_{i_1 j_2}} = \hat{s}_{36} \langle f_5^i f_6^j \rangle_\psi, && \hat{A}_{1_{i_4 j_1}} = \langle f_3^i f_4^j \rangle_\psi, && \hat{A}_{1_{i_5 j_2}} = -\tfrac{1}{\psi} \langle f_2^i f_{6,\xi}^j \rangle_\psi, \\
&\hat{A}_{1_{i_6 j_1}} = -\tfrac{1}{\psi} \langle f_1^i f_{4,\xi}^j \rangle_\psi, && \tilde{A}_{0_{i_1 j_4}} = \hat{s}_{13} \langle f_4^i f_5^j \rangle_\psi, && \tilde{A}_{0_{i_2 j_4}} = \hat{s}_{36} \langle f_6^i f_5^j \rangle_\psi \\
&\tilde{A}_{1_{i_1 j_1}} = -\langle f_4^i f_3^j \rangle_\psi, && \tilde{A}_{1_{i_1 j_2}} = -\tfrac{1}{\psi} \langle f_4^i f_{1,\xi}^j \rangle_\psi, && \tilde{A}_{1_{i_2 j_3}} = -\tfrac{1}{\psi} \langle f_6^i f_{2,\xi}^j \rangle_\psi, \\
&K_{i_1 j_1} = \hat{s}_{11} \langle f_4^i f_4^j \rangle_\psi, && K_{i_1 j_2} = -\hat{s}_{16} \langle f_4^i f_6^j \rangle_\psi, && K_{i_2 j_1} = -\hat{s}_{16} \langle f_6^i f_4^j \rangle_\psi, \\
&K_{i_2 j_2} = -\hat{s}_{66} \langle f_6^i f_6^j \rangle_\psi
\end{aligned} \tag{3.23}$$

where $i_p = (p-1)n + i$ and $j_q = (q-1)n + j$ for $p, q = 1, 2, \ldots, 8$. $\bar{\mathbf{Q}}_\mathbf{p0}$, $\bar{\mathbf{Q}}_\mathbf{p1}$, $\bar{\mathbf{Q}}_\mathbf{p2}$, $\tilde{\mathbf{Q}}_\mathbf{p0}$ and $\tilde{\mathbf{Q}}_\mathbf{p1}$ are load vectors of size $6n$, $6n$, $6n$, $2n$ and $2n$, respectively, whose non-zero terms are given by:

$$\begin{aligned}
&\bar{Q}_{p0_{i_1}} = \hat{s}_{33} p_a \langle f_5^i \rangle_\psi, && \bar{Q}_{p0_{i_4}} = -2 p_d \langle f_3^i \rangle_\psi, && \bar{Q}_{p1_{i_4}} = -p_a \langle f_3^i \rangle_\psi, \\
&\bar{Q}_{p2_{i_1}} = \hat{s}_{33} p_d \langle f_5^i \rangle_\psi, && \tilde{Q}_{p0_{i_1}} = \hat{s}_{13} p_a \langle f_4^i \rangle_\psi, && \tilde{Q}_{p0_{i_2}} = \hat{s}_{36} p_a \langle f_6^i \rangle_\psi, \\
&\tilde{Q}_{p1_{i_1}} = \hat{s}_{13} p_d \langle f_4^i \rangle_\psi, && \tilde{Q}_{p1_{i_2}} = \hat{s}_{36} p_d \langle f_6^i \rangle_\psi
\end{aligned} \tag{3.24}$$

These elements of the matrices defined in Eqs. (3.23) and (3.24) have been evaluated in close form as the functions f_l^i are known analytical functions.

Substituting back the Eq. (3.21) in Eq. (3.20) gives a simultaneous system of $6n$ first-order non-homogeneous ODEs with variable coefficients expressed as:

$$\bar{\mathbf{G}}_{,\zeta} = t[\{\mathbf{A_0} + (\mathbf{A_1}/(\zeta t + R_1)) + (\mathbf{A_2}/(\zeta t + R_1)^2)\}\,\bar{\mathbf{G}} + \mathbf{Q_{p0}} + (\mathbf{Q_{p1}}/(\zeta t + R_1)) + \mathbf{Q_{p2}}(\zeta t + R_1)] \tag{3.25}$$

where, $\mathbf{A_0} = [\mathbf{M}^{-1}\bar{\mathbf{A}}_\mathbf{0}] + [\mathbf{M}^{-1}\hat{\mathbf{A}}_\mathbf{0}\mathbf{K}^{-1}\tilde{\mathbf{A}}_\mathbf{0}]$, $\mathbf{A_1} = [\mathbf{M}^{-1}\bar{\mathbf{A}}_\mathbf{1}] + [\mathbf{M}^{-1}\hat{\mathbf{A}}_\mathbf{0}\mathbf{K}^{-1}\tilde{\mathbf{A}}_\mathbf{1}] + [\mathbf{M}^{-1}\hat{\mathbf{A}}_\mathbf{1}\mathbf{K}^{-1}\tilde{\mathbf{A}}_\mathbf{0}]$,

$\mathbf{A_2} = [\mathbf{M}^{-1}\hat{\mathbf{A}}_\mathbf{1}\mathbf{K}^{-1}\tilde{\mathbf{A}}_\mathbf{1}]$,

$\mathbf{Q_{p0}} = [\mathbf{M}^{-1}\bar{\mathbf{Q}}_\mathbf{p0}] + [\mathbf{M}^{-1}\hat{\mathbf{A}}_\mathbf{0}\mathbf{K}^{-1}\tilde{\mathbf{Q}}_\mathbf{p0}] + [\mathbf{M}^{-1}\hat{\mathbf{A}}_\mathbf{1}\mathbf{K}^{-1}\tilde{\mathbf{Q}}_\mathbf{p1}]$,

$\mathbf{Q_{p1}} = [\mathbf{M}^{-1}\bar{\mathbf{Q}}_\mathbf{p1}] + [\mathbf{M}^{-1}\hat{\mathbf{A}}_\mathbf{1}\mathbf{K}^{-1}\tilde{\mathbf{Q}}_\mathbf{p0}]$, $\mathbf{Q_{p2}} = [\mathbf{M}^{-1}\bar{\mathbf{Q}}_\mathbf{p2}] + [\mathbf{M}^{-1}\hat{\mathbf{A}}_\mathbf{0}\mathbf{K}^{-1}\tilde{\mathbf{Q}}_\mathbf{p1}]$

Defining a shell geometric constant $s = R_1/t$ and substituting it in Eq. (3.25) further simplifies to:

$$\begin{aligned}
(s+\zeta)^2\bar{\mathbf{G}}_{,\zeta} &= [(R_1/s)\mathbf{A_0}(s+\zeta)^2 + \mathbf{A_1}(s+\zeta) + \mathbf{A_2}(s/R_1)]\bar{\mathbf{G}} \\
&\quad +[\mathbf{Q_{p0}}(R_1/s)(s+\zeta)^2 + \mathbf{Q_{p1}}(s+\zeta) + \mathbf{Q_{p2}}(R_1/s)^2(s+\zeta)^3] \\
\Rightarrow \quad (s^2+2s\zeta+\zeta^2)\bar{\mathbf{G}}_{,\zeta} &= [s^2((\mathbf{A_0}R_1 + \mathbf{A_1} + \mathbf{A_2}/R_1)/s) + (2R_1\mathbf{A_0} + \mathbf{A_1})\zeta + (R_1/s)\mathbf{A_0}\zeta^2]\bar{\mathbf{G}} \\
&\quad +[(s^2(R_1\mathbf{Q_{p0}} + \mathbf{Q_{p1}} + {R_1}^2\mathbf{Q_{p2}})/s) + \zeta(2R_1\mathbf{Q_{p0}} + \mathbf{Q_{p1}} + 3{R_1}^2\mathbf{Q_{p2}}) \\
&\quad +(\zeta^2(R_1\mathbf{Q_{p0}} + 3{R_1}^2\mathbf{Q_{p2}})/s) + (\zeta^3({R_1}^2\mathbf{Q_{p2}})/s^2)]
\end{aligned} \tag{3.26}$$

The closed form solution of system of equations in Eq. (3.26) is obtained by using the modified power series expansion method [206]. Thus, expanding along dimensionless radial coordinate ζ $(0 \le \zeta \le 1)$ as:

$$\bar{\mathbf{G}}(\zeta) = \sum_{i=0}^{\infty}(\mathbf{Y}_i\zeta^i/i!), \qquad \bar{\mathbf{G}}_{,\zeta}(\zeta) = \sum_{i=1}^{\infty}(\mathbf{Y}_i\zeta^{(i-1)}/(i-1)!) \tag{3.27}$$

And substituting Eq. (3.27) in Eq. (3.26) gives:

$$\begin{aligned}
&\sum_{i=1}^{\infty}\left[\left(\frac{\mathbf{Y}_i\zeta^{(i+1)}}{(i-1)!}\right) + \left(2s\frac{\mathbf{Y}_i\zeta^{i}}{(i-1)!}\right) + \left(s^2\frac{\mathbf{Y}_i\zeta^{i-1}}{(i-1)!}\right)\right] = \\
&\sum_{i=0}^{\infty}\left[s^2((\mathbf{A_0}R_1 + \mathbf{A_1} + \mathbf{A_2}/R_1)/s)\left(\frac{\mathbf{Y}_i\zeta^{i}}{i!}\right) + (2R_1\mathbf{A_0} + \mathbf{A_1})\left(\frac{\mathbf{Y}_i\zeta^{(i+1)}}{i!}\right) + (R_1/s)\mathbf{A_0}\left(\frac{\mathbf{Y}_i\zeta^{(i+2)}}{i!}\right)\right] \\
&\quad +[(s^2(R_1\mathbf{Q_{p0}} + \mathbf{Q_{p1}} + {R_1}^2\mathbf{Q_{p2}})/s) + \zeta(2R_1\mathbf{Q_{p0}} + \mathbf{Q_{p1}} + 3{R_1}^2\mathbf{Q_{p2}}) \\
&\quad +(\zeta^2(R_1\mathbf{Q_{p0}} + 3{R_1}^2\mathbf{Q_{p2}})/s) + (\zeta^3({R_1}^2\mathbf{Q_{p2}})/s^2)]
\end{aligned} \tag{3.28}$$

where the coefficient $\mathbf{Y}_i$s are column vectors of size $6n$ and a term $\mathbf{Y}_i$ is included only if $i \geq 0$. Assuming the following simplified relations:

$$\begin{aligned}
\mathbf{q_0} &= (R_1\mathbf{Q_{p0}} + \mathbf{Q_{p1}} + {R_1}^2\mathbf{Q_{p2}})/s, & \mathbf{A} &= (\mathbf{A_0}R_1 + \mathbf{A_1} + \mathbf{A_2}/R_1)/s, \\
\mathbf{q_1} &= (2R_1\mathbf{Q_{p0}} + \mathbf{Q_{p1}} + 3{R_1}^2\mathbf{Q_{p2}})/s^2, & \mathbf{A_3} &= (2R_1\mathbf{A_0} + \mathbf{A_1})/s^2, \\
\mathbf{q_2} &= (R_1\mathbf{Q_{p0}} + 3{R_1}^2\mathbf{Q_{p2}})/s^3, & \mathbf{A_4} &= ((R_1/s)\mathbf{A_0})/s^2, \\
\mathbf{q_3} &= ({R_1}^2\mathbf{Q_{p2}})/s^4, & \mathbf{I} &= \text{unit matrix}
\end{aligned} \tag{3.29}$$

and equating the coefficients of ζ^0, ζ^1, ζ^2 & ζ^3 from $L.H.S$ & $R.H.S$ of Eq. (3.28), yields:

$$\begin{aligned}
\mathbf{Y}_1 &= [\mathbf{A}\mathbf{Y}_0] + [\mathbf{q_0}],\ \mathbf{Y}_2 = [\{\mathbf{A} - 2\mathbf{I}/s\}\mathbf{Y}_1] + [\mathbf{A_3}\mathbf{Y}_0] + [\mathbf{q_1}], \\
\mathbf{Y}_3 &= [\{\mathbf{A} - 4\mathbf{I}/s\}\,\mathbf{Y}_2] + [2\{\mathbf{A_3} - \mathbf{I}/s^2\}\mathbf{Y}_1] + [2\mathbf{A_4}\mathbf{Y}_0] + [2\mathbf{q_2}], \\
\mathbf{Y}_4 &= [\{\mathbf{A} - 6\mathbf{I}/s\}\,\mathbf{Y}_3] + \left[3\left\{\mathbf{A_3} - 2\mathbf{I}/s^2\right\}\mathbf{Y}_2\right] + [6\mathbf{A_4}\mathbf{Y}_1] + [6\mathbf{q_3}]
\end{aligned} \tag{3.30}$$

and a recursive relation for $\mathbf{Y}_i$ is obtained, when comparing coefficients of (ζ^i, $\forall\ i \geq 4$) as given below:

$$\mathbf{Y}_{(i+1)} = \left[\left\{\mathbf{A} - \frac{2i\mathbf{I}}{s}\right\}\mathbf{Y}_i\right] + \left[i\left\{\mathbf{A_3} - \frac{(i-1)\mathbf{I}}{s^2}\right\}\mathbf{Y}_{(i-1)}\right] + \left[i(i-1)\mathbf{A_4}\mathbf{Y}_{(i-2)}\right] \tag{3.31}$$

On segregating $\mathbf{Y}_i$ of the form, $\mathbf{Y}_i = \hat{\mathbf{Z}}_i + \hat{\mathbf{H}}_i\mathbf{C}_o$, $\forall\ i = 0, 1, 2, \ldots$ and substituting it in Eqs. (3.30) & (3.31), following relations for $\hat{\mathbf{Z}}_i$ & $\hat{\mathbf{H}}_i$ are obtained respectively:

$$\begin{aligned}
&\hat{\mathbf{Z}}_0 = 0,\ \hat{\mathbf{Z}}_1 = [\mathbf{q_0}],\ \hat{\mathbf{Z}}_2 = [\{\mathbf{A} - 2\mathbf{I}/s\}\hat{\mathbf{Z}}_1] + [\mathbf{q_1}], \\
&\hat{\mathbf{Z}}_3 = \left[\{\mathbf{A} - 4\mathbf{I}/s\}\,\hat{\mathbf{Z}}_2\right] + [2\{\mathbf{A_3} - \mathbf{I}/s^2\}\hat{\mathbf{Z}}_1] + [2\mathbf{q_2}], \\
&\hat{\mathbf{Z}}_4 = \left[\{\mathbf{A} - 6\mathbf{I}/s\}\,\hat{\mathbf{Z}}_3\right] + \left[3\left\{\mathbf{A_3} - 2\mathbf{I}/s^2\right\}\hat{\mathbf{Z}}_2\right] + [6\mathbf{A_4}\hat{\mathbf{Z}}_1] + [6\mathbf{q_3}] \text{ and a recursive relation} \\
&\hat{\mathbf{Z}}_{(i+1)} = \left[\left\{\mathbf{A} - \frac{2i\mathbf{I}}{s}\right\}\hat{\mathbf{Z}}_i\right] + \left[i\left\{\mathbf{A_3} - \frac{(i-1)\mathbf{I}}{s^2}\right\}\hat{\mathbf{Z}}_{(i-1)}\right] + \left[i(i-1)\mathbf{A_4}\hat{\mathbf{Z}}_{(i-2)}\right] \quad \forall\ i \geq 4
\end{aligned} \tag{3.32}$$

$$\begin{aligned}
&\hat{\mathbf{H}}_0 = [\mathbf{I}],\ \hat{\mathbf{H}}_1 = [\mathbf{A}],\ \hat{\mathbf{H}}_2 = [\{(\mathbf{A} - 2\mathbf{I}/s\}\hat{\mathbf{H}}_1] + [\mathbf{A_3}], \\
&\hat{\mathbf{H}}_3 = \left[\{\mathbf{A} - 4\mathbf{I}/s\}\,\hat{\mathbf{H}}_2\right] + [2\{\mathbf{A_3} - \mathbf{I}/s^2\}\hat{\mathbf{H}}_1] + [2\mathbf{A_4}],
\end{aligned}$$

$$\hat{\mathbf{H}}_4 = \left[\{\mathbf{A} - 6\mathbf{I}/s\}\,\hat{\mathbf{H}}_3\right] + \left[3\left\{\mathbf{A_3} - \mathbf{I}/s^2\right\}\hat{\mathbf{H}}_2\right] + [6\mathbf{A_4}\hat{\mathbf{H}}_1] \text{ and a recursive relation}$$

$$\hat{\mathbf{H}}_{(i+1)} = \left[\left\{\mathbf{A} - \frac{2i\mathbf{I}}{s}\right\}\hat{\mathbf{H}}_i\right] + \left[i\left\{\mathbf{A_3} - \frac{(i-1)\mathbf{I}}{s^2}\right\}\hat{\mathbf{H}}_{(i-1)}\right] + \left[i(i-1)\mathbf{A_4}\hat{\mathbf{H}}_{(i-2)}\right] \;\forall\; i \geq 4 \quad (3.33)$$

It should be noted that, $\hat{\mathbf{Z}}_i$ & $\mathbf{C}_o$ are $6n \times 2n$ column vectors, where as $\hat{\mathbf{H}}_i$ is a $6n \times 6n$ matrix. Hence, general solution for Eq. (3.26) is acquired in the form of:

$$[\bar{\mathbf{G}}(\zeta)] = \left[\sum_{i=0}^{\infty}\left(\frac{\hat{\mathbf{Z}}_i\zeta^i}{i!}\right)\right] + \left[\sum_{i=0}^{\infty}\left(\frac{\hat{\mathbf{H}}_i\zeta^i}{i!}\right)\right][\mathbf{C_o}] \quad (3.34)$$

The series is truncated when the contribution of any more terms is negligibly small which is less than 10^{-10}. Again, the boundary and interface conditions in Eqs. (3.12)-(3.13) can be written in terms of functions $g_l^i(\zeta)$ as

$$\begin{aligned} &\text{for } k = 1, \quad \text{at } \zeta = 0: \quad g_5^i = 0, \quad g_7^i = 0, \quad g_8^i = 0, \\ &\text{for } k = L, \quad \text{at } \zeta = 1: \quad g_5^i = 0, \quad g_7^i = 0, \quad g_8^i = 0, \end{aligned} \quad (3.35)$$

$$[(g_1^i,\, g_2^i,\, g_3^i,\, g_5^i,\, g_7^i,\, g_8^i)|_{\zeta=1}]^{(k)} = [(g_1^i,\, g_2^i,\, g_3^i,\, g_5^i,\, g_7^i,\, g_8^i)|_{\zeta=0}]^{(k+1)} \quad (3.36)$$

for $i = 1, 2, \ldots, n$. The $6n \times L$ constants $C_o^{(k)}$'s for L layers are obtained from the $6n$ boundary conditions and $6n \times (L-1)$ interface continuity conditions given by Eqs. (3.35) and (3.36). This completely determines $\bar{\mathbf{G}}(\zeta)$. $\hat{\mathbf{G}}(\zeta)$ can now be obtained by solving the algebraic equation (3.21). This completes the first iteration step. The initial trial functions for $f_l^i(\xi)$ for the first iteration and the corresponding matrices are given in Sec. 3.5 below.

3.4.2 Solution along circumferential direction (θ)

In this step, the solution of the previous step is taken as the known functions for $g_l^i(\zeta)$ while latest $f_l^i(\xi)$ functions are evaluated. Thus, $f_l^i(\xi)$ being unknown the variation δX_l this time is given by

$$\delta X_l = \sum_{i=1}^{n} g_l^i \delta f_l^i(\xi), \qquad l = 1, 2, \ldots 8. \quad (3.37)$$

Further, the functions $f_l^i(\xi)$ are partitioned into vector $\bar{\mathbf{F}}$ consisting of those variables that appear in the boundary conditions along θ-axis and a vector $\hat{\mathbf{F}}$ of the remaining variables. The vectors

include the following field variables:

$$\bar{\mathbf{F}} = \left[f_3^1 \dots f_3^n \; f_1^1 \dots f_1^n \; f_2^1 \dots f_2^n \; f_4^1 \dots f_4^n \; f_6^1 \dots f_6^n \; f_8^1 \dots f_8^n\right]^{\mathrm{T}}$$
$$\hat{\mathbf{F}} = \left[f_5^1 \dots f_5^n \; f_7^1 \dots f_7^n\right]^{\mathrm{T}} \tag{3.38}$$

Again, by substituting Eqs. (3.16) and (3.37) in Eq. (3.10) and realising the coefficients of any arbitrary $\delta f_l^i(\xi)$ as zero $8n$ differential-algebraic equations are derived for $\bar{\mathbf{F}}_{,\xi}$ and $\hat{\mathbf{F}}$, respectively. Here, the integration is performed over ζ direction on the known functions of ζ and wherever necessary integration by parts is applied. By back substituting the $2n$ algebraic equations for $\hat{\mathbf{F}}$ obtained in the form of:

$$\mathbf{L}\hat{\mathbf{F}} = \tilde{\mathbf{B}}\bar{\mathbf{F}} + \tilde{\mathbf{P}}_{\mathbf{m}} \tag{3.39}$$

into the $6n$ system of first-order ODEs for $\bar{\mathbf{F}}_{,\xi}$:

$$\mathbf{N}\bar{\mathbf{F}}_{,\xi} = \bar{\mathbf{B}}\bar{\mathbf{F}} + \hat{\mathbf{B}}\hat{\mathbf{F}} + \bar{\mathbf{P}}_{\mathbf{m}} \tag{3.40}$$

the final $6n$ system of non-homogeneous first-order ODEs with constant coefficients are obtained as:

$$\bar{\mathbf{F}}_{,\xi} = \mathbf{B}\bar{\mathbf{F}} + \mathbf{P}_{\mathbf{m}} \tag{3.41}$$

where, $\mathbf{B} = \mathbf{N}^{-1}[\bar{\mathbf{B}} + \hat{\mathbf{B}}\mathbf{L}^{-1}\tilde{\mathbf{B}}]$ and $\mathbf{P}_{\mathbf{m}} = \mathbf{N}^{-1}[\bar{\mathbf{P}}_{\mathbf{m}} + \hat{\mathbf{B}}\mathbf{L}^{-1}\tilde{\mathbf{P}}_{\mathbf{m}}]$. Further, $\mathbf{N}$, $\bar{\mathbf{B}}$, $\hat{\mathbf{B}}$, $\mathbf{L}$ and $\tilde{\mathbf{B}}$ are $6n \times 6n$, $6n \times 6n$, $6n \times 2n$, $2n \times 2n$ and $2n \times 6n$ matrices respectively, and $\bar{\mathbf{P}}_{\mathbf{m}}$ and $\tilde{\mathbf{P}}_{\mathbf{m}}$ are $6n \times 1$ and $2n \times 1$ column vectors comprising of the loading terms.

For integration across the thickness a notation $\langle \dots \rangle_h = \sum_{k=1}^{L} t^{(k)} \int_0^1 (\dots)^{(k)} \, d\zeta$ is used to denote the following non-zero elements of these matrices:

$$N_{i_1 j_1} = N_{j_6 i_6} = \frac{1}{\psi}\langle \frac{g_8^i g_3^j}{\zeta t + R_1} \rangle_h, N_{i_2 j_2} = N_{j_4 i_4} = \frac{1}{\psi}\langle \frac{g_4^i g_1^j}{\zeta t + R_1} \rangle_h,$$
$$N_{i_3 j_3} = N_{j_5 i_5} = \frac{1}{\psi}\langle \frac{g_6^i g_2^j}{\zeta t + R_1} \rangle_h$$
$$\bar{B}_{i_1 j_2} = \langle \frac{g_8^i g_1^j}{\zeta t + R_1} \rangle_h - \frac{1}{t}\langle g_8^i g_{1,\zeta}^j \rangle_h, \bar{B}_{i_1 j_6} = \bar{s}_{55}\langle g_8^i g_8^j \rangle_h, \bar{B}_{i_2 j_1} = \langle \frac{g_4^i g_3^j}{\zeta t + R_1} \rangle_h,$$

$$\bar{B}_{i_2j_4} = \hat{s}_{11}\langle g_4^i g_4^j\rangle_h, \bar{B}_{i_2j_5} = \hat{s}_{16}\langle g_4^i g_6^j\rangle_h, \bar{B}_{i_3j_4} = \hat{s}_{16}\langle g_6^i g_4^j\rangle_h,$$

$$\bar{B}_{i_3j_5} = \hat{s}_{66}\langle g_6^i g_6^j\rangle_h, \bar{B}_{i_4j_6} = -2\langle\frac{g_1^i g_8^j}{\zeta t + R_1}\rangle_h - \frac{1}{t}\langle g_1^i g_{8,\zeta}^j\rangle_h, \bar{B}_{i_6j_4} = \langle\frac{g_3^i g_4^j}{\zeta t + R_1}\rangle_h,$$

$$\hat{B}_{i_1j_2} = \bar{s}_{45}\langle g_8^i g_7^j\rangle_h, \hat{B}_{i_2j_1} = \hat{s}_{13}\langle g_4^i g_5^j\rangle_h, \hat{B}_{i_3j_1} = \hat{s}_{36}\langle g_6^i g_5^j\rangle_h,$$

$$\hat{B}_{i_5j_2} = -\langle\frac{g_2^i g_7^j}{\zeta t + R_1}\rangle_h - \frac{1}{t}\langle g_2^i g_{7,\zeta}^j\rangle_h, \hat{B}_{i_6j_1} = -\langle\frac{g_3^i g_5^j}{\zeta t + R_1}\rangle_h - \frac{1}{t}\langle g_3^i g_{5,\zeta}^j\rangle_h,$$

$$\tilde{B}_{i_1j_1} = -\frac{1}{t}\langle g_5^i g_{3,\zeta}^j\rangle_h, \tilde{B}_{i_1j_4} = \hat{s}_{13}\langle g_5^i g_4^j\rangle_h, \tilde{B}_{i_1j_5} = \hat{s}_{36}\langle g_5^i g_6^j\rangle_h,$$

$$\tilde{B}_{i_2j_3} = -\frac{1}{t}\langle g_7^i g_{2,\zeta}^j\rangle_h, \tilde{B}_{i_2j_6} = \bar{s}_{45}\langle g_7^i g_8^j\rangle_h,$$

$$L_{i_1j_1} = -\hat{s}_{33}\langle g_5^i g_5^j\rangle_h, L_{i_2j_2} = -\bar{s}_{44}\langle g_7^i g_7^j\rangle_h \tag{3.42}$$

$$\begin{aligned}
\bar{P}_{m_{i2}} &= \hat{s}_{13}p_a\langle g_4^i\rangle_h + \hat{s}_{13}p_d\langle g_4^i(\zeta t + R_1)\rangle_h,\\
\bar{P}_{m_{i3}} &= \hat{s}_{36}p_a\langle g_6^i\rangle_h + \hat{s}_{36}p_d\langle g_6^i(\zeta t + R_1)\rangle_h,\\
\bar{P}_{m_{i6}} &= -2p_d\langle g_3^i\rangle_h - \tfrac{p_a\langle g_3^i\rangle}{(\zeta t + R_1)}\rangle_h,\\
\tilde{P}_{m_{i1}} &= \hat{s}_{33}p_a\langle g_5^i\rangle_h + \hat{s}_{33}p_d\langle g_5^i(\zeta t + R_1)\rangle_h
\end{aligned} \tag{3.43}$$

Since $g_l^i(\zeta)$ are known in close form, all integrations in Eqs. (3.42) and (3.43) are evaluated exactly in close form.

Equation (3.41) represents a system of $6n$ nonhomogeneous first order ODEs with constant coefficients. Its complementary solution is of the form $\bar{\mathbf{F}}_\mathbf{c}(\xi) = e^{\lambda\xi}\mathbf{Y}$, which on substitution in the homogeneous part of Eq. (3.41) yields an eigenvalue problem

$$\mathbf{BY} = \lambda\mathbf{Y} \tag{3.44}$$

Hence, the exponent λ and $\mathbf{Y}$ are the $6n$ eigenvalue and eigenvector pairs of matrix $\mathbf{B}$. The eigenvalues λ can be either real or occur in complex conjugate pairs. The solution for a distinct real eigenvalue $\lambda = p$ with eigenvector $\mathbf{Y}_1$ in terms of arbitrary real constant C_1 is

$$\bar{\mathbf{F}}_\mathbf{c} = \mathbf{H}_1(\zeta)C_1 \qquad \text{with} \qquad \mathbf{H}_1(\zeta) = \mathbf{Y}_1 e^{p\xi} \tag{3.45}$$

For a complex conjugate pair of eigenvalues λ_2, $\lambda_3 = \alpha \pm i\beta$ with complex eigenvector $\mathbf{Y}_2$ corresponding to λ_2, the complementary solution can be expressed in terms of two real constants C_2

and C_3 as

$$\mathbf{F_c}(\xi) = \mathbf{H}_2(\xi)C_2 + \mathbf{H}_3(\xi)C_3 \tag{3.46}$$

$$\mathbf{H}_2(\xi) = \mathrm{e}^{\alpha\xi}\Big[\Re(\mathbf{Y}_2)\cos\beta\xi - \Im(\mathbf{Y}_2)\sin\beta\xi\Big] \tag{3.47}$$

$$\mathbf{H}_3(\xi) = \mathrm{e}^{\alpha\xi}\Big[\Re(\mathbf{Y}_2)\sin\beta\xi + \Im(\mathbf{Y}_2)\cos\beta\xi\Big] \tag{3.48}$$

$\Re$ and $\Im$ indicate real and imaginary parts of a complex number. Where the functional form of the column vector $\mathbf{H}_i(\xi)$ is given by the Eq. (3.45) or Eqs. (3.47) and (3.48) as per the nature of λ_i.

Thus, the complete complementary solution $\bar{\mathbf{F}}_\mathbf{c}(\xi)$ can be expressed in terms of $6n$ real constants C_i as

$$\bar{\mathbf{F}}_\mathbf{c} = \sum_{i=1}^{6n} \mathbf{H}_i(\xi)C_i \tag{3.49}$$

Equation (3.41) implies that $\mathbf{P_m}$ is a linear function of ξ. Thus, the general solution of Eq. (3.41) is

$$\bar{\mathbf{F}}(\xi) = \sum_{i=1}^{6n} \mathbf{H}_i(\xi)C_i + \mathbf{U_0} \tag{3.50}$$

where

$$\mathbf{U_0} = -\mathbf{B}^{-1}[\mathbf{P_m}] \tag{3.51}$$

Across the circumferential span of the shell panel, the boundary conditions in Eq. (3.11) can be written in terms of functions $f_l^i(\xi)$ as

$$\begin{aligned}
&\text{Simply supported (S)}: \quad f_3^i = 0, \quad f_4^i = 0, \quad f_6^i = 0 \\
&\text{Clamped (C)}: \quad\quad\quad f_3^i = 0, \quad f_1^i = 0, \quad f_2^i = 0 \\
&\text{Free (F)}: \quad\quad\quad\quad f_4^i = 0, \quad f_6^i = 0, \quad f_8^i = 0, \qquad (i = 1, 2, \ldots, n)
\end{aligned} \tag{3.52}$$

After obtaining the solution for $\bar{\mathbf{F}}$, functions $\hat{\mathbf{F}}$ can be determined from Eq. (3.39). This completes the second iterative step. These two iteration steps (Secs. 3.4.1 and 3.4.2) of alternating directions

for approximate and analytical solutions are repeated until a prescribed level of convergence is achieved. For higher order terms in the integral functions, matrix **B** in Eq. (3.41) often have large positive eigenvalues, whose exponentials, being very large, may cause numerical instability to the solution. To prevent this, for positive eigenvalues, the exponential term $e^{\alpha\xi}$ in Eq. (3.45) is replaced with $e^{\alpha(\xi-1)}$, which limits the maximum value of the exponential to one. Obviously, this does not alter the final solution, since the arbitrary constants corresponding to these eigenvectors are computed accordingly.

3.5 INITIAL TRIAL FUNCTIONS

A nice feature of the EKM, not shared by many other approximate methods is that the initial trial functions are required to satisfy neither the essential (displacement) nor the natural (stress) boundary conditions. A bad quality of trial function can at most lead to one or two more iteration steps. Taking advantage of this feature, the following trial functions are considered, which actually correspond to the simply supported boundary conditions at $\xi = 0, 1$:

$$\begin{aligned} f_1^i(\xi) = f_2^i(\xi) = f_7^i(\xi) = f_8^i(\xi) = \cos i\pi\xi \\ f_3^i(\xi) = f_4^i(\xi) = f_5^i(\xi) = f_6^i(\xi) = \sin i\pi\xi \end{aligned} \tag{3.53}$$

Substituting Eq. (3.53) into Eq. (3.23) yields the following non-zero terms of matrices $\mathbf{M}$, $\bar{\mathbf{A}}_\mathbf{0}$, $\bar{\mathbf{A}}_\mathbf{1}$, $\hat{\mathbf{A}}_\mathbf{0}$, $\hat{\mathbf{A}}_\mathbf{1}$, $\tilde{\mathbf{A}}_\mathbf{0}$, $\tilde{\mathbf{A}}_\mathbf{1}$, $\mathbf{K}$, $\bar{\mathbf{Q}}_\mathbf{p0}$, $\bar{\mathbf{Q}}_\mathbf{p1}$, $\bar{\mathbf{Q}}_\mathbf{p2}$, $\tilde{\mathbf{Q}}_\mathbf{p0}$ and $\tilde{\mathbf{Q}}_\mathbf{p1}$:

$$\begin{aligned} &\bar{A}_{0_{i_1j_4}} = \hat{s}_{33}, \quad \bar{A}_{0_{i_2j_5}} = \bar{s}_{45}, \quad \bar{A}_{0_{i_2j_6}} = \bar{s}_{55}, \quad \bar{A}_{0_{i_3j_5}} = \bar{s}_{44}, \\ &\bar{A}_{0_{i_3j_6}} = \bar{s}_{45}, \quad \bar{A}_{1_{i_2j_1}} = -\bar{n}, \quad \bar{A}_{1_{i_2j_2}} = 1, \quad \bar{A}_{1_{i_4j_4}} = -1, \\ &\bar{A}_{1_{i_4j_6}} = -\bar{n}, \quad \bar{A}_{1_{i_5j_5}} = -1, \quad \bar{A}_{1_{i_6j_6}} = -2, \quad \hat{A}_{0_{i_1j_1}} = \hat{s}_{31}, \\ &\hat{A}_{0_{i_1j_2}} = \hat{s}_{36}, \quad \hat{A}_{1_{i_4j_1}} = 1, \quad \hat{A}_{1_{i_5j_2}} = -\bar{n}, \quad \hat{A}_{1_{i_6j_1}} = -\bar{n}, \end{aligned} \tag{3.54}$$

$$\tilde{A}_{0_{i_1 j_4}} = \hat{s}_{13}, \quad \tilde{A}_{0_{i_2 j_4}} = \hat{s}_{36}, \quad \tilde{A}_{1_{i_1 j_1}} = -1, \quad \tilde{A}_{1_{i_1 j_2}} = -\bar{n},$$
$$\tilde{A}_{1_{i_2 j_3}} = -\bar{n}, \quad K_{i_1 j_1} = \hat{s}_{11}, \quad K_{i_1 j_2} = -\hat{s}_{16}, \quad K_{i_2 j_1} = -\hat{s}_{16},$$
$$K_{i_2 j_2} = -\hat{s}_{66}, \quad \bar{n} = i\pi/\psi$$

$$\bar{Q}_{p0_{i_1}} = 4\hat{s}_{33} p_a / i\pi, \quad \bar{Q}_{p0_{i_4}} = -8 p_d / i\pi, \quad \bar{Q}_{p1_{i_4}} = -4 p_a / i\pi,$$
$$\bar{Q}_{p2_{i_1}} = 4\hat{s}_{33} p_d / i\pi, \quad \tilde{Q}_{p0_{i_1}} = 4\hat{s}_{13} p_a / i\pi, \quad \tilde{Q}_{p0_{i_2}} = 4\hat{s}_{36} p_a / i\pi, \tag{3.55}$$
$$\tilde{Q}_{p1_{i_1}} = 4\hat{s}_{13} p_d / i\pi, \quad \tilde{Q}_{p1_{i_2}} = 4\hat{s}_{36} p_d / i\pi$$

and **M** reduces to an identity matrix.

3.6 EVALUATION OF THE INTEGRALS

The integrals in Eqs. (3.42) and (3.43) are of the following types:

$$\sum_{k=1}^{L} t^{(k)} \int_0^1 [\bar{g}_p^i(\zeta)\bar{g}_q^j(\zeta)]^{(k)}\, d\zeta; \quad \sum_{k=1}^{L} t^{(k)} \int_0^1 [\bar{g}_{p,\zeta}^i(\zeta)\bar{g}_q^j(\zeta)]^{(k)}\, d\zeta; \quad \sum_{k=1}^{L} t^{(k)} \int_0^1 \left[\frac{\bar{g}_p^i(\zeta)\bar{g}_q^j(\zeta)}{(\zeta t + R_1)}\right]^{(k)} d\zeta;$$
$$\sum_{k=1}^{L} t^{(k)} \int_0^1 [\bar{g}_p^i(\zeta)\hat{g}_q^j(\zeta)]^{(k)}\, d\zeta; \quad \sum_{k=1}^{L} t^{(k)} \int_0^1 \left[\frac{\bar{g}_p^i(\zeta)\hat{g}_q^j(\zeta)}{(\zeta t + R_1)}\right]^{(k)} d\zeta; \quad \sum_{k=1}^{L} t^{(k)} \int_0^1 [\bar{g}_p^i(\zeta)]^{(k)}\, d\zeta;$$
$$\sum_{k=1}^{L} t^{(k)} \int_0^1 [\bar{g}_p^i(\zeta)(\zeta t + R_1)]^{(k)}\, d\zeta; \quad \sum_{k=1}^{L} t^{(k)} \int_0^1 [\hat{g}_p^i(\zeta)]^{(k)}\, d\zeta \tag{3.56}$$

Using Eqs. (3.20) and (3.21), the integrals in Eq. (3.56) involve the evaluation of the following basic integrals which can be evaluated in closed form as follows:

$$J_1 = \int \zeta^n d\zeta = \frac{\zeta^{n+1}}{(n+1)} \tag{3.57}$$

$$J_2 = \int \frac{1}{\left(1 + \frac{\zeta}{s}\right)} d\zeta = s \log(s + \zeta) \tag{3.58}$$

$$J_3 = \int \frac{\zeta^n}{\left(1 + \frac{\zeta}{s}\right)} d\zeta = \sum_{k=1}^{n} \frac{(-1)^{(n-k)} \zeta^k s^{(n-k+1)}}{k} + (-1)^n s^{(n+1)} \log\left(\frac{s+\zeta}{s}\right) \tag{3.59}$$

$$J_4 = \int \frac{1}{\left(1 + \frac{\zeta}{s}\right)^2} d\zeta = \frac{-s^2}{(s+\zeta)} \tag{3.60}$$

$$J_5 = \int \frac{\zeta^n}{\left(1 + \frac{\zeta}{s}\right)^2} d\zeta =$$
$$\sum_{k=1}^{(n-1)} \frac{(-1)^{(k-1)} \zeta^{(n-k)} k s^{(k+1)}}{(n-k)} + \left(\frac{(-1)^{(n-1)} s^{(n+2)}}{(s+\zeta)}\right) + (-1)^{(n+1)} s^{(n+1)} n \log\left(\frac{s+\zeta}{s}\right) \tag{3.61}$$

On the other hand, the integrals in Eqs. (3.23) and (3.24) have the following basic forms:

$$\int_0^1 \bar{f}_p^i(\xi)\bar{f}_q^j(\xi)d\xi; \quad \int_0^1 \hat{f}_p^i(\xi)\hat{f}_q^j(\xi)d\xi; \quad \int_0^1 \bar{f}_p^i(\xi)\hat{f}_q^j(\xi)d\xi; \quad \int_0^1 \bar{f}_{p,\xi}^i(\xi)\bar{f}_q^j(\xi)d\xi;$$
$$\int_0^1 \bar{f}_p^i(\xi)d\xi; \quad \int_0^1 \hat{f}_p^i(\xi)d\xi \tag{3.62}$$

Using Eqs. (3.39) and (3.40), the integrals in Eq. (3.62) can be further expressed in terms of the following basic integrals:

$$\int_0^1 F_r^p(\xi)F_s^q(\xi)d\xi, \quad \int_0^1 F_{r\,,\xi}^p(\xi)F_s^q(\xi)d\xi, \quad \int_0^1 F_r^p(\xi)d\xi \tag{3.63}$$

The evaluation of $\int_0^1 F_r^p(\xi)F_s^q(\xi)d\xi$ will depend on the nature of the eigenvalues λ_r and λ_s. If both λ_r and λ_s are complex with $(\lambda_r = \alpha_r \pm \beta_r)$ and $(\lambda_s = \alpha_s \pm \beta_s)$, the product of $F_r^p(\xi)$ and $F_s^q(\xi)$ can be evaluated and summed over $(r, r+1)$ and $(s, s+1)$ as

$$\begin{aligned}
&[C_r e^{\alpha_r\xi}(R_p\cos\beta_r\xi - I_p\sin\beta_r\xi) + C_{r+1}e^{\alpha_r\xi}(R_p\sin\beta_r\xi + I_p\cos\beta_r\xi)] \times [C_s e^{\alpha_s\xi}(R_q\cos\beta_s\xi \\
&-I_q\sin\beta_s\xi) + C_{s+1}e^{\alpha_s\xi}(R_q\sin\beta_s\xi + I_q\cos\beta_s\xi)] \\
&= e^{(\alpha_r+\alpha_s)\xi}\left\{\frac{1}{2}\left[\cos(\beta_r-\beta_s)\xi + \cos(\beta_r+\beta_s)\xi\right]C_{rs}^1 + \frac{1}{2}\left[\sin(\beta_r+\beta_s)\xi + \sin(\beta_r-\beta_s)\xi\right]C_{rs}^2\right. \\
&\quad \left.+\frac{1}{2}\left[\sin(\beta_r+\beta_s)\xi - \sin(\beta_r-\beta_s)\xi\right]C_{rs}^3 + \frac{1}{2}\left[\cos(\beta_r-\beta_s)\xi + \cos(\beta_r+\beta_s)\xi\right]C_{rs}^4\right\}
\end{aligned} \tag{3.64}$$

where

$$\begin{aligned}
C_{rs}^1 &= (C_rR_p + C_{r+1}I_p)(C_sR_q + C_{s+1}I_q); \quad C_{rs}^2 = (C_{r+1}R_p - C_rI_p)(C_sR_q + C_{s+1}I_q) \\
C_{rs}^3 &= (C_rR_p + C_{r+1}I_p)(C_{s+1}R_q - C_sI_q); \quad C_{rs}^4 = (-C_rI_p + C_{r+1}R_p)(-C_sI_q + C_{s+1}R_q)
\end{aligned} \tag{3.65}$$

For all other cases of λ_r and λ_s, the integrands can be expressed as a special case of Eq. (3.64) in terms of the products of trigonometric and exponential functions or only exponential functions (when both the roots are real). For integrals involving $F_{r\,,\xi}^p$, the derivative can be expressed as

$$F_{r\,,\xi}^p = e^{\lambda_s\xi}[R_p'\cos\beta_s\xi - I_p'\sin\beta_s\xi] \tag{3.66}$$

where $R_p' = (\alpha_rR_p - \beta_rI_p)$, $\quad I_p' = (\beta_rR_p + \alpha_rI_p)$. Using Eq. (3.66), the integrand $F_{r\,,\xi}^p\,F_s^q$ can be expressed in the same form as in Eq. (3.62). It is now evident that all integrals in Eq. (3.64) involve

the evaluation of the following basic integrals which can be evaluated in closed form as follows:

$$I_1 = \int_0^1 e^{\alpha\xi}\cos(\beta\xi)d\xi = \frac{e^{\alpha}(\alpha\cos\beta + \beta\sin\beta) - \alpha}{\alpha^2+\beta^2} \tag{3.67}$$

$$I_2 = \int_0^1 e^{\alpha\xi}\sin(\beta\xi)d\xi = \frac{e^{\alpha}(\alpha\sin\beta - \beta\cos\beta) + \beta}{\alpha^2+\beta^2} \tag{3.68}$$

$$I_3 = \int_0^1 e^{\alpha\xi}d\xi = \left[\frac{e^{\alpha}-1}{\alpha}\right] \tag{3.69}$$

$$I_4 = \int_0^1 \xi e^{\alpha\xi}\cos(\beta\xi)d\xi = \frac{e^{\alpha}(\alpha\cos\beta + \beta\sin\beta) - \alpha I_1 - \beta I_2}{\alpha^2+\beta^2} \tag{3.70}$$

$$I_5 = \int_0^1 \xi e^{\alpha\xi}\sin(\beta\xi)d\xi = \frac{e^{\alpha}(\alpha\sin\beta - \beta\cos\beta) - (\alpha I_2 - \beta I_1)}{\alpha^2+\beta^2} \tag{3.71}$$

$$I_6 = \int_0^1 \xi e^{\alpha\xi}d\xi = \left[\frac{1+(\alpha-1)e^{\alpha}}{\alpha^2}\right] \tag{3.72}$$

The special cases of the above integrals for $\alpha = 0$ and/or $\beta = 0$ are computed in closed form separately.

3.7 NUMERICAL RESULTS - SINGLE TERM SOLUTION

So far, most of the studies have employed a single term (n=1) in the EKM solution for 2D problems, as it yields a reasonably accurate result. In order to assess the accuracy of the single term solution for a 3D elasticity problem of cylindrical bending of a shell, numerical study is conducted in this section for shell panels of different thicknesses made up of angle-ply laminate scheme.

An infinitely long composite panel with angle-ply stacking sequence of [30/-30/-30/30] and circumferential span of 90^o is taken (as shown in Fig. 3.6c). Plies are of equal thickness and are composed of Mat. 1 of Table 3.1 corresponding to that of graphite epoxy T300/934. Uniformly distributed loads are applied which are represented as $p_2 = p_0 = 1N/m^2$ on the outer surface and $p_1 = 0$ at the inner surface, respectively. Nomenclature of the shell panels are done as per the designation, for instance CF panel means it is clamped (C) at $\xi = 0$ and free (F) at $\xi = 1$, respectively. The obtained results are nondimensionalized using

$$(\bar{v},\, \bar{u}) = (v/S, 10u)Y_0/p_0hS^3, \qquad (\bar{\sigma}_\theta,\, \bar{\tau}_{z\theta},\, \bar{\tau}_{r\theta},\, \bar{\tau}_{zr}) = (\sigma_\theta,\, S\tau_{z\theta},\, S\tau_{r\theta},\, S\tau_{zr})/p_0S^2$$

where $S = R/h$ and $Y_0 = Y_2$.

Table 3.1: Material constants.

Material	Y_1	Y_2	Y_3	G_{23}	G_{13}	G_{12}	ν_{12}	ν_{13}	ν_{23}
Mat. 1*	131.0	10.34	10.34	6.895	6.205	6.895	0.22	0.22	0.49
Mat. 2†	181.0	10.3	10.3	2.87	7.17	7.17	0.28	0.28	0.33
Face(Al)	70.0	70.0	70.0	26.3	26.3	26.3	0.33	0.33	0.33
Core ‡	0.1457	0.1457	0.186	0.056	0.056	0.056	0.3	0.3	0.33

Units: Young's moduli Y_i and shear moduli G_{ij} in GPa.
* [253]; † [254]; ‡ [255]

Table 3.2: Comparison of present single-term EKM results with simulated 3D FE and 3D exact results.

S	Entity $\bar{X}(\xi,\zeta)$	3D exact [83]	3D FE [256]	Present (n=1)
5	$\bar{v}(0,-0.5)$	-0.18576	-0.18638	-0.18622
	$\bar{u}(0.5,0)$	2.9278	2.9307	2.9299
	$\bar{\sigma}_\theta(0.5,-0.5)$	-3.0497	-3.0443	-3.0658
	$\bar{\tau}_{r\theta}(0,0)$	1.5902	1.5991	1.6220
	$\bar{\tau}_{z\theta}(0.5,-0.5)$	-7.0435	-7.0108	-7.0878
	$\bar{\tau}_{zr}(0,0)$	0.34799	0.3453	0.34384
20	$\bar{v}(0,-0.5)$	-0.12176		-0.12139
	$\bar{u}(0.5,0)$	-2.2582		-2.2584
	$\bar{\sigma}_\theta(0.5,-0.5)$	2.6031		2.6034
	$\bar{\tau}_{r\theta}(0,0)$	-1.1606		-1.1726
	$\bar{\tau}_{z\theta}(0.5,-0.5)$	1.2256		1.2258
	$\bar{\tau}_{zr}(0,0)$	-0.54529		-0.54527

3.7.1 Panels with Simply-Supported Edges

The circumferential variation of displacement field variable $\bar{u}$, normal stress $\bar{\sigma}_\theta$ and transverse stresses $\bar{\tau}_{r\theta}$ and $\bar{\tau}_{zr}$ are shown in Fig. 3.2 for thick and thin shell panels corresponding to the mid-

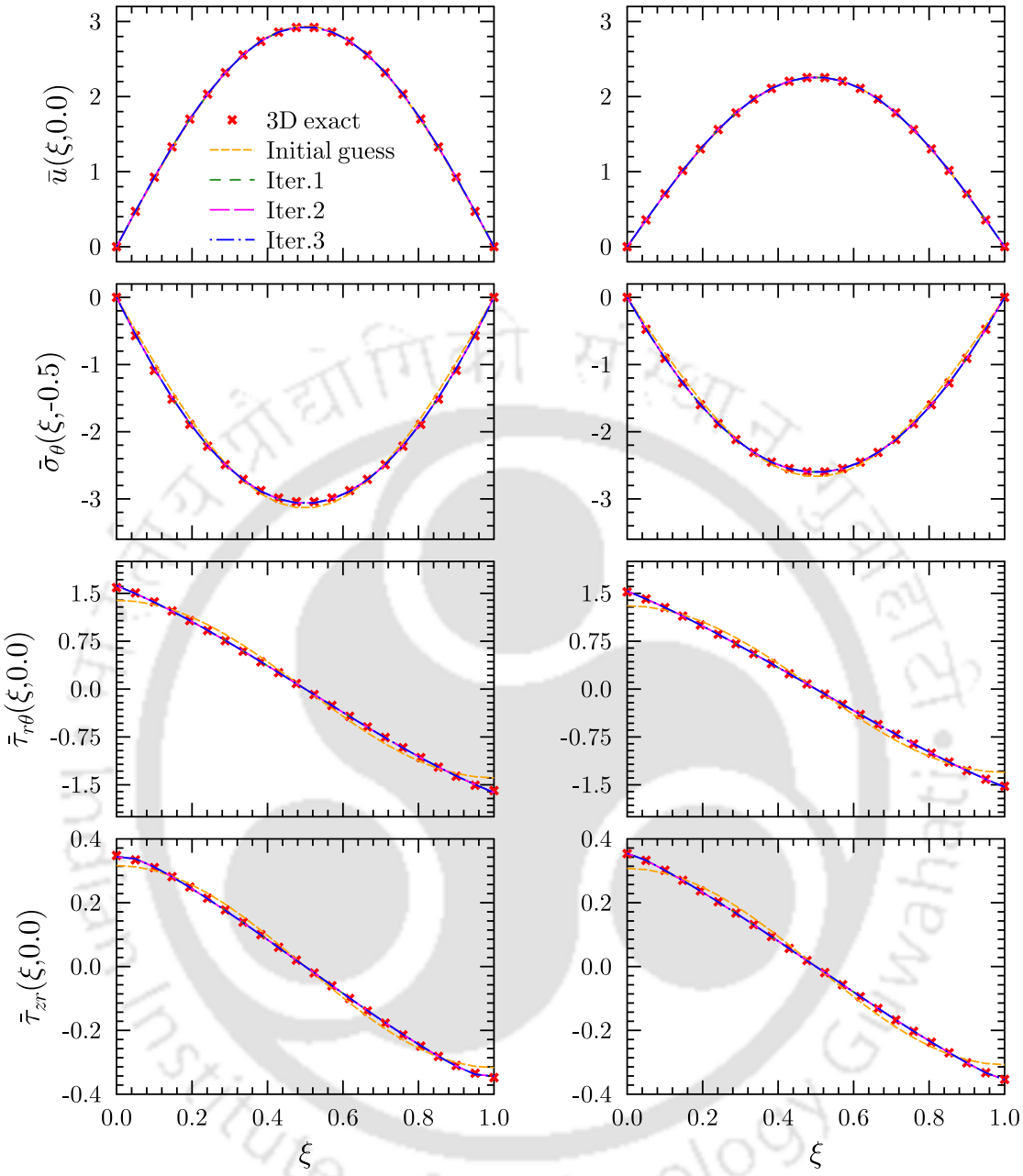

Fig. 3.2: Circumferential variation showing convergence of deflection and stresses for simply supported panels (c) of S=5 and 20.

surface radius to thickness ratios $S = 5$ and 20. In the figure, the individual plots are shown at those r-locations where the variables are maximum. Further, for the present case the convergence of the method for different iterations can be studied with the choice of initial trial functions $f_i(\xi)$. Referring to the Sec. 3.5, $f_i(\xi)$ at the boundaries $\xi = 0, 1$ is chosen which satisfied the simply-supported conditions initially.

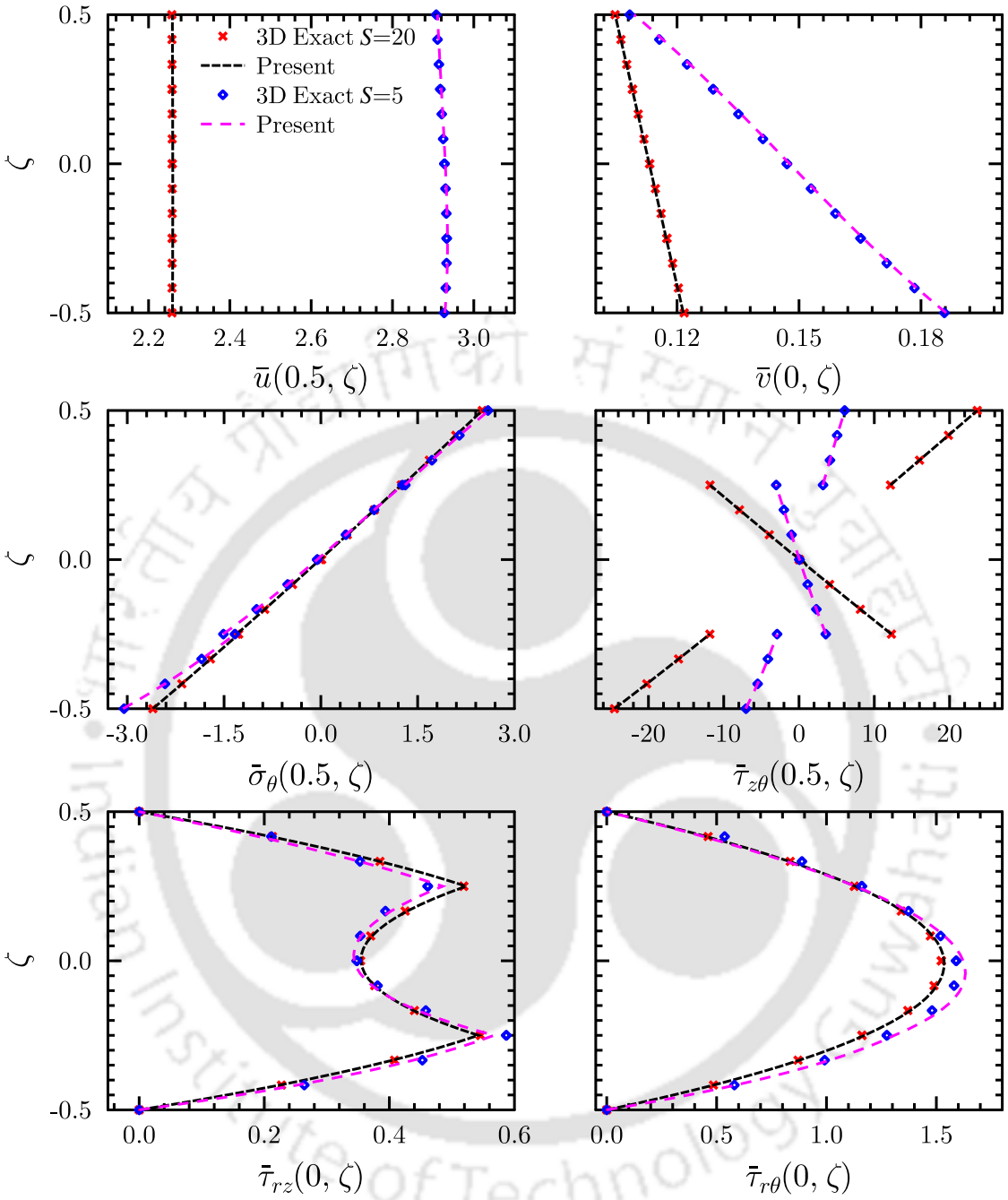

Fig. 3.3: Through-the-thickness variation of deflection and stresses for simply supported panels (c) of S=5 and 20.

The present iterative solution converged very rapidly even for the angle-ply laminate scheme which is as low as just one or two iteration steps for different thickness shell panels. The solution also predicts through-the-thickness variations accurately with lower number of iterations. Through-the-thickness plots are presented in the Fig. 3.3 for all the non-zero field variables such as the

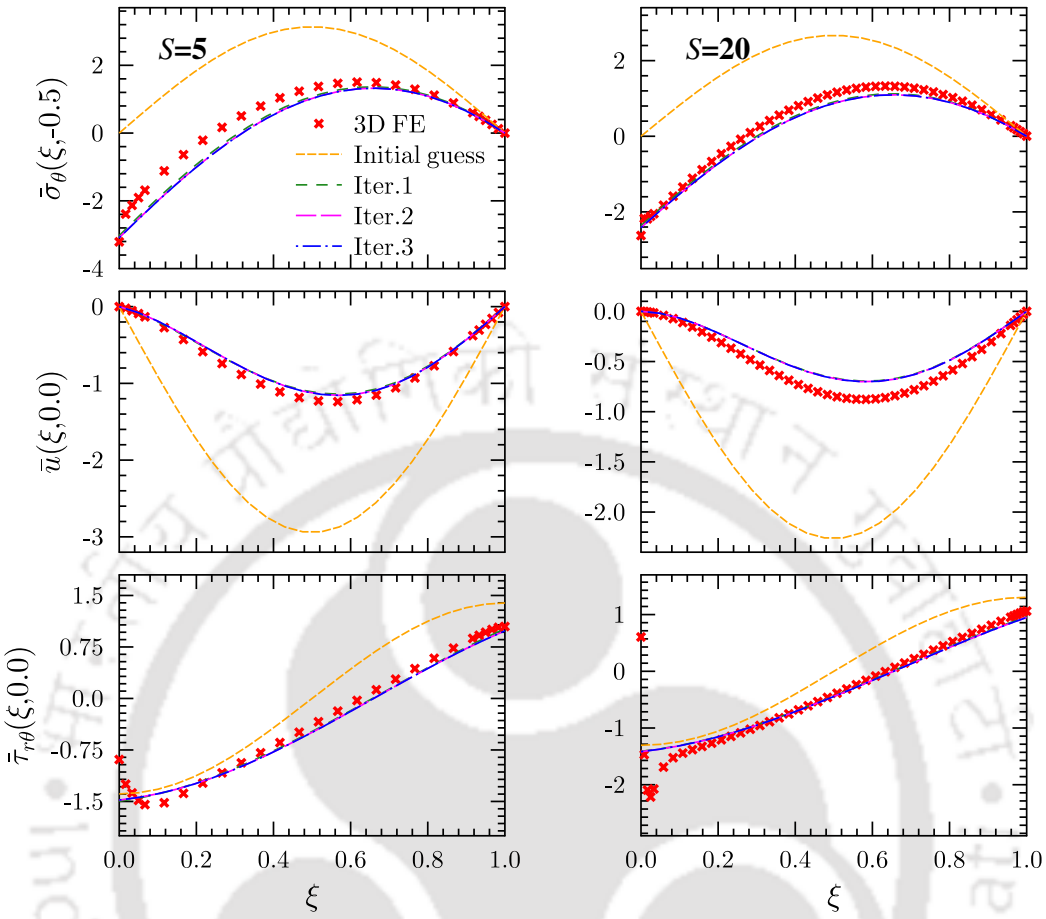

Fig. 3.4: Circumferential variation showing convergence of deflection and stresses for CS panels (c) of S=5 and 20.

displacement components $(\bar{u}, \bar{v})$, normal stress $(\bar{\sigma}_\theta)$ and transverse stress components $(\bar{\tau}_{r\theta}, \bar{\tau}_{z\theta}$ and $\bar{\tau}_{zr})$, respectively. The nature of the mentioned variables are plotted in the figure at those ξ-locations where they are largest for both the thick and thin shell panels. There is a comparison between the 3D exact results and third iteration results of the present solution which reveals very good match between both of them. The exact analytical solution used here are generated from the computer program developed by Dumir [83] which is similar to the analytical exact solution presented by Pagano [257] for the 3D elasticity equations. As an extension, Dumir has obtained the results for the simply-supported piezoelectric shell panel under uniformly distributed loading. There they had used Fourier series expansion, which requires a set of differential equations to be solved for each Fourier component. Converged results for such approach are obtained using 26 non-

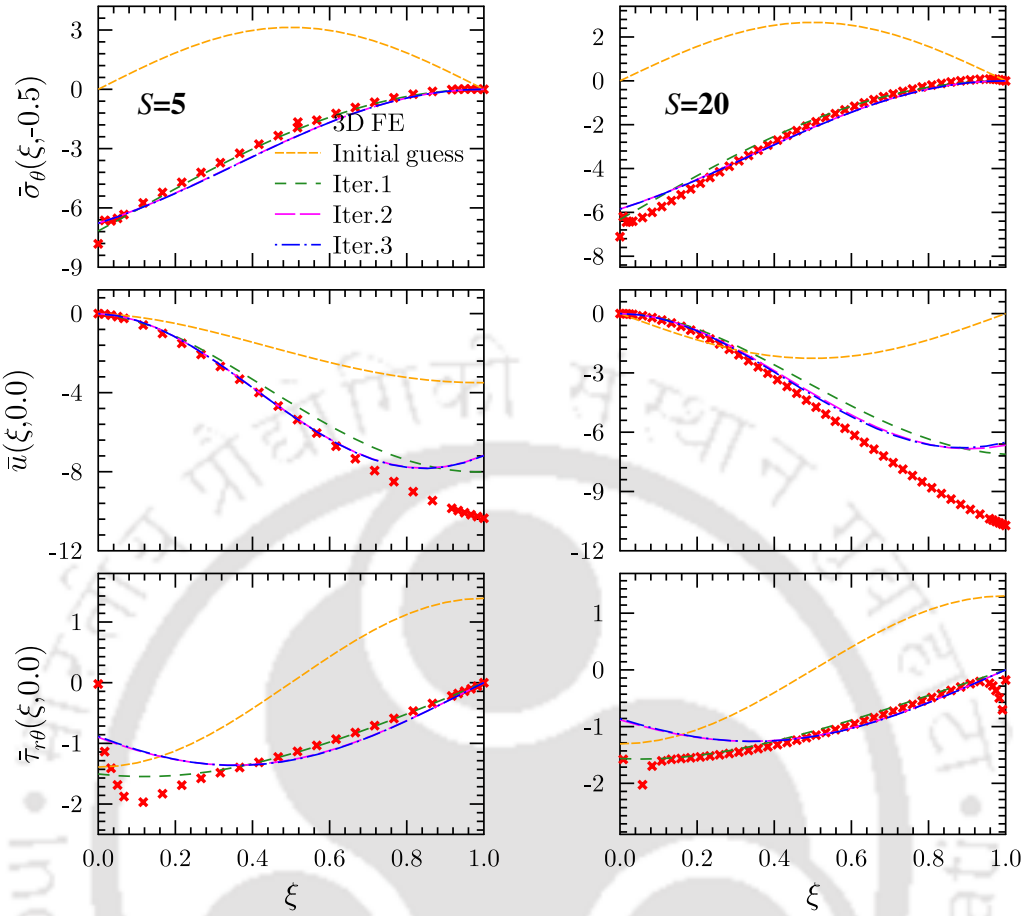

Fig. 3.5: Circumferential variation showing convergence of deflection and stresses for CF panels (c) of S=5 and 20.

zero Fourier terms, whereas the EKM solution has only one term, and its convergence is achieved in a single or two iterations. This ensured EKM to be computationally efficient with respect to the 3D exact solution using Fourier expansion. Adding to that, the 3D exact solution is valid for only simply-supported boundary conditions, whereas the present EKM has been proved to be applicable for arbitrary boundary conditions in case of plate structures [199]. As the solution for the shell panel (c) subjected to arbitrary boundary conditions is not available in the literature, 3D FE model is done in ABAQUS [256] for obtaining the results. For accurate stress behavior and mimicking the present model exactly, the cylindrical shell is constructed as a very long panel along z-axis having axial length (l) ($\frac{l}{R} = 50$). This established a plane strain condition and obtained results remained constant for further increase of $\frac{l}{R}$ ratio. A 20 noded quadratic serendipity hexahedral elements with reduced integration (C3D20R) is used with mesh size of $(12 \times 60 \times 40)$ along r, θ and z directions,

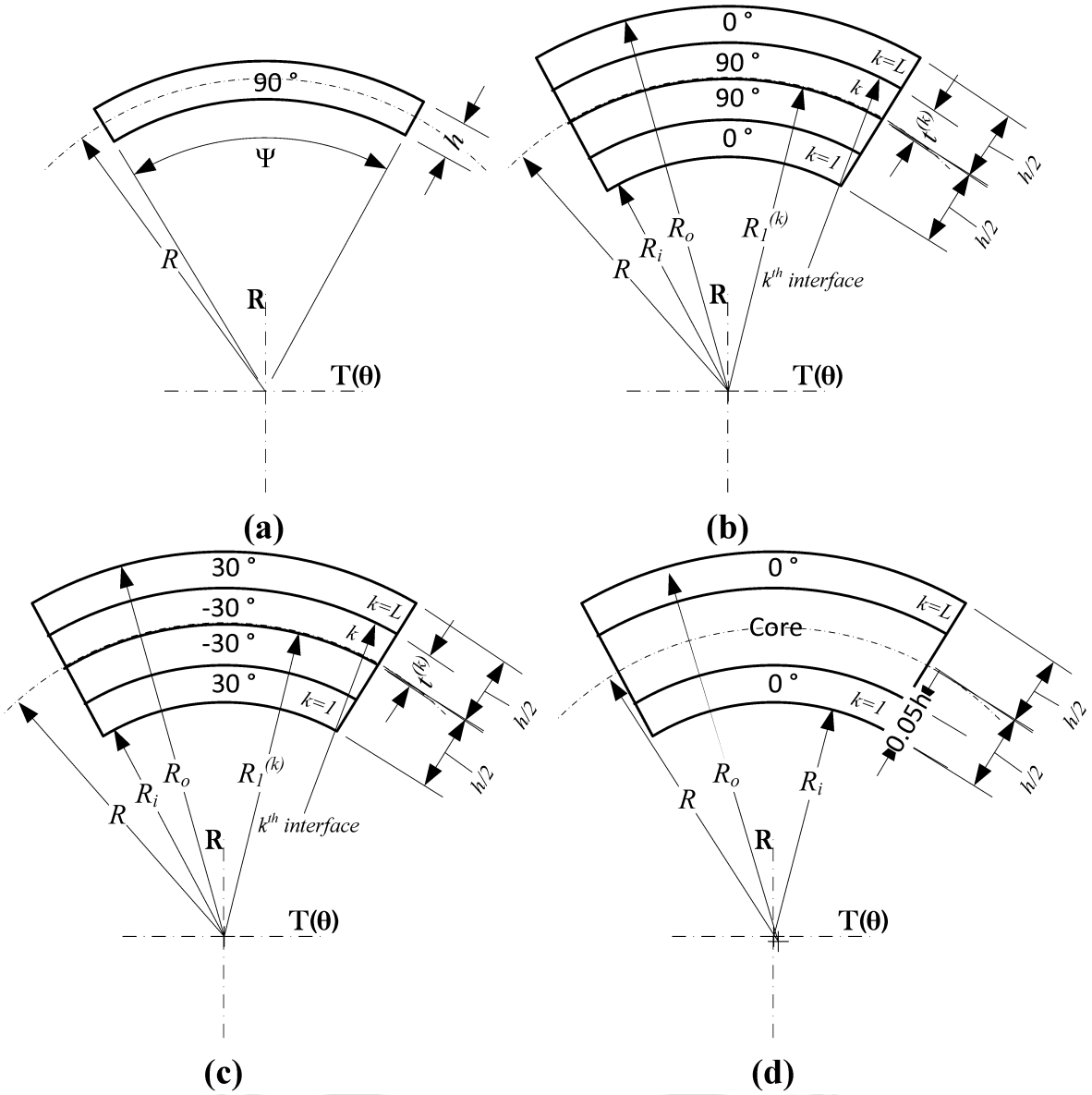

Fig. 3.6: Laminate lay-up of the cylindrical panels

respectively. The reduced integration is adopted to avoid shear locking, and hourglassing for the same will be inconsequential for the quadratic element specially in presence of multiple elements in the thickness direction. The present results are compared with the 3D exact and modeled 3D FE results in the Table 3.2. For the comparison, the present results are obtained after third iteration for the displacement and stress components at those specific locations where they attain the largest value in the geometry. The results are shown for the simply-supported shell panels (c) with $S = 5$ and 20. Very good agreement with a maximum error of 1.5% is revealed for both the thick and thin

shell panels on comparing of the results. Further, the close agreement of the 3D FE results with the 3D exact solution validates the FE modeling which will be used to obtain the reference solutions for non-simply supported boundary conditions. Noteworthily, accurate prediction is obtained for all the field variables with just one-term in the EKM solution.

3.7.2 Panels with other Boundary Conditions

The present method is examined in this section for its accuracy and convergence rate corresponding to the analysis of a shell panel with non-simply supported boundary conditions. For the opposite circumferential boundary conditions of clamped-simply supported (CS) and clamped-free (CF) case, the variation along the circumference of the displacement and stress field variables are shown in the Figs. 3.4 and 3.5 for both thick and thin (S=5, 20) shell panel (c), respectively. Recollecting that the initially guessed functions need not satisfy the non-simply supported boundary conditions, convergence is achieved very fast after just the second iteration step even for shell panels with these arbitrary boundary conditions. Successive iterations are performed and computed results are plotted in the figures for comparison with 3D FE results obtained from the mimicking ABAQUS model discussed above. Variation of the displacement $\bar{u}$ and excluding the region near the clamped edge, stresses $\bar{\sigma}_\theta$ and $\bar{\tau}_{r\theta}$ also show good agreement with 3D FE results. The thickness of the shell panels is also observed to affect the accuracy of prediction, with more deviations occurring in the EKM results of thick shell panel. This indicates the necessity of considering multiple terms in the assumed expression of Eq. (3.16) to achieve higher accuracy and predict the stress concentration zones arising at certain boundaries and interfaces.

3.8 NUMERICAL RESULTS - MULTI-TERM SOLUTION

The single-term solutions discussed above could predict the response in the domain of the shell panel, but did not yield the stress field near the boundaries. Although, the solution is computationally very cheap for preliminary predictions. The single-term solution deviated more for the thick shell panels even for the displacements. Hence, a multi-term solution with ($n > 1$) in the

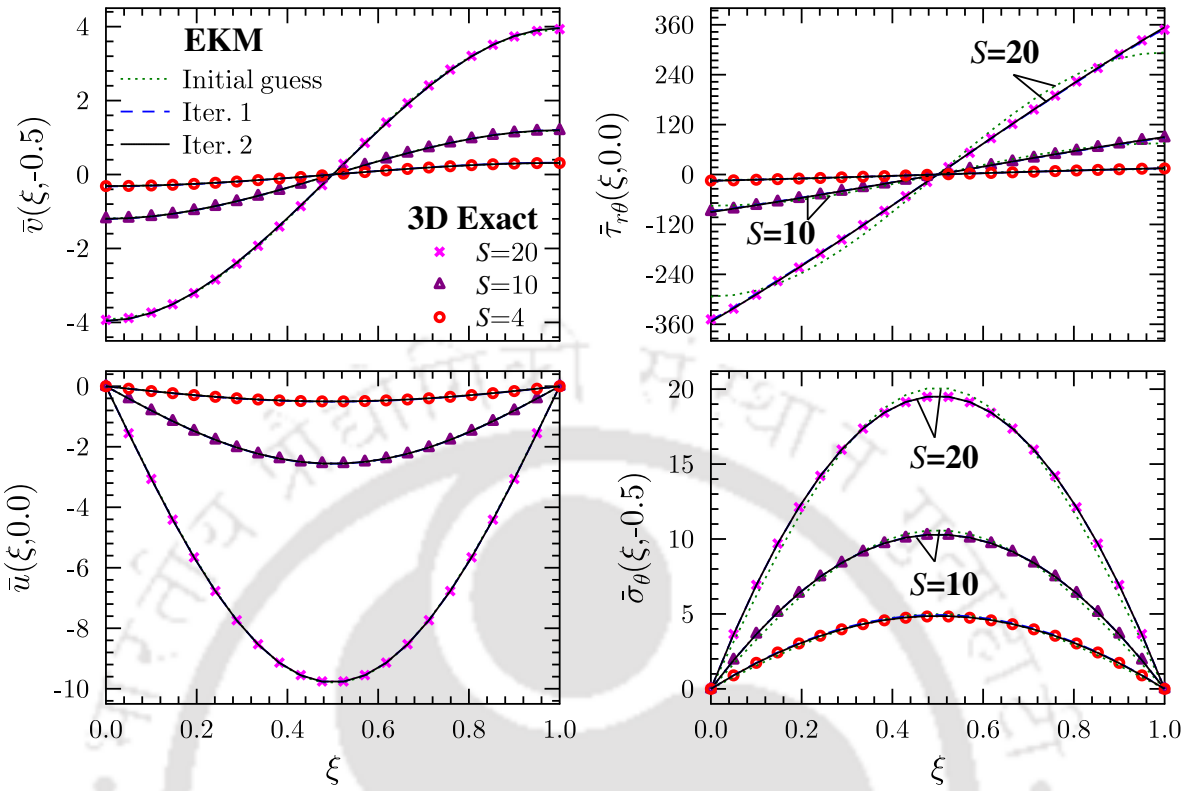

Fig. 3.7: Circumferential variation of deflections and stresses in cylindrical shell panel (a) of span 60^0 with SS boundary condition.

trial function is used for numerical study in this section with an aim to examine the improvement in accuracy of prediction for the field variables.

3.8.1 Response of Cross-ply Composite Shell Panels

For the analysis of cross-ply laminates, no special treatment is required in the developed general solution for angle-ply laminates in which case variables w, $\tau_{z\theta}$ and τ_{zr} vanishes. Numerical results are presented for single layer composite cylindrical shell panel (a) and a multilayered laminated composite shell panel (b). The lay-up of panel (a) & panel (b) are shown in Fig. 3.6. The mechanical response of the cylindrical shell panels are obtained for a uniform pressure loading (UDL) applied at the outer surface. The span angle (ψ) is taken as 60^0 in general and R is taken unity.

The present results are compared with 3D exact solution for simply supported case whereas 3D finite element (3D FE) solutions are used for comparing results of arbitrary support conditions. For the present case, 3D exact results are generated using the computer program developed by [83]. The

3D FE results are obtained from FE software [256]. As previously done for shell panel (c), similar model is constructed in the ABAQUS with C3D20R 3D elements and mesh size of $(12 \times 60 \times 40)$ to mimic the behavior of shell panels (a) and (b).

Initially, the panel (a) is considered for the analysis. Circumferential (along ξ) variation of displacements $(\bar{u}, \bar{v})$ & stresses $(\bar{\sigma}_\theta, \bar{\tau}_{r\theta})$ for thick, moderately thick and thin panels corresponding to S=4, 10 and 20 are plotted in Fig. 3.7 for simply-supported (SS) (at ξ=0,1) boundary condition. Through-the-thickness variation of these variables are also plotted in Fig. 3.8.

Presently developed multiterm EKM results are compared with 3D exact results obtained from solution technique developed by Dumir et al. [83]. The results for all the entities $(\bar{v}, \bar{u}, \bar{\sigma}_\theta, \bar{\tau}_{r\theta})$ show excellent agreement for thin, moderately thick & even for a considerably thick cylindrical shell panel (S=4), which is noteworthy. For the 3D exact solution, Dumir et al. [83] used the single

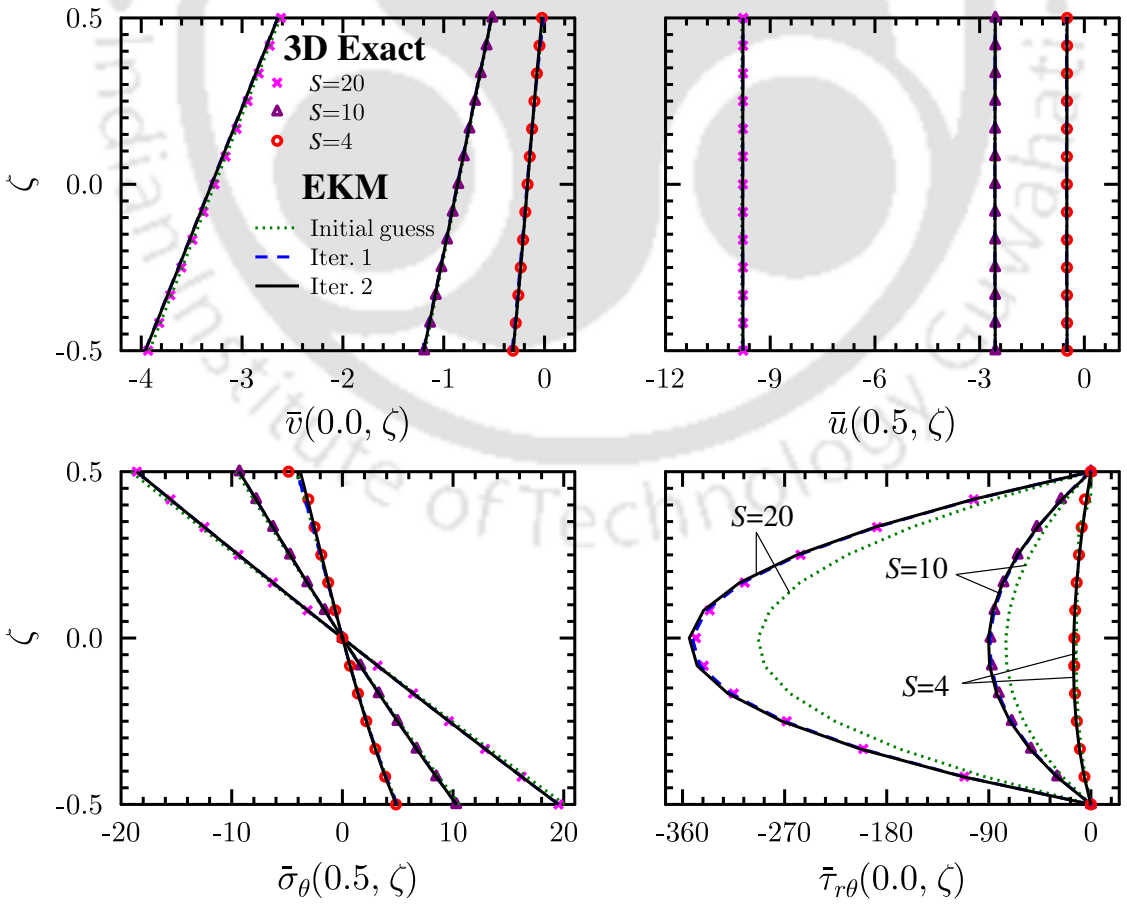

Fig. 3.8: Through-the-thickness variation of deflections and stresses in cylindrical shell panel (a) of span 60^0 with SS boundary condition.

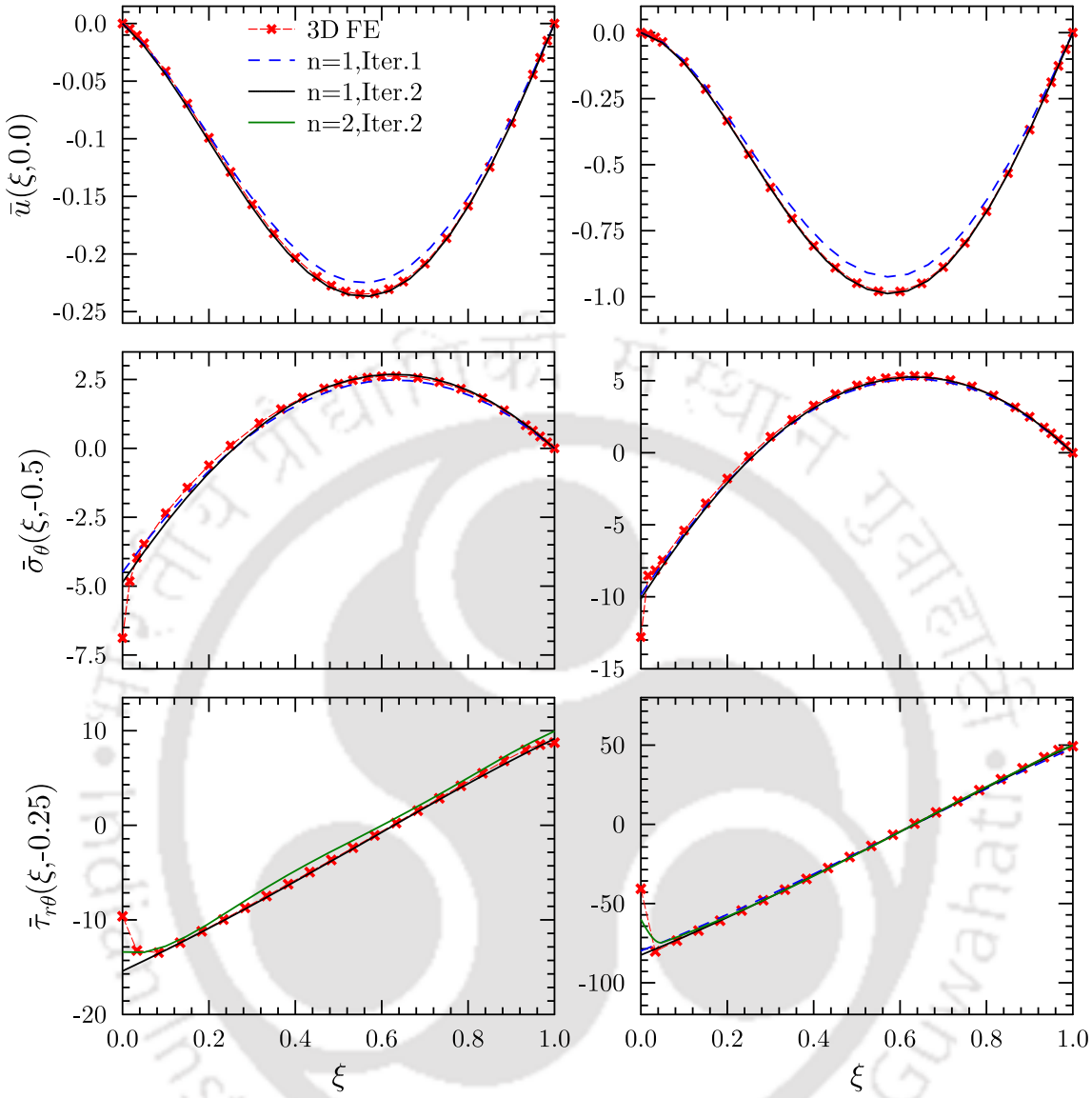

Fig. 3.9: Circumferential variation of deflections and stresses in cylindrical shell panel (a) of span 60^0 with CS boundary condition.

Fourier series expansion along circumferential direction. Due to which, 21 non-zero Fourier terms are required to obtain the converged results under UDL. On the other hand, EKM solutions are converged using just single term (n=1) in one or two iterations ($Iter.$=1/2). Therefore, it is proved that EKM is more computationally efficient than 3D exact solution based on Fourier expansion. Adding to that, the 3D exact solution is valid for only simply-supported boundary conditions, whereas the present EKM can also handle arbitrary support conditions.

Circumferential variation of deflections and stresses developed during static bending of thick &

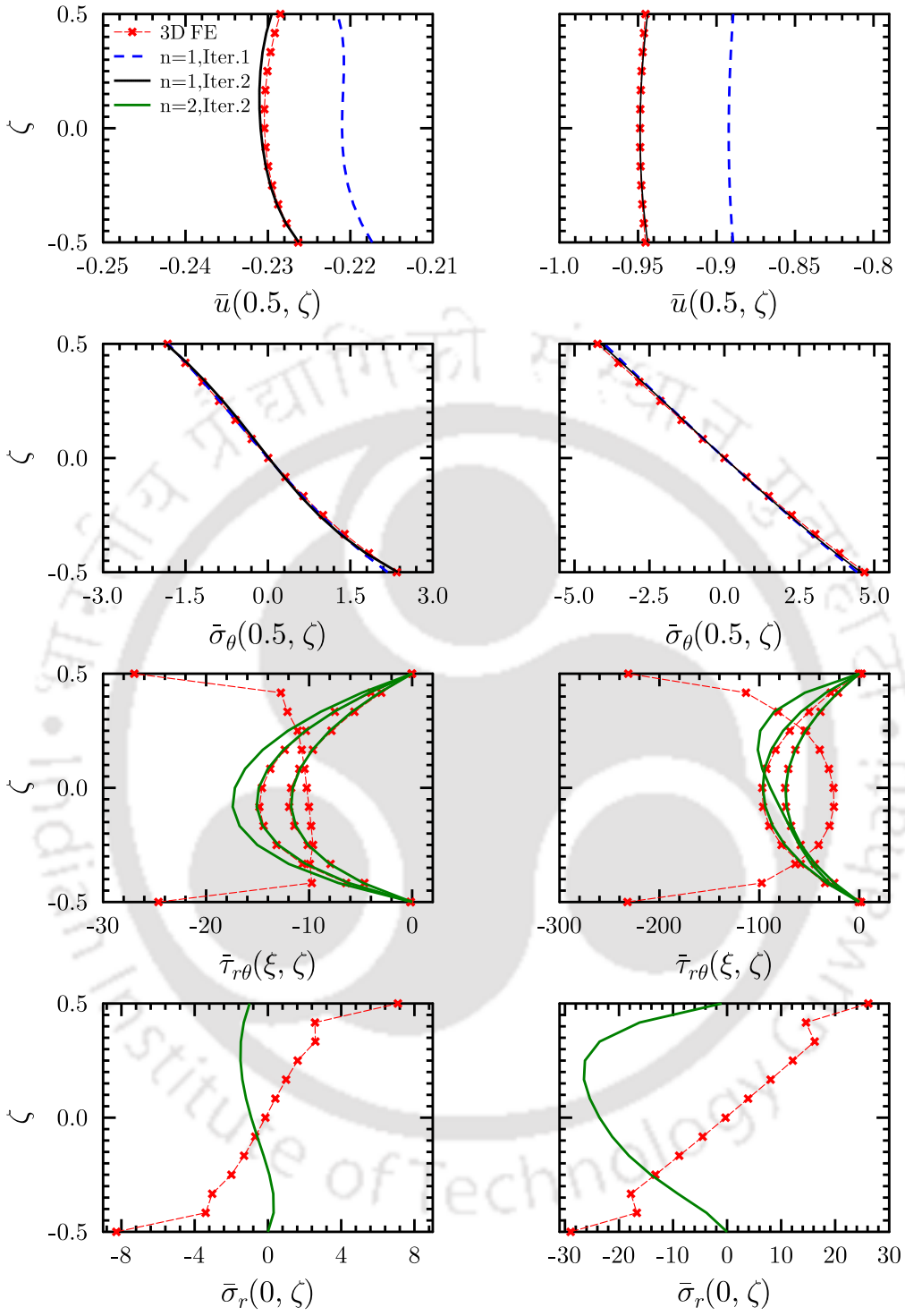

Fig. 3.10: Through-the-thickness variation of deflections and stresses in cylindrical shell panel (a) of span 60^0 with CS boundary condition.

moderately thick clamped-simply supported (CS) cylindrical shell panels are plotted in Fig. 3.9. Here, present results are compared with 3D FE results (ABAQUS). Excellent agreement between

present results and 3D FE are obtained for $\bar{u}$ through out the ξ span and stresses for most part of the ξ span except at the clamped edge (ξ=0). Through-the-thickness variations are also presented in Fig. 3.10. It is observed that $\bar{\tau}_{r\theta}$ and $\bar{\sigma}_r$ (obtained through 3D FE) do not satisfy the boundary condition at the inner and outer surfaces of panel at the very clamped edge. But slightly away from the clamped edge, it exactly matches with the present EKM results. A cantilevered (CF) panel is also analysed and its circumferential variation is given in Fig. 3.11. In-plane stress ($\bar{\sigma}_\theta$) is maximum at clamped edge for CF configuration as compared to SS & CS cases. Whereas transverse

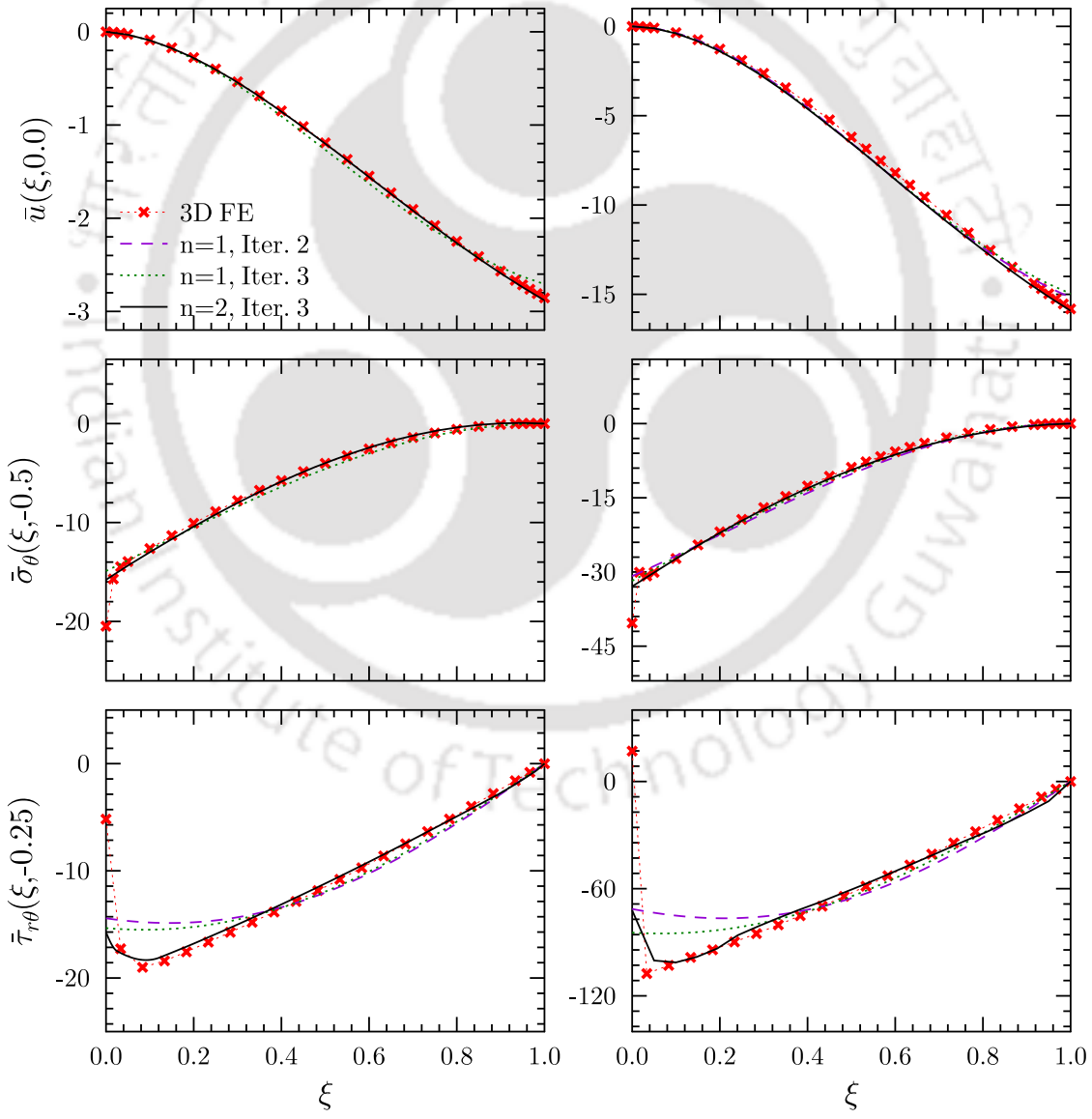

Fig. 3.11: Circumferential variation of deflections and stresses in cylindrical shell panel (a) of span 60^0 with CF boundary condition.

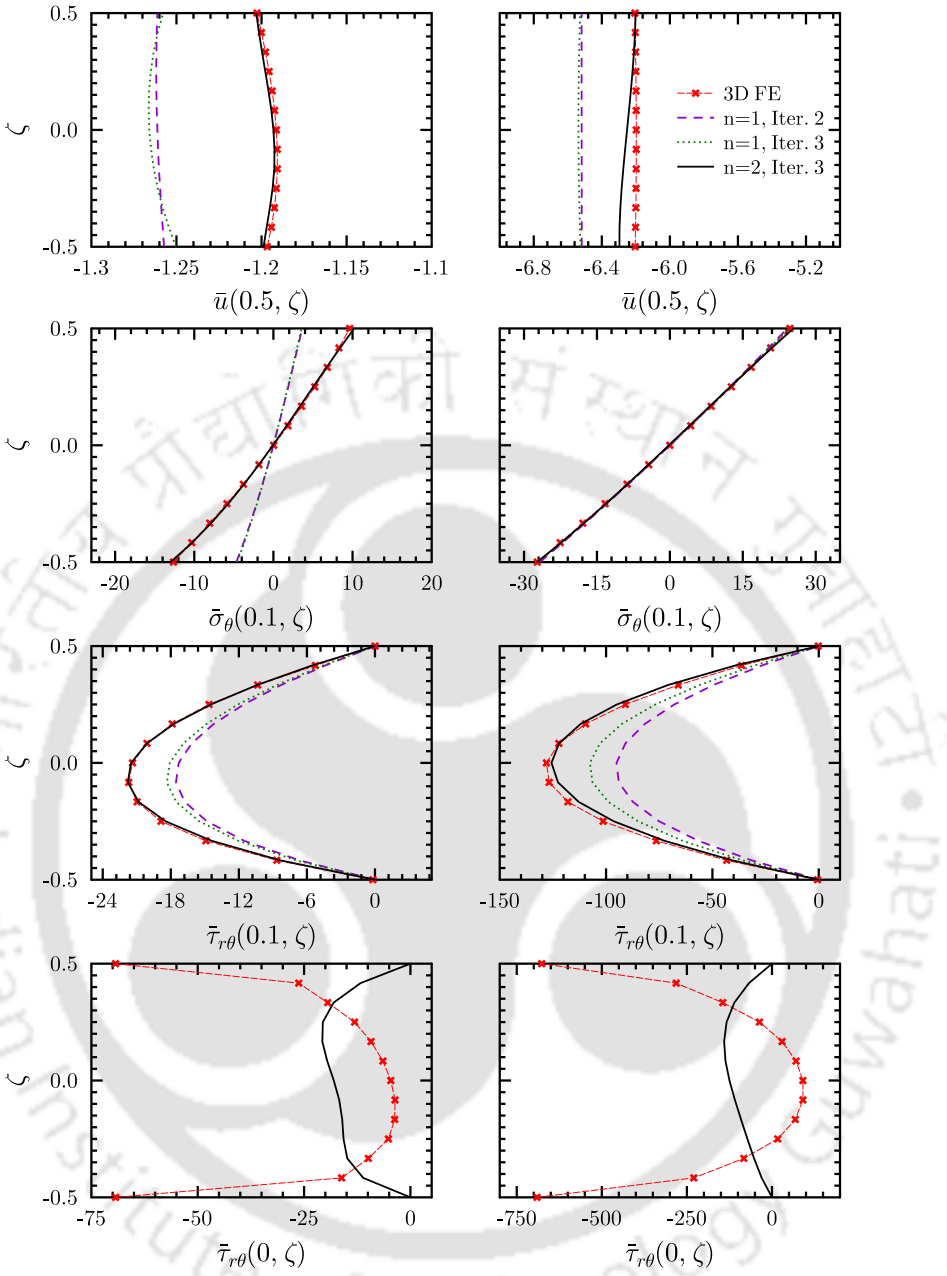

Fig. 3.12: Through-the-thickness variation of deflections and stresses in cylindrical shell panel (a) of span 60^0 with CF boundary condition.

shear stress is similar as that developed in CS but lower than that of SS panel. Higher bending displacements at free edge and stress irregularity in the vicinity of clamped edge are excellently estimated by present technique. Through-the-thickness variation is also obtained for CF shell panel and is plotted in Fig. 3.12. Steep variation of $\bar{\tau}_{r\theta}$ is observed near the clamped edge for both CS & CF cases. Transverse displacement is non-uniform across the thickness for thick panel.

In relevance to computational elegance of present technique, unlike in SS case, an extra or two

iteration steps and inclusion of just an additional term (n=2) in the trial function is required for exactly tracking the circumferential distribution for CF cases.

Next, a multi-layered composite panel (b) is considered for numerical study under various support conditions, here. Displacements and stresses developed along the circumference (along ξ) of a SS cylindrical shell panel (b) is analysed in Fig. 3.13.

It can be seen from the figure that present results are in excellent agreement with 3D exact results. Displacements and stresses are observed to be lower than those of panel (a). Thicker panel has higher transverse ($\bar{u}$) and circumferential ($\bar{v}$) displacements, which decreases for moderately thick to thin panels. Stresses ($\bar{\tau}_{r\theta}$,$\bar{\sigma}_{\theta}$) developed for thin and moderately thick laminates are similar although considerable variations in deflections ($\bar{u}$,$\bar{v}$) are observed. Through-the-thickness variations

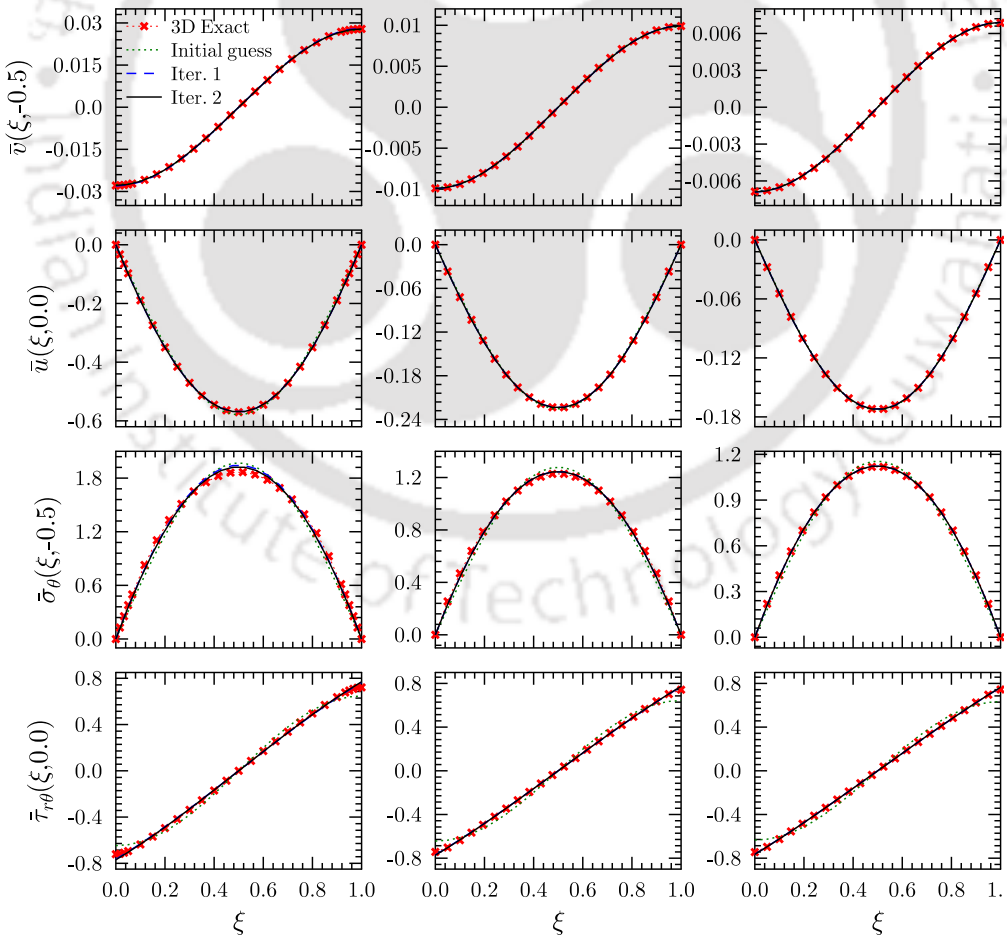

Fig. 3.13: Circumferential variation of deflections and stresses in a multi-layered laminated cylindrical shell panel (b) of span 60^0 with SS boundary condition.

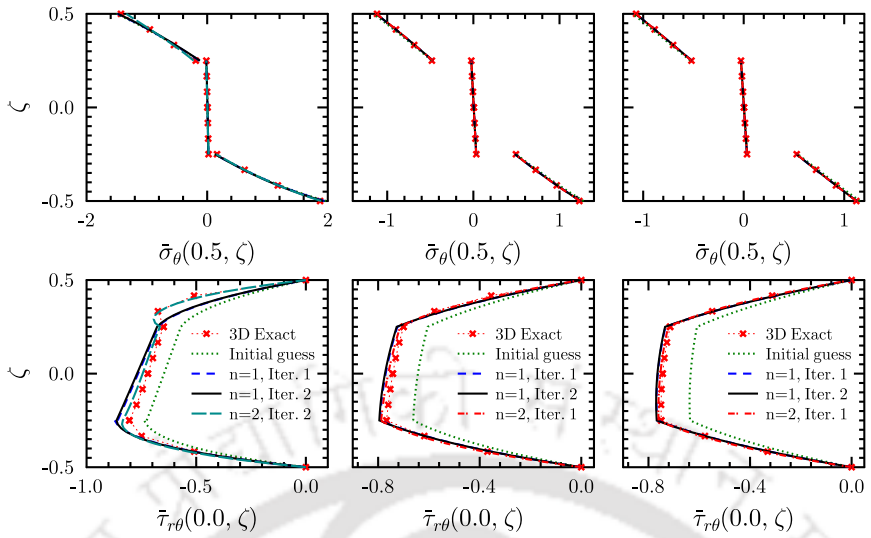

Fig. 3.14: Through-the-thickness variation of deflections and stresses in a multi-layered laminated cylindrical shell panel (b) of span 60^0 with SS boundary condition.

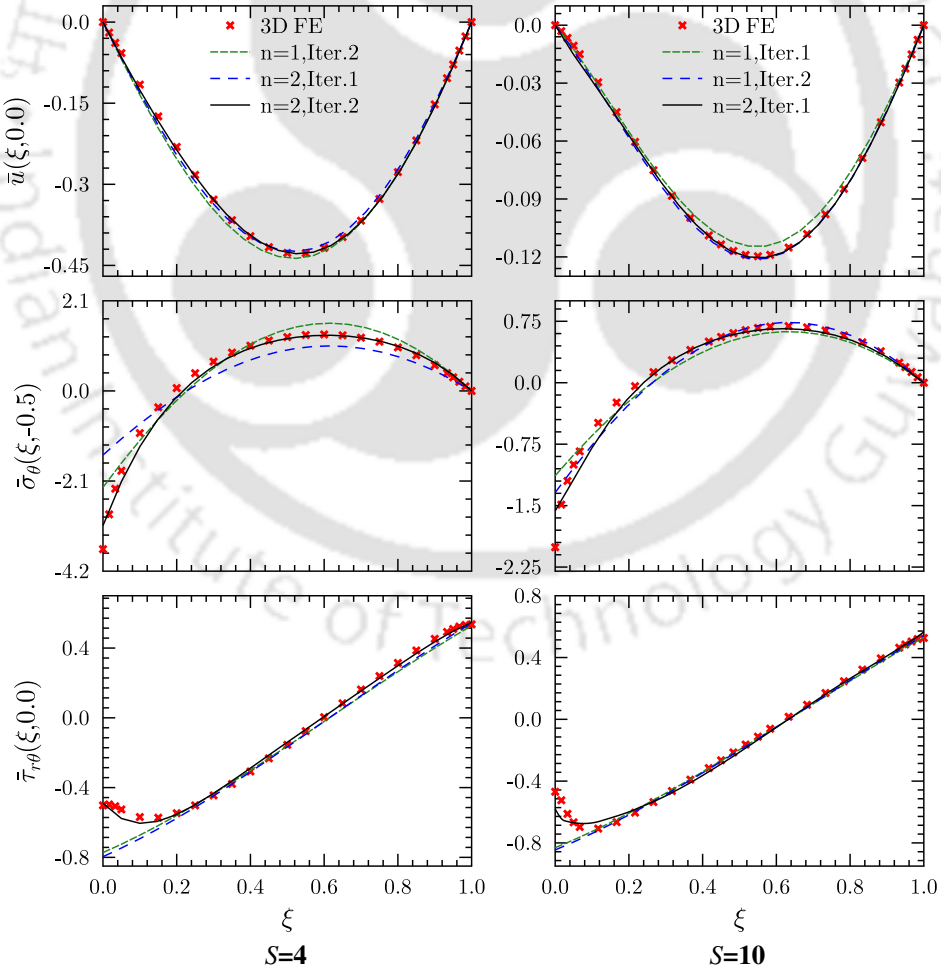

Fig. 3.15: Circumferential variation of deflections and stresses in a multi-layered laminated cylindrical shell panel (b) of span 60^0 with CS boundary condition.

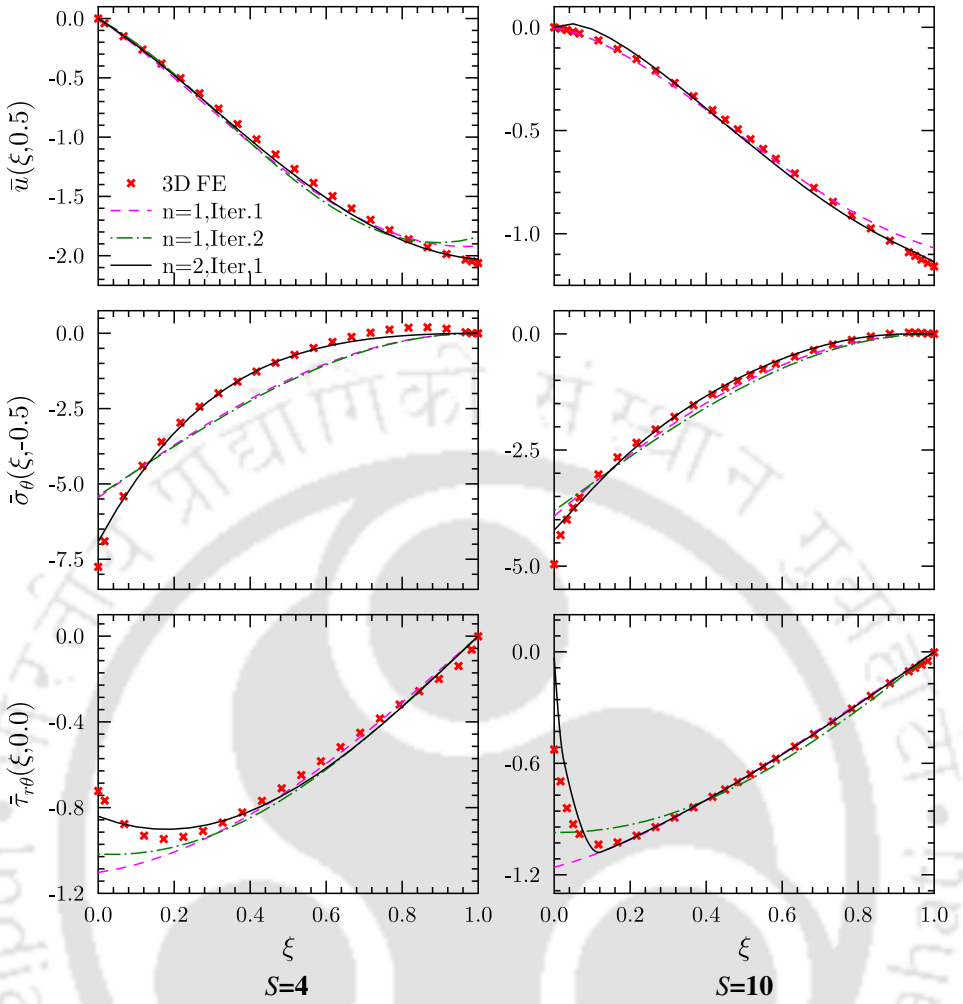

Fig. 3.16: Circumferential variation of deflections and stresses in a multi-layered laminated cylindrical shell panel (b) of span 60^0 with CF boundary condition.

of stresses are also plotted in Fig. 3.14 and compared with 3D exact. Thus, a thorough validation is conducted for verification & validation of present technique.

Circumferential variation of displacements and stresses for the thick and moderately thick panels are depicted in Fig. 3.15 & Fig. 3.16 subjected to CS and CF support conditions, respectively. Similarly like panel (a), the present results are in good agreement with 3D FE results except at the very clamped edge. However, the reason behind mismatch of stresses can be found in the through thickness plots at the very clamped edge and its close vicinity as shown in Fig. 3.17a.

Transverse shear stress ($\bar{\tau}_{r\theta}$) is observed to be non-continuous at the layer interfaces and the required traction free boundary conditions are also not satisfied on inner and outer surfaces at the very clamped edge. Due to this although the numerical values are slightly affected, the pattern of

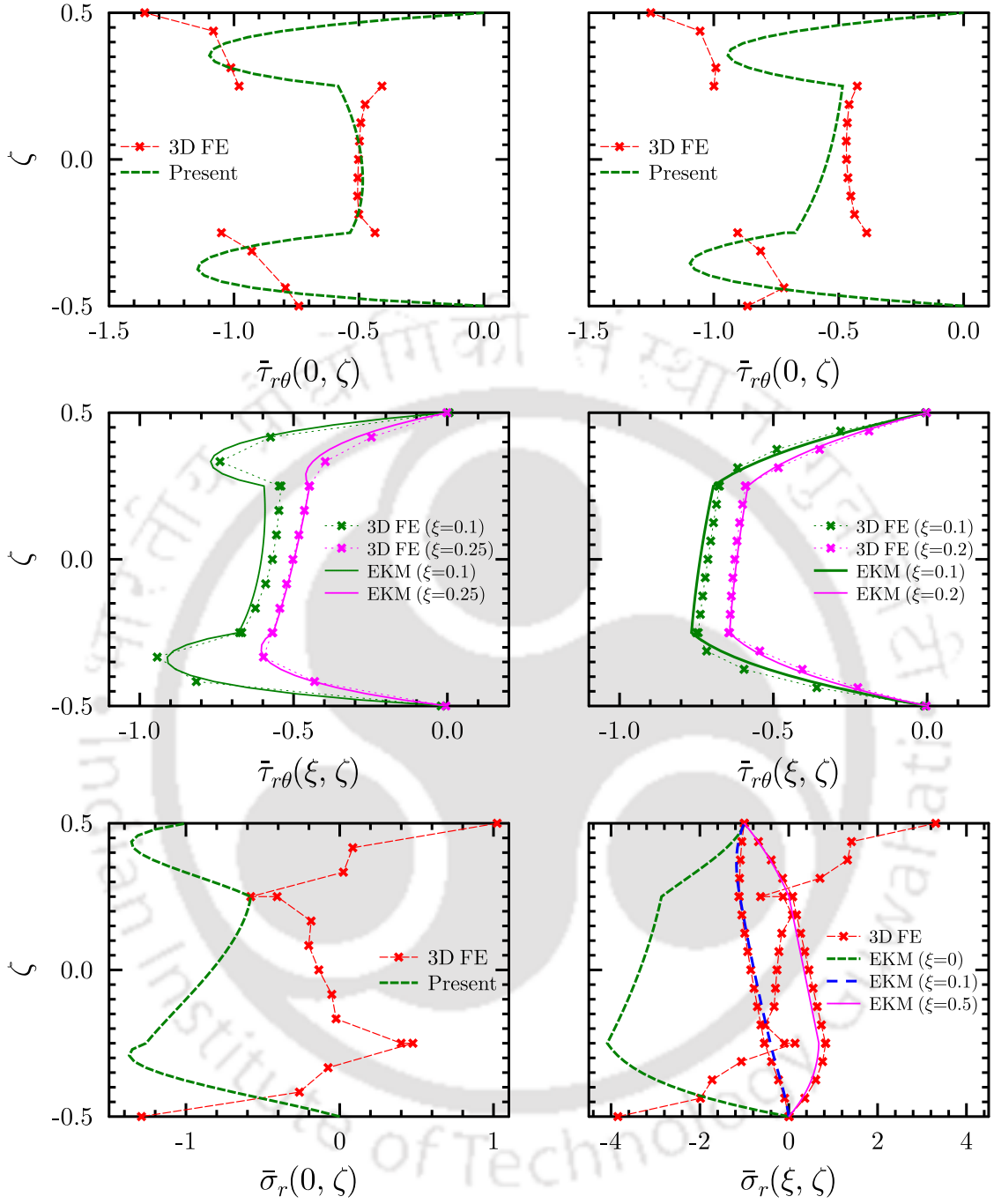

Fig. 3.17: Comparison of stress distribution with 3D FE solutions at the ξ boundaries for a multilayered laminated CS cylindrical shell panel (b) of span 60^0.

the stresses exactly match with 3D FE at locations very near to the clamped edge. In this region, the sudden spike in the transverse stress ($\bar{\tau}_{r\theta}$) at the interfaces of the outer layers is also obtained efficiently which is prime cause of delamination in laminates. Further, all the entities exactly match after this boundary layer region whose span is observed to be proportional to the panel thickness.

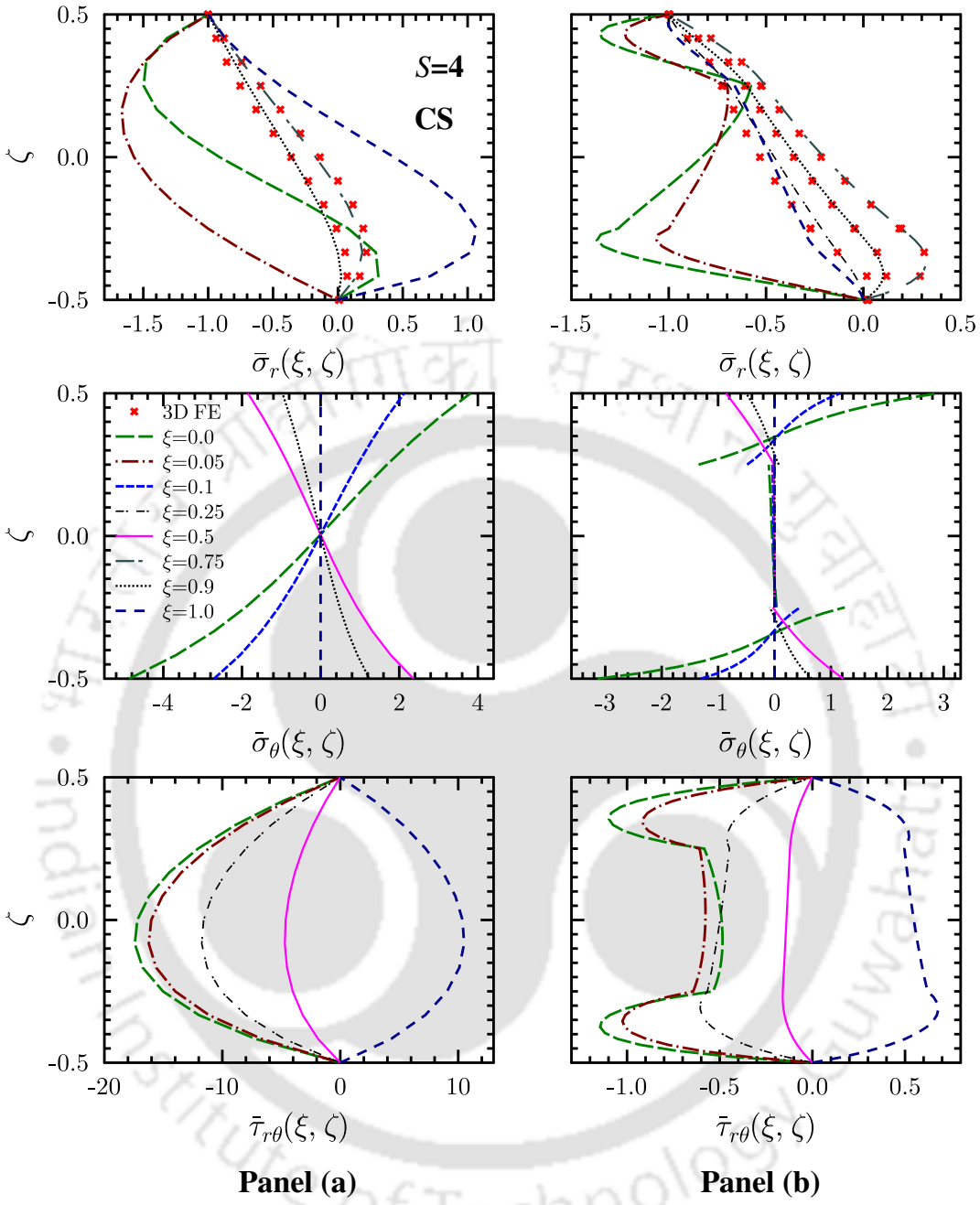

Fig. 3.18: Effect of ξ locations on the through-the-thickness distributions of stresses developed in CS supported thick (S=4) cylindrical shell panels (a) and (b).

Therefore, in case of thinner panel, the agreement between present and 3D FE results are observed from locations closer (as close as ξ=0.1 for panel of S=10) to clamped edge. Similarly $\bar{\sigma}_r$ does not satisfy interface continuity and applied force boundary condition on inner and outer surfaces at the clamped edge of both thick and moderately thick panels (Ref. Fig. 3.17b). $\bar{\sigma}_r$ obtained through present EKM starts matching at ξ locations from (ξ=0.1 for panel of S=10 and beyond ξ=0.25 for

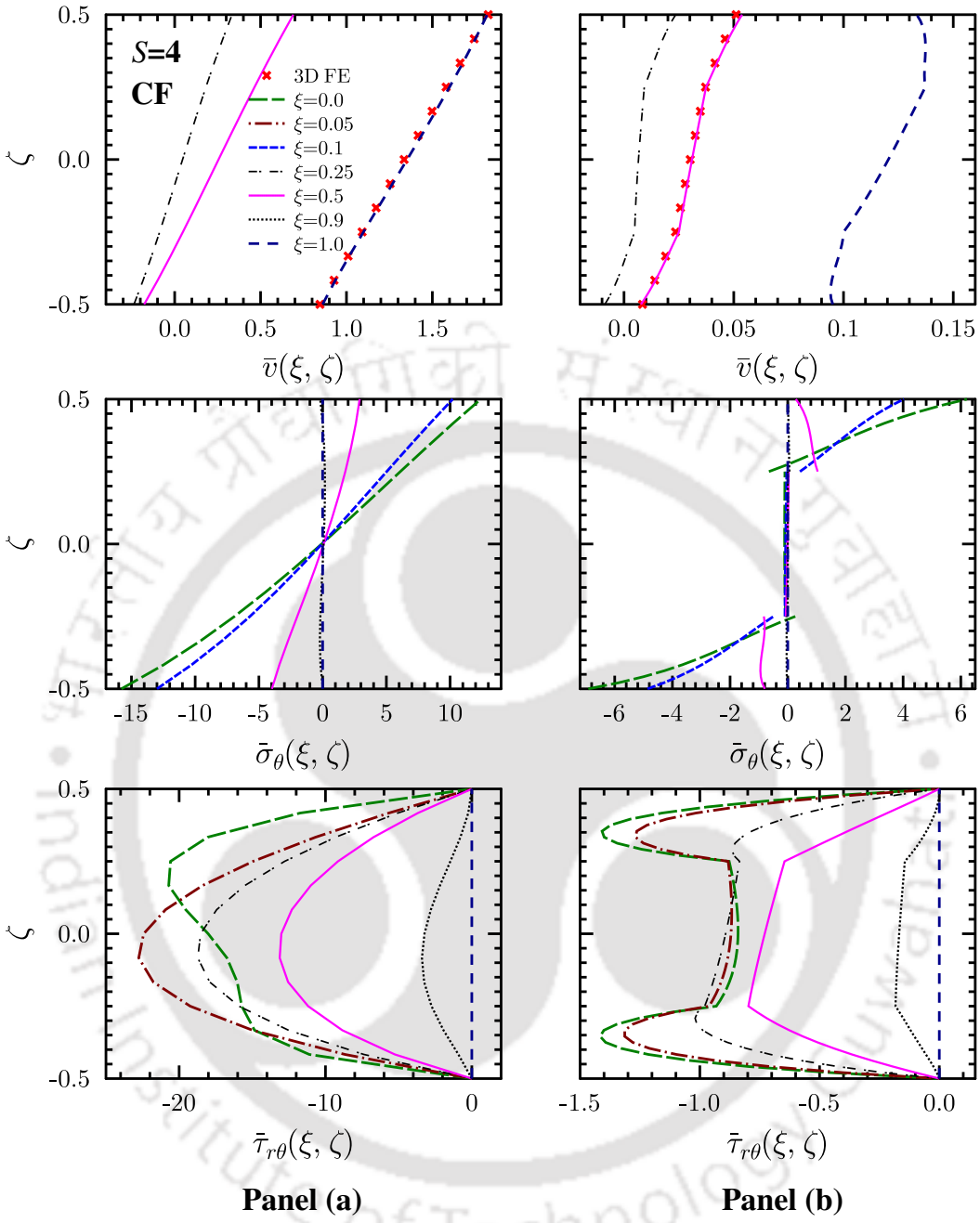

Fig. 3.19: Effect of ξ locations on the through-the-thickness distributions of stresses developed in CF supported thick (S=4) cylindrical shell panels (a) and (b).

panel of S=4 (Ref. Fig. 3.18) which again suggests the presence of boundary layer region near the clamped edge.

Distribution along ξ for CF shell panel is accurately obtained using n=2, but lesser iteration step, *Iter.*=1 is required for both the shell panels as compared to CS configuration.

3.8.1.1 Effect of ξ-location

Pattern of stresses through-the-thickness at various ξ locations (along the circumferential θ span) for a CS shell panel are shown in Fig. 3.18. Thick shell panels (S=4) with laminate scheme (a) & (b) are studied. For panel (b), the nature of distribution of the $\bar{\sigma}_r$ in the vicinity of clamped edge is very different from those at the simply supported edge. Transverse normal stress ($\bar{\sigma}_r$) is predominantly compressive in the upper quarter thickness of the shell on which pressure load is applied, although the slope of distribution varies at different ξ locations. But in the lower quarter thickness of the shell, the distribution of out-of-plane normal stress $\bar{\sigma}_r$ varies from compressive in the vicinity of clamped edge to tensile beyond ξ=0.25 and again compressive at the simply supported edge. Similar pattern is observed for upper quarter thickness of panel (a), but $\bar{\sigma}_r$ varies from being compressive to tensile while moving from clamped to simply supported edge. It is also noted that the present $\bar{\sigma}_r$ distribution matched well with the 3D FE solution beyond ξ=0.25 in the interior, but 3D FE fails completely in predicting $\bar{\sigma}_r$, in the vicinity of the edges. As shown in Fig. Fig. 3.10 & Fig. 3.17, neither the condition of applied normal, nor the continuity condition at layer interfaces were satisfied by FE-predicted stresses. In-plane normal stress ($\bar{\sigma}_\theta$) shows anti-symmetric variation about the mid-surface ζ=0.0 which further changes from tensile at the clamped edge to compressive around the middle in the upper quarter thickness. Transverse shear stress ($\bar{\tau}_{r\theta}$) is observed to be compressive at clamped edge and tensile at the simply supported edge varying parabolically through the thickness.

Similarly distribution of in-plane deformation and stresses at various ξ locations for a cantilevered (CF) panel are plotted in Fig. 3.19. It is found that $\bar{v}$ follows layer-wise (zig-zag) nonlinear variations with slope discontinuities at the layer interfaces for panel (b). This variation is different from global linear or higher order variations assumed in smeared 2D theories. In-plane stress ($\bar{\sigma}_\theta$) is tensile in the upper quarter thickness and compressive in the lower quarter thickness. Out-of plane stress ($\bar{\tau}_{r\theta}$) is predominantly compressive throughout the span of the shell panel.

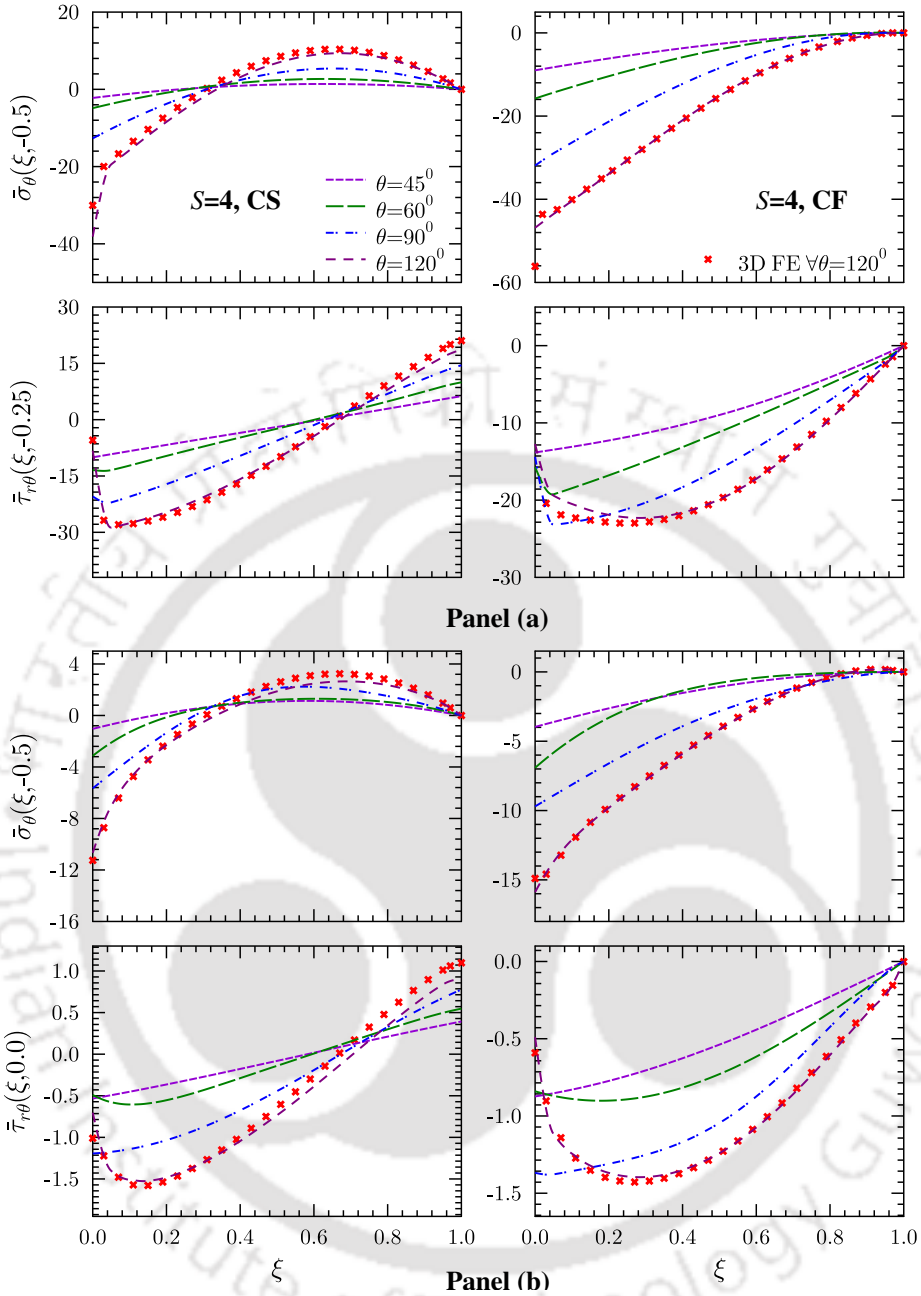

Fig. 3.20: Effect of circumferential span θ on the boundary effects in in-plane and out-of plane stresses for thick (S=4) panels (a) and (b).

3.8.1.2 Effect of θ span on boundary effects of stresses

The effect of span angle on the variation of variables is plotted in Fig. 3.20 for thick panel (a) & panel (b). Unlike SS support, the CS & CF supported shell panels are subjected to boundary effects in developed stresses due to orthotropy. Deformations in deep shells (θ high) are higher than those in shallow shells (θ low), thus stresses developed are also higher in the deep shells. Presently

computed stresses ($\bar{\sigma}_\theta$, $\bar{\tau}_{r\theta}$) matched perfectly with 3D FE also for deep shell panels as shown for $\theta = 120^0$. The extent of boundary effects in both the lay-ups were observed to be independent of circumferential θ span, but were observed to be dependent on the geometric constant S as observed in earlier through thickness plots.

3.8.2 Response of Angle-ply Composite and Sandwich Shell Panel

A single layer angle-ply composite thick cylindrical shell panel is considered for the numerical analysis. Geometrical parameters of the cylindrical shell panel are of circumferential span $\psi = 90^o$, thickness is defined as $S = R/h = 4$ and is considered to be infinitely long along its z-axis. The

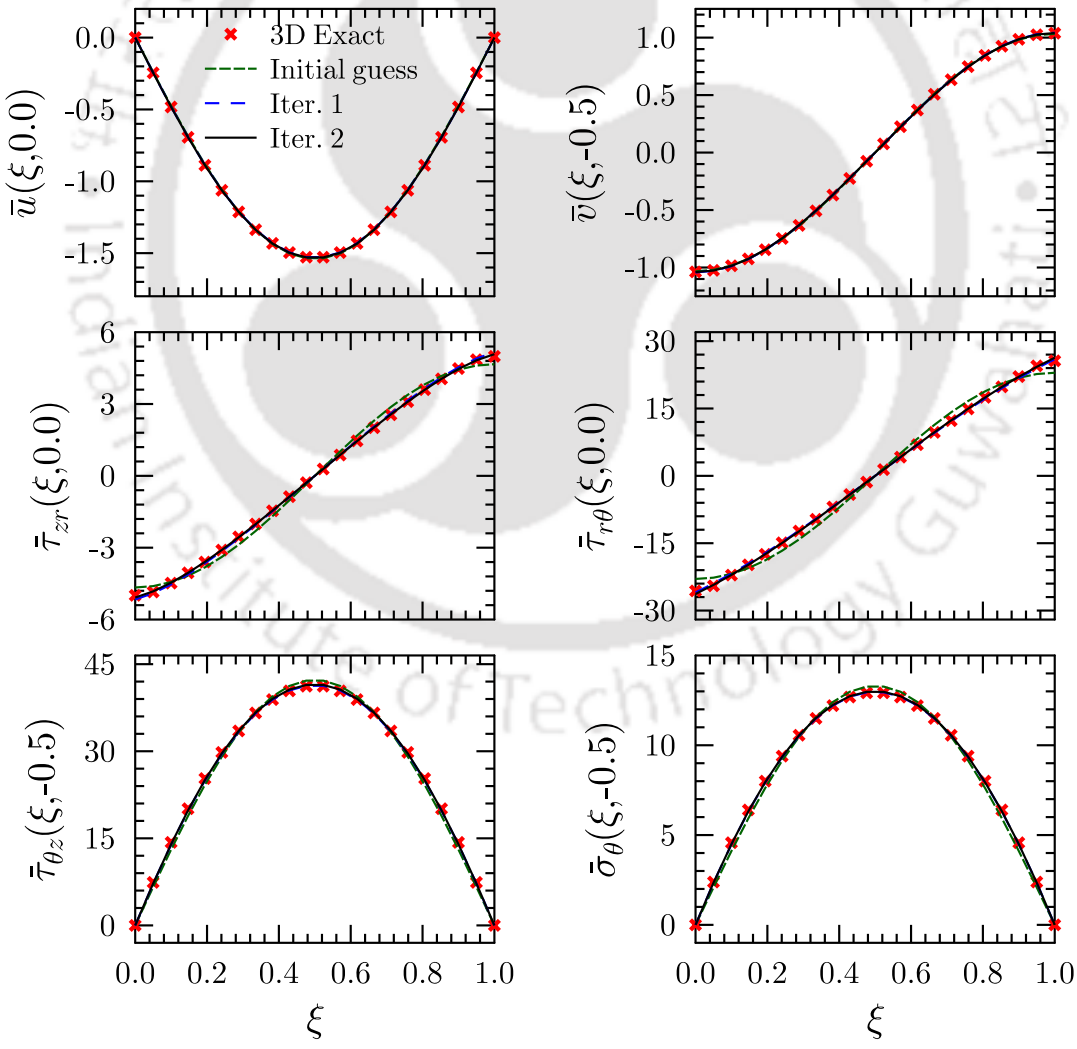

Fig. 3.21: Circumferential variation of deflections and stresses in a thick (S=4) angle-ply cylindrical shell panel (a) of span 90^0 with SS boundary condition.

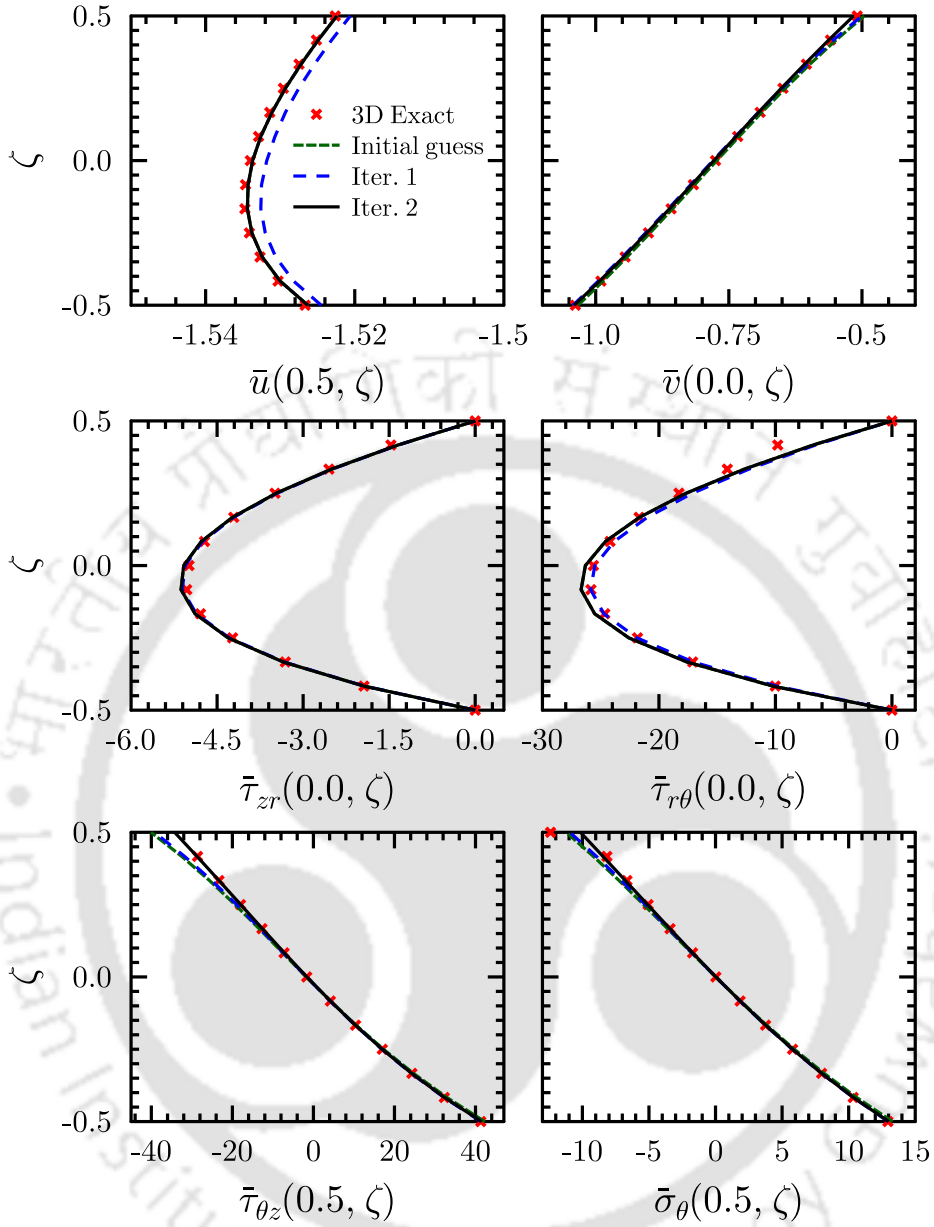

Fig. 3.22: Through-the-thickness variation of deflections and stresses in a thick (S=4) angle-ply cylindrical shell panel (a) of span 90^0 with SS boundary condition.

laminate scheme is similar to that of cylindrical shell panel (a), except for the fibers are oriented at 60^0 here. The shell panel is subjected to an uniformly distributed load (UDL) $p_2(\theta) = 1N/m^2$ on its outer surface. The material properties considered for the study are taken as Mat 2. of Table 3.1 and the nondimensionalization equations for the field variables are as follows:

Non-dim.: $\bar{u} = uY_0/10P_0S^2h$, $\bar{v} = vY_0/10P_0S^2h$, $\bar{\sigma_r} = \sigma_r/P_0$, $\bar{\sigma_\theta} = \sigma_\theta/P_0S^2$, $\bar{\tau_{r\theta}} = \tau_{r\theta}/P_0S$,

$\bar{\tau_{zr}} = \tau_{zr}/P_0$ and $\bar{\tau_{\theta z}} = \tau_{\theta z}/P_0$, $(Y_0 = Y_T \ \& \ P_0 = p_2(\theta))$.

Again, for comparing the presently obtained results, 3D exact results are used for simply-supported shell panel [83]. For comparing the results corresponding to the arbitrarily supported shell panel, the 3D FE results through ABAQUS [256] model analysis are used which is build similar

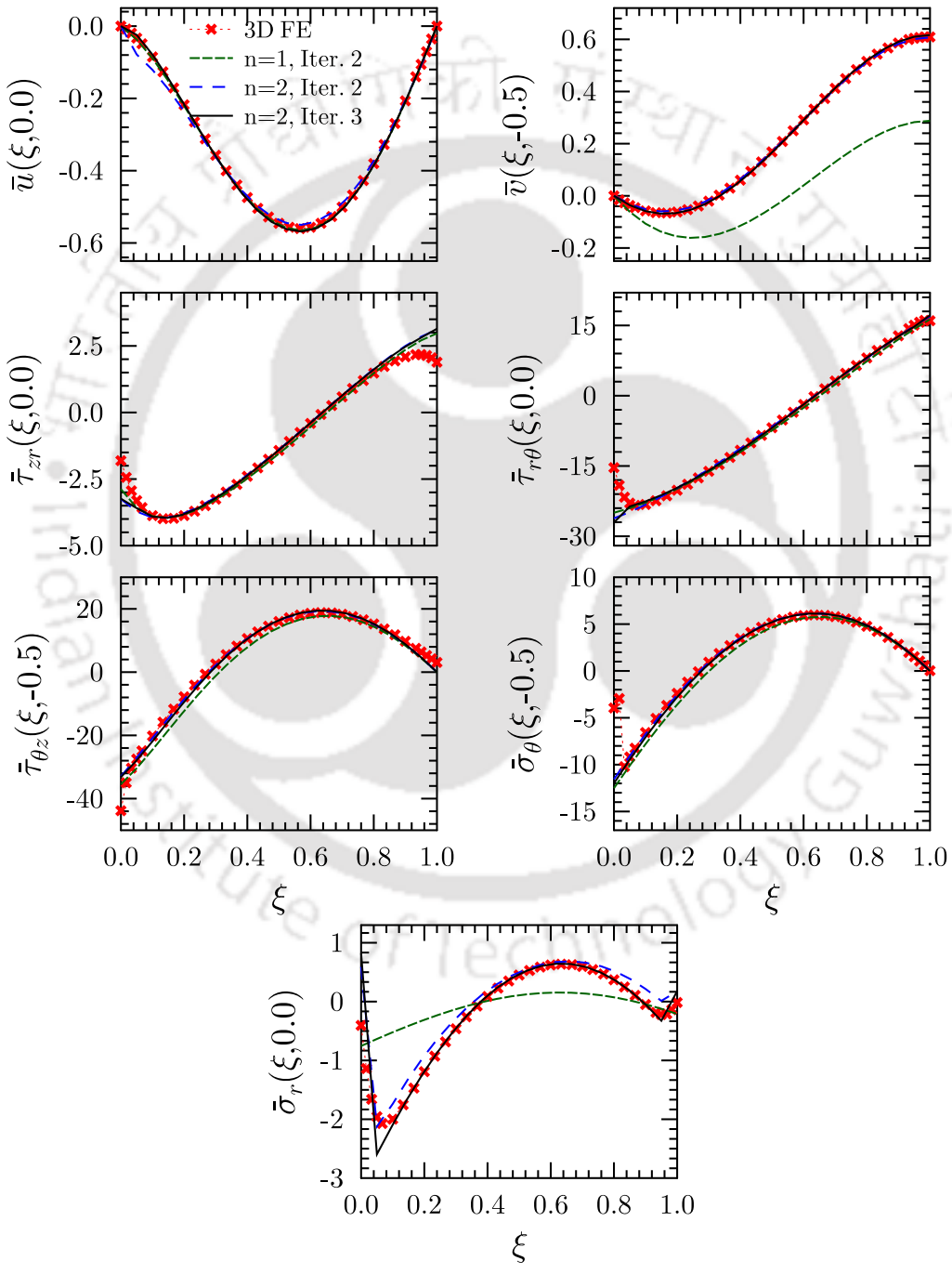

Fig. 3.23: Circumferential variation of deflections and stresses in a thick (S=4) angle-ply cylindrical shell panel (a) of span 90^0 with CS boundary condition.

to that done previously in Sec. 3.7.1 with equal mesh size.

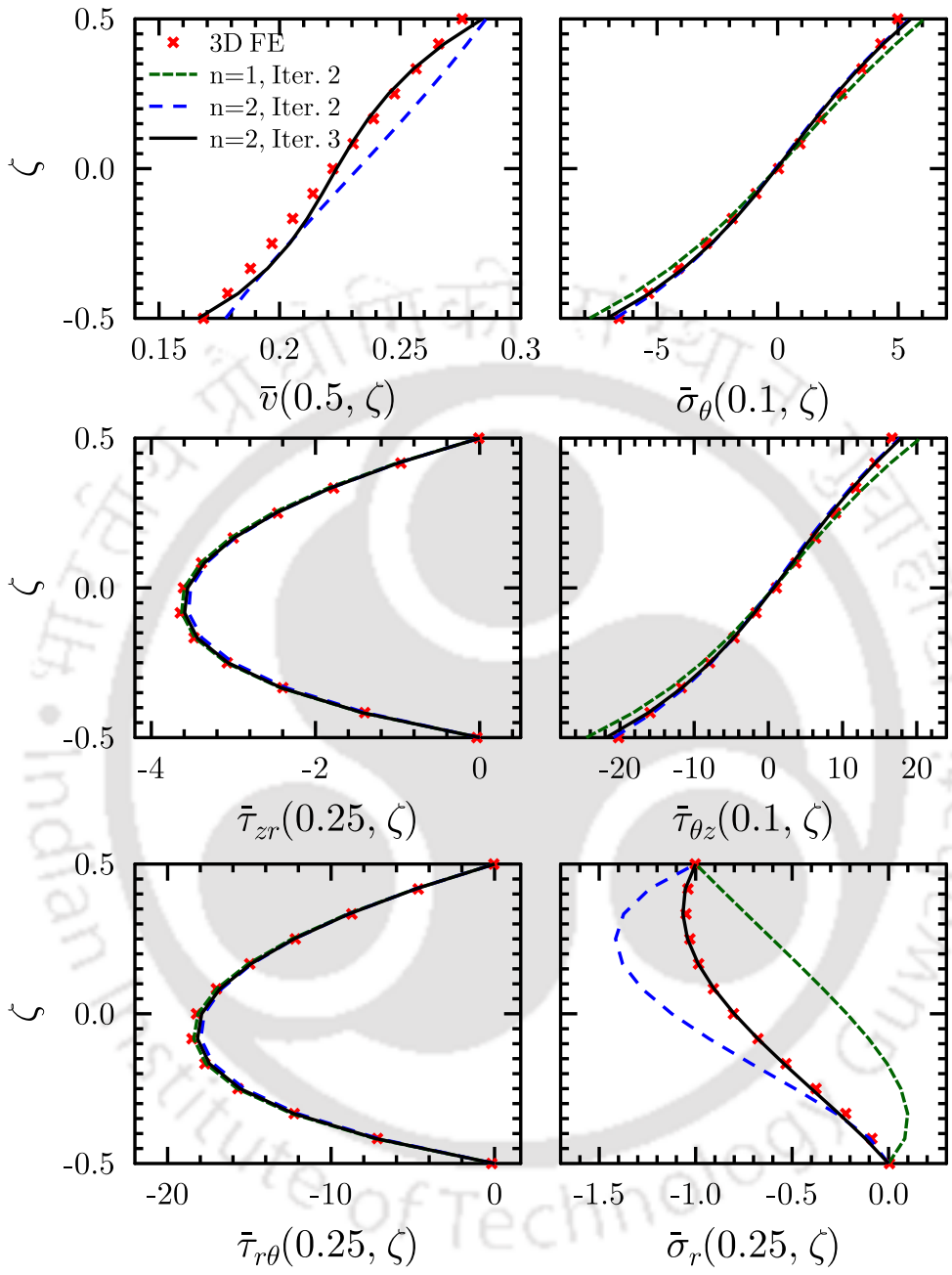

Fig. 3.24: Through-the-thickness variation of deflections and stresses in a thick (S=4) angle-ply cylindrical shell panel (a) of span 90^0 with CS boundary condition.

For a thick ($S = 4$) SS shell panel (a), the circumferential variation of displacements & stresses are plotted in Fig. 3.21. 3D exact results for this case are available and are generated from the Ref. [83]. On comparing the presently developed results of the multiterm EKM with the 3D exact

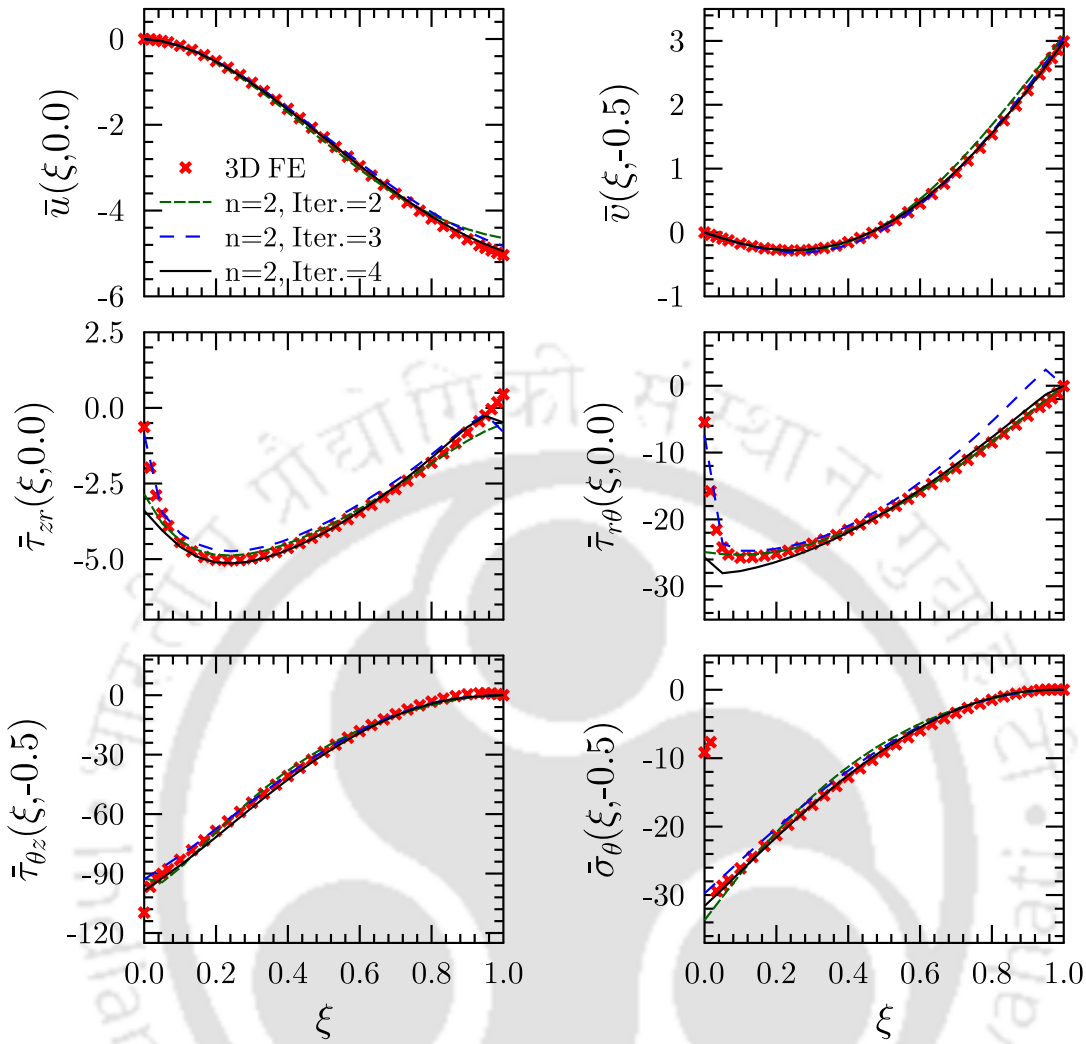

Fig. 3.25: Circumferential variation of deflections and stresses in a thick (S=4) angle-ply cylindrical shell panel (a) of span 90^0 with CF boundary condition.

ones an excellent match between them is seen. This is shown in Fig. 3.21 for all the field variables ($\bar{v}, \bar{u}, \bar{\sigma}_\theta, \bar{\tau}_{r\theta}, \bar{\tau}_{zr}, \bar{\tau}_{\theta z}$) where they are maximum at a radial coordinate for all the corresponding ξ of the shell panel. Through-the-thickness variation of these variables are also plotted and compared in Fig. 3.22. As can be observed, excellent match throughout the domain of the shell panel between 3D exact and presently developed multiterm EKM solution is noteworthy. It should be noted that the results are accurate even for a thick shell panel in both through-the-thickness and circumferential directions. Further as shown in the Figs. 3.21 & 3.22, the EKM results are obtained with just one term (n=1) in the multiterm expansion and the solution converged within 2 iterations ($Iter.$=1/2).

On the other hand, the generated 3D exact solution converged after considering 21 non-zero Fourier terms in the single Fourier series expansion along circumferential direction for the shell panel under UDL. This proves the computational power of the presently developed solution with excellent accuracy in analysis of the present problem. Moreover, the multiterm EKM solution is valid for other arbitrarily supported cylindrical shell panels unlike the 3D exact Fourier series based solution applicable for solving only the SS case.

Table 3.3: Convergence of present multi-term EKM for arbitrarily supported angle-ply shell panels (S=4) of span ($\psi = \pi/2$) under UDL= $1Nm^{-2}$.

			SS			
Entities	$\bar{u}(0.5, 0.0)$	$\bar{v}(0.0, -0.5)$	$\bar{\sigma}_\theta(0.5, -0.5)$	$\bar{\tau}_{\theta z}(0.5, -0.5)$	$\bar{\tau}_{zr}(0.0, 0.0)$	$\bar{\tau}_{r\theta}(0.0, 0.0)$
3D Exact [83]	-1.5325	-1.0381	12.947	41.3	-4.99425	-25.624
n=1, Iter. 1	-1.5317	-1.0426	12.976	41.368	-5.1624	-25.963
n=1, Iter. 2	-1.5337	-1.0402	13.003	41.516	-5.0819	-26.313
n=1, Iter. 3	-1.5337	-1.0402	13.003	41.513	-5.0820	-26.313
			CS			
Entities	$\bar{u}(0.5, 0.0)$	$\bar{v}(1.0, -0.5)$	$\bar{\sigma}_\theta(0.1, -0.25)$	$\bar{\tau}_{\theta z}(0.1, -0.25)$	$\bar{\tau}_{zr}(0.25, 0.0)$	$\bar{\tau}_{r\theta}(0.25, 0.0)$
3D FE [256]	-0.5457	0.60916	-2.95067	-7.93384	-3.60878	-18.2288
n=2, Iter. 2	-0.5502	0.60742	-2.7258	-7.7202	-3.5216	-17.760
n=2, Iter. 3	-0.5531	0.61655	-2.7451	-7.8645	-3.5580	-17.915
			CF			
Entities	$\bar{u}(0.5, -0.5)$	$\bar{v}(1.0, 0.5)$	$\bar{\sigma}_\theta(0.25, -0.25)$	$\bar{\tau}_{\theta z}(0.25, -0.5)$	$\bar{\tau}_{zr}(0.25, 0.0)$	$\bar{\tau}_{r\theta}(0.25, 0.0)$
3D FE [256]	-2.29660	4.39768	-8.8718	-61.2760	-5.0500	-24.4726
n=2, Iter. 3	-2.2443	4.5965	-8.4096	-60.541	-4.4687	-24.336
n=2, Iter. 4	-2.2873	4.3778	-8.5991	-60.467	-4.7380	-25.455

The response of the same shell panel considered above but, with arbitrarily supported circumferential boundary edges is studied next. Cylindrical bending of the single layer angle-ply panel is analysed under similar loading. The variation of the displacements $(\bar{v}, \bar{u})$ and the corresponding stresses $(\bar{\sigma}_\theta, \bar{\sigma}_r, \bar{\tau}_{r\theta}, \bar{\tau}_{zr}, \bar{\tau}_{\theta z})$ developed along the circumference are presented in the Fig. 3.23 for CS case. In the figure, the results obtained from the presently developed solution are shown and compared with 3D FE results. The multiterm EKM results of different terms (n) and iterations ($Iter.$) are seen to converge and there is exact match between the two results. Throughout the ξ span, the

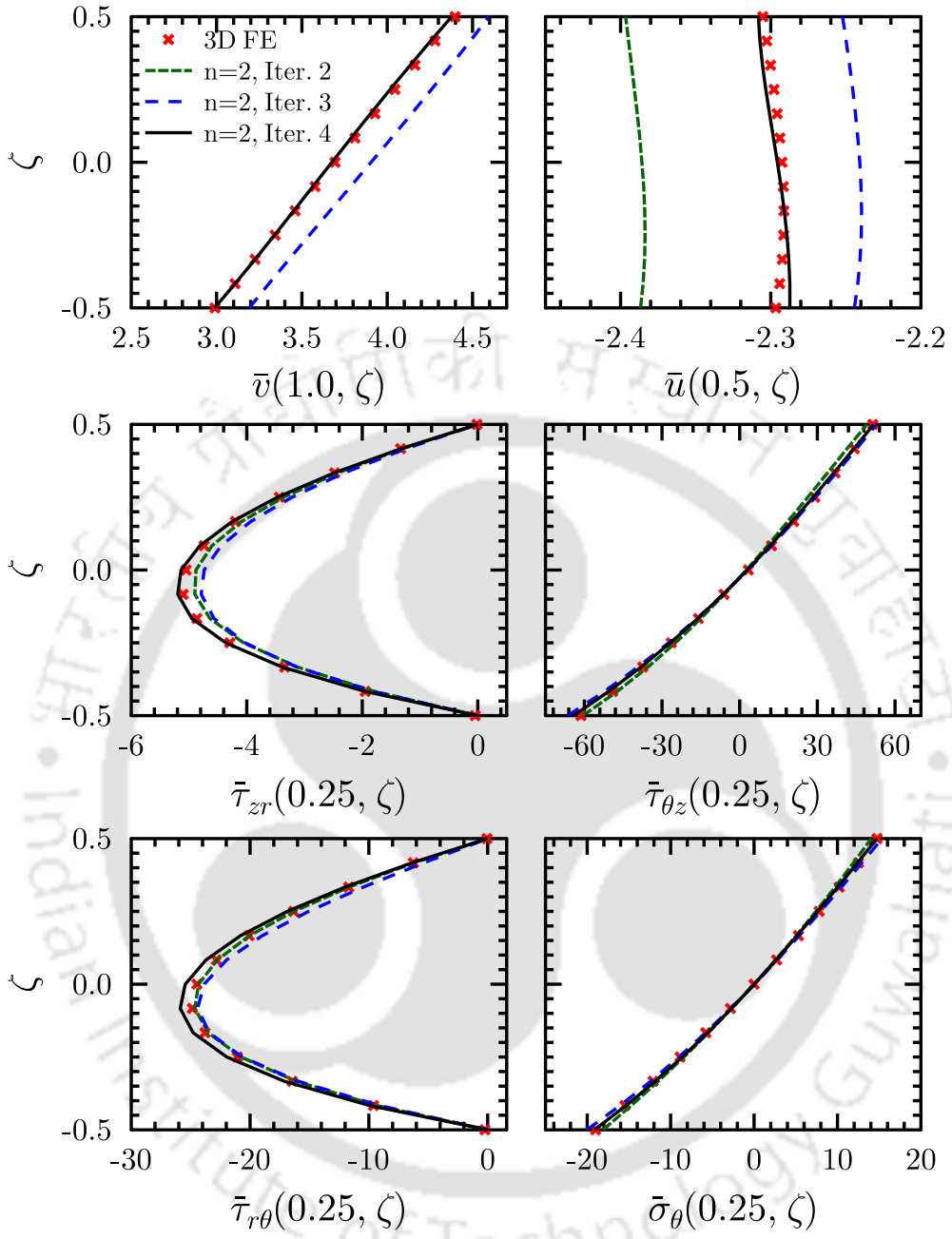

Fig. 3.26: Through-the-thickness variation of deflections and stresses in a thick (S=4) angle-ply cylindrical shell panel (a) of span 90^0 with CF boundary condition.

displacements ($\bar{v}, \bar{u}$) match exactly. However, although the stresses ($\bar{\sigma}_\theta, \bar{\sigma}_r, \bar{\tau}_{r\theta}, \bar{\tau}_{zr}, \bar{\tau}_{\theta z}$) matched for most part of the ξ span, it is deviated in the very vicinity of the clamped edge (ξ=0). Earlier, it has been verified that the numerical solution (3D FE) is not consistent with the traction boundary conditions on R_o & R_i surfaces at and very near to the clamped edge (ξ=0). Subsequently, two

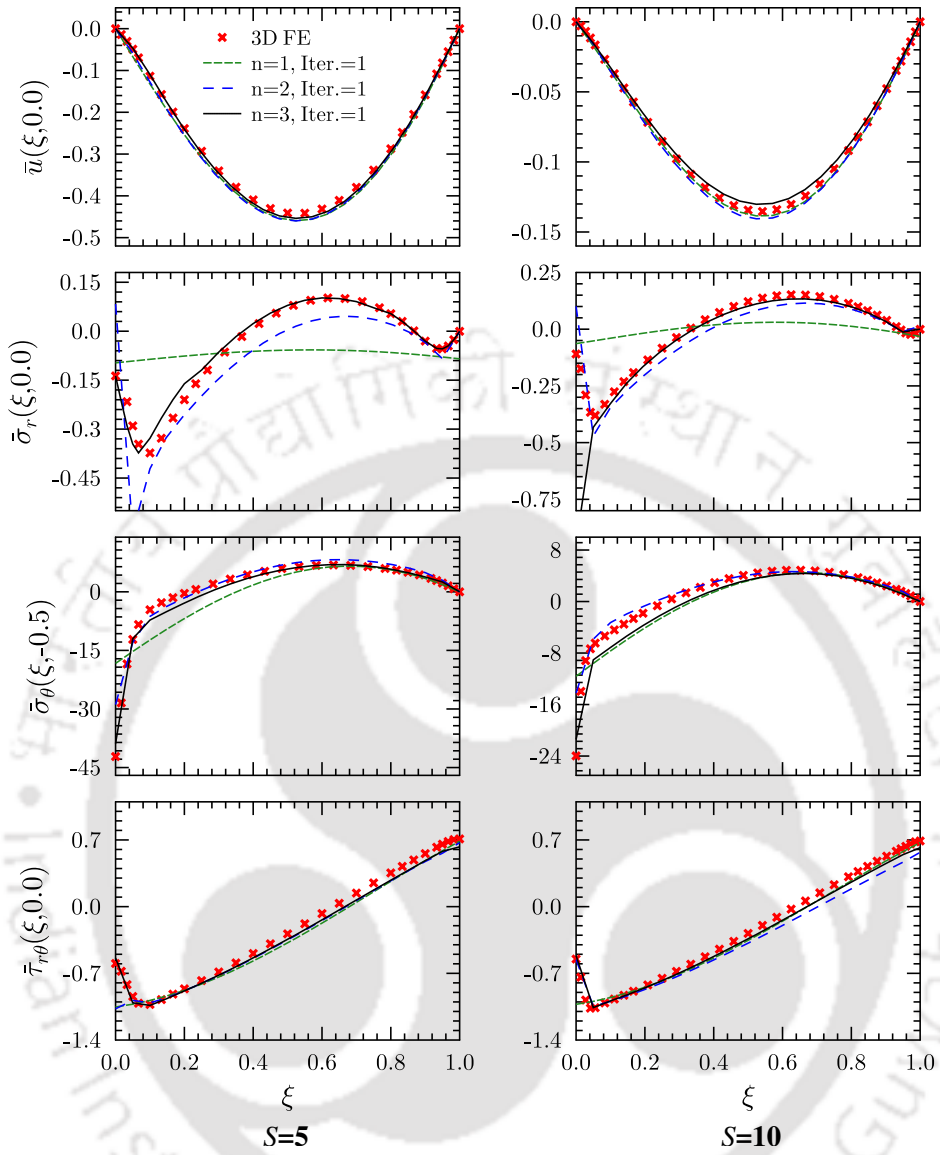

Fig. 3.27: Circumferential variation of deflections and stresses in cylindrical shell panel (d) (S=5, 10) of span 90^0 with CS boundary condition.

solutions match where 3D FE solution is consistent with boundary and interface continuity conditions, at some distance away from the clamped edge [258]. There, it was also inferred that this distance is dependent on the thickness S of the shell panel. Therefore, through-the-thickness variation of the stresses are compared at ξ locations where the 3D FE satisfies the concerned boundary and interface continuity conditions in Fig. 3.24 for the CS shell panel. The displacements and stresses accurately match throughout the thickness for the thick shell panel. Similar studies are conducted for the CF shell panel with similar configuration and loading. The circumferential and

through-the-thickness variations are represented in Figs. 3.25 & 3.26, respectively. Similar edge effects are also observed at the clamped edge (ξ=0) of the CF panel. But, the multiterm EKM results converge and match excellently with the 3D FE results at other locations throughout the domain of the shell panel. Further, the edge effects are also predicted near the clamped edge which is consistent with the outer and inner surface boundary condition at ξ=0. Apart from accurate prediction of mechanical response by the multiterm EKM, its computational power is also elegant. Realising that only n=1 was enough for the SS case, addition of just one more term in the multiterm expansion (n=2), exactly predicted the results for the arbitrarily supported (CS, CF) cylindrical shell panels. However, comparably higher number of iterations are required for the CF and CS cases. This is because in the present case the initial trial functions (f^i) are chosen such that they satisfy the simply supported boundary conditions at $\xi = 0, 1$ in the first iteration. For CS & CF shell panels one or two extra iterations are required. However, it should be noted that the initial choice of f^i do not require them to satisfy any boundary condition. For ill-chosen f^i the result will converge after few more iterations. This is the beauty of this powerful EKM solution. The convergence for the present solution can be studied from Table 3.3.

In general, the stresses developed in the CF panel are larger than those for CS and SS panels as both in-plane and out-of plane deflections are higher in CF panel. Further, following the constitutive relation for the angle-ply laminate, the developed transverse stresses ($\bar{\tau}_{r\theta}, \bar{\tau}_{zr}$) are larger corresponding to larger strain in the CF panel compared to CS & SS panels. However, the inplane normal stress ($\bar{\sigma}_\theta$) developed in the SS panel is higher than that in the CS panel in the mid-span of the shell panel. The transverse normal stress ($\bar{\sigma}_r$) follows a non-linear trend through-the-thickness of the shell panel.

The cylindrical shell panels with sandwich laminate (i.e., shell panel (d)) are also analysed in a similar fashion as done for other laminates. Typical benchmark results for the arbitrarily supported shell panel has been presented. The face sheets are of $0.05h$ on the outer and inner surfaces of the shell panel and the core is made up of Klegecell foam which has thickness of $0.9h$.

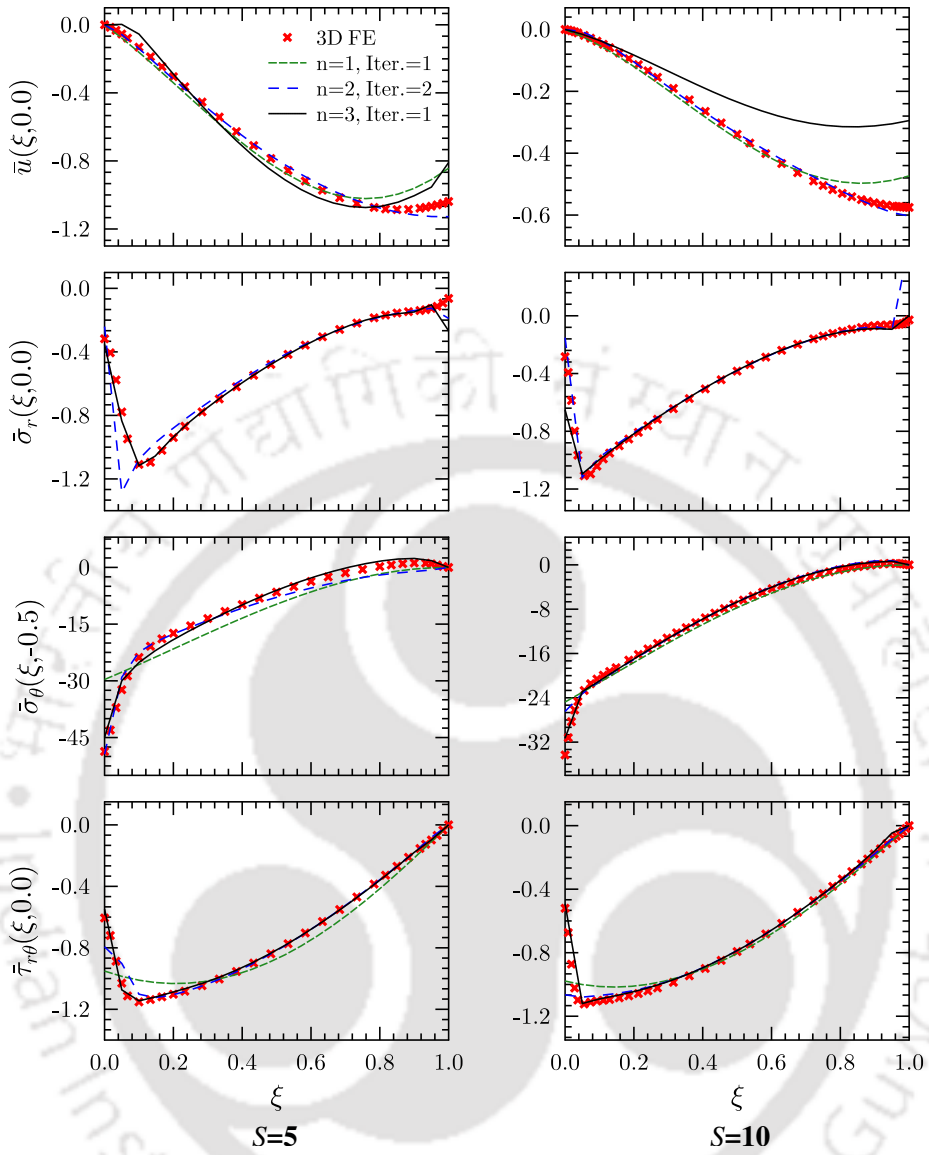

Fig. 3.28: Circumferential variation of deflections and stresses in cylindrical shell panel (d) (S=5, 10) of span 90^0 with CF boundary condition.

The circumferential span is ψ=90^o. For non-dimensionalization, $Y_0 = Y_2$ of core is taken. The material properties are take from the Table 3.1. The circumferential deflection and stress variation along the θ direction are plotted in Fig. 3.27 for CS configuration and under same loading the variations for the CF shell panel is shown in the Fig. 3.28 for a thick S=5 and moderately thick S=10 thicknesses. Through-the-thickness plot for thick S=5 sandwich laminates has been depicted in the Fig. 3.29 for CS and CF cases. On further analysing, the stress varies abruptly corresponding to the layerwise inhomogeneity as this is more pronounced in sandwich laminates which possess

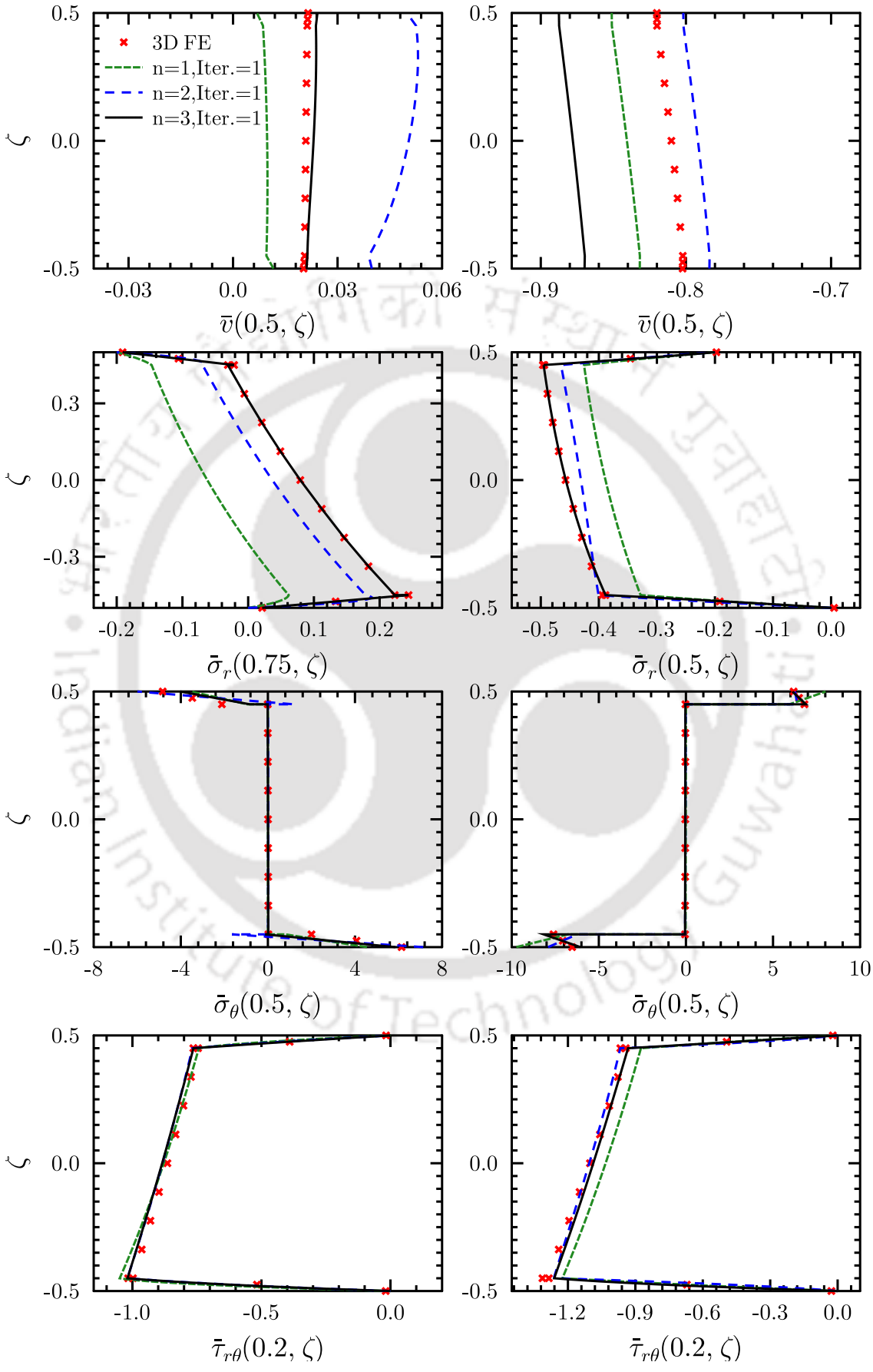

Fig. 3.29: Through-the-thickness variation of deflections and stresses in a thick (S=5) sandwich cylindrical shell panel (d) of span 90^0 with CS (left), CF (right) boundary condition.

substantial change in material properties in the face sheet and core across the interface. Unlike, previous cases where interest lies on accurate prediction of non-linear variations of field variables through-the-thickness or large variations in the transverse stresses at the boundary layer region for angle-ply laminates, computing the drastic interfacial stress variation in the sandwiched laminates is predominantly important. Furthermore, the edge effects are also very accurately predicted as can be inferred from the circumferential plots. This study can help in designing the face sheet of appropriate thickness and appropriate adhesive strength required to instill the structural integrity of sandwiched laminates.

3.9 SUMMARY

An elasticity based 3D solution has been developed and its extensive numerical study has also been done for different composite laminates, angle-ply and sandwich schemes. This novel 3D solution provides computationally faster and accurate results in case of arbitrarily supported cylindrical shells. Further, some benchmark results are presented which can be beneficial for assessing other theories.

By application of the extended Kantorovich method along with mixed formulation based on displacements and stresses, it has been generalised to obtain 3D analytical solution for static bending of thick, moderately thick and thin cylindrical shell panels. In the formulation of this 3D analytical elasticity solution, power series is used to solve the ODE through-the-thickness and ODE along the circumference is solved using the Pagano's approach. A single-term EKM solution was not in good agreement with the 3D FE results for CS and CF shell panels although for SS shell panels it was very accurate. To predict the boundary layer effect in the laminates, multiple number of terms in the expression for EKM has been proposed and extensive numerical study has been conducted. In spite of multi-term formulation, just one more term could predict the boundary effects and other stress concentration zones near exactly, where 3D FE results were affected because it did not satisfy the traction boundary conditions on the inner and outer surfaces at and near the clamped

edge. Similar observations were found for arbitrarily supported angle-ply, cross-ply and sandwich composite shell panels. In addition, the solution converged within few iterations with n=2 terms which proves it to be computationally powerful as compared to other numerical solutions. The 3D exact solution required more than 20 number of Fourier terms for solving SS boundary case.

The cross-ply laminated composite shell panel showed abrupt change in nature of the stresses from compressive to tensile at the clamped edge which should be considered during design of laminates. In general, CF shell panels are subjected to higher stresses. The interlaminar transverse stresses could also be minimised by optimal choice of ply-angle. In case of deep shell panels the deflections are larger and a larger boundary layer region is formed. In case of sandwiched laminated composite, there is abrupt change in stress at the interface through the thickness. The present 3D solution can be readily employed for pursuing structural data analyses.

Chapter 4

Three-dimensional analytical solution of cylindrical shell panels with interlaminar weak interfaces

4.1 INTRODUCTION

In this chapter, an infinitely long laminated composite cylindrical shell panel with imperfectly bonded laminae and having arbitrary boundary conditions is considered for investigating its static response. In the frame of cylindrical coordinate system, a generalized 3D analytical elasticity solution is developed for the cylindrical shell panel consisting of imperfectly bonded composite plies, which is an advancement over previously developed solution for those with perfectly bonded plies [258]. Based on the Reissner's-type mixed variational principle, the governing equations are derived which consistently include the contribution of bonding imperfection. Imperfect bonding at the interface is modeled using the linear spring-layer model and the governing PDEs are converted into sets of non-homogeneous first order ODEs by applying the multi-term EKM. One of the sets of ODEs obtained along the radial direction has variable coefficients and the set along the circumferential direction are constant coefficient ODEs. These are solved iteratively using different approaches as presented by Kumari et al. [206, 258]. After validation with available results for simply-supported panels, the convergence of the presently developed solution is studied for arbitrary boundary conditions. Further, parametric study is also conducted to study the design aspects.

The utilization of a mixed type variational equation in this technique allow boundary conditions to be satisfied exactly at all points unlike displacement based ones where they are satisfied

only averagely. Consequently, near-exact prediction of stresses at the interlaminar interfaces and other stress concentration locations has been achieved. Moreover, the partial differential equations (PDE)s are converted to the ordinary differential equations (ODE)s which reduces the complexity and allows to get closed-form solutions. Earlier, Kapuria and Dhanesh [259] had investigated the effect of imperfect bonding at the lamina interface by developing a 3D solution for arbitrarily supported plates using the multi-term EKM. Hence, a similar solution for the shells has been developed here and the physical aspects of bonding imperfection in cylindrical shell panels made up of laminated composites are studied.

4.2 CYLINDRICAL SHELL PANEL WITH WEAK INTERFACES

Consider an infinitely long L-layered composite cylindrical shell panel (Fig. 4.1) of circumferential span ψ along θ-axis, total thickness h and mid-surface radius at R along the radial r-axis from the origin on z-axis. $R_i, R_o = R \mp h/2$ are the inner and outer surface radii of the panel, respectively.

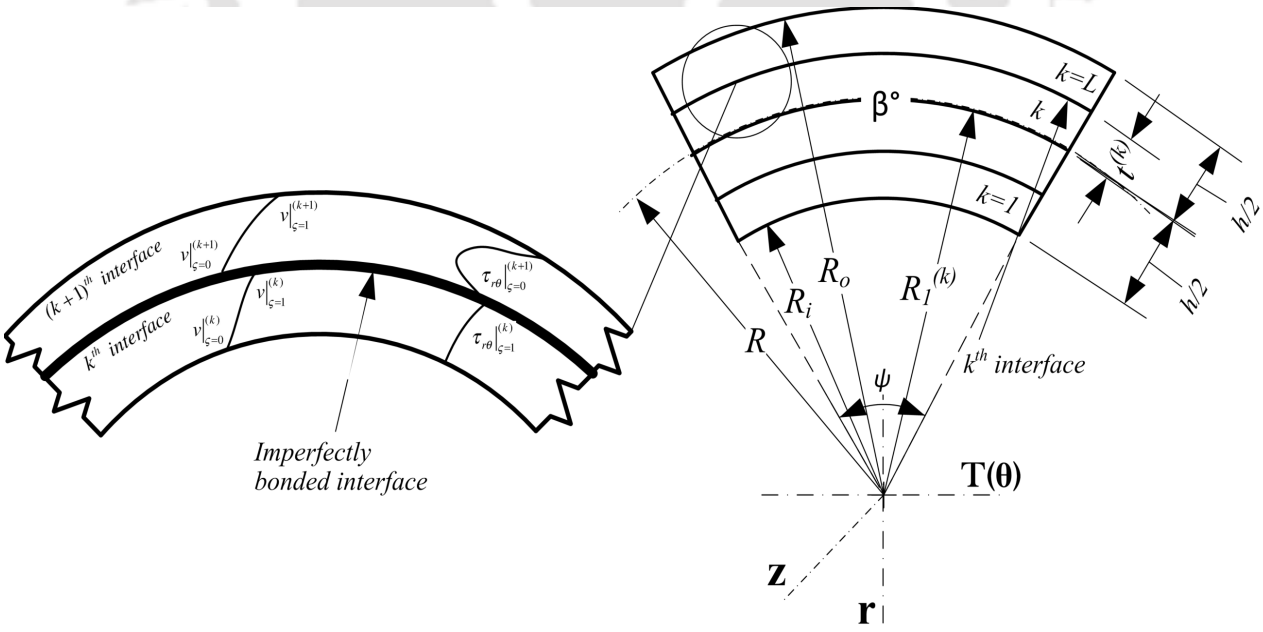

Fig. 4.1: Geometry of weakly bonded cylindrical shell panel and typical trend of field entities at the imperfectly bonded interface.

The kth layer numbered from the inner surface of the panel is of thickness $t^{(k)}$ and has its inner

surface at a radius of $R_1^{(k)}$. The layers are orthotropic with their fibre axis orientated at an angle of $\beta^{(k)}$ from the θ-axis. Hence, for kth layer, a 3D linear elastic constitutive relation between the induced normal, shear stresses ($\sigma_i^{(k)}$& $\tau_{ij}^{(k)}$) and the corresponding strains ($\varepsilon_i^{(k)}$ & $\gamma_{ij}^{(k)}$) for $i, j = \theta, z, r$ is given as

$$\begin{bmatrix} \varepsilon_\theta^{(k)} \\ \varepsilon_z^{(k)} \\ \varepsilon_r^{(k)} \\ \gamma_{zr}^{(k)} \\ \gamma_{r\theta}^{(k)} \\ \gamma_{z\theta}^{(k)} \end{bmatrix} = \begin{bmatrix} \bar{s}_{11} & \bar{s}_{12} & \bar{s}_{13} & 0 & 0 & \bar{s}_{16} \\ \bar{s}_{12} & \bar{s}_{22} & \bar{s}_{23} & 0 & 0 & \bar{s}_{26} \\ \bar{s}_{13} & \bar{s}_{23} & \bar{s}_{33} & 0 & 0 & \bar{s}_{36} \\ 0 & 0 & 0 & \bar{s}_{44} & \bar{s}_{45} & 0 \\ 0 & 0 & 0 & \bar{s}_{45} & \bar{s}_{55} & 0 \\ \bar{s}_{16} & \bar{s}_{26} & \bar{s}_{36} & 0 & 0 & \bar{s}_{66} \end{bmatrix}^{(k)} \begin{bmatrix} \sigma_\theta^{(k)} \\ \sigma_z^{(k)} \\ \sigma_r^{(k)} \\ \tau_{zr}^{(k)} \\ \tau_{r\theta}^{(k)} \\ \tau_{z\theta}^{(k)} \end{bmatrix} \tag{4.1}$$

where $\bar{s}_{ij}^{(k)}$ ($\forall\ i, j = 1-6$) are the components of transformed compliance matrix from material $(1, 2, 3)$ to cylindrical panel coordinate system (θ, z, r). Compliances are expressed in terms of engineering constants namely Young's, shear moduli ($Y_i^{(k)}$, $G_{ij}^{(k)}$) and major Poisson's ratios $\nu_{ij}^{(k)}$ [260]. For a cross-ply lamina, $\bar{s}_{i6}^{(k)} = \bar{s}_{45}^{(k)} = 0$ ($\forall\ i = 1-3$). Furthermore, the kth interface condition between (k) & $(k+1)$th layer at $r = R_1^{(k+1)}$ is considered to be imperfectly bonded, uniformly.

4.2.1 Modeling of imperfectly bonded interface

The displacement field u_i ($\forall\ i = \theta, z, r$) for the cylindrical panel has components v, w and u along θ, z and r coordinate directions, respectively. As there is an imperfect bonding at the kth interface, a normal & two tangential displacement jumps ($\Delta u_i^{(k)}$) are introduced. However, assuming the interface to be made up of a zero thickness adhesive layer, the transverse stresses ($\sigma_{3i}^{(k)}$) on either side of the interface are in equilibrium. Pertaining to which the stress continuity relations are established in form of

$$\sigma_{3i}^{(k+1)} = \sigma_{3i}^{(k)} \quad \& \quad \text{displacement jumps as } \Delta u_i^{(k)} = u_i^{(k+1)} - u_i^{(k)} \quad \text{at } k\text{th interface} \tag{4.2}$$

In the present work, the linear spring-layer model [165] is adopted to model the imperfectly bonded interface. According to which, a linear relation between $\sigma_{3i}^{(k)}$ and $\Delta u_i^{(k)}$ through a nonnegative interfacial bonding stiffness coefficient ($K_i^{(k)}$) is expressed as [143, 261]

$$\sigma_{3i}^{(k)} = K_i^{(k)} \Delta u_i^{(k)} \quad (\forall\ i = \theta, z, r) \tag{4.3}$$

and no summation over i is obeyed. Conventionally, $K_i^{(k)}$ is determined through experiments but, Lu and Liu [262] had also proposed a model for its estimation from the mechanical properties and geometry of the adhesive layer. A large value of $K_i^{(k)} \to \infty$ physically represents a perfect bonding whereas $K_i^{(k)} = 0$ indicates the case of complete debonding between the adjacent layers. Cases such as interlaminar shear slips are represented by nonzero tangential components $K_\theta^{(k)}$, $K_z^{(k)}$ and normal opening delamination by the normal component $K_r^{(k)} \geq 0$, respectively. $K_r^{(k)} = 0$ is imposed to ensure no material penetration in case of $\sigma_{rr}^{(k)} < 0$. Presently, an interface compliance $\bar{\mathbf{R}}_i^{(k)} = 1/c_{22}^{(1)} K_i^{(k)} h$ is defined for parametric study in terms of stiffness coefficient $c_{22}^{(1)}$ corresponding to the normal strain along z direction caused due to the normal stress along same direction in the material of $(k = 1)$th layer. Henceforth, layer superscript (k) is omitted for brevity, unless required.

4.2.2 Governing equations

The Reissner's-type mixed variational principle for a cylindrical shell is used to derive the governing equations of motion. Mixed variational principle includes both displacements and stresses as the primary variables. Hence, advantageously all the field variables are computed with equal order of accuracy pointwise unlike the displacement based variational principles. An uniformly distributed load (UDL) invariant along z-axis is applied, which are of the magnitude of p_1 & p_2 acting on inner and outer surfaces of a cross-ply cylindrical shell panel, respectively. It undergoes a cylindrical bending and the components of the geometrical strain (ε_{ij}^G) are obtained from the following strain displacement relations

$$\varepsilon_\theta = (u + v_{,\theta})/r,\ \varepsilon_z = 0,\ \varepsilon_r = u_{,r},\ \gamma_{r\theta} = (u_{,\theta} - v)/r + v_{,r},\ \gamma_{zr} = \gamma_{\theta z} = 0 \tag{4.4}$$

These are reduced since all the field variables are independent of z and $w = 0$ gives $\gamma_{zr} = \gamma_{\theta z} = 0$. Note that subscript comma is used to designate partial differentiation of the field variable with respect to coordinate variable which follows the comma. The relation $\varepsilon_z = 0$ simplifies the constitutive equations in Eq. (4.1) as

$$\sigma_z = \tilde{s}_{21}\sigma_\theta + \tilde{s}_{23}\sigma_r; \qquad \varepsilon_\theta = \hat{s}_{11}\sigma_\theta + \hat{s}_{13}\sigma_r, \qquad \varepsilon_r = \hat{s}_{31}\sigma_\theta + \hat{s}_{33}\sigma_r, \qquad \gamma_{r\theta} = \bar{s}_{55}\tau_{r\theta} \tag{4.5}$$

where $\hat{s}_{ij} = \bar{s}_{ij} + \bar{s}_{i2}\tilde{s}_{2j},\ \tilde{s}_{2i} = -\bar{s}_{2i}/\bar{s}_{22},\ (\forall i,j = 1,3)$.

Similarly, the obtained geometrical displacement jump is denoted as $\Delta u_i^{G(k)}$. Using, surface traction vector $T_i^n = \sigma_{ij}n_j$ (n_j are direction cosines of outward normal $\bar{n}$ to the surface), the Reissner's-type mixed variational principle is expressed without accounting for any body forces as

$$\int_V \left[\sigma_{ij,j}\delta u_i + (\varepsilon_{ij} - \varepsilon_{ij}^G)\delta\sigma_{ij}\right] dV - \int_{A_T} \left(T_i^n - \bar{T}_i^n\right) \delta u_i dA - \int_{A_u} T_i^n \delta u_i dA$$
$$+ \sum_{k=1}^{L-1} \int_{A_k} \left[\Delta u_i^{(k)} - \Delta u_i^{G(k)}\right] \delta\sigma_{3i}^{(k)} dA = 0, \quad \forall\ \delta u_i,\ \delta\sigma_{ij} \tag{4.6}$$

where V denotes the volume of the panel per unit length in the z direction, A_u, A_T are the boundary surfaces where displacements ($\bar{u}_i$) and tractions ($\bar{T}_i^n$) are prescribed and A_k refers to the area of the kth interface. The 3D equations of momentum balance [91], $\Delta u_i^{(k)}$ from Eq. (4.3) and ε_{ij} obtained from Eqs. (4.4) and (4.5) are used to expand Eq. (4.6) by applying the summation over indices i, j $(= \theta, z, r)$ in the following manner

$$\int_r \int_\theta [\delta u \left(-\sigma_{r,r} - \tau_{r\theta,\theta}/r - (\sigma_r - \sigma_\theta)/r\right) + \delta v \left(-\tau_{r\theta,r} - \sigma_{\theta,\theta}/r - 2\tau_{r\theta}/r\right)$$
$$+\delta\sigma_\theta \left(\hat{s}_{11}\sigma_\theta + \hat{s}_{13}\sigma_r - (u + v_{,\theta})/r\right) + \delta\sigma_r \left(\hat{s}_{31}\sigma_\theta + \hat{s}_{33}\sigma_r - u_{,r}\right)$$
$$+\delta\tau_{r\theta} \left(\bar{s}_{55}\tau_{r\theta} - (u_{,\theta} - v)/r - v_{,r}\right)] r d\theta dr$$
$$+ \sum_{k=1}^{L-1} \int_\theta [\delta\tau_{r\theta}^{(k)}((\tau_{r\theta}^{(k)}/K_\theta^{(k)}) - \Delta v^{G(k)}) + \delta\sigma_r^{(k)}((\sigma_r^{(k)}/K_r^{(k)}) - \Delta u^{G(k)})] r d\theta = 0,$$
$$\forall\ \ \delta u_i,\ \delta\sigma_i,\ \delta\tau_{ij} \tag{4.7}$$

and area integrals over A_T & A_u are zero as corresponding boundary conditions are exactly satisfied.

4.2.2.0.1 Boundary conditions: At the radial r-axis boundaries,

$$R_i = -\frac{h}{2} \qquad \text{tractions:} \qquad \sigma_r = -p_1,\ \tau_{r\theta} = \tau_{rz} = 0$$
$$R_o = +\frac{h}{2} \qquad \text{tractions:} \qquad \sigma_r = -p_2,\ \tau_{r\theta} = \tau_{rz} = 0 \tag{4.8}$$

and at circumferential θ-axis boundaries ($\theta = 0, \psi$) following displacement/traction conditions corresponding to

$$\text{Simply supported (S)}: \ u = \sigma_\theta = 0;$$

$$\text{Clamped (C)}: \ u = v = 0;$$

$$\text{Free (F)}: \ \sigma_\theta = \tau_{r\theta} = 0; \tag{4.9}$$

and interface continuity relations of Eq. (4.2) are exactly satisfied. Henceforward, the circumferential coordinate θ and thickness coordinate r are non-dimensionalised to be defined separately over the whole circumferential span and locally for kth layer respectively as:

$$\xi = \theta/\psi, \qquad \zeta^{(k)} = (r - R_1^{(k)})/t^{(k)} \quad \text{with} \quad R_1^{(k)} = R - h/2 + \sum_{i=1}^{k-1} t^{(i)} \tag{4.10}$$

such that $0 \leq \xi \leq 1$ & $0 \leq \zeta^{(k)} \leq 1$ for $R_1^{(k)} \leq r \leq R_1^{(k)} + t^{(k)}$ respectively.

4.3 GENERALIZED MULTI-TERM EKM SOLUTION

The EKM is an iterative method for analytically solving partial differential equations (PDEs) by reducing them into ordinary differential equations (ODEs). The method had been elaborately discussed in the previous chapters. Through similar approach, the present technique will be employed to accurately solve the field variables simultaneously. The field variables u_i & σ_{ij} are approximated as a series of the product of univariate separable functions which are iteratively obtained in closed-form. They are included in the field variable vector $\mathbf{X}$ as:

$$\mathbf{X} = \begin{bmatrix} v & u & \sigma_\theta & \sigma_r & \tau_{r\theta} \end{bmatrix}^{\mathrm{T}} \tag{4.11}$$

However, Eq. (4.5) is used to obtain σ_z after solving for other variables in $\mathbf{X}$ simultaneously. The expression for $\mathbf{X}$ based on multi-term EKM and integrated loading function is expressed. Hence, the lth field variable X_l of $\mathbf{X}$ for the kth layer is assumed as a n-term series of products of univariate functions $f_l^i(\xi)$ and $g_l^i(\zeta)$ in two independent variables ξ and ζ of the following form:

$$X_l(\xi, \zeta) = \sum_{i=1}^{n} f_l^i(\xi) g_l^i(\zeta) + \delta_{l4}[p_a + r p_d] \qquad \text{for} \qquad l = 1, 2, \ldots 5 \tag{4.12}$$

where no summation over repeated index l is considered. A term satisfying Kronecker delta property is added to σ_r for satisfying the non-homogeneous part arising of applied loads p_1 & p_2. Loads are further simplified into $p_a = p_1 - (R - h/2)(p_2 - p_1)/h$ and $p_d = (p_2 - p_1)/h$. The functions $f_l^i(\xi)$ and $g_l^i(\zeta)$ are to be determined stepwise in a two-step iteration process as discussed further.

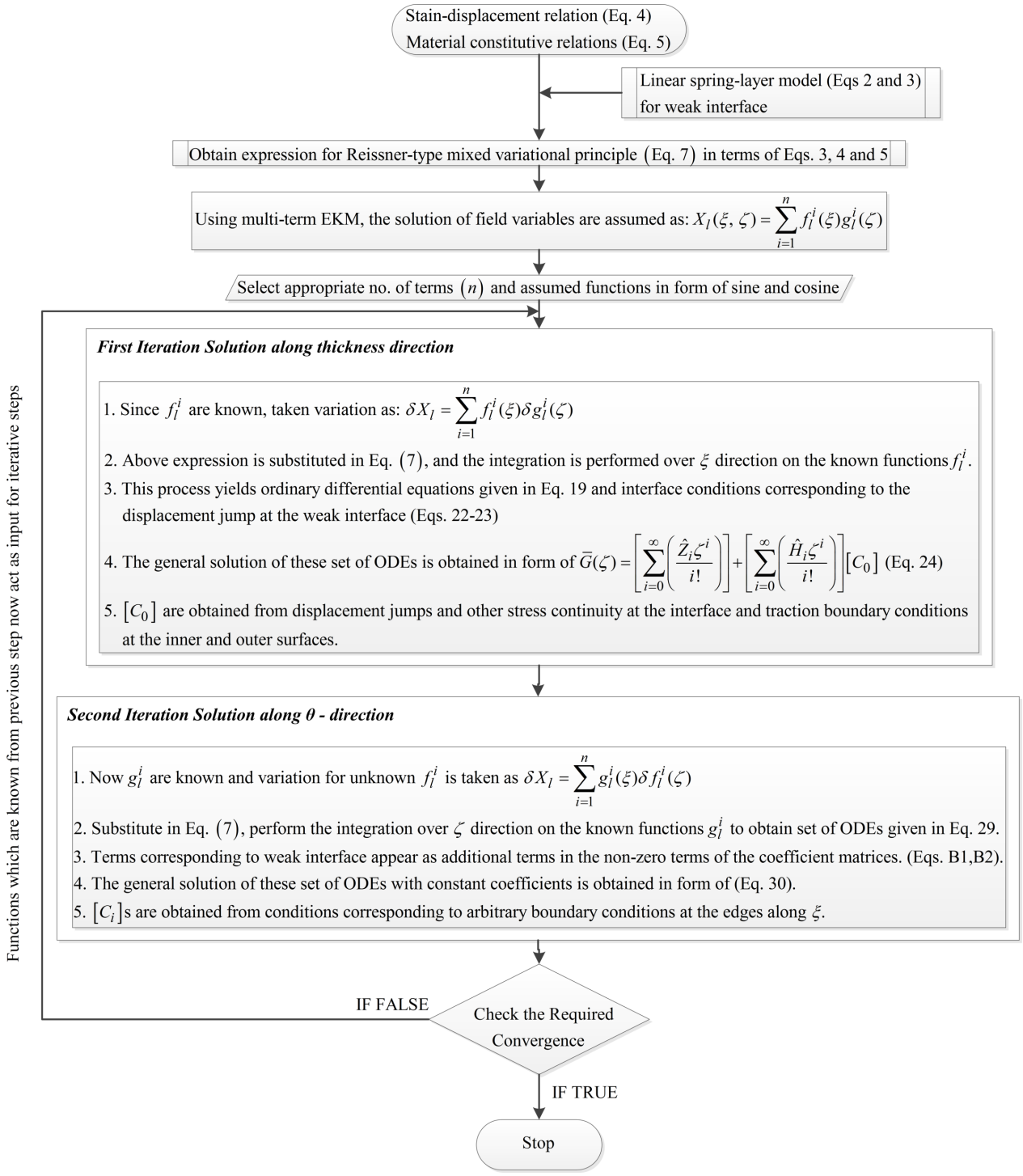

Fig. 4.2: A flowchart of the multi-term EKM solution.

4.3.1 Solution along radial direction (r)

The first step of the iteration requires finding a closed form g_l^i function for each of the kth layer. Note that, there are 4 independent variables $(u, v, \sigma_r, \tau_{r\theta})$ corresponding to 4 differential equations

along ζ-direction in Eq. (4.7). This facilitates the $5n$ g_l^i functions to be included separately into vectors with $4n$ & $1n$ components in

$$\bar{\mathbf{G}} = \left[g_2^1 \dots g_2^n \; g_1^1 \dots g_1^n \; g_4^1 \dots g_4^n \; g_5^1 \dots g_5^n\right]^{\mathrm{T}}$$
$$\hat{\mathbf{G}} = \left[g_3^1 \dots g_3^n\right]^{\mathrm{T}} \tag{4.13}$$

However, the f_l^i functions are assumed to be known. The present multi-term EKM solution discards the necessity of chosen f_l^i functions to satisfy the prescribed conditions at the $\xi = 0$ & 1 boundaries. Hence following trigonometric functions are chosen as trial functions

$$f_1^i = f_5^i = \cos i\pi\xi$$
$$f_2^i = f_3^i = f_4^i = \sin i\pi\xi \tag{4.14}$$

Choice of above normalised trial functions gets rid of potential computational discrepancy which might otherwise arise after any iteration because of large difference in magnitudes of f_l^i & g_l^i [263]. Since f_l^i are known, the variation of lth field variable X_l of $\mathbf{X}$ is reduced to:

$$\delta X_l = \sum_{i=1}^{n} f_l^i \delta g_l^i, \qquad l = 1, 2, \dots 5 \tag{4.15}$$

The variables in the expanded form of Reissner's variational Eq. (4.7), are substituted with corresponding X_l and δX_l from Eqs. (4.12) and (4.15), respectively to perform the integration on the known function $f_l^i(\xi)$ over ξ direction. Note that, f_l^i is assumed trial function in first iteration and iteratively calculated for later iterations. On rearranging Eq. (4.7), the coefficient of arbitrary function δg_l^i is individually zero. Thus $4n$ simultaneous ODEs and $1n$ algebraic equations for the kth layer are obtained as follows

$$\mathbf{M}\bar{\mathbf{G}}_{,\zeta} = t[\bar{\mathbf{A}}_{\mathbf{m}}\bar{\mathbf{G}} + \hat{\mathbf{A}}_{\mathbf{m}}\hat{\mathbf{G}} + \bar{\mathbf{Q}}_{\mathbf{pm}}] \tag{4.16}$$

$$\mathbf{K}\hat{\mathbf{G}} = \tilde{\mathbf{A}}_{\mathbf{m}}\bar{\mathbf{G}} + \tilde{\mathbf{Q}}_{\mathbf{pm}} \tag{4.17}$$

$$\bar{\mathbf{A}}_{\mathbf{m}} = \bar{\mathbf{A}}_{\mathbf{0}} + (\bar{\mathbf{A}}_{\mathbf{1}}/(\zeta t + R_1)), \; \hat{\mathbf{A}}_{\mathbf{m}} = \hat{\mathbf{A}}_{\mathbf{0}} + (\hat{\mathbf{A}}_{\mathbf{1}}/(\zeta t + R_1)), \; \tilde{\mathbf{A}}_{\mathbf{m}} = \tilde{\mathbf{A}}_{\mathbf{0}} + (\tilde{\mathbf{A}}_{\mathbf{1}}/(\zeta t + R_1))$$

$$\bar{\mathbf{Q}}_{\mathbf{pm}} = \bar{\mathbf{Q}}_{\mathbf{p0}} + (\bar{\mathbf{Q}}_{\mathbf{p1}}/(\zeta t + R_1)) + \bar{\mathbf{Q}}_{\mathbf{p2}}(\zeta t + R_1),\ \tilde{\mathbf{Q}}_{\mathbf{pm}} = \tilde{\mathbf{Q}}_{\mathbf{p0}} + \tilde{\mathbf{Q}}_{\mathbf{p1}}(\zeta t + R_1) \tag{4.18}$$

where $\mathbf{M}$, $\bar{\mathbf{A}}_{\mathbf{0}}$, $\bar{\mathbf{A}}_{\mathbf{1}}$ are $4n \times 4n$, $\hat{\mathbf{A}}_{\mathbf{0}}$, $\hat{\mathbf{A}}_{\mathbf{1}}$ are $4n \times 1n$, $\tilde{\mathbf{A}}_{\mathbf{0}}$, $\tilde{\mathbf{A}}_{\mathbf{1}}$ are $1n \times 4n$ and $\mathbf{K}$ is $1n \times 1n$ matrix. $\bar{\mathbf{Q}}_{\mathbf{p0}}$, $\bar{\mathbf{Q}}_{\mathbf{p1}}$, $\bar{\mathbf{Q}}_{\mathbf{p2}}$ are load column vectors of size $4n$ and $\tilde{\mathbf{Q}}_{\mathbf{p0}}$, $\tilde{\mathbf{Q}}_{\mathbf{p1}}$ are load column vectors of size $1n$ respectively. The nonzero terms of $\mathbf{M}$, $\bar{\mathbf{A}}_{\mathbf{0}}$, $\bar{\mathbf{A}}_{\mathbf{1}}$, $\hat{\mathbf{A}}_{\mathbf{0}}$, $\hat{\mathbf{A}}_{\mathbf{1}}$, $\tilde{\mathbf{A}}_{\mathbf{0}}$, $\tilde{\mathbf{A}}_{\mathbf{1}}$, $\mathbf{K}$, $\bar{\mathbf{Q}}_{\mathbf{pi}}$ and $\tilde{\mathbf{Q}}_{\mathbf{pj}}$ for $(i = 0, 1, 2;\ j = 0, 1)$ matrices are defined, using the notation

$$\langle \ldots \rangle_\psi = \psi \int_0^1 (\ldots) d\xi$$

for integration over the span length ψ wherever required, as

$$\begin{aligned}
&M_{i_1 j_1} = M_{j_3 i_3} = \langle f_4^i f_2^j \rangle_\psi,\ M_{i_2 j_2} = M_{j_4 i_4} = \langle f_5^i f_1^j \rangle_\psi \\
&\bar{A}_{0_{i_1 j_3}} = \hat{s}_{33} \langle f_4^i f_4^j \rangle_\psi, \quad \bar{A}_{0_{i_2 j_4}} = \bar{s}_{55} \langle f_5^i f_5^j \rangle_\psi, \quad \bar{A}_{1_{i_4 j_4}} = -2\langle f_1^i f_5^j \rangle_\psi \\
&\bar{A}_{1_{i_2 j_1}} = -\tfrac{1}{\psi} \langle f_5^i f_{2,\xi}^j \rangle_\psi, \quad \bar{A}_{1_{i_2 j_2}} = \langle f_5^i f_1^j \rangle_\psi, \quad \bar{A}_{1_{i_3 j_3}} = -\langle f_2^i f_4^j \rangle_\psi \\
&\bar{A}_{1_{i_3 j_4}} = -\tfrac{1}{\psi} \langle f_2^i f_{5,\xi}^j \rangle_\psi, \quad \hat{A}_{0_{i_1 j_1}} = \hat{s}_{31} \langle f_4^i f_3^j \rangle_\psi, \quad \hat{A}_{1_{i_3 j_1}} = \langle f_2^i f_3^j \rangle_\psi \\
&\hat{A}_{1_{i_4 j_1}} = -\tfrac{1}{\psi} \langle f_1^i f_{3,\xi}^j \rangle_\psi, \quad \tilde{A}_{0_{i_1 j_3}} = \hat{s}_{13} \langle f_3^i f_4^j \rangle_\psi, \quad \tilde{A}_{1_{i_1 j_1}} = -\langle f_3^i f_2^j \rangle_\psi \\
&\tilde{A}_{1_{i_1 j_2}} = -\tfrac{1}{\psi} \langle f_3^i f_{1,\xi}^j \rangle_\psi, \quad K_{i_1 j_1} = \hat{s}_{11} \langle f_3^i f_3^j \rangle_\psi
\end{aligned} \tag{4.19}$$

where $i_p = (p-1)n + i$ and $j_q = (q-1)n + j$ for $p, q = 1, 2, \ldots, 5$. $\bar{\mathbf{Q}}_{\mathbf{p0}}$, $\bar{\mathbf{Q}}_{\mathbf{p1}}$, $\bar{\mathbf{Q}}_{\mathbf{p2}}$, $\tilde{\mathbf{Q}}_{\mathbf{p0}}$ and $\tilde{\mathbf{Q}}_{\mathbf{p1}}$ are load vectors of size $4n$, $4n$, $4n$, $1n$ and $1n$, respectively, whose non-zero terms are given by

$$\begin{aligned}
&\bar{Q}_{p0_{i_1}} = \hat{s}_{33} p_a \langle f_4^i \rangle_\psi, \quad \bar{Q}_{p0_{i_3}} = -2 p_d \langle f_2^i \rangle_\psi, \quad \bar{Q}_{p1_{i_3}} = -p_a \langle f_2^i \rangle_\psi \\
&\bar{Q}_{p2_{i_1}} = \hat{s}_{33} p_d \langle f_4^i \rangle_\psi, \quad \tilde{Q}_{p0_{i_1}} = \hat{s}_{13} p_a \langle f_3^i \rangle_\psi, \quad \tilde{Q}_{p1_{i_1}} = \hat{s}_{13} p_d \langle f_3^i \rangle_\psi
\end{aligned} \tag{4.20}$$

Since the functions f_l^i are known analytical functions, elements of the matrices defined in Eqs. (4.36) and (4.20) have been evaluated in closed form.

Back substituting expressions for $\hat{\mathbf{G}}$ simplified from Eq. (4.17) in Eq. (4.16), yields a system of $4n$ non-homogeneous first order ODEs with variable coefficients as follows:

$$\begin{aligned}
\bar{\mathbf{G}}_{,\zeta} = t[&\left\{ \mathbf{A_0} + (\mathbf{A_1}/(\zeta t + R_1)) + (\mathbf{A_2}/(\zeta t + R_1)^2) \right\} \bar{\mathbf{G}} \\
&+ \mathbf{Q_{p0}} + (\mathbf{Q_{p1}}/(\zeta t + R_1)) + \mathbf{Q_{p2}}(\zeta t + R_1)]
\end{aligned} \tag{4.21}$$

where, $\mathbf{A_0} = [\mathbf{M}^{-1}\bar{\mathbf{A}}_{\mathbf{0}}] + [\mathbf{M}^{-1}\hat{\mathbf{A}}_{\mathbf{0}}\mathbf{K}^{-1}\tilde{\mathbf{A}}_{\mathbf{0}}]$, $\mathbf{A_1} = [\mathbf{M}^{-1}\bar{\mathbf{A}}_{\mathbf{1}}] + [\mathbf{M}^{-1}\hat{\mathbf{A}}_{\mathbf{0}}\mathbf{K}^{-1}\tilde{\mathbf{A}}_{\mathbf{1}}] + [\mathbf{M}^{-1}\hat{\mathbf{A}}_{\mathbf{1}}\mathbf{K}^{-1}\tilde{\mathbf{A}}_{\mathbf{0}}]$, $\mathbf{A_2} = [\mathbf{M}^{-1}\hat{\mathbf{A}}_{\mathbf{1}}\mathbf{K}^{-1}\tilde{\mathbf{A}}_{\mathbf{1}}]$, $\mathbf{Q_{p0}} = [\mathbf{M}^{-1}\bar{\mathbf{Q}}_{\mathbf{p0}}] + [\mathbf{M}^{-1}\hat{\mathbf{A}}_{\mathbf{0}}\mathbf{K}^{-1}\tilde{\mathbf{Q}}_{\mathbf{p0}}] + [\mathbf{M}^{-1}\hat{\mathbf{A}}_{\mathbf{1}}\mathbf{K}^{-1}\tilde{\mathbf{Q}}_{\mathbf{p1}}]$,

$\mathbf{Q_{p1}} = [\mathbf{M}^{-1}\bar{\mathbf{Q}}_{\mathbf{p1}}] + [\mathbf{M}^{-1}\hat{\mathbf{A}}_{\mathbf{1}}\mathbf{K}^{-1}\tilde{\mathbf{Q}}_{\mathbf{p0}}]$, $\mathbf{Q_{p2}} = [\mathbf{M}^{-1}\bar{\mathbf{Q}}_{\mathbf{p2}}] + [\mathbf{M}^{-1}\hat{\mathbf{A}}_{\mathbf{0}}\mathbf{K}^{-1}\tilde{\mathbf{Q}}_{\mathbf{p1}}]$

Additional $2n(L-1)$ equations are obtained from the area integrals as follows

$$\int_{\xi=0}^{1}\left(\sum_{i=1}^{n} f_5^i\delta g_5^i\right)\left[\left(\sum_{j=1}^{n}\frac{f_5^j g_5^j}{K_\theta}\right)\Bigg|_{\zeta=1}^{(k)} - \sum_{j=1}^{n}\left(f_1^j\Delta g_1^j\big|^{(k)}\right)\right](\zeta t+R_1)\psi d\xi = 0 \quad \& \tag{4.22}$$

$$\int_{\xi=0}^{1}\left(\sum_{i=1}^{n} f_4^i\delta g_4^i\right)\left[\left(\sum_{j=1}^{n}\frac{f_4^j g_4^j + p_a + (\zeta t+R_1)p_d}{K_r}\right)\Bigg|_{\zeta=1}^{(k)} - \sum_{j=1}^{n}\left(f_2^j\Delta g_2^j\big|^{(k)}\right)\right](\zeta t+R_1)\psi d\xi = 0 \tag{4.23}$$

Equating the coefficients of arbitrary δg_l^i to zero and evaluating the integral of known f_l^i in closed form give n equations each for $g_1^j\big|^{(k)}$ and $g_2^j\big|^{(k)}$ written in matrix form as

$$\mathbf{F}_{51}\Delta\mathbf{G}_1 - \frac{\mathbf{F}_{55}\mathbf{G}_5}{K_\theta} = 0 \quad \Rightarrow \Delta\mathbf{G}_1 = \frac{\mathbf{F}_{51}^{-1}\mathbf{F}_{55}\mathbf{G}_5}{K_\theta} \quad \& \tag{4.24}$$

$$\mathbf{F}_{42}\Delta\mathbf{G}_2 - \frac{\mathbf{F}_{44}\mathbf{G}_4 + \mathbf{P}_4}{K_r} = 0 \quad \Rightarrow \Delta\mathbf{G}_2 = \frac{\mathbf{F}_{42}^{-1}\left[\mathbf{F}_{44}\mathbf{G}_4 + \mathbf{P}_4\right]}{K_r} \tag{4.25}$$

where elements of $\mathbf{G}_l = \left[g_l^1\big|_{\zeta=1}^{(k)} \quad g_l^2\big|_{\zeta=1}^{(k)} \ldots \quad g_l^n\big|_{\zeta=1}^{(k)}\right]^T$ and $\mathbf{\Delta G}_l = \left[\Delta g_l^1\big|^{(k)} \quad \Delta g_l^2\big|^{(k)} \ldots \quad \Delta g_l^n\big|^{(k)}\right]^T$ with $\Delta g_l^j\big|^{(k)} = g_l^j\big|_{\zeta=0}^{(k+1)} - g_l^j\big|_{\zeta=1}^{(k)}$. Using the notation $\langle\ldots\rangle_\psi$ for $\psi\int_0^1(\ldots)d\xi$, non-zero elements of the matrices $\mathbf{F}$ and $\mathbf{P_4}$ are $F_{l_1p_1} = \langle f_l^i f_p^j\rangle_\psi$, and $P_{4_1} = \langle f_4^j\rangle_\psi\left(p_a + p_d R_1^{(k+1)}\right)$ where $i_p = (p-1)n + i$ and $j_q = (q-1)n + j$ for $p, q = 1, 2, \ldots, 5$. Including other interfaces, these are the $2n(L-1)$ conditions on $g_l^j\big|^{(k)}$ $(\forall\ l = 1, 2)$ in addition with other $2n(L-1)$ interface conditions expressed for the kth interface as $(g_4^j, g_5^j)\big|_{\zeta=1}^{(k)} = (g_4^j, g_5^j)\big|_{\zeta=0}^{(k+1)}$ which are obtained from Eq. (4.2). Besides, more $4n$ outer and inner traction boundary conditions from Eq. (4.8) are used to evaluate the constant matrix $\mathbf{C}_o$ in the general closed form solution obtained as

$$[\bar{\mathbf{G}}(\zeta)] = \left[\sum_{i=0}^{\infty}\left(\frac{\hat{\mathbf{Z}}_i\zeta^i}{i!}\right)\right] + \left[\sum_{i=0}^{\infty}\left(\frac{\hat{\mathbf{H}}_i\zeta^i}{i!}\right)\right][\mathbf{C_o}] \tag{4.26}$$

for the aforementioned system of first-order ODEs expressed in (Eq. (4.21)) which has been shown earlier by Kumari and Kar [258]. In Eq. (4.26), $\hat{\mathbf{Z}}_i$ & $\mathbf{C}_o$ are $4n \times 1n$ column vectors, where as $\hat{\mathbf{H}}_i$ is a $4n \times 4n$ matrix and the series' are finitely truncated when difference between two consecutive terms in the series' is $< 10^{-10}$.

4.3.2 Solution along circumferential direction (θ)

This section discusses the second step where the latest f_l^i functions are obtained from g_l^i functions determined in Sec.4.3.1. Hence, the known g_l^i facilitates the variation of X_l in the form

$$\delta X_l = \sum_{i=1}^{n} g_l^i(\zeta)\delta f_l^i, \qquad l=1,2,\ldots,5. \tag{4.27}$$

As the f_l^i functions are function of the whole circumference, they are partitioned into a vector $\bar{\mathbf{F}}$ consisting of those variables that appear in the displacement/ traction boundary conditions at circumferential edges $\theta = 0$, ψ (Ref.Eq. (4.9)) and a vector $\hat{\mathbf{F}}$ of the remaining variables as follows:

$$\begin{aligned}\bar{\mathbf{F}} &= \left[f_2^1 \ldots f_2^n \; f_1^1 \ldots f_1^n \; f_3^1 \ldots f_3^n \; f_5^1 \ldots f_5^n\right]^{\mathrm{T}} \\ \hat{\mathbf{F}} &= \left[f_4^1 \ldots f_4^n\right]^{\mathrm{T}}\end{aligned} \tag{4.28}$$

After substituting X_l expressed in Eq. (4.12) and its variation δX_l mentioned above, integration is performed over ζ direction on the known g_l^i functions in closed form. Again, the coefficients of δf_l^i are individually equated to zero to obtain the following system of $5n$ differential-algebraic equations for f_l^i:

$$\mathbf{N}\bar{\mathbf{F}}_{,\xi} = \bar{\mathbf{B}}\bar{\mathbf{F}} + \hat{\mathbf{B}}\hat{\mathbf{F}} + \bar{\mathbf{P}}_{\mathbf{m}} \tag{4.29}$$

$$\mathbf{L}\hat{\mathbf{F}} = \tilde{\mathbf{B}}\bar{\mathbf{F}} + \tilde{\mathbf{P}}_{\mathbf{m}} \tag{4.30}$$

where $\mathbf{N}$, $\bar{\mathbf{B}}$, $\hat{\mathbf{B}}$, $\mathbf{L}$ and $\tilde{\mathbf{B}}$ are $4n \times 4n$, $4n \times 4n$, $4n \times 1n$, $1n \times 1n$ and $1n \times 4n$ matrices respectively, and $\bar{\mathbf{P}}_{\mathbf{m}}$ and $\tilde{\mathbf{P}}_{\mathbf{m}}$ are $4n \times 1$ and $1n \times 1$ column vectors comprising of the loading terms.

Using the notation $\langle \ldots \rangle_h = \sum_{k=1}^{L} t^{(k)} \int_0^1 (\ldots)^{(k)} \, d\zeta$ for integration across the thickness, the nonzero elements of $\mathbf{N}$, $\bar{\mathbf{B}}$, $\hat{\mathbf{B}}$, $\mathbf{L}$ and $\tilde{\mathbf{B}}$, $\bar{\mathbf{P}}_{\mathbf{m}}$ and $\tilde{\mathbf{P}}_{\mathbf{m}}$ matrices are following:

$$N_{i_1 j_1} = N_{j_4 i_4} = \frac{1}{\psi}\langle \frac{g_5^i g_2^j}{(\zeta t + R_1)} \rangle_h, \qquad N_{i_2 j_2} = N_{j_3 i_3} = \frac{1}{\psi}\langle \frac{g_1^i g_3^j}{(\zeta t + R_1)} \rangle_h$$

$$\bar{B}_{i_1j_2} = \langle \frac{g_5^i g_1^j}{(\zeta t+R_1)} \rangle_h - \frac{1}{t}\langle g_5^i g_{1,\zeta}^j \rangle_h - \sum_{k=1}^{L-1} g_5^i\big|_{\zeta=1}^{(k)} \Delta g_1^j\big|^{(k)}, \quad \bar{B}_{i_1j_4} = \bar{s}_{55}\langle g_5^i g_5^j \rangle_h + \sum_{k=1}^{L-1} \frac{1}{K_\theta^{(k)}} g_5^i\big|_{\zeta=1}^{(k)} g_5^j\big|_{\zeta=1}^{(k)},$$

$$\bar{B}_{i_2j_1} = -\langle \frac{g_3^i g_2^j}{(\zeta t+R_1)} \rangle_h, \qquad \bar{B}_{i_2j_3} = \hat{s}_{11}\langle g_3^i g_3^j \rangle_h,$$

$$\bar{B}_{i_3j_4} = -\langle \frac{g_1^i g_{5,\zeta}^j}{t} \rangle_h - 2\langle \frac{g_1^i g_5^j}{(\zeta t+R_1)} \rangle_h, \qquad \bar{B}_{i_4j_3} = \langle \frac{g_2^i g_3^j}{(\zeta t+R_1)} \rangle_h$$

$$\hat{B}_{i_2j_1} = \hat{s}_{13}\langle g_3^i g_4^j \rangle_h, \qquad \hat{B}_{i_4j_1} = -\langle \frac{g_2^i g_{4,\zeta}^j}{t} \rangle_h - \langle \frac{g_2^i g_4^j}{(\zeta t+R_1)} \rangle_h,$$

$$\tilde{B}_{i_1j_1} = -\langle \frac{g_4^i g_{2,\zeta}^j}{t} \rangle_h - \sum_{k=1}^{L-1} g_4^i\big|_{\zeta=1}^{(k)} \Delta g_2^j\big|^{(k)}, \qquad \tilde{B}_{i_1j_3} = \hat{s}_{31}\langle g_4^i g_3^j \rangle_h,$$

$$L_{i_1j_1} = \hat{s}_{33}\langle g_4^i g_4^j \rangle_h + \sum_{k=1}^{L-1} \frac{1}{K_r^{(k)}} g_4^i\big|_{\zeta=1}^{(k)} g_4^j\big|_{\zeta=1}^{(k)} \tag{4.31}$$

$$\bar{P}_{m_{i2}} = \hat{s}_{13} p_a \langle g_3^i \rangle_h + \hat{s}_{13} p_d \langle g_3^i(\zeta t + R_1) \rangle_h,$$

$$\bar{P}_{m_{i4}} = -2p_d\langle g_2^i \rangle_h - p_a\langle g_2^i(\zeta t + R_1) \rangle_h \tag{4.32}$$

$$\tilde{P}_{m_{i1}} = \hat{s}_{33} p_a \langle g_4^i \rangle_h + \hat{s}_{33} p_d \langle g_4^i(\zeta t + R_1) \rangle_h + \sum_{k=1}^{L-1} \frac{1}{K_r^{(k)}} g_4^i\big|_{\zeta=1}^{(k)} P_a^{(k+1)}$$

where $P_a^{(k+1)} = (P_a + (\zeta t + R_1)P_d)\big|_{\zeta=1}^{(k)}$ Since $g_l^i(\zeta)$ are known in close form, all integrations in Eq. (4.31) and (4.32) are evaluated exactly in close form.

Further, back substitution of $\hat{\mathbf{F}}$ from Eq. (4.30) into Eq. (4.29) gives system of $4n$ nonhomogeneous first order ODEs with constant coefficients dissimilar to that obtained for $\bar{\mathbf{G}}$ in Sec.4.3.1:

$$\bar{\mathbf{F}}_{,\xi} = \mathbf{B}\bar{\mathbf{F}} + \mathbf{P_m} \tag{4.33}$$

where, $\mathbf{B} = \mathbf{N}^{-1}[\bar{\mathbf{B}} + \hat{\mathbf{B}}\mathbf{L}^{-1}\tilde{\mathbf{B}}]$ and $\mathbf{P_m} = \mathbf{N}^{-1}[\bar{\mathbf{P}}_\mathbf{m} + \hat{\mathbf{B}}\mathbf{L}^{-1}\tilde{\mathbf{P}}_\mathbf{m}]$. General solution of Eq. (4.33) is given in the following form (Ref. [201]):

$$\bar{\mathbf{F}}(\xi) = \sum_{i=0}^{4n}((\mathbf{Y}_i e^{\lambda_i \xi})\mathbf{C}_i) + \mathbf{U_0} \tag{4.34}$$

where, $\mathbf{Y}_i$s and λ_is are the eigenvalues and eigenvectors of $\mathbf{B}$ comprising the complimentary part of the ODE along with real arbitrary constants $\mathbf{C}_i$s. Vector $\mathbf{U_0}$ correspond to the particular part of the non-homogeneous ODE in Eq. (4.33). Conclusively, above mentioned 2 steps in Sec.4.3.1 and 4.3.2 comprise the 1st iteration which is continued for accurate convergence. The flowchart in Fig. 4.2 is intended to highlight the steps involved in the presently developed multi-term EKM solution.

4.4 INITIAL TRIAL FUNCTIONS

The initial trial functions considered for the known $f_l^i(\xi)$ functions in the first iteration step are those corresponding to the case of simply supported boundary condition at $\xi = 0, 1$. Although, this choice does not affect the convergence of the solution and there might be increase in one or two iterations. The considered functions are in the form of

$$f_1(\xi) = f_2(\xi) = \cos i\pi\xi$$
$$f_3(\xi) = f_4(\xi) = f_5(\xi) = \sin i\pi\xi \tag{4.35}$$

Substituting these trial functions from Eq. (4.35) into Eq. (4.36) yields the following non-zero terms of matrices

$\mathbf{M}$, $\bar{\mathbf{A}}_\mathbf{0}$, $\bar{\mathbf{A}}_\mathbf{1}$, $\hat{\mathbf{A}}_\mathbf{0}$, $\hat{\mathbf{A}}_\mathbf{1}$, $\tilde{\mathbf{A}}_\mathbf{0}$, $\tilde{\mathbf{A}}_\mathbf{1}$, $\mathbf{K}$, $\bar{\mathbf{Q}}_\mathbf{p0}$, $\bar{\mathbf{Q}}_\mathbf{e0}$, $\bar{\mathbf{Q}}_\mathbf{p1}$, $\bar{\mathbf{Q}}_\mathbf{p2}$, $\tilde{\mathbf{Q}}_\mathbf{p0}$ and $\tilde{\mathbf{Q}}_\mathbf{p1}$:

$$\begin{aligned}
&\bar{A}_{0_{i_1j_3}} = \hat{s}_{33},\ \bar{A}_{0_{i_2j_4}} = \bar{s}_{55},\ \bar{A}_{1_{i_4j_4}} = -2\\
&\bar{A}_{1_{i_2j_1}} = -\bar{n},\ \bar{A}_{1_{i_2j_2}} = 1, \quad \bar{A}_{1_{i_3j_3}} = -1\\
&\bar{A}_{1_{i_3j_4}} = -\bar{n},\ \hat{A}_{0_{i_1j_1}} = \hat{s}_{31},\ \hat{A}_{1_{i_3j_1}} = 1\\
&\hat{A}_{1_{i_4j_1}} = -\bar{n},\ \tilde{A}_{0_{i_1j_3}} = \hat{s}_{13},\ \tilde{A}_{1_{i_1j_1}} = -1\\
&\tilde{A}_{1_{i_1j_2}} = -\bar{n},\ \ K_{i_1j_1} = \hat{s}_{11}
\end{aligned} \tag{4.36}$$

where $\bar{n} = i\pi/\psi$ and the loading terms are as follows

$$\begin{aligned}
&\bar{Q}_{p0_{i_1}} = 4\hat{s}_{33}p_a/i\pi, \qquad \bar{Q}_{p0_{i_3}} = -8p_d/i\pi, \qquad \bar{Q}_{p1_{i_3}} = -4p_a/i\pi,\\
&\bar{Q}_{p2_{i_1}} = 4\hat{s}_{33}p_d/i\pi, \qquad \tilde{Q}_{p0_{i_1}} = 4\hat{s}_{13}p_a/i\pi, \qquad \tilde{Q}_{p0_{i_1}} = 4\hat{s}_{13}p_a/i\pi
\end{aligned} \tag{4.37}$$

and $\mathbf{M}$ reduces to an identity matrix.

4.5 NUMERICAL RESULTS

4.5.1 Validation of 3D FE Model

Authors shall first validate 3D finite element (3D FE) cylindrical shell model (ABAQUS [256]) with Chen et al. [165] due to non-availability of analytical solution for arbitrarily supported cylindrical shell panels with weak interfaces. For this purpose, a three-ply shell is considered for study and results of Table 3 of Ref. [165] is compared for thick (S=(R/h)=4) and moderately thick shell

(S=10). In Ref. [165], fiber orientation (β^0) is measured from the z-axis to the fiber direction. But, in present formulation fiber orientation is designated by an angle making with θ-axis. Therefore, the present configuration $[0^0/90^0/0^0]$ is equivalent to $[90^0/0^0/90^0]$ of Ref. [165]. The laminate scheme, material, loading and the non-dimensionalization used for reporting the field variables are as follows:

Cylindrical shell configuration: $[0^0/90^0/0^0]$ of equal thickness plies; Young's, shear moduli & Poisson's ratios: $Y_L = 172.5$ GPa, $Y_T = 6.9$ GPa, $G_{TT} = 1.38$ GPa, $G_{LT} = 3.45$ GPa; $\nu_{LT} = \nu_{TT} = 0.25$; Loading: Sinusoidal load $p = -p_0 sin(\pi\theta/\psi) sin(\pi z/l)$ on the inner surface of the shell of span psi and axial length l. Non-dim.: $\bar{u} = (10uY_L)/(p_0 S^4 h)$, $\bar{\sigma_\theta} = (10\sigma_\theta)/(p_0 S^2)$, $\bar{\sigma_z} = (10\sigma_z)/(p_0 S^2)$, $\bar{\tau_{r\theta}} = (10\tau_{r\theta})/(p_0 S)$ (Ref. Eq.25 of [165]).

where L & T are directions parallel and transverse to fiber direction, respectively. A shell having circumferential span of ($\psi = \pi/4$), thickness (S=4, 10) and length (l) along z-axis ($l/h = 4S$) is modeled in the commercial software ABAQUS. For meshing, a 20 noded quadratic serendipity

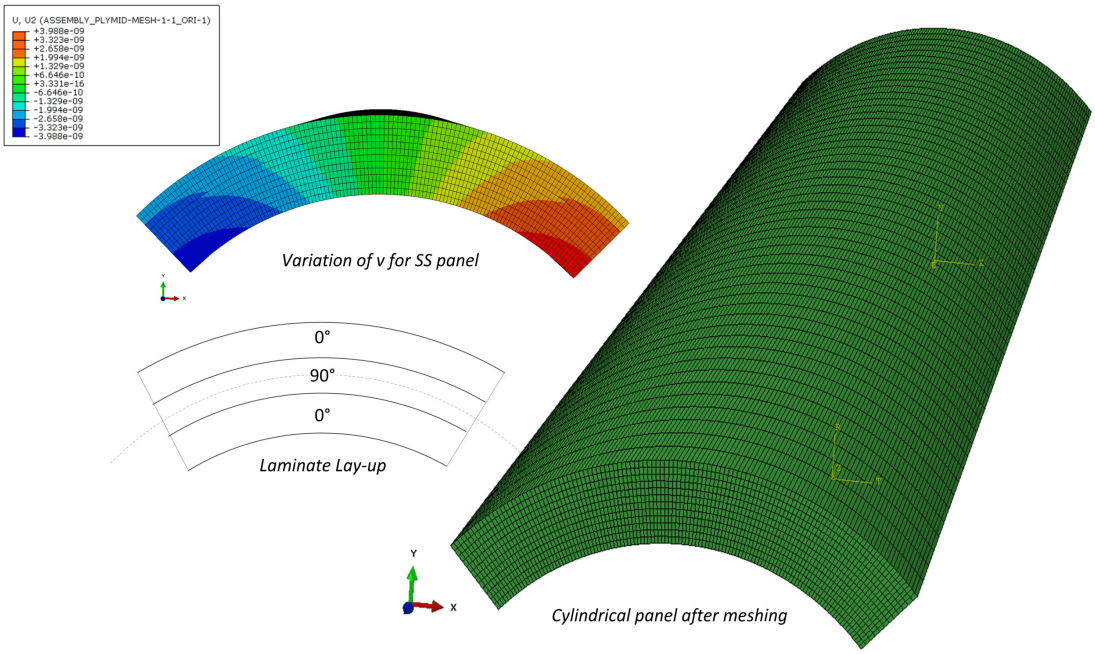

Fig. 4.3: The FE model of cylindrical cross-ply panel with a simulated in-plane deflection (v) variation for SS panel under $P_0 = 1Nm^{-2}$.

hexahedral element with reduced integration (C3D20R) is used for the lamina. The mesh size of

$(12 \times 25 \times 40)$ along r, θ and z directions, respectively is taken after convergence study. Further, a zero thickness interface layer made of eight-node cohesive element (COH3D8) is introduced to analyse the weak interface between the adjacent lamina. For an adhesive interface, mesh size of $(1 \times 50 \times 80)$ number of cohesive elements are considered. The cohesive elements are employed as these can be used to model the initial loading, the initiation of damage, and the propagation of damage leading to eventual failure in the material. Further, such cohesive elements are used in areas of the model where cracks are expected to be developed. However, the model need not have any crack to begin with. Furthermore, the cohesive elements are analogous to effect of spring at the interface. Thus for studying the behavior in the initial loading phase, the cohesive elements have been considered in the 3D FE model in ABAQUS as results for arbitrarily supported cylindrical shells is not available in the literature. The linear elastic traction-separation behavior has been used where the normal stiffness has been given a very high value for avoiding any peel up or material overlap in the normal direction to the interface. The parameters of the cohesive elements are defined by the elastic traction stiffnesses in the normal (E_{nn}) and along the two local shear directions (E_{ss} and E_{tt}). E_{nn} is obtained from Y_T, E_{ss} & E_{tt} are calculated from G_{LT} and the given imperfection compliances $\mathbf{R}$. A very large value is taken for the corresponding normal stiffness coefficient (E_{nn}) in case of perfectly bonded interface. Converged results of 3D FE are presented in Table 4.1 for different $\mathbf{R}_\theta = \mathbf{R_z} = \mathbf{R}$ and thickness ratios (S) of shell panels.

4.5.2 New Benchmark Results

In this section, the accuracy and convergence of the present formulation is investigated for a three-ply laminated cylindrical panel having arbitrarily supported boundary conditions. Following laminate scheme, material, loading and non-dimensionalization are used for the later discussions: Cylindrical shell panel of ($\psi = \pi/2$); Configuration $[0/90/0^0]$; Young's, shear moduli & Poisson's ratios: $Y_L = 137.9$ GPa, $Y_T = 14.4$ GPa, $G_{TT} = G_{LT} = 5.86$ GPa; $\nu_{LT} = \nu_{TT} = 0.21$ [264]; Loading: Uniformly distributed load (UDL) $p = -p_0$ on the outer surface; Non-dim.: $\bar{u} = (10uY_T)/(p_0 S^4 h)$,

Table 4.1: Comparison of deflection and stresses for simply supported shell with different interface conditions.

Non-dim. Variables (ζ, ξ, z)	S	$\mathbf{R} = 0$ Ref.†	FE	$\mathbf{R} = 0.6$ Ref.†	FE	$\mathbf{R} = 0.9$ Ref.†	FE
$\bar{u}(0.0, 0.5, L/2)$	4	4.00897	4.00149	5.01155	5.01375	5.37336	5.37080
	10	1.22329	1.22299	1.54034	1.58170	1.68613	1.68028
$\bar{\sigma}_z(-0.5, 0.5, L/2)$	4	-0.27009	-0.27069	-0.29131	-0.29254	-0.29858	-0.29970
	10	-0.07910	-0.07928	-0.08639	-0.08744	-0.07248	-0.07353
$\bar{\sigma}_z(0.5, 0.5, L/2)$	4	0.12702	0.12497	0.15235	0.15029	0.16133	0.15884
	10	0.07392	0.07368	0.08618	0.08740	0.09179	0.09208
$\bar{\sigma}_\theta(-0.5, 0.5, L/2)$	4	-9.32297	-9.05037	-11.21592	-10.92956	-11.91532	-11.59293
	10	-5.22390	-5.2009	-5.90440	-5.96791	-6.85332	-6.92714
$\bar{\sigma}_\theta(0.5, 0.5, L/2)$	4	6.54448	6.437	7.86913	7.76512	8.35815	8.23293
	10	4.68271	4.66889	5.25316	5.31311	5.51549	5.56374
$\bar{\tau}_{r\theta}(0.0, 0.0, L/2)$	4	2.34883	2.35202	1.96304	1.95793	1.81160	1.81854
	10	3.26357	3.26493	3.09703	3.07762	3.02049	3.0139

† Data were obtained by Chen et al. [165]

$\bar{v} = (10vY_T)/(p_0S^4h)$, $\bar{\sigma_r} = \sigma_r$, $\bar{\sigma_\theta} = (10\sigma_\theta)/(p_0S^2)$, $\bar{\tau_{r\theta}} = (10\tau_{r\theta})/(p_0S)$ and $\mathbf{R} = SY_T\bar{\mathbf{R}}$.

The FE model for the cylindrical panel is shown in Fig. 4.3 which gives converged results with mesh size of $(12 \times 120 \times 50)$ number of C3D20R elements for the plies and $(1 \times 240 \times 100)$ number of COH3D8 cohesive elements in the cohesive layer. The model for the cylindrical panel has a longer z-axial length $(l)(\frac{l}{R} = 50)$ to establish a plane strain condition and to mimic the stress behaviour of a cylindrical panel exactly. The following nomenclature for the shells are followed during the discussion. A CS cylindrical panel means it has clamped (C) edge at ξ=0 and is simply supported (S) at ξ=1. The values of the field variables $\bar{\mathbf{X}}(\xi, \zeta)$ are plotted at selected locations along the circumferential and through-the-thickness locus points.

4.5.2.1 Simply Supported Boundary Edges

In Fig. 4.4, the circumferential variation of displacements $(\bar{u}, \bar{v})$ & stresses $(\bar{\sigma}_\theta, \bar{\tau}_{r\theta})$ for thick $(S = 4)$ and moderately thick $(S = 10)$ SS panel are plotted. Besides, the panels have an uniform shear slip at one of the interfaces $(k = 2)$ with imperfection compliance $\mathbf{R}_\theta = \mathbf{R} = 0.4$ and $\mathbf{R}_r = \mathbf{R}_z = 0$,

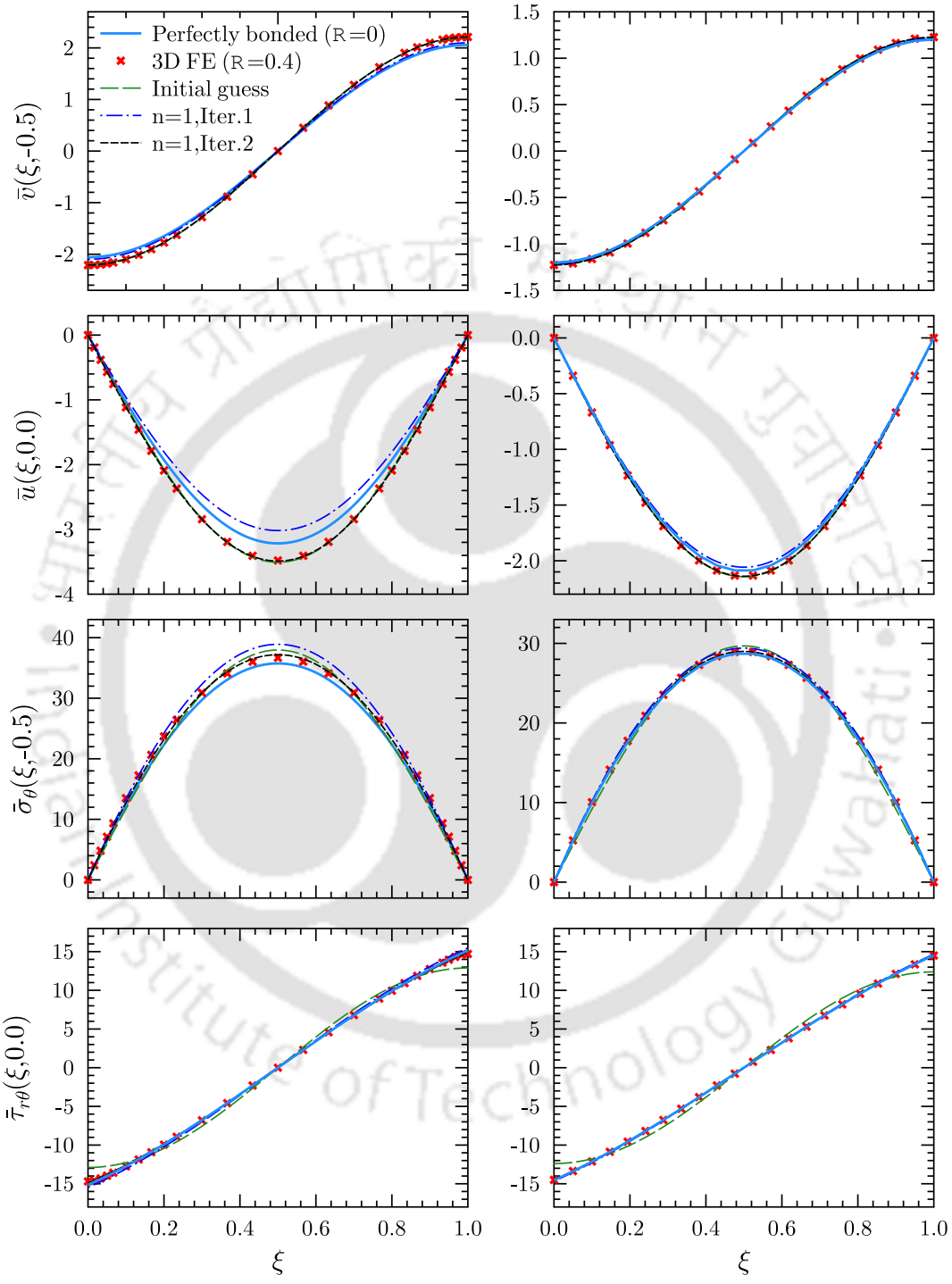

Fig. 4.4: Circumferential variations of displacements and stresses for simply supported (SS) composite panel with weak interface of **R**=0.4 at the 2nd interface.

respectively. Through-the-thickness variation of various entities are depicted in Fig. 4.5. The results for perfectly bonded panels are also presented in these figures for comparison. The in-plane

and transverse displacements are larger than those for the perfectly bonded case which indicates reduction in stiffness of the shell panel due to weak interfaces. Further, in-plane displacement $\bar{v}$ undergoes a jump at the weak interface observable in the through-thickness plot.

Significant jump is observed for thick panel (S=4) than moderately thick shell panels. Consequently, there is further increase in the difference of in-plane stress $\bar{\sigma}_\theta$ across the interface. However, the transverse shear stress $\bar{\tau}_{r\theta}$ is slightly reduced at the weak interface as seen in the through-thickness plot because of reduced shear transfer. These effects are accurately predicted from multi-term EKM and are in close agreement with 3D FE. It is worth to note that, present technique is able to predict the behavior using just n=1 term (2 iterations) which proves the efficiency and elegancy of powerful EKM technique.

4.5.2.2 Non-Simply Supported Boundary Edges

The numerical results in order to conduct the convergence study for the presently developed technique for cases of different boundary conditions is shown in Table 4.2. The results are shown for

Table 4.2: Convergence of present multi-term EKM for arbitrarily supported shell panels (S=4) of span ($\psi = \pi/2$) and uniform $\mathbf{R} = 0.4$ at (k=2) interface under UDL= $1Nm^{-2}$.

SS				
Entities	$\bar{u}(0.5, 0.0)$	$\bar{v}(0.0, -0.5)$	$\bar{\sigma}_\theta(0.5, -0.5)$	$\bar{\tau}_{r\theta}(0.0, 0.0)$
Abaqus (3D FE)	-3.4793	-2.2115	36.680	-14.696
n=1, Iter. 1	-3.5061	-2.1949	37.952	-12.899
n=1, Iter. 2	-3.4880	-2.2099	36.184	-14.893
n=2, Iter. 1	-3.4780	-2.2049	36.618	-14.620
CS				
Entities	$\bar{u}(0.5, 0.0)$	$\bar{v}(0.5, -0.5)$	$\bar{\sigma}_\theta(0.1, -0.5)$	$\bar{\tau}_{r\theta}(0.1, 0.0)$
Abaqus (3D FE)	-1.6724	0.67431	-21.0751	-12.1142
n=2, Iter. 1	-1.6892	0.67090	-21.900	-12.889
n=2, Iter. 2	-1.6899	0.67625	-21.429	-12.381
CF				
Entities	$\bar{u}(1.0, 0.0)$	$\bar{v}(1.0, -0.5)$	$\bar{\sigma}_\theta(0.1, -0.5)$	$\bar{\tau}_{r\theta}(0.1, 0.0)$
Abaqus (3D FE)	-8.9469	6.27885	-75.28	-13.9503
n=2, Iter. 4	-8.9862	6.2046	-75.972	-13.982
n=2, Iter. 5	-8.9921	6.2994	-75.155	-13.945

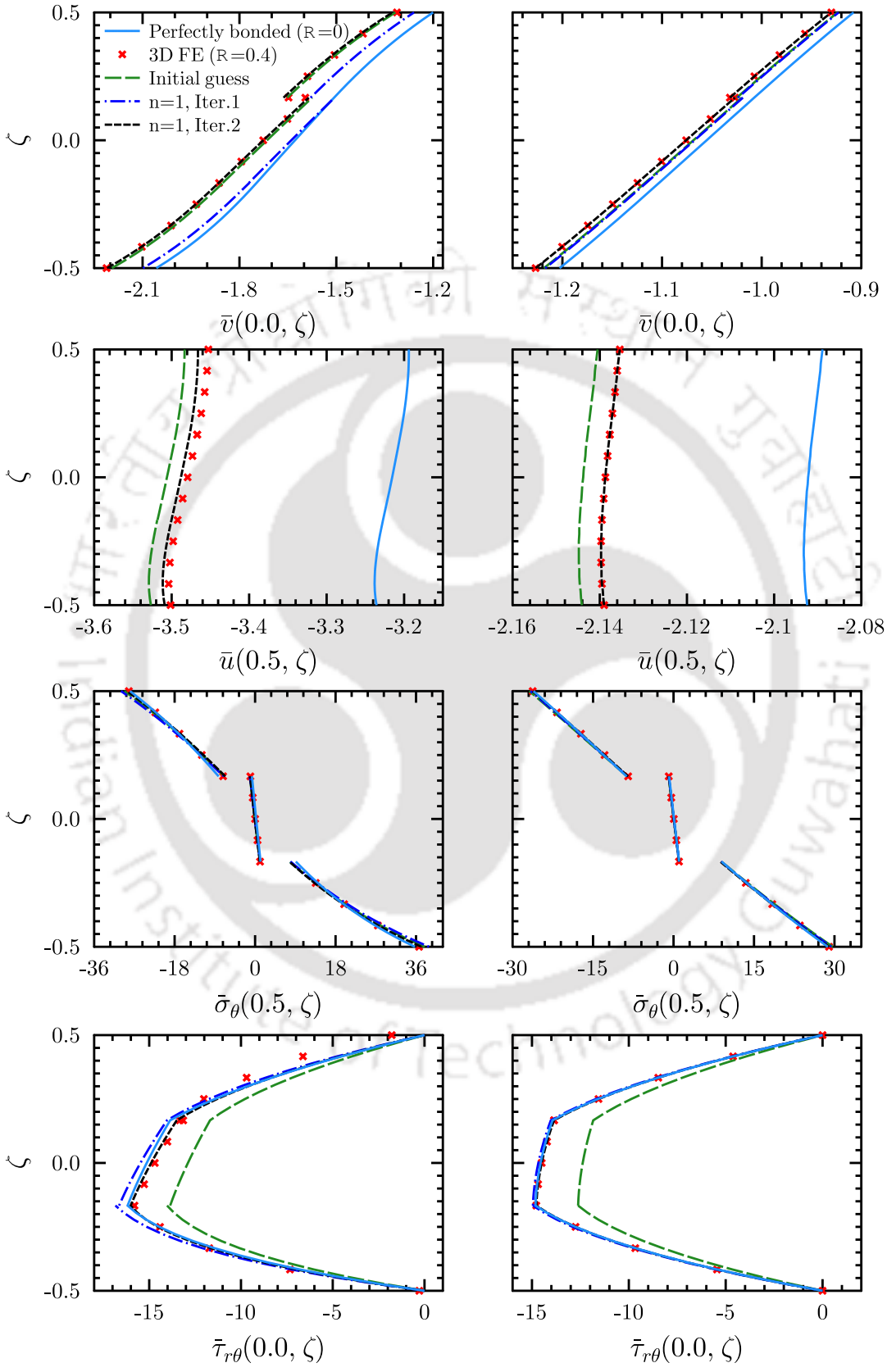

Fig. 4.5: Through-the-thickness variations of displacements and stresses for simply supported (SS) composite panel with weak interface of **R**=0.4 at the 2nd interface.

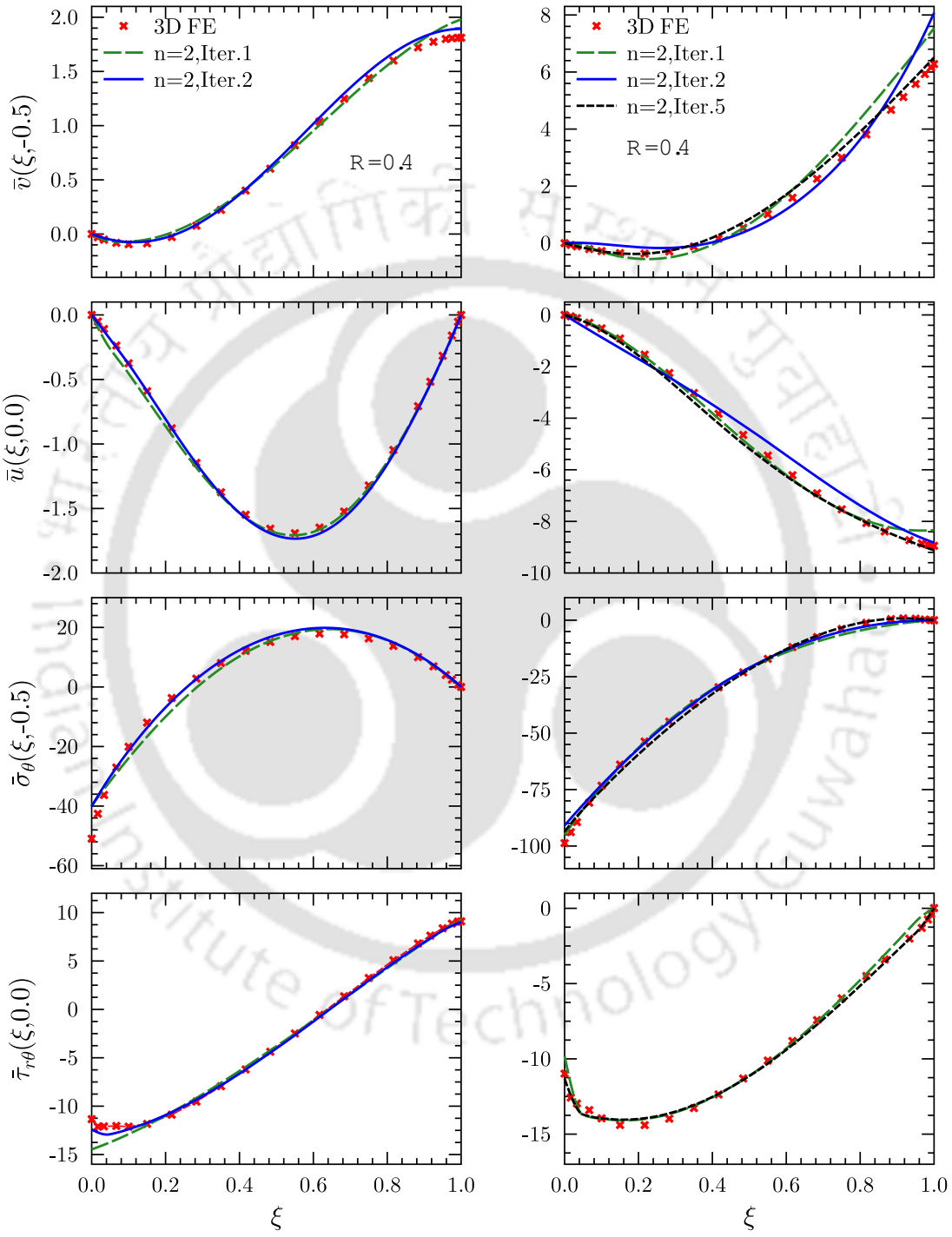

Fig. 4.6: Circumferential variations of displacements and stresses for composite panel with **R**=0.4 subjected to CS and CF support conditions.

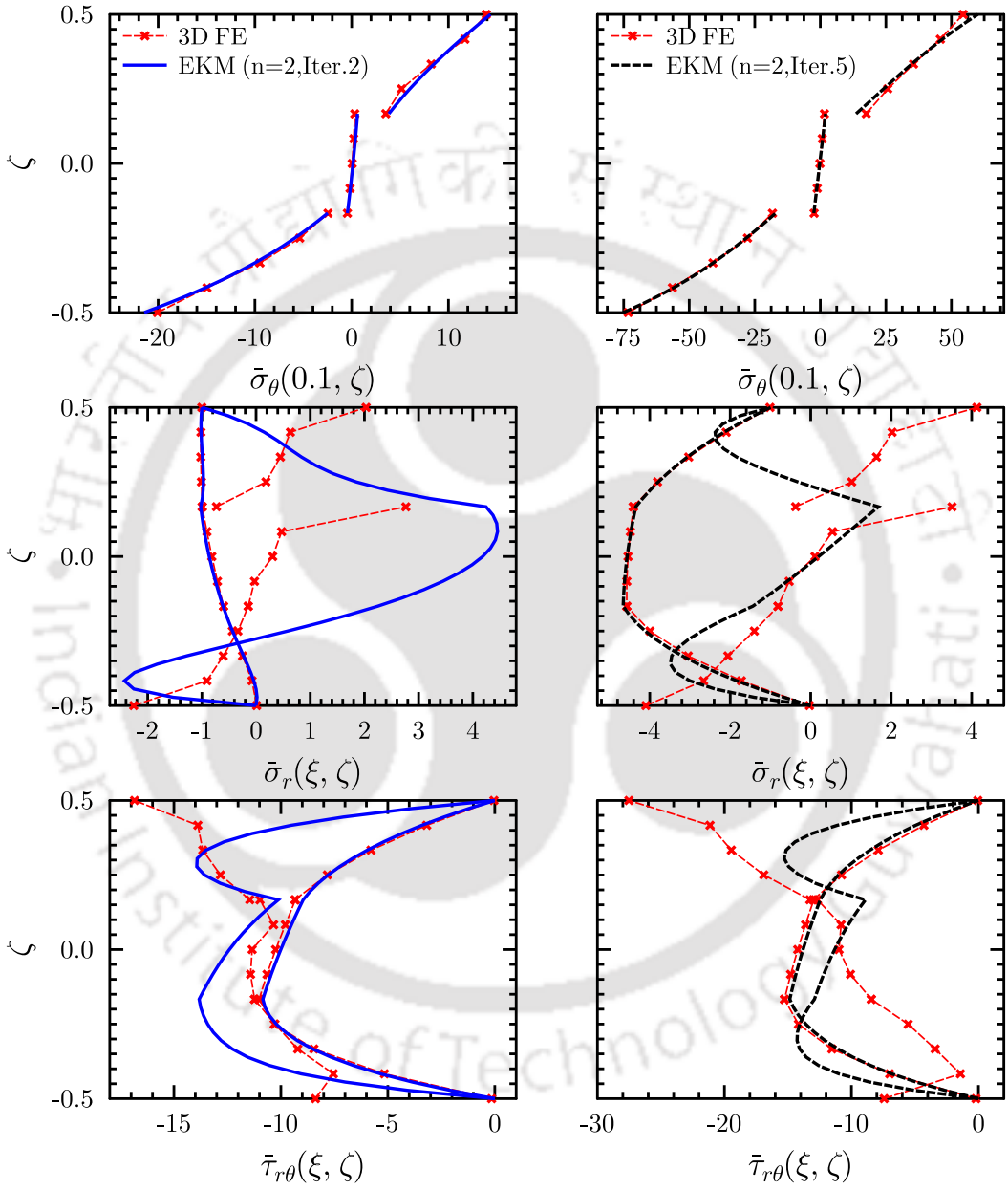

Fig. 4.7: Through-the-thickness variations of stresses for composite panel with **R**=0.4 subjected to CS and CF support conditions.

the peak values of the field variables. Only $n = 1$ term predicts the result for SS panel and addition of just one more term is adequate for accurately predicting the effects in non-simply supported boundary conditions. Although few more iterations are required for CF case. Circumferential and through-the-thickness variation for imperfectly bonded thick shells ($S = 4$) having arbitrarily supported boundary conditions are presented next with similar interlaminar shear-slip condition as SS panel. The circumferential variation of field variables are presented in Fig. 4.6 for CS and CF shell panels. For this case, only two terms (n=2) are required to predict the edge effects and interfacial stresses accurately. The present results for displacements excellently match with 3D FE. It is observed that at the very clamped edge, stresses are not in agreement with 3D FE results. And, earlier it has been already verified that 3D FE solutions do not satisfy the boundary and interface conditions at the very clamped support. This can also be verified by studying the plots for through-the-thickness variation of stresses in Fig. 4.7. However, at some distance away from the clamped support, two solutions match where 3D FE solution is consistent with boundary and interface continuity conditions. Through-the-thickness variation for transverse stress $\bar{\sigma}_r$ changes its sign across the thickness for both CS and CF cases at the very clamped edge which is non-intuitive. However, just slightly away from the clamped edge, $\bar{\sigma}_r$ remain compressive across the thickness. This is due to the difference in stiffness and Poisson's ratio of the plies owing to their orientation. Moreover, the reaction force developed at the clamped edge is higher which eventually vanishes along the circumference of the shell panel. Further, the nature of $\bar{\sigma}_r$ changes abruptly across the weak interface for both the CS and CF shell panels due to substantial difference in stiffness between the interfacial cohesive zone and the adjoining plies. Similarly, for SS panel the transverse shear stress $\bar{\tau}_{r\theta}$ is reduced at the weak interface again because of reduced shear transfer. Moreover, the in-plane normal stress difference ($\Delta\bar{\sigma}_\theta$) across the interface due to imperfection is depicted in Fig. 4.8.

Singularity in $\Delta\bar{\sigma}_\theta$ is observed in the vicinity of the clamped edge due to material discontinuity at the two adjacent plies across the weak interface. Hence, clamped edge is vulnerable to stress

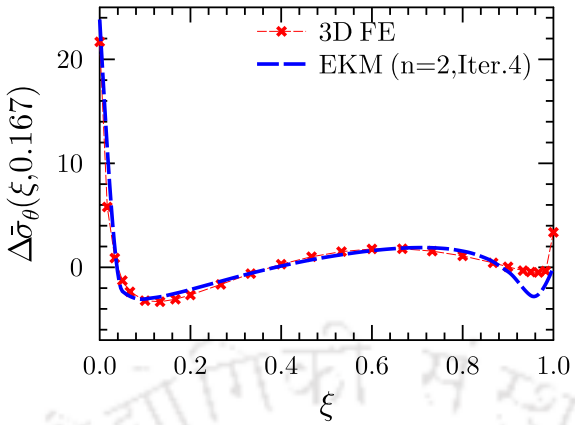

Fig. 4.8: Circumferential variation of in-plane stress difference $\Delta\sigma_\theta$ across the weak interface of **R**=0.4 for a CS composite panel.

concentrations. The effect of boundary conditions on the variation of $\Delta\bar{\sigma}_\theta$ match closely with 3D FE.

4.5.3 Effect of imperfection compliance R

The arbitrarily supported CS and CF thick (S=4) cylindrical panels are considered for studying the effect of imperfection compliance **R** on their bending. It is assumed that, a uniform shear slip imperfection is present at both the interfaces. The circumferential variation of displacements and stresses of the cylindrical panel is presented for different values of **R** in Fig. 4.9 with the results for the perfectly bonded case (**R** = 0). It is observed that owing to bonding imperfection at the interface, the in-plane ($\bar{v}$) and transverse ($\bar{u}$) deflections of the cylindrical panel are increased. This is due to reduction in stiffness of the panel with weaker bonding at the interfaces. In response to this higher strain in the panels the stress also increase at the clamped support and other mid-span location of the panel as shown in Fig. 4.9. As expected, there is discontinuity in the in-plane displacement ($\bar{v}$) at the imperfectly bonded interfaces which further increases with increase in **R** as shown in the through-the-thickness plots for displacement and stress in Fig. 4.10. It should be observed that similar to Fig. 4.8, there is change in the sign of $\Delta\bar{\sigma}_\theta$ in the region near to the clamped edge along the circumference. This is to satisfy the force-equilibrium requirement with no development of stress resultant along the θ-direction. The $\Delta\bar{\sigma}_\theta$ is extremely high at the clamped

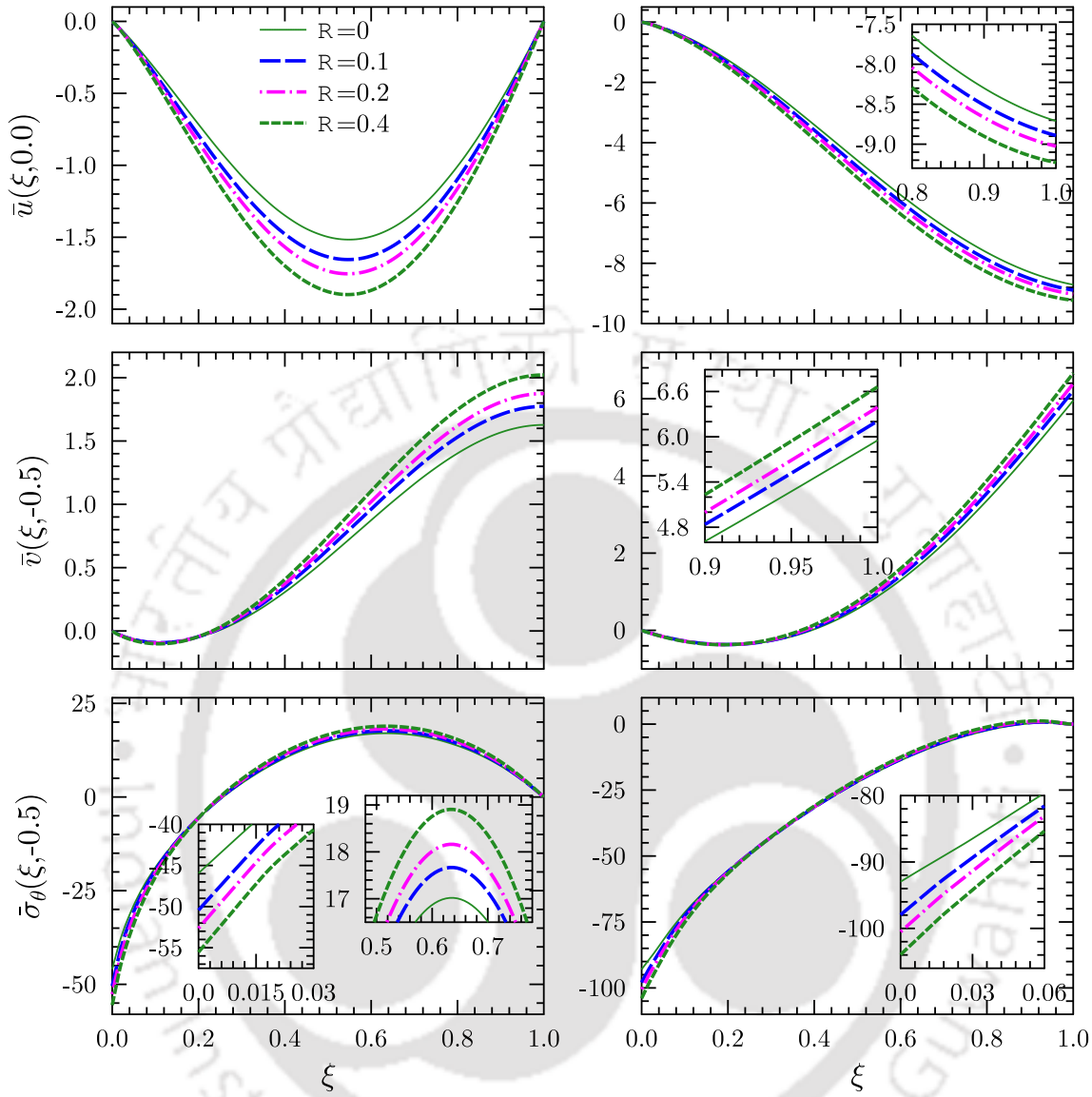

Fig. 4.9: Effect of imperfection compliance **R** on the circumferential variations of displacements and stresses for the CS and CF composite panels having same imperfection at both the interfaces.

edge which increases in direct proportion with **R** but, in the region very close to it the sign of $\Delta\bar{\sigma}_\theta$ changes across the thickness. This change is shown in the through-the-thickness trend of $\bar{\sigma}_\theta$ at $\xi = 0.1$ in Fig. 4.10. The $\bar{\tau}_{r\theta}$ reduces as **R** increases which can be seen in the Fig. 4.10. As the interface is weaker, it can not transfer the shear stress.

A quantitative study for the increased trend of peak displacements and stresses can be conducted from Fig. 4.11a. There, percentage increase of field variables $\bar{\mathbf{X}}$ and imperfection compliance **R** are denoted as $\tilde{X} = (\bar{\mathbf{X}} - \bar{\mathbf{X}}|_{\mathbf{R=0.1}}) \times 100/\bar{\mathbf{X}}|_{\mathbf{R=0.1}}$ and $\tilde{\mathbf{R}} = (\mathbf{R} - 0.1) \times 100/0.1$, respectively. For an

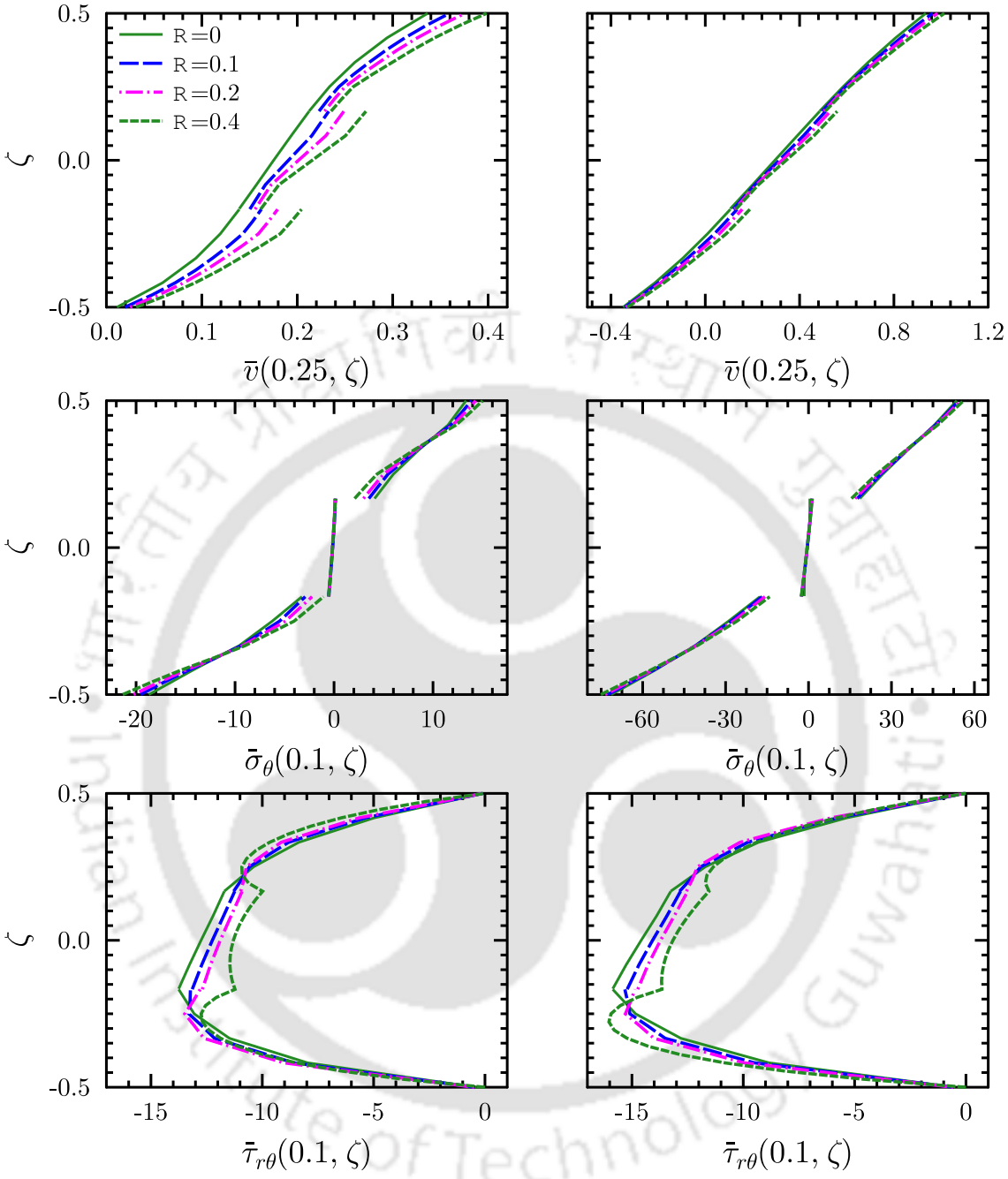

Fig. 4.10: Effect of imperfection compliance **R** on the through-the-thickness distribution of displacements and stresses for the CS and CF composite panels having same imperfection at both the interfaces.

imperfectly bonded CS shell panel, the displacement field variables are more sensitive than stresses. For CS panel when **R** is increased approximately by 4 times, deflections of cylindrical panel are increased 3 folds where as induced in-plane stress $\tilde{\sigma}_\theta$ increased with a factor of 2 approximately.

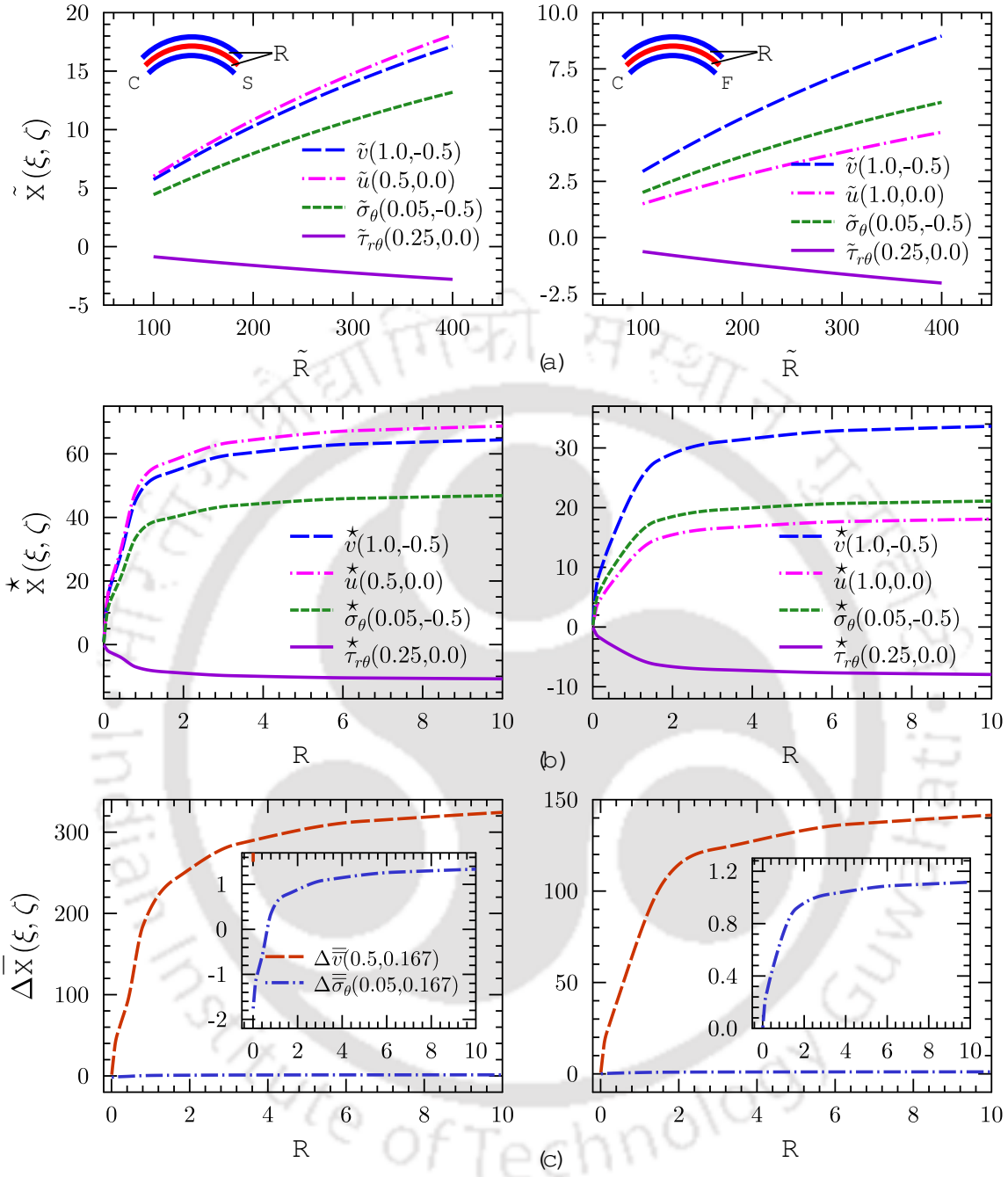

Fig. 4.11: Variation trends for the displacements and stresses with increasing **R** for CS and CF composite panels (S=4) with bonding imperfection at both the interfaces.

However, although there is a decrease in the transverse shear stress $\tilde{\tau}_{r\theta}$ in the 90^o ply with increase in **R** (Ref.Fig. 4.10) but stresses are higher in the outer 0^o plies. This difference of $\tilde{\tau}_{r\theta}$ between adjacent plies increased with increase in **R**. For the CF cylindrical panel, displacements and stresses increase approximately in similar fashion with that of CS panel, however the magnitude of increase

is lower and the peak transverse displacement ($\tilde{u}$) is less sensitive (i:e, lower slope) to $\mathbf{R}$ as compared to the peak $\tilde{u}$ of CS panel. Fig. 4.11b shows a wider range of study for the effect of $\mathbf{R}$ where the displacements and stresses are expressed with respect to the corresponding values of a perfectly bonded case as $X^{\star} = (\bar{\mathbf{X}} - \bar{\mathbf{X}}|_{\mathbf{R=0}}) \times 100/\bar{\mathbf{X}}|_{\mathbf{R=0}}$. The curves for all entities show a steep variation at lower value of $\mathbf{R}$ but the slopes decrease with increase in $\mathbf{R}$ which later becomes constant. This indicates no further reduction in the cylindrical panel stiffness and the laminas are completely debonded. For both CS and CF panels, complete debonding at higher $\mathbf{R}$ can also be concluded from constant values of normalised in-plane displacement jump ($\Delta\bar{\bar{v}} = (\Delta\bar{v} - \Delta\bar{v}|_{\mathbf{R=0.0625}})/\Delta\bar{v}|_{\mathbf{R=0.0625}}$) and normalised in-plane stress difference ($\Delta\bar{\bar{\sigma}}_{\theta} = (\Delta\bar{\sigma}_{\theta} - \Delta\bar{\sigma}_{\theta}|_{\mathbf{R=0.0625}})/\Delta\bar{\sigma}_{\theta}|_{\mathbf{R=0.0625}}$) across the interface as shown in Fig. 4.11c. The magnitude of displacement and induced stress variation with $\mathbf{R}$ is lower for CF than CS panel.

4.5.4 Effect of span angle ψ

In this section, effect of span angle (ψ) of thick (S=4) CS and CF cylindrical panels with a weak interface of uniform imperfection compliance $\mathbf{R} = 0.3$ at the 2nd interface is illustrated. The Fig. 4.12a presents variation of $\bar{u}$ along the circumference and the variation of shear stress $\bar{\tau}_{r\theta}$ across the thickness for different span angles under CS and CF support conditions. Displacement increases with increase in span angle for both support conditions and is maximum for $\psi = 120^{o}$. It can be seen in Fig. 4.12a that the stress also increases with ψ. It shows that deeper shells are less stiffer. At the interface, shear stress dips and continues to increase inside the ply. The normalised field variables displacements and stresses ($\tilde{X} = (\bar{\mathbf{X}} - \bar{\mathbf{X}}|_{\psi=60^{o}})/\bar{\mathbf{X}}|_{\psi=60^{o}}$) are plotted in Fig. 4.12b with normalised span angle ($\tilde{\psi} = (\psi - 60^{o})/60^{o}$). The in-plane displacement ($\tilde{v}$) is more sensitive than the transverse displacement ($\tilde{u}$) for both CS and CF cases due to the shear slip compliance $\mathbf{R}_{\theta}$. It is found that inplane stress $\tilde{\sigma}_{\theta}$ increases more abruptly than the transverse shear stress $\tilde{\tau}_{r\theta}$ for all the boundary conditions. The displacements increase almost exponentially and the slope is more for CF panel than CS panel. Further, the increment in stresses is higher in CS panel than

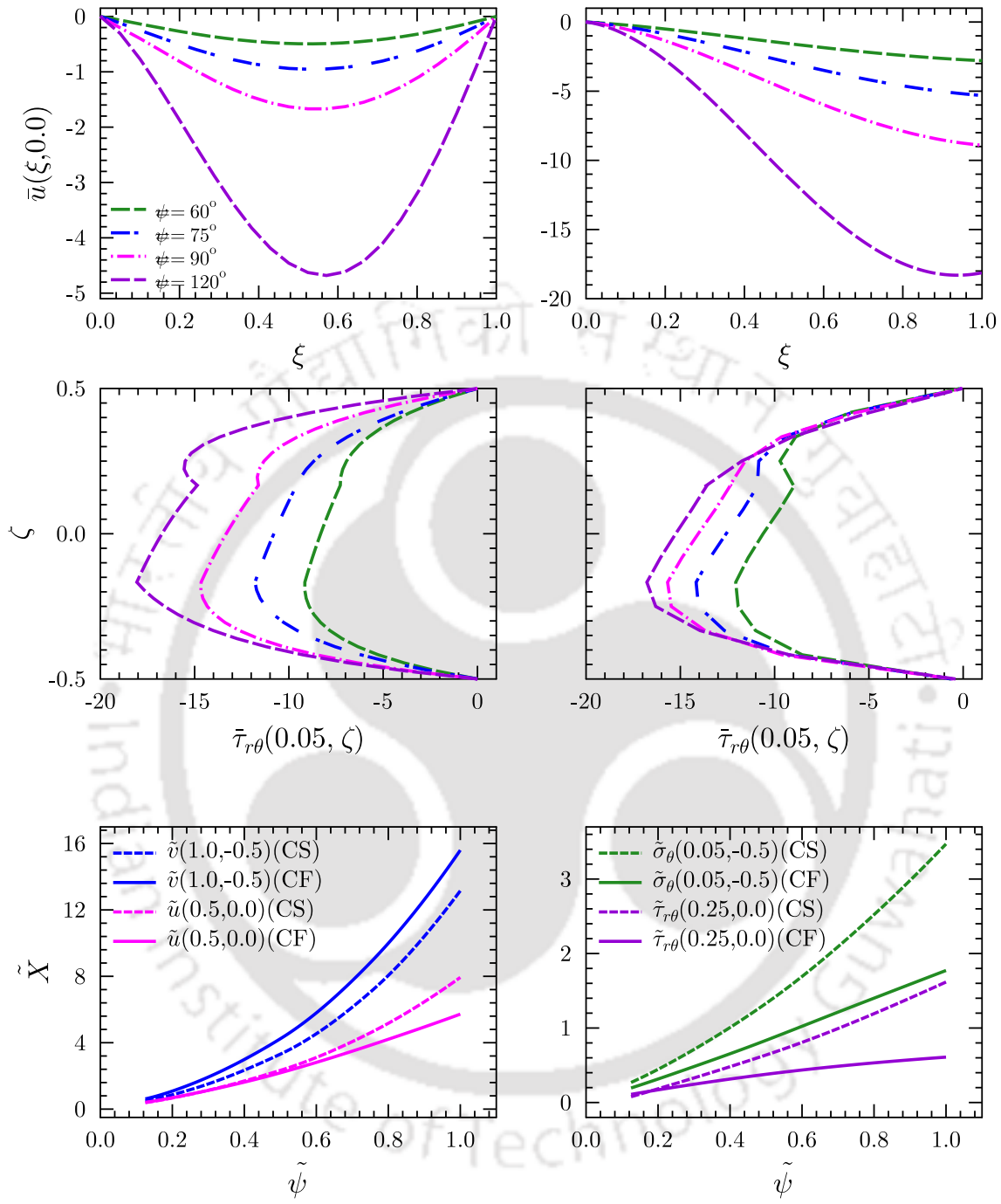

Fig. 4.12: Effect of span angle ψ on the distribution of transverse displacement ($\bar{u}$) and transverse stress ($\bar{\tau}_{r\theta}$) for the CS and CF composite panels with weak interfaces of **R**=0.3 at the 2nd interface.

the CF panel.

4.6 SUMMARY

A generalised 3D elasticity based solution for the laminated composites with imperfectly bonded layers has been developed. There is shear-slip between the lamina due to weak bonding. Through a linear spring-layer model, the shear-slip phenomena is incorporated in a mixed type variational principle where the shear-slip appears in an area integral at the lamina interfaces. The shear-slip is quantified in terms of imperfection compliance. By obtaining the governing equations from mixed variational form, the displacement and stress components could attain same degree of accuracy even for the solution of the thick shell panel subjected to arbitrary boundary conditions which ideally is the novelty of this development. The cylindrical bending has been analysed by studying the effects of the span angle, arbitrary boundary conditions and imperfection compliances used for quantifying the bond strength between the plies and geometry of the cylindrical shell panel. Presently developed 3D solution could predict more realistic behavior of the laminated composites which has been demonstrated through numerical study. As per intuition, larger displacements and stresses were observed for laminates with imperfect interlaminar bonding, which has been also quantitatively obtained here as compared to perfectly bonded laminates. Further, this created stress concentration zones in the interface at the clamped region due to slip between the adjacent plies. The sensitivity of the imperfectly bonded laminated structure is large in the lower range of imperfection compliances which gradually decreased to a constant value referring to occurrence of complete debonding between the plies. Moreover, stresses are high for deep shell panels. Furthermore, from the computed solution of a SS cross-ply laminate, only single term EKM provided accurate results although n=2 terms were required for obtaining results for shell panels with CS and CF boundaries. As convergence could be achieved in lower number of iterations the multi-term EKM facilitated the development of a computationally efficient and powerful 3D solution even for weakly bonded laminates in shell structure.

Chapter 5

3D piezoelasticity solution for static analysis of angle-ply piezolaminated cylindrical shell panel

5.1 INTRODUCTION

Smart cylindrical shells under cylindrical bending has been considered for obtaining the generalised multi-field multi-term EKM (MMEKM) solution in this chapter. The smart/ hybrid structure is integrated with piezoelectricity effect for sensing and actuation applications. Recently, these structures are considered for high fidelity and intricate functional replacements as they are superior to the conventional options. Along with improved functionality, advent of noble PFRCs which has complied with shape irregularities has intrigued research towards accurate prediction of electromechanical response of such structures. Coupling effect, high layer wise inhomogeneity and geometric parameters are the challenges in development of a exact solution for the structures.

Using a similar approach earlier used for 3D elasticity case in the chapter 3, a different analytical solution is obtained here for piezo-laminated cylindrical shell panel which is subjected to arbitrary boundary conditions. At its circumferential boundaries, the supports can arbitrarily be chosen as simply supported (S), clamped (C) or freely supported (F), respectively. Electrically, the boundary surfaces can be applied with charge potential or left open circuited. A coupled three-dimensional (3D) constitutive model for laminated smart composite is utilized to develop the 3D piezoelasticity equations. An angle-ply hybrid piezoelectric shell in cylindrical bending, integrated with piezoelectric/PFRC sensors and actuators is considered. Further, the electromechanical coupling

equations, such as the momentum, strain-displacement, electric field-potential, and charge balance relations are substituted in a mixed variational equation. There, the components of displacement, stress, electric displacement and potential components are considered as the primary variables. To attain the same degree of accuracy for all the field variables, the Reissner's-type mixed variational principle has been extended to the piezoelectricity case. Subsequently, the MMEKM is applied, whose expression also treats the nonhomogeneous boundary condition in the thickness direction corresponding to the pressure and electric potential loads over the inner/ outer surfaces.

As an advancement over any two-dimensional (2D) formulation where only the inplane directions are involved, an inplane and a thickness direction is involved for the 3D problem. By the application of the mentioned formulation along the inplane (θ) and the radial (r) directions, it yields two different systems of $8n$ ODEs with $3n$ algebraic equations in terms of θ and r, respectively. The obtained system of ODEs with constant coefficients along θ is solved through the Pagano's approach, whereas the closed-form solution for the radial system of ODEs with variable coefficients is obtained in form of the modified power series. The closed-form solutions are iteratively obtained till convergence, while starting with assumption of an initial trial function along θ. As a result, the developed solution is able to exactly satisfy the interface continuity and boundary conditions. Moreover, when higher order terms arise, the issue with large eigenvalues has also been addressed. The numerical study of the method has been conducted for different angle-ply hybrid composite panels under various boundary conditions. Irrespective of the choice of initial trial functions, the iterative solution converged very fast (n=1, 2 or 3 terms). This work will provide an analytical solution for coupled electro-mechanical response of shell structures and the 3D solution will facilitate near-exact prediction of stress concentration zones with provision of electrical control.

5.2 PIEZOELECTRIC CYLINDRICAL SHELL PANEL

The laminate scheme for the hybrid composite may consist of surface mounted or embedded piezoelectric layers along with the elastic plies. All the piles are generally made up of orthotropic

material and additionally, for the orthotropic piezoelectricity layer, the poling direction is along the radial r coordinate. The piezoelectric materials are considered to be of orthorhombic class mm2 symmetry or of PFRC with effective properties having orthorhombic symmetry with respect to the principal material axes x_1, x_2 and x_3. The x_3 axis is aligned along the r-direction. As shown in Fig. 5.1, in the frame of cylindrical coordinate system (r, θ, z), an L-layered angle-ply hybrid cylindrical shell with infinite axial length, total thickness h and circumferential span ψ is considered.

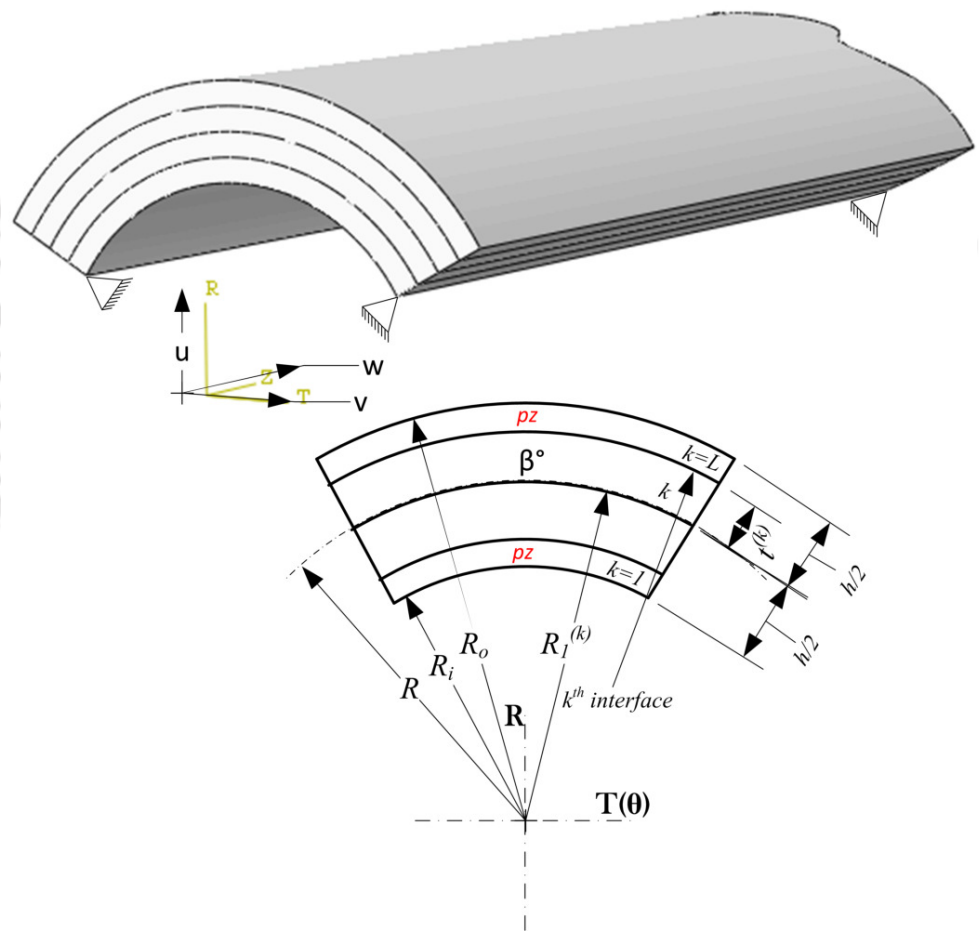

Fig. 5.1: Geometry of a Piezoelectric Shell panel

The local thickness $t^{(k)}$ of each kth layer along radial direction and global circumferential coordinates are introduced as dimensionless entities ξ & ζ defined in the range $\theta = 0, \psi$ and

$r = R_1^{(k)}, R_1^{(k)} + t^{(k)}$, respectively as:

$$\xi = \theta/\psi, \qquad \zeta^{(k)} = (r - R_1^{(k)})/t^{(k)} \quad \text{with} \quad R_1^{(k)} = R - h/2 + \sum_{i=1}^{k-1} t^{(i)} \tag{5.1}$$

Where, $R_1^{(k)}$ is the inner radius of kth layer. And, kth layer is numbered from the inner surface of the shell panel. Physically, the outer surface of the shell panel is at $R_o = R + h/2$ and the inner surface at $R_i = R - h/2$. Here, R & h are the mean radius and total thickness along the radial direction r of the shell panel, respectively. Fiber directions of the perfectly bonded plies can be oriented at an angle $\beta^{(k)}$ with respect to the θ-axis in θz plane. In the following sections, superscript 'k' for the layers is omitted unless needed for clarity. Arbitrary boundary conditions of the shell panel on its opposite circumferential edges (i.e., at $\theta = 0, \psi$) can be clamped (C), free (F) or simply-supported (S). The electrical boundary conditions can also be changed with or without the application of electric potential denoted respectively as closed circuit (CC) and open circuit (OC) conditions.

5.3 GOVERNING EQUATIONS

The Young's moduli Y_i, major Poisson's ratios ν_{ij}, shear moduli G_{ij} are the engineering elastic material constants, along with the coupling piezoelectric terms, namely, piezoelectric coefficients d_{ij} and constant strain dielectric permittivities η_{ij} are used to obtain the expressions of the transformed constants as detailed in Eqs. (A.2)-(A.7) of Appendix A.

$$\begin{bmatrix} \varepsilon_\theta \\ \varepsilon_z \\ \varepsilon_r \\ \gamma_{zr} \\ \gamma_{r\theta} \\ \gamma_{\theta z} \\ D_\theta \\ D_z \\ D_r \end{bmatrix} = \begin{bmatrix} \bar{s}_{11} & \bar{s}_{12} & \bar{s}_{13} & 0 & 0 & \bar{s}_{16} & 0 & 0 & \bar{d}_{31} \\ \bar{s}_{12} & \bar{s}_{22} & \bar{s}_{23} & 0 & 0 & \bar{s}_{26} & 0 & 0 & \bar{d}_{32} \\ \bar{s}_{13} & \bar{s}_{23} & \bar{s}_{33} & 0 & 0 & \bar{s}_{36} & 0 & 0 & \bar{d}_{33} \\ 0 & 0 & 0 & \bar{s}_{44} & \bar{s}_{45} & 0 & \bar{d}_{14} & \bar{d}_{24} & 0 \\ 0 & 0 & 0 & \bar{s}_{54} & \bar{s}_{55} & 0 & \bar{d}_{15} & \bar{d}_{25} & 0 \\ \bar{s}_{16} & \bar{s}_{26} & \bar{s}_{36} & 0 & 0 & \bar{s}_{66} & 0 & 0 & \bar{d}_{36} \\ 0 & 0 & 0 & \bar{d}_{14} & \bar{d}_{15} & 0 & \bar{\epsilon}_{11} & \bar{\epsilon}_{12} & 0 \\ 0 & 0 & 0 & \bar{d}_{24} & \bar{d}_{25} & 0 & \bar{\epsilon}_{21} & \bar{\epsilon}_{22} & 0 \\ \bar{d}_{31} & \bar{d}_{32} & \bar{d}_{33} & 0 & 0 & \bar{d}_{36} & 0 & 0 & \bar{\epsilon}_{33} \end{bmatrix} \begin{bmatrix} \sigma_\theta \\ \sigma_z \\ \sigma_r \\ \tau_{zr} \\ \tau_{r\theta} \\ \tau_{\theta z} \\ E_\theta \\ E_z \\ E_r \end{bmatrix} \tag{5.2}$$

According to a linear 3D piezoelasticity and using the transformation derived in Appendix A, the coupled material constitutive relations has been shown below in cylindrical coordinate system. The

notations, σ_i and τ_{ij} are the stress components, D_i are electric displacement components which are related to corresponding strain components ε_i and γ_{ij} along with electric field components E_i. These are related through the transformed elastic compliances ($\bar{s}_{ij}$), piezoelectric strain constants ($\bar{d}_{ij}$) and dielectric permittivities ($\bar{\epsilon}_{ij}$) at constant stress field, respectively. Furthermore, identical governing equations to those of the original ones are used with dimensionless forms of all the entities. The dimensionless entities for the mechanical variables have been defined in Eq. (3.14) of Chapter 3. The remaining electrical variables are nondimensionalized as

$$\begin{aligned} (D_\theta^*, D_z^*, D_r^*) &= (D_\theta, D_z, D_r)S/Y_0 d_0, & \epsilon_{ij}^* &= \epsilon_{ij}/Y_0 d_0^2 \\ (\phi^*) &= (\phi)d_0/h, & (E_\theta^*, E_z^*, E_r^*) &= (E_\theta, E_z, E_r)d_0 S \end{aligned} \tag{5.3}$$

Where d_0 and Y_0 used for nondimensionalisation, correspond to the values of the material piezoelectric constant and Young's modulus, respectively. However, for simplicity, the superscript * is removed from the dimensionless entities and the equations with dimensionless entities are used henceforth.

When the nature of all the field variables is independent of z, cylindrical bending occurs which is a case of generalised plane strain condition. Corresponding to which the mechanical strain-displacement and electric field-potential relations are in the following form:

$$\begin{aligned} \varepsilon_\theta &= (u + v_{,\theta})/r, & \gamma_{zr} &= w_{,r}, & E_\theta &= -\phi_{,\theta}/r, \\ \varepsilon_z &= 0, & \gamma_{r\theta} &= (u_{,\theta} - v)/r + v_{,r}, & E_z &= 0, \\ \varepsilon_r &= u_{,r}, & \gamma_{\theta z} &= w_{,\theta}/r, & E_r &= -\phi_{,r} \end{aligned} \tag{5.4}$$

where a comma in the subscript denotes differentiation. Using Eq. $(5.2)_9$, the expression for E_r in terms of D_r can be obtained as:

$$E_r = \frac{1}{\bar{\epsilon}_{33}} D_r - \bar{d}'_{31}\sigma_\theta - \bar{d}'_{32}\sigma_z - \bar{d}'_{33}\sigma_r - \bar{d}'_{36}\tau_{\theta z} \tag{5.5}$$

where $\bar{d}'_{ij} = \bar{d}_{ij}/\bar{\epsilon}_{33}$. Substituting E_r from Eq. (5.5) and ε_z from Eq. $(5.4)_2$ in Eq. $(5.2)_2$, σ_z is obtained as

$$\sigma_z = -(\bar{s}'_{12}/\bar{s}'_{22})\sigma_\theta - (\bar{s}'_{26}/\bar{s}'_{22})\tau_{z\theta} - (\bar{s}'_{23}/\bar{s}'_{22})\sigma_r - (\bar{d}'_{32}/\bar{s}'_{22})D_r \tag{5.6}$$

where $\bar{s}'_{ij} = \bar{s}_{ij} - \bar{d}_{3i}\bar{d}_{3j}/\bar{\epsilon}_{33}$. Using Eqs. (5.5) and (5.6), σ_z and E_r are eliminated from Eqs. $(5.2)_1$, $(5.2)_3$, $(5.2)_6$ and Eq. (5.5) to yield

$$\begin{aligned}
\varepsilon_\theta &= p_{11}\sigma_\theta + p_{16}\tau_{\theta z} + p_{13}\sigma_r + p_{18}D_r \\
\varepsilon_r &= p_{31}\sigma_\theta + p_{36}\tau_{\theta z} + p_{33}\sigma_r + p_{38}D_r \\
\gamma_{\theta z} &= p_{61}\sigma_\theta + p_{66}\tau_{\theta z} + p_{63}\sigma_r + p_{68}D_r \\
E_r &= -(p_{81}\sigma_\theta + p_{86}\tau_{\theta z} + p_{83}\sigma_r + p_{88}D_r)
\end{aligned} \tag{5.7}$$

where

$$\begin{aligned}
p_{ij} &= \bar{s}'_{ij} - \bar{s}'_{2i}\bar{s}'_{2j}/\bar{s}'_{22}, \qquad & p_{88} &= -1/\bar{\epsilon}_{33} - \bar{d}'^2_{32}/\bar{s}'_{22} \\
p_{i8} &= p_{8i} = \bar{d}'_{3i} - \bar{s}'_{2i}\bar{d}'_{32}/\bar{s}'_{22}, \quad \text{for} \quad (i,j) = 1,3,6 &&
\end{aligned} \tag{5.8}$$

Further, using the Eq. $(5.2)_2$ in Eq. $(5.4)_2$, σ_z can be differently expressed as

$$\sigma_z = -(\bar{s}_{12}/\bar{s}_{22})\sigma_\theta - (\bar{s}_{26}/\bar{s}_{22})\tau_{\theta z} - (\bar{s}_{23}/\bar{s}_{22})\sigma_r - (\bar{d}_{32}/\bar{s}_{22})E_r \tag{5.9}$$

Substituting σ_z from Eq. (5.9) into Eqs. $(5.2)_1$, $(5.2)_3$, $(5.2)_6$ and $(5.2)_9$, ε_θ, ε_r, $\gamma_{\theta z}$ and E_r can be expressed in terms of σ_θ, $\tau_{\theta z}$, σ_r and E_r as

$$\begin{aligned}
\varepsilon_\theta &= \bar{p}_{11}\sigma_\theta + \bar{p}_{16}\tau_{\theta z} + \bar{p}_{13}\sigma_r + \bar{p}_{18}E_r \\
\varepsilon_r &= \bar{p}_{31}\sigma_\theta + \bar{p}_{36}\tau_{\theta z} + \bar{p}_{33}\sigma_r + \bar{p}_{38}E_r \\
\gamma_{\theta z} &= \bar{p}_{61}\sigma_\theta + \bar{p}_{66}\tau_{\theta z} + \bar{p}_{63}\sigma_r + \bar{p}_{68}E_r \\
E_r &= -(\bar{p}_{81}\sigma_\theta + \bar{p}_{86}\tau_{\theta z} + \bar{p}_{83}\sigma_r + \bar{p}_{88}D_r)
\end{aligned} \tag{5.10}$$

where

$$\begin{aligned}
\bar{p}_{ij} &= \bar{s}_{ij} - \bar{s}_{2i}\bar{s}_{2j}/\bar{s}_{22}, \qquad & \bar{p}_{8i} &= (\bar{d}_{3i} - \bar{s}_{2i}\bar{d}_{32}/\bar{s}_{22})/[\bar{\epsilon}_{33} - (\bar{d}_{32})^2/\bar{s}_{22}] \\
\bar{p}_{i8} &= \bar{d}_{3i} - \bar{s}_{2i}\bar{d}_{32}/\bar{s}_{22}, \quad \text{for} \quad (i,j) = 1,3,6, & \bar{p}_{88} &= -1/[\bar{\epsilon}_{33} - (\bar{d}_{32})^2/\bar{s}_{22}]
\end{aligned}$$

Using Eqs. $(5.2)_4$, $(5.2)_5$ and $(5.2)_7$, γ_{zr}, $\gamma_{r\theta}$ and E_θ can be expressed in terms of τ_{zr}, $\tau_{r\theta}$ and D_θ as

$$\gamma_{zr} = p_{44}\tau_{zr} + p_{45}\tau_{r\theta} + p_{47}D_\theta \tag{5.11}$$

$$\gamma_{r\theta} = p_{54}\tau_{zr} + p_{55}\tau_{r\theta} + p_{57}D_\theta \tag{5.12}$$

$$E_\theta = -p_{74}\tau_{zr} - p_{75}\tau_{r\theta} + p_{77}D_\theta \tag{5.13}$$

where

$$p_{ij} = \bar{s}_{ij} - \bar{d}_{1i}\bar{d}_{1j}/\bar{\epsilon}_{11}, \quad \text{for} \quad (i,j) = (4,5), \qquad p_{47} = \bar{d}_{14}/\bar{\epsilon}_{11}$$

$$p_{74} = p_{47}, \qquad p_{77} = 1/\bar{\epsilon}_{11}, \qquad p_{57} = p_{75} = \bar{d}_{15}/\bar{\epsilon}_{11}$$

In case of cylindrical bending without consideration of any body forces or internal charge sources, the extended Reissner-type mixed variational principle gives the following expression for the piezoelectric medium:

$$\begin{aligned}
&\int_V [\delta u \left(\sigma_{r,r} + \frac{\tau_{r\theta,\theta}}{r} + \frac{(\sigma_r - \sigma_\theta)}{r}\right) + \delta v \left(\tau_{r\theta,r} + \frac{\sigma_{\theta,\theta}}{r} + \frac{2\tau_{r\theta}}{r}\right) + \delta w \left(\tau_{zr,r} + \frac{\tau_{\theta z,\theta}}{r} + \frac{\tau_{zr}}{r}\right) \\
&+\delta\sigma_\theta \left(\varepsilon_\theta - \frac{(u + v_{,\theta})}{r}\right) + \delta\sigma_r(\varepsilon_r - u_{,r}) + \delta\tau_{\theta z}\left(\gamma_{\theta z} - \frac{w_{,\theta}}{r}\right) + \delta\tau_{zr}\left(\gamma_{zr} - w_{,r}\right) \\
&+\delta\tau_{r\theta}\left(\gamma_{r\theta} - \frac{(u_{,\theta} - v)}{r} - v_{,r}\right) - \delta\phi\left(D_{r,r} + \frac{D_r}{r} + \frac{D_{\theta,\theta}}{r}\right) + \delta D_\theta\left(E_\theta + \frac{\phi_{,\theta}}{r}\right) \\
&+\delta D_r\left(E_r - \phi_{,r}\right)]dV = 0, \forall\ \delta u_i,\ \delta\sigma_i,\ \delta\tau_{ij},\ \delta\phi,\ \delta D_i
\end{aligned} \tag{5.14}$$

where V denotes the volume of the panel per unit width in the z direction. The variationally consistent boundary conditions associated with the Eq. (5.14) are to be exactly satisfied as:

$$u_i - \bar{u}_i = 0 \quad \text{on} \quad A_u, \quad \text{and} \quad \sigma_{ij}n_j - \bar{T}_i^n = 0 \quad \text{on} \quad A_T$$

$$\phi - \bar{\phi} = 0 \quad \text{on} \quad A_\phi, \quad \text{and} \quad D_i n_i - \bar{D}_n = 0 \quad \text{on} \quad A_D$$

where $\bar{T}_i^n$ and $\bar{D}_i^n$ are components of the prescribed surface traction vector $\bar{T}^n$ and electric displacement on a surface with outward normal $\bar{n} = n_i\hat{e}_i$, where $\hat{e}_i$ $(i = 1, 2, 3)$ are the unit vectors along θ, z, and r directions. A_u, A_T, A_D, A_ϕ are the boundaries of the surfaces where surface traction $(\bar{T}_i^n)$, displacements $(\bar{u}_i)$, electric displacements $(\bar{D}_i^n)$ and potentials $(\bar{\phi}_i)$ are respectively prescribed.

Substituting the expressions from Eqs. (5.7) and (5.11)-(5.13) for ε_θ, ε_r, $\gamma_{z\theta}$, γ_{zr}, $\gamma_{r\theta}$, E_r and E_θ corresponding to the strain and electric field components, into Eq. (5.14) yields

$$\begin{aligned}
\int_r \int_\theta \ [\ &\delta v(-\tau_{r\theta,r} - \sigma_{\theta,\theta}/r - 2\tau_{r\theta}/r) \\
&+ \delta w(-\tau_{zr,r} - \tau_{z\theta,\theta}/r - \tau_{zr}/r) \\
&+ \delta u(-\sigma_{r,r} - \tau_{r\theta,\theta}/r - (\sigma_r - \sigma_\theta)/r)
\end{aligned}$$

$$
\begin{aligned}
&+ \delta\sigma_\theta(p_{11}\sigma_\theta + p_{13}\sigma_r + p_{16}\tau_{z\theta} + p_{18}D_r - (u + v_{,\theta})/r) \\
&+ \delta\sigma_r(p_{13}\sigma_\theta + p_{33}\sigma_r + p_{36}\tau_{z\theta} + p_{38}D_r - u_{,r}) \\
&+ \delta\tau_{z\theta}(p_{16}\sigma_\theta + p_{36}\sigma_r + p_{66}\tau_{\theta z} + p_{68}D_r - (w_{,\theta}/r)) \\
&+ \delta\tau_{zr}(p_{44}\tau_{zr} + p_{45}\tau_{r\theta} + p_{47}D_\theta - (w_{,r})) \\
&+ \delta\tau_{r\theta}(p_{45}\tau_{zr} + p_{55}\tau_{r\theta} + p_{57}D_\theta - (u_{,\theta} - v)/r - v_{,r}) \\
&- \delta\phi(D_{r,r} + D_r/r + D_{\theta,\theta}/r) \\
&+ \delta D_\theta(p_{77}D_\theta - p_{74}\tau_{zr} - p_{75}\tau_{r\theta} + \phi_{,\theta}/r) \\
&+ \delta D_r(p_{81}\sigma_\theta + p_{83}\sigma_r + p_{86}\tau_{z\theta} + p_{88}D_r - \phi_{,r})]rd\theta dr = 0
\end{aligned} \tag{5.15}
$$

For the instance when the solution in θ direction is considered to be known and for the r direction the corresponding ODEs are to be formed, above Eq. (5.15) is employed. Whereas, for forming the ODEs corresponding to θ direction when r direction solutions are known, the alternative expressions for ε_θ, ε_r, $\gamma_{\theta z}$ and E_r from Eq. (5.10) are substituted in Eq. (5.14) to yield

$$
\begin{aligned}
\int_r\int_\theta\ [\ &\delta v(-\tau_{r\theta,r} - \sigma_{\theta,\theta}/r - 2\tau_{r\theta}/r) \\
&+ \delta w(-\tau_{zr,r} - \tau_{z\theta,\theta}/r - \tau_{zr}/r) \\
&+ \delta u(-\sigma_{r,r} - \tau_{r\theta,\theta}/r - (\sigma_r - \sigma_\theta)/r) \\
&+ \delta\sigma_\theta(\bar{p}_{11}\sigma_\theta + \bar{p}_{13}\sigma_r + \bar{p}_{16}\tau_{z\theta} + \bar{p}_{18}E_r - (u + v_{,\theta})/r) \\
&+ \delta\sigma_r(\bar{p}_{13}\sigma_\theta + \bar{p}_{33}\sigma_r + \bar{p}_{36}\tau_{z\theta} + \bar{p}_{38}E_r - u_{,r}) \\
&+ \delta\tau_{z\theta}(\bar{p}_{16}\sigma_\theta + \bar{p}_{36}\sigma_r + \bar{p}_{66}\tau_{\theta z} + \bar{p}_{68}E_r - (w_{,\theta}/r)) \\
&+ \delta\tau_{zr}(p_{44}\tau_{zr} + p_{45}\tau_{r\theta} + p_{47}D_\theta - (w_{,r})) \\
&+ \delta\tau_{r\theta}(p_{45}\tau_{zr} + p_{55}\tau_{r\theta} + p_{57}D_\theta - (u_{,\theta} - v)/r - v_{,r}) \\
&- \delta\phi(D_{r,r} + D_r/r + D_{\theta,\theta}/r) \\
&+ \delta D_\theta(p_{77}D_\theta - p_{74}\tau_{zr} - p_{75}\tau_{r\theta} - E_\theta) \\
&+ \delta D_r(\bar{p}_{81}\sigma_\theta + \bar{p}_{83}\sigma_r + \bar{p}_{86}\tau_{z\theta} + \bar{p}_{88}D_r + E_r)]rd\theta dr = 0
\end{aligned} \tag{5.16}
$$

However, it may be noted that Eqs. (5.15) and (5.16) are identical for the elastic case.

5.4 BOUNDARY AND INTERFACE CONDITIONS

The loading of magnitude p_1 and p_2 as uniformly distributed pressure load (UDL) is applied at the inner and outer surfaces, respectively. In addition, electric potential ϕ_i can be prescribed or the transverse electric displacement (charge density) D_i can be applied at those surfaces of the shell panel, which are uniformly distributed over θ. Hence, mathematically the inner and outer surfaces are subjected to following conditions:

$$\begin{aligned} &\text{at } r = -\frac{h}{2} \qquad \sigma_r = -p_1,\ \tau_{r\theta} = \tau_{rz} = 0, \quad \phi = \phi_1 \ \text{ or } \ D_r = D_1 \\ &\text{at } r = +\frac{h}{2} \qquad \sigma_r = -p_2,\ \tau_{r\theta} = \tau_{rz} = 0, \quad \phi = \phi_2 \ \text{ or } \ D_r = D_2 \end{aligned} \tag{5.17}$$

The kth interface between adjacent layers are under the following equilibrium and compatibility conditions

$$[(v,\, w,\, u,\, \sigma_r,\, \tau_{zr},\, \tau_{z\theta},\, \phi,\, D_r)|_{\zeta=1}]^{(k)} = [(v,\, w,\, u,\, \sigma_r,\, \tau_{zr},\, \tau_{z\theta},\, \phi,\, D_r)|_{\zeta=0}]^{(k+1)} \tag{5.18}$$

for $k = 1, \ldots, L-1$,. However, the n_q $(q = 1, ..., L_a)$ number of interfaces of elastic layers with the adjacent piezoelectricity layers are grounded for effective sensing/ actuating applications. There the electric potential is 0 in the form of:

$$[\phi|_{\zeta=1}]^{(n_q)} = 0, \qquad q = 1, \ldots, L_a \tag{5.19}$$

At the interfaces $k = n_q,\ (q = 1, \ldots, L_a)$, D_r is discontinuous due to which the otherwise continuity condition for it is replaced by the above Eq. (5.19)

The circumferential edges at $\xi = 0$ and 1 can be arbitrarily chosen among the following cases for numerical study, where the field variables are physically 0.

$$\begin{aligned} &\text{Simply Supported (S)}: \qquad u = 0, \qquad \sigma_\theta = 0, \qquad \tau_{z\theta} = 0 \\ &\text{Clamped (C)}: \qquad\qquad u = 0, \qquad v = 0, \qquad w = 0 \end{aligned}$$

$$\text{Free (F)}: \qquad \tau_{r\theta} = 0, \qquad \sigma_\theta = 0, \qquad \tau_{z\theta} = 0 \tag{5.20}$$

The electric condition at such edges can have a prescribed potential to be closed circuited or the ends can have $D_\theta = 0$ under an open circuit condition.

5.5 GENERALIZED MULTI-FIELD MULTI-TERM EKM SOLUTION

A n-term series of the products of separable functions in the two independent variables ξ and ζ is assumed as the solution of the field variables. Those are simultaneously considered in the $\mathbf{X}$ vector as $\mathbf{X} = \begin{bmatrix} v & w & u & \sigma_\theta & \sigma_r & \tau_{\theta z} & \tau_{zr} & \tau_{r\theta} & \phi & D_\theta & D_r \end{bmatrix}^{\mathrm{T}}$. According to MMEKM, each component $X_l(\xi, \zeta)$ can be assumed as the product of separable univariate functions $f_l^i(\xi)$ and $g_l^i(\zeta)$, in the form of:

$$X_l(\xi, \zeta) = \sum_{i=1}^{n} f_l^i(\xi) g_l^i(\zeta) + \delta_{l5}[p_a + r p_d] + \delta_{l9}\bar{g}_9 \qquad \text{for} \qquad l = 1, 2, \ldots 11 \tag{5.21}$$

Where a solution satisfying the nonhomogeneous part is superimposed on solution constructed for X_l of a kth layer, corresponding to σ_r and ϕ. This is to take care of the nonhomogeneous boundary conditions indicated in Eq. (5.17) for σ_r and ϕ. Hence, only the homogeneous boundary conditions are required to be satisfied by the later. It can be realised that $g_l^i(\zeta)$ and $f_l^i(\xi)$ functions are valid for the kth layer and whole laminate, respectively. Satisfying all homogenous boundary conditions, the functions $g_l^i(\zeta)$ and $f_l^i(\xi)$ are iteratively obtained. In Eq. (5.21) no summation is meant for the repeated index l. Nonhomogeneous boundary conditions are incorporated through the Kronecker's delta function δ_{lm}. Due to applied pressure, the load is obtained as $p_a = p_1 - \{R - (h/2)\}\{(p_2 - p_1)/h\}$ and $p_d = (p_2 - p_1)/h$. And, for the nonhomogeneous boundary condition of ϕ, the solution $\bar{g}_9$ is given by

$$\bar{g}_9 = \begin{cases} \phi_1(1 - \zeta) & \text{for} \quad k = 1 \\ \phi_2 \zeta & \text{for} \quad k = L \end{cases} \tag{5.22}$$

5.5.1 First Iteration Step

Assuming the $f_l^i(\xi)$ functions in this step, the variation δX_i for it is obtained as

$$\delta X_l = \sum_{i=1}^{n} f_l^i(\xi)\delta g_l^i, \qquad l = 1, 2, \ldots 11 \tag{5.23}$$

Referring back to the through-the-thickness boundary conditions in Eqs. (5.17) and (5.18), the $g_l^i(\zeta)$ functions corresponding to those eight field variables are taken in a $\bar{\mathbf{G}}$ vector, while the remaining three $g_l^i(\zeta)$ functions appear in another vector $\hat{\mathbf{G}}$ as shown below:

$$\begin{aligned}
\bar{\mathbf{G}} &= \left[g_3^1 \ldots g_3^n \; g_1^1 \ldots g_1^n \; g_2^1 \ldots g_2^n \; g_5^1 \ldots g_5^n \; g_7^1 \ldots g_7^n \; g_8^1 \ldots g_8^n \; g_9^1 \ldots g_9^n \; g_{11}^1 \ldots g_{11}^n\right]^{\mathrm{T}} \\
\hat{\mathbf{G}} &= \left[g_4^1 \ldots g_4^n \; g_6^1 \ldots g_6^n \; g_{10}^1 \ldots g_{10}^n\right]^{\mathrm{T}}
\end{aligned} \tag{5.24}$$

Substituting X_l and δX_l from the Eqs. (5.21) and (5.23) in Eq. (5.15), results in a set of following $11n$ differential-algebraic equations.

$$\mathbf{M}\bar{\mathbf{G}}_{,\zeta} = t[\bar{\mathbf{A}}_\mathbf{m}\bar{\mathbf{G}} + \hat{\mathbf{A}}_\mathbf{m}\hat{\mathbf{G}} + \bar{\mathbf{Q}}_\mathbf{pem}] \tag{5.25}$$

$$\mathbf{K}\hat{\mathbf{G}} = \tilde{\mathbf{A}}_\mathbf{m}\bar{\mathbf{G}} + \tilde{\mathbf{Q}}_\mathbf{pm} \tag{5.26}$$

$$\begin{aligned}
\text{where, } \bar{\mathbf{A}}_\mathbf{m} &= \bar{\mathbf{A}}_\mathbf{0} + \left(\frac{\bar{\mathbf{A}}_\mathbf{1}}{(\zeta t + R_1)}\right), \; \hat{\mathbf{A}}_\mathbf{m} = \hat{\mathbf{A}}_\mathbf{0} + \left(\frac{\hat{\mathbf{A}}_\mathbf{1}}{(\zeta t + R_1)}\right), \\
\tilde{\mathbf{A}}_\mathbf{m} &= \tilde{\mathbf{A}}_\mathbf{0} + \left(\frac{\tilde{\mathbf{A}}_\mathbf{1}}{(\zeta t + R_1)}\right), \\
\bar{\mathbf{Q}}_\mathbf{pem} &= \bar{\mathbf{Q}}_\mathbf{p0} + \bar{\mathbf{Q}}_\mathbf{e0} + \left(\frac{\bar{\mathbf{Q}}_\mathbf{p1}}{(\zeta t + R_1)}\right) + \bar{\mathbf{Q}}_\mathbf{p2}(\zeta t + R_1), \\
\tilde{\mathbf{Q}}_\mathbf{pm} &= \tilde{\mathbf{Q}}_\mathbf{p0} + \tilde{\mathbf{Q}}_\mathbf{p1}(\zeta t + R_1)
\end{aligned} \tag{5.27}$$

where, Eq. (5.25) is the set of $8n$ ODE and $3n$ algebraic equations are expressed in Eq. (5.26). These are obtained by equating the coefficients of the arbitrary variations δg_l^i ($l = 1, \ldots, 11$; $i = 1, 2, \ldots, n$) individually to zero and performing the integrations over ξ direction. The elements of the matrices $\bar{\mathbf{A}}_\mathbf{0}$, $\bar{\mathbf{A}}_\mathbf{1}$, $\hat{\mathbf{A}}_\mathbf{0}$, $\hat{\mathbf{A}}_\mathbf{1}$, $\tilde{\mathbf{A}}_\mathbf{0}$, $\tilde{\mathbf{A}}_\mathbf{1}$, $\mathbf{K}$ and $\mathbf{M}$ which are non-zero are listed in the following page:

$$
\begin{aligned}
&M_{i_1j_1} = M_{j_4i_4} = \langle f_5^i f_3^j\rangle_\psi, \quad M_{i_2j_2} = M_{j_6i_6} = \langle f_8^i f_1^j\rangle_\psi, \quad M_{i_3j_3} = M_{j_5i_5} = \langle f_7^i f_2^j\rangle_\psi,\\
&M_{i_7j_7} = M_{j_8i_8} = \langle f_{11}^i f_9^j\rangle_\psi\\
&\bar{A}_{0_{i_1j_4}} = p_{33}\langle f_5^i f_5^j\rangle_\psi, \quad \bar{A}_{0_{i_1j_8}} = p_{38}\langle f_5^i f_{11}^j\rangle_\psi, \quad \bar{A}_{0_{i_2j_5}} = p_{45}\langle f_8^i f_7^j\rangle_\psi,\\
&\bar{A}_{0_{i_2j_6}} = p_{55}\langle f_8^i f_8^j\rangle_\psi, \quad \bar{A}_{0_{i_3j_5}} = p_{44}\langle f_7^i f_7^j\rangle_\psi, \quad \bar{A}_{0_{i_3j_6}} = p_{45}\langle f_7^i f_8^j\rangle_\psi,\\
&\bar{A}_{0_{i_7j_4}} = p_{38}\langle f_{11}^i f_5^j\rangle_\psi, \quad \bar{A}_{0_{i_7j_8}} = p_{88}\langle f_{11}^i f_{11}^j\rangle_\psi, \quad \bar{A}_{1_{i_2j_1}} = -\tfrac{1}{\psi}\langle f_8^i f_{3,\xi}^j\rangle_\psi\\
&\bar{A}_{1_{i_2j_2}} = \langle f_8^i f_1^j\rangle_\psi, \quad \bar{A}_{1_{i_4j_4}} = -\langle f_3^i f_5^j\rangle_\psi, \quad \bar{A}_{1_{i_4j_6}} = -\tfrac{1}{\psi}\langle f_3^i f_{8,\xi}^j\rangle_\psi\\
&\bar{A}_{1_{i_5j_5}} = -\langle f_2^i f_7^j\rangle_\psi, \quad \bar{A}_{1_{i_6j_6}} = -2\langle f_1^i f_8^j\rangle_\psi, \quad \bar{A}_{1_{i_8j_8}} = -\langle f_9^i f_{11}^j\rangle_\psi,\\
&\hat{A}_{0_{i_1j_1}} = p_{31}\langle f_5^i f_4^j\rangle_\psi, \quad \hat{A}_{0_{i_1j_2}} = p_{36}\langle f_5^i f_6^j\rangle_\psi, \quad \hat{A}_{0_{i_2j_3}} = p_{57}\langle f_8^i f_{10}^j\rangle_\psi,\\
&\hat{A}_{0_{i_7j_1}} = p_{81}\langle f_{11}^i f_4^j\rangle_\psi, \quad \hat{A}_{0_{i_7j_2}} = p_{86}\langle f_{11}^i f_6^j\rangle_\psi, \quad \hat{A}_{1_{i_4j_1}} = \langle f_3^i f_4^j\rangle_\psi,\\
&\hat{A}_{1_{i_5j_2}} = -\tfrac{1}{\psi}\langle f_2^i f_{6,\xi}^j\rangle_\psi, \quad \hat{A}_{1_{i_6j_1}} = -\tfrac{1}{\psi}\langle f_1^i f_{4,\xi}^j\rangle_\psi, \quad \hat{A}_{1_{i_6j_1}} = -\tfrac{1}{\psi}\langle f_1^i f_{4,\xi}^j\rangle_\psi,\\
&\tilde{A}_{0_{i_1j_4}} = p_{13}\langle f_4^i f_5^j\rangle_\psi, \quad \tilde{A}_{0_{i_1j_8}} = p_{18}\langle f_4^i f_{11}^j\rangle_\psi, \quad \tilde{A}_{0_{i_2j_4}} = p_{36}\langle f_6^i f_5^j\rangle_\psi,\\
&\tilde{A}_{0_{i_2j_8}} = p_{68}\langle f_6^i f_{11}^j\rangle_\psi, \quad \tilde{A}_{0_{i_3j_5}} = -p_{47}\langle f_{10}^i f_7^j\rangle_\psi, \quad \tilde{A}_{0_{i_3j_6}} = -p_{57}\langle f_{10}^i f_8^j\rangle_\psi,\\
&\tilde{A}_{1_{i_1j_1}} = -\langle f_4^i f_3^j\rangle_\psi, \quad \tilde{A}_{1_{i_1j_2}} = -\tfrac{1}{\psi}\langle f_4^i f_{1,\xi}^j\rangle_\psi, \quad \tilde{A}_{1_{i_2j_3}} = -\tfrac{1}{\psi}\langle f_6^i f_{2,\xi}^j\rangle_\psi,\\
&\tilde{A}_{1_{i_3j_7}} = -\tfrac{1}{\psi}\langle f_{10}^i f_{9,\xi}^j\rangle_\psi, \quad K_{i_1j_1} = -p_{11}\langle f_4^i f_4^j\rangle_\psi, \quad K_{i_1j_2} = -p_{16}\langle f_4^i f_6^j\rangle_\psi,\\
&K_{i_2j_1} = -p_{16}\langle f_6^i f_4^j\rangle_\psi, \quad K_{i_2j_2} = -p_{66}\langle f_6^i f_6^j\rangle_\psi, \quad K_{i_3j_3} = -p_{77}\langle f_{10}^i f_{10}^j\rangle_\psi
\end{aligned}
\tag{5.28}
$$

where for integration over the circumferential span ψ, a notation $\langle\ldots\rangle_\psi = \psi\int_0^1(\ldots)d\xi$ has been used. The indices are calculated as $i_p = (p-1)n+i$ and $j_q = (q-1)n+j$ for $p,q = 1,2,\ldots,8$. The matrices, $\mathbf{M}$, $\bar{\mathbf{A}}_\mathbf{0}$, $\bar{\mathbf{A}}_\mathbf{1}$ are $8n\times 8n$, $\hat{\mathbf{A}}_\mathbf{0}$, $\hat{\mathbf{A}}_\mathbf{1}$ are $8n\times 3n$, $\tilde{\mathbf{A}}_\mathbf{0}$, $\tilde{\mathbf{A}}_\mathbf{1}$ are $3n\times 8n$ and $\mathbf{K}$ is $3n\times 3n$ matrix. $\bar{\mathbf{Q}}_\mathbf{p0}$, $\bar{\mathbf{Q}}_\mathbf{e0}$, $\bar{\mathbf{Q}}_\mathbf{p1}$, $\bar{\mathbf{Q}}_\mathbf{p2}$ are vectors containing $8n$ components and $\tilde{\mathbf{Q}}_\mathbf{p0}$, $\tilde{\mathbf{Q}}_\mathbf{p1}$ have $3n$ components, respectively. The non-zero terms in these load vectors are given by

$$
\begin{aligned}
&\bar{Q}_{p0_{i_1}} = p_{33}p_a\langle f_5^i\rangle_\psi, \quad \bar{Q}_{p0_{i_4}} = -2p_d\langle f_3^i\rangle_\psi,\\
&\bar{Q}_{p1_{i_4}} = -p_a\langle f_3^i\rangle_\psi, \quad \bar{Q}_{p2_{i_1}} = p_{33}p_d\langle f_5^i\rangle_\psi
\end{aligned}
$$

$$\bar{Q}_{p2_{i_7}} = p_{83}p_d\langle f_{11}^i\rangle_\psi, \quad \tilde{Q}_{p0_{i_1}} = p_{13}p_a\langle f_4^i\rangle_\psi$$
$$\tilde{Q}_{p0_{i_2}} = p_{36}p_a\langle f_6^i\rangle_\psi, \quad \tilde{Q}_{p1_{i_1}} = p_{13}p_d\langle f_4^i\rangle_\psi$$
$$\tilde{Q}_{p1_{i_2}} = p_{36}p_d\langle f_6^i\rangle_\psi, \quad \bar{Q}_{e0_{i_7}} = \begin{cases} \frac{f_{11}\phi_1}{t} & \text{for } k=1 \\ \frac{-f_{11}\phi_2}{t} & \text{for } k=L \\ 0 & \text{otherwise} \end{cases} \tag{5.29}$$

Since the functions f_l^i are known analytical functions, elements of the matrices defined in Eqs. (5.28) and (5.29) are evaluated in close form, as described in Sec. 3.6 of Chapter 3. Solving the system of algebraic equations (5.26) for $\hat{\mathbf{G}}$ and substituting it back into the Eq. (5.25) yields the following first-order ODE after using a shell geometric constant $s = R_1/t$.

$$(\zeta+s)^2\bar{\mathbf{G}}_{,\zeta} = [s^2\mathbf{A} + \zeta\mathbf{A_3} + \zeta^2\mathbf{A_4}]\bar{\mathbf{G}} + [\zeta^3\mathbf{G_{3mat}} + \zeta^2\mathbf{G_{2mat}} + \zeta\mathbf{G_{1mat}} + s^2\mathbf{G_{0mat}}] \tag{5.30}$$

where

$$\begin{aligned}
\mathbf{A_4} &= \left(\frac{R_1}{s}\right)\mathbf{M}^{-1}\bar{\mathbf{A}}_\mathbf{0} + \left(\frac{R_1}{s}\right)\mathbf{M}^{-1}\hat{\mathbf{A}}_\mathbf{0}\mathbf{K}^{-1}\tilde{\mathbf{A}}_\mathbf{0} \\
\mathbf{A_3} &= 2R_1\mathbf{M}^{-1}\bar{\mathbf{A}}_\mathbf{0} + \mathbf{M}^{-1}\bar{\mathbf{A}}_\mathbf{1} + 2R_1\mathbf{M}^{-1}\hat{\mathbf{A}}_\mathbf{0}\mathbf{K}^{-1}\tilde{\mathbf{A}}_\mathbf{0} + \mathbf{M}^{-1}\hat{\mathbf{A}}_\mathbf{0}\mathbf{K}^{-1}\tilde{\mathbf{A}}_\mathbf{1} + \mathbf{M}^{-1}\hat{\mathbf{A}}_\mathbf{1}\mathbf{K}^{-1}\tilde{\mathbf{A}}_\mathbf{0} \\
\mathbf{A} &= \frac{R_1}{s}\mathbf{M}^{-1}\bar{\mathbf{A}}_\mathbf{0} + \frac{1}{s}\mathbf{M}^{-1}\bar{\mathbf{A}}_\mathbf{1} + \frac{R_1}{s}\mathbf{M}^{-1}\hat{\mathbf{A}}_\mathbf{0}\mathbf{K}^{-1}\tilde{\mathbf{A}}_\mathbf{0} + \frac{1}{s}\mathbf{M}^{-1}\hat{\mathbf{A}}_\mathbf{0}\mathbf{K}^{-1}\tilde{\mathbf{A}}_\mathbf{1} + \frac{1}{s}\mathbf{M}^{-1}\hat{\mathbf{A}}_\mathbf{1}\mathbf{K}^{-1}\tilde{\mathbf{A}}_\mathbf{0} \\
&\quad + \left(\frac{1}{sR_1}\right)\mathbf{M}^{-1}\hat{\mathbf{A}}_\mathbf{1}\mathbf{K}^{-1}\tilde{\mathbf{A}}_\mathbf{1}
\end{aligned} \tag{5.31}$$

And

$$\begin{aligned}
\mathbf{G_{3mat}} &= \left(\frac{R_1}{s}\right)^2\mathbf{M}^{-1}\bar{\mathbf{Q}}_\mathbf{p2} + \left(\frac{R_1}{s}\right)^2\mathbf{M}^{-1}\hat{\mathbf{A}}_\mathbf{0}\mathbf{K}^{-1}\tilde{\mathbf{Q}}_\mathbf{p1} \\
\mathbf{G_{2mat}} &= \left(\frac{R_1}{s}\right)\mathbf{M}^{-1}\left[\bar{\mathbf{Q}}_\mathbf{p0} + \bar{\mathbf{Q}}_\mathbf{e0}\right] + \left(\frac{3R_1^2}{s}\right)\mathbf{M}^{-1}\bar{\mathbf{Q}}_\mathbf{p2} + \left(\frac{R_1}{s}\right)\mathbf{M}^{-1}\hat{\mathbf{A}}_\mathbf{0}\mathbf{K}^{-1}\tilde{\mathbf{Q}}_\mathbf{p0} \\
&\quad + \left(\frac{3R_1^2}{s}\right)\mathbf{M}^{-1}\hat{\mathbf{A}}_\mathbf{0}\mathbf{K}^{-1}\tilde{\mathbf{Q}}_\mathbf{p1} + \left(\frac{R_1}{s}\right)\mathbf{M}^{-1}\hat{\mathbf{A}}_\mathbf{1}\mathbf{K}^{-1}\tilde{\mathbf{Q}}_\mathbf{p1} \\
\mathbf{G_{1mat}} &= 3R_1^2\mathbf{M}^{-1}\bar{\mathbf{Q}}_\mathbf{p2} + 2R_1\mathbf{M}^{-1}\left[\bar{\mathbf{Q}}_\mathbf{p0} + \bar{\mathbf{Q}}_\mathbf{e0}\right] + \mathbf{M}^{-1}\bar{\mathbf{Q}}_\mathbf{p1} + 2R_1\mathbf{M}^{-1}\hat{\mathbf{A}}_\mathbf{0}\mathbf{K}^{-1}\tilde{\mathbf{Q}}_\mathbf{p0} \\
&\quad + 3R_1^2\mathbf{M}^{-1}\hat{\mathbf{A}}_\mathbf{0}\mathbf{K}^{-1}\tilde{\mathbf{Q}}_\mathbf{p1} + \mathbf{M}^{-1}\hat{\mathbf{A}}_\mathbf{1}\mathbf{K}^{-1}\tilde{\mathbf{Q}}_\mathbf{p0} + 2R_1\mathbf{M}^{-1}\hat{\mathbf{A}}_\mathbf{1}\mathbf{K}^{-1}\tilde{\mathbf{Q}}_\mathbf{p1} \\
\mathbf{G_{0mat}} &= \frac{R_1}{s}\mathbf{M}^{-1}\left[\bar{\mathbf{Q}}_\mathbf{p0} + \bar{\mathbf{Q}}_\mathbf{e0}\right] + \frac{1}{s}\mathbf{M}^{-1}\bar{\mathbf{Q}}_\mathbf{p1} + \frac{{R_1}^2}{s}\mathbf{M}^{-1}\bar{\mathbf{Q}}_\mathbf{p2} + \frac{R_1}{s}\mathbf{M}^{-1}\hat{\mathbf{A}}_\mathbf{0}\mathbf{K}^{-1}\tilde{\mathbf{Q}}_\mathbf{p0} \\
&\quad + \frac{{R_1}^2}{s}\mathbf{M}^{-1}\hat{\mathbf{A}}_\mathbf{0}\mathbf{K}^{-1}\tilde{\mathbf{Q}}_\mathbf{p1} + \frac{1}{s}\mathbf{M}^{-1}\hat{\mathbf{A}}_\mathbf{1}\mathbf{K}^{-1}\tilde{\mathbf{Q}}_\mathbf{p0} + \frac{R_1}{s}\mathbf{M}^{-1}\hat{\mathbf{A}}_\mathbf{1}\mathbf{K}^{-1}\tilde{\mathbf{Q}}_\mathbf{p1}
\end{aligned} \tag{5.32}$$

Equation (5.30) represents a set of nonhomogeneous linear ODEs with variable coefficients. By using the method of modified power series expansion, a closed form solution for the system of

equations (5.30) is obtained. Hence, a general solution is acquired in the following form for the variable coefficient ODE in Eq. (5.30) as:

$$[\bar{\mathbf{G}}(\zeta)] = \left[\sum_{i=0}^{\infty}\left(\frac{\hat{\mathbf{Z}}_i\zeta^i}{i!}\right)\right] + \left[\sum_{i=0}^{\infty}\left(\frac{\hat{\mathbf{H}}_i\zeta^i}{i!}\right)\right][\mathbf{C_o}] \tag{5.33}$$

The boundary and interface conditions in Eqs. (5.17)-(5.19) can be written in terms of functions $g_l^i(\zeta)$ as

$$\text{for } k=1, \quad \text{at } \zeta=0: \quad g_5^i=0, \quad g_7^i=0, \quad g_8^i=0, \quad g_9^i \quad \text{or} \quad g_{11}^i=0$$

$$\text{for } k=L, \quad \text{at } \zeta=1: \quad g_5^i=0, \quad g_7^i=0, \quad g_8^i=0, \quad g_9^i \quad \text{or} \quad g_{11}^i=0 \tag{5.34}$$

$$[(g_1^i,\, g_2^i,\, g_3^i,\, g_5^i,\, g_7^i,\, g_8^i,\, g_9^i,\, g_{11}^i)|_{\zeta=1}]^{(k)} = [(g_1^i,\, g_2^i,\, g_3^i,\, g_5^i,\, g_7^i,\, g_8^i,\, g_9^i,\, g_{11}^i)|_{\zeta=0}]^{(k+1)} \tag{5.35}$$

At the $k=n_q$ $(q=1,\dots L_a)$ interfaces for $k=1,2,\dots,L-1$ except for g_{11}^i where ϕ is prescribed, the following condition is replaced instead of the continuity condition on g_{11}^i

$$g_9^i|_{\zeta=1}=0; \qquad q=1,...,L_a \tag{5.36}$$

Equations (5.34)-(5.36) give the $8n$ boundary conditions and $8n\times(L-1)$ interface continuity conditions which are used to obtain the $8n\times L$ constants $C_o^{(k)}$'s for L layers. This determines $\bar{\mathbf{G}}(\zeta)$ completely and subsequently, $\hat{\mathbf{G}}(\zeta)$ can now be obtained by solving the algebraic equation (5.26). For elaboration, in the Sec. 5.6 below, the elements of the matrices are obtained using the initial trial functions for $f_l^i(\xi)$ in the first iteration which are also given there. Hence, the first iteration step is completed.

5.5.2 Second Iteration Step

In this step, the solution of the previous step is taken as the known approximate solution for $g_l^i(\zeta)$, while functions f_l^i are considered unknown. The variation δX for this case is given by

$$\delta X_l^i = \sum_{i=1}^{n} g_l^i(\zeta)\delta f_l^i \quad \text{for} \quad l=1,2,\dots,11 \tag{5.37}$$

According to Eq. (5.20) $f_l^i(\xi)$ functions are partitioned into

$$\bar{\mathbf{F}} = \left[f_3^1\dots f_3^n\ f_1^1\dots f_1^n\ f_2^1\dots f_2^n\ f_4^1\dots f_4^n\ f_6^1\dots f_6^n\ f_8^1\dots f_8^n\ f_9^1\dots f_9^n\ f_{10}^1\dots f_{10}^n\right]^{\mathrm{T}}$$

$$\hat{\mathbf{F}} = \left[f_5^1 \dots f_5^n \; f_7^1 \dots f_7^n \; f_{11}^1 \dots f_{11}^n \right]^{\mathrm{T}} \tag{5.38}$$

Substituting Eqs. (5.37) and (5.21) in Eq. (5.16), and the arbitrary coefficients of δf_l^i are individually equated to zero to yield the $8n$ system of differential equations and $3n$ simultaneous algebraic equations for f_l^i which are in the form of

$$\mathbf{N}\bar{\mathbf{F}}_{,\xi} = \bar{\mathbf{B}}\bar{\mathbf{F}} + \hat{\mathbf{B}}\hat{\mathbf{F}} + \bar{\mathbf{P}}_{\mathbf{m}} \tag{5.39}$$

$$\mathbf{L}\hat{\mathbf{F}} = \tilde{\mathbf{B}}\bar{\mathbf{F}} + \tilde{\mathbf{P}}_{\mathbf{m}} + \tilde{\mathbf{P}}_{\mathbf{em}} \tag{5.40}$$

The non-zero elements of the matrices are listed below

$$N_{i_1j_1} = N_{j_6i_6} = \tfrac{1}{\psi}\langle \tfrac{g_8^i g_3^j}{\zeta t + R_1}\rangle_h, \quad N_{i_2j_2} = N_{j_4i_4} = \tfrac{1}{\psi}\langle \tfrac{g_4^i g_1^j}{\zeta t + R_1}\rangle_h,$$

$$N_{i_3j_3} = N_{j_5i_5} = \tfrac{1}{\psi}\langle \tfrac{g_6^i g_2^j}{\zeta t + R_1}\rangle_h, \quad N_{i_7j_7} = N_{j_8i_8} = \tfrac{1}{\psi}\langle \tfrac{g_{10}^i g_9^j}{\zeta t + R_1}\rangle_h,$$

$$\bar{B}_{i_1j_2} = \langle \tfrac{g_8^i g_1^j}{\zeta t + R_1}\rangle_h - \tfrac{1}{t}\langle g_8^i g_{1,\zeta}^j\rangle_h, \quad \bar{B}_{i_1j_6} = \bar{p}_{55}\langle g_8^i g_8^j\rangle_h, \quad \bar{B}_{i_1j_8} = p_{57}\langle g_8^i g_{10}^j\rangle_h,$$

$$\bar{B}_{i_2j_1} = \langle \tfrac{g_4^i g_3^j}{\zeta t + R_1}\rangle_h, \quad \bar{B}_{i_2j_4} = \bar{p}_{11}\langle g_4^i g_4^j\rangle_h, \quad \bar{B}_{i_2j_5} = \bar{p}_{16}\langle g_4^i g_6^j\rangle_h,$$

$$\bar{B}_{i_2j_7} = -\tfrac{\bar{p}_{18}}{t}\langle g_4^i g_{9,\zeta}^j\rangle_h, \quad \bar{B}_{i_3j_4} = \bar{p}_{16}\langle g_6^i g_4^j\rangle_h, \quad \bar{B}_{i_3j_5} = \bar{p}_{66}\langle g_6^i g_6^j\rangle_h,$$

$$\bar{B}_{i_3j_7} = -\tfrac{\bar{p}_{68}}{t}\langle g_6^i g_{9,\zeta}^j\rangle_h, \quad \bar{B}_{i_4j_6} = -2\langle \tfrac{g_1^i g_8^j}{\zeta t + R_1}\rangle_h - \tfrac{1}{t}\langle g_1^i g_{8,\zeta}^j\rangle_h, \quad \bar{B}_{i_6j_4} = \langle \tfrac{g_3^i g_4^j}{\zeta t + R_1}\rangle_h,$$

$$\bar{B}_{i_7j_6} = p_{75}\langle g_{10}^i g_8^j\rangle_h, \quad \bar{B}_{i_3j_4} = -\bar{p}_{77}\langle g_{10}^i g_{10}^j\rangle_h,$$

$$\hat{B}_{i_1j_2} = \bar{p}_{45}\langle g_8^i g_7^j\rangle_h, \quad \hat{B}_{i_2j_1} = \bar{p}_{13}\langle g_4^i g_5^j\rangle_h, \quad \hat{B}_{i_3j_1} = \bar{p}_{36}\langle g_6^i g_5^j\rangle_h,$$

$$\hat{B}_{i_5j_2} = -\langle \tfrac{g_2^i g_7^j}{\zeta t + R_1}\rangle_h - \tfrac{1}{t}\langle g_2^i g_{7,\zeta}^j\rangle_h, \quad \hat{B}_{i_6j_1} = -\langle \tfrac{g_3^i g_5^j}{\zeta t + R_1}\rangle_h - \tfrac{1}{t}\langle g_3^i g_{5,\zeta}^j\rangle_h,$$

$$\hat{B}_{i_7j_2} = p_{74}\langle g_{10}^i g_7^j\rangle_h, \quad \hat{B}_{i_8j_3} = -\langle \tfrac{g_9^i g_{11}^j}{\zeta t + R_1}\rangle_h - \tfrac{1}{t}\langle g_9^i g_{11,\zeta}^j\rangle_h,$$

$$\tilde{B}_{i_1j_1} = -\tfrac{1}{t}\langle g_5^i g_{3,\zeta}^j\rangle_h, \quad \tilde{B}_{i_1j_4} = \bar{p}_{13}\langle g_5^i g_4^j\rangle_h, \quad \tilde{B}_{i_1j_5} = \bar{p}_{36}\langle g_5^i g_6^j\rangle_h,$$

$$\tilde{B}_{i_1j_7} = -\tfrac{\bar{p}_{38}}{t}\langle g_5^i g_{9,\zeta}^j\rangle_h, \quad \tilde{B}_{i_2j_3} = -\tfrac{1}{t}\langle g_7^i g_{2,\zeta}^j\rangle_h, \quad \tilde{B}_{i_2j_6} = \bar{p}_{45}\langle g_7^i g_8^j\rangle_h,$$

$$\tilde{B}_{i_2j_8} = \bar{p}_{47}\langle g_7^i g_{10}^j\rangle_h, \quad \tilde{B}_{i_3j_4} = \bar{p}_{81}\langle g_{11}^i g_4^j\rangle_h, \quad \tilde{B}_{i_3j_5} = \bar{p}_{86}\langle g_{11}^i g_6^j\rangle_h,$$

$$\tilde{B}_{i_3j_7} = -\tfrac{1}{t}\langle g_{11}^i g_{9,\zeta}^j\rangle_h, \quad L_{i_1j_1} = -\bar{p}_{33}\langle g_5^i g_5^j\rangle_h, \quad L_{i_2j_2} = -\bar{p}_{44}\langle g_7^i g_7^j\rangle_h,$$

$$L_{i_3j_1} = -\bar{p}_{83}\langle g_{11}^i g_5^j\rangle_h, \quad L_{i_3j_3} = -\bar{p}_{88}\langle g_{11}^i g_{11}^j\rangle_h$$

where $\langle \dots \rangle_h = \sum_{k=1}^{L} t^{(k)} \int_0^1 (\dots)^{(k)}\, d\zeta$ denotes integration across the thickness. Above integrations are performed over the ζ direction on the known functions of ζ and by applying integration by parts

wherever necessary. Thus size of the obtained matrices, $\mathbf{N}$, $\bar{\mathbf{B}}$, $\hat{\mathbf{B}}$, $\mathbf{L}$ and $\tilde{\mathbf{B}}$ are $8n \times 8n$, $8n \times 8n$, $8n \times 3n$, $3n \times 3n$ and $3n \times 8n$, respectively. $\bar{\mathbf{P}}_{\mathbf{m}}$, $\tilde{\mathbf{P}}_{\mathbf{m}}$ and $\tilde{\mathbf{P}}_{\mathbf{em}}$ are column vectors of size $8n$, $3n$ and $3n$ respectively, comprising of the loading terms with the following non-zero elements.

$$\bar{P}_{m_{i2}} = \bar{p}_{13} p_a \langle g_4^i \rangle_h + \bar{p}_{13} p_d \langle g_4^i(\zeta t + R_1) \rangle_h,$$

$$\bar{P}_{m_{i3}} = \bar{p}_{36} p_a \langle g_6^i \rangle_h + \bar{p}_{36} p_d \langle g_6^i(\zeta t + R_1) \rangle_h,$$

$$\bar{P}_{m_{i6}} = -2 p_d \langle g_3^i \rangle_h - p_a \langle \tfrac{g_3^i}{(\zeta t + R_1)} \rangle_h,$$

$$\tilde{P}_{m_{i1}} = \bar{p}_{33} p_a \langle g_5^i \rangle_h + \bar{p}_{33} p_d \langle g_5^i(\zeta t + R_1) \rangle_h,$$

$$\tilde{P}_{m_{i3}} = \bar{p}_{83} p_a \langle g_5^i \rangle_h + \bar{p}_{83} p_d \langle g_5^i(\zeta t + R_1) \rangle_h +$$

$$\tilde{P}_{em_{i3}} = \langle \left[-g_{11}\phi_1 \Big|^{(k=1)} \text{ or } g_{11}\phi_2 \Big|^{(k=L)} \right] \rangle_h$$

Referring back to the Sec. 3.6 of Chapter 3 as discussed, all the above integrations are evaluated in closed form because the general solution obtained in Eq. (5.33) gives close form $g_l^i(\zeta)$ functions. Substituting $\hat{\mathbf{F}}$ which is algebraically solved in Eq. (5.40) back into Eq. (5.39) yields the following set of first order ODEs for $\bar{\mathbf{F}}$:

$$\bar{\mathbf{F}}_{,\xi} = \mathbf{B}\bar{\mathbf{F}} + \mathbf{P}_{\mathbf{m}} \tag{5.41}$$

with $\mathbf{B} = \mathbf{N}^{-1}[\bar{\mathbf{B}} + \hat{\mathbf{B}}\mathbf{L}^{-1}\tilde{\mathbf{B}}]$ and $\mathbf{P}_{\mathbf{m}} = \mathbf{N}^{-1}[\bar{\mathbf{P}}_{\mathbf{m}} + \hat{\mathbf{B}}\mathbf{L}^{-1}[\tilde{\mathbf{P}}_{\mathbf{m}} + \tilde{\mathbf{P}}_{\mathbf{em}}]]$. Equation (5.41) represents a set of nonhomogeneous linear ODEs with constant coefficients. Its complementary solution is of the form $\bar{\mathbf{F}}_{\mathbf{c}}(\xi) = e^{\lambda\xi}\mathbf{Y}$, which on substitution in the homogeneous part of Eq. (5.41) yields

$$\mathbf{B}\mathbf{Y} = \lambda\mathbf{Y} \tag{5.42}$$

Hence, the exponent λ and $\mathbf{Y}$ are the $8n$ eigenvalue and eigenvector pairs of matrix $\mathbf{B}$. Thus, the complete complementary solution $\bar{\mathbf{F}}_{\mathbf{c}}(\xi)$ can be expressed in terms of $8n$ real constants C_i as

$$\bar{\mathbf{F}}_{\mathbf{c}} = \sum_{i=1}^{8n} \mathbf{F}_i(\zeta) C_i \tag{5.43}$$

where $\mathbf{F}_i(\xi)$ are column vectors of functions corresponding to the eigen pair λ_i and Y_i, whose functional forms depend on the nature of λ_i (real or complex), details of which can be found in

Sec. 3.4.2 of Chapter 3. It is seen from Eq. (5.41) that $\mathbf{P_m}$ is a linear function of ξ. Thus, the general solution of Eq. (5.41) is obtained in similar fashion of the form

$$\bar{\mathbf{F}}(\xi) = \sum_{i=1}^{8n} \mathbf{H}_i(\xi) C_i + \mathbf{U_0} \tag{5.44}$$

The prescribed circumferential edge boundary conditions (5.20) which are homogeneous are expressed in terms of $\bar{\mathbf{F}}$ to be satisfied by the general solution in Eq. (5.44) for obtaining the constants C_i

$$\begin{aligned}
&\text{Simply Supported (S) :} && f_3^i = 0, \quad f_4^i = 0, \quad f_6^i = 0 \\
&\text{Clamped (C) :} && f_3^i = 0, \quad f_1^i = 0, \quad f_2^i = 0 \\
&\text{Free (F) :} && f_8^i = 0, \quad f_4^i = 0, \quad f_6^i = 0, \qquad (i = 1, 2, \ldots, n)
\end{aligned} \tag{5.45}$$

The electric boundary condition is given by

$$f_9^i \quad \text{or} \quad f_{10}^i = 0 \tag{5.46}$$

The complete solution for $\bar{\mathbf{F}}$ functions is constructed after obtaining the $8n$ constants C_i which are valid for all the layers. Further, from the algebraic equation Eq. (5.40), functions $\hat{\mathbf{F}}$ can be determined. Hence, the second iteration step is completed. These two iteration steps (Secs. 5.5.1 and 5.5.2) of alternating directions for approximate and analytical solutions are repeated until a prescribed level of convergence is achieved. It is noteworthy, that the exponential term $e^{\alpha(\xi-1)}$ is used in place of $e^{\alpha\xi}$ for the positive eigenvalues in order to limit the maximum value of the exponential to one. This prevents possibility of any numerical instability in the solution which might be caused due to occurrence of very large exponentials corresponding to large positive eigenvalues of the $\mathbf{B}$ matrix in Eq. (5.41) for higher order terms in the integral functions. Since the arbitrary constants corresponding to these eigenvectors are computed accordingly, there is no alteration in the final solution obviously.

5.6 INITIAL TRIAL FUNCTIONS

The initial trial functions considered for the known $f_l^i(\xi)$ functions in the first iteration step are those corresponding to the case of simply supported boundary condition at $\xi = 0, 1$. Although, this choice does not affect the convergence of the solution and there might be increase in one or two iterations. The considered functions are in the form of

$$f_1(\xi) = f_2(\xi) = f_7(\xi) = f_8(\xi) = f_{10}(\xi) = \cos i\pi\xi$$
$$f_3(\xi) = f_4(\xi) = f_5(\xi) = f_6(\xi) = f_9(\xi) = f_{11}(\xi) = \sin i\pi\xi \tag{5.47}$$

Substituting these trial functions from Eq. (5.47) into Eq. (5.28) yields the following non-zero terms of matrices $\mathbf{M}$, $\bar{\mathbf{A}}_\mathbf{0}$, $\bar{\mathbf{A}}_\mathbf{1}$, $\hat{\mathbf{A}}_\mathbf{0}$, $\hat{\mathbf{A}}_\mathbf{1}$, $\tilde{\mathbf{A}}_\mathbf{0}$, $\tilde{\mathbf{A}}_\mathbf{1}$, $\mathbf{K}$, $\bar{\mathbf{Q}}_\mathbf{p0}$, $\bar{\mathbf{Q}}_\mathbf{e0}$, $\bar{\mathbf{Q}}_\mathbf{p1}$, $\bar{\mathbf{Q}}_\mathbf{p2}$, $\tilde{\mathbf{Q}}_\mathbf{p0}$ and $\tilde{\mathbf{Q}}_\mathbf{p1}$:

$$\begin{aligned}
&\bar{A}_{0_{i_1j_4}} = p_{33}, \quad \bar{A}_{0_{i_1j_8}} = p_{38}, \quad \bar{A}_{0_{i_2j_5}} = p_{45},\\
&\bar{A}_{0_{i_2j_6}} = p_{55}, \quad \bar{A}_{0_{i_3j_5}} = p_{44}, \quad \bar{A}_{0_{i_3j_6}} = p_{45},\\
&\bar{A}_{0_{i_7j_4}} = p_{38}, \quad \bar{A}_{0_{i_7j_8}} = p_{88}, \quad \bar{A}_{1_{i_2j_1}} = -\bar{n}\\
&\bar{A}_{1_{i_2j_2}} = 1, \quad \bar{A}_{1_{i_4j_4}} = -1, \quad \bar{A}_{1_{i_4j_6}} = -\bar{n}\\
&\bar{A}_{1_{i_5j_5}} = -1, \quad \bar{A}_{1_{i_6j_6}} = -2, \quad \bar{A}_{1_{i_8j_8}} = -1,\\
&\hat{A}_{0_{i_1j_1}} = p_{31}, \quad \hat{A}_{0_{i_1j_2}} = p_{36}, \quad \hat{A}_{0_{i_2j_3}} = p_{57},\\
&\hat{A}_{0_{i_7j_1}} = p_{81}, \quad \hat{A}_{0_{i_7j_2}} = p_{86}, \quad \hat{A}_{1_{i_4j_1}} = 1,\\
&\hat{A}_{1_{i_5j_2}} = -\bar{n}, \quad \hat{A}_{1_{i_6j_1}} = -\bar{n}, \quad \hat{A}_{1_{i_6j_1}} = -\bar{n},\\
&\tilde{A}_{0_{i_1j_4}} = p_{13}, \quad \tilde{A}_{0_{i_1j_8}} = p_{18}, \quad \tilde{A}_{0_{i_2j_4}} = p_{36},\\
&\tilde{A}_{0_{i_2j_8}} = p_{68}, \quad \tilde{A}_{0_{i_3j_5}} = -p_{47}, \quad \tilde{A}_{0_{i_3j_6}} = -p_{57},\\
&\tilde{A}_{1_{i_1j_1}} = -1, \quad \tilde{A}_{1_{i_1j_2}} = -\bar{n}, \quad \tilde{A}_{1_{i_2j_3}} = -\bar{n},\\
&\tilde{A}_{1_{i_3j_7}} = -\bar{n}, \quad K_{i_1j_1} = -p_{11}, \quad K_{i_1j_2} = -p_{16},\\
&K_{i_2j_1} = -p_{16}, \quad K_{i_2j_2} = -p_{66}, \quad K_{i_3j_3} = -p_{77}
\end{aligned} \tag{5.48}$$

where $\bar{n} = i\pi/\psi$ and the loading terms are as follows

$$\bar{Q}_{p0_{i_1}} = 4p_{33}p_a/i\pi, \quad \bar{Q}_{p0_{i_4}} = -8p_d/i\pi,$$

$$\bar{Q}_{p1_{i_4}} = -4p_a/i\pi, \quad \bar{Q}_{p2_{i_1}} = 4p_{33}p_d/i\pi$$

$$\bar{Q}_{p2_{i_7}} = 4p_{83}p_d/i\pi, \quad \tilde{Q}_{p0_{i_1}} = 4p_{13}p_a/i\pi$$

$$\tilde{Q}_{p0_{i_2}} = 4p_{36}p_a/i\pi, \quad \tilde{Q}_{p1_{i_1}} = 4p_{13}p_d/i\pi$$

$$\tilde{Q}_{p1_{i_2}} = 4p_{36}p_d/i\pi, \quad \bar{Q}_{e0_{i_7}} = \begin{cases} \frac{4\phi_1}{i\pi t} & \text{for } k = 1 \\ \frac{-4\phi_2}{i\pi t} & \text{for } k = L \\ 0 & \text{otherwise} \end{cases}$$

and $\mathbf{M}$ reduces to an identity matrix.

5.7 NUMERICAL RESULTS

5.7.1 Simply-supported hybrid cylindrical shell panels

The numerical study is conducted to validate and present the efficacy of the developed solution. Initially, this MMEKM based analytical solution is validated for a physically simply-supported cross-ply laminated cylindrical shell panel having surface mounted piezoelectricity PFRC layers which can act as actuators and sensors. The comparison has been done with the results obtained from a 3D exact solution through a computer program [83].

Table 5.1: Material constants.

Material	Y_1	Y_2	Y_3	G_{23}	G_{13}	G_{12}	ν_{12}	ν_{13}	ν_{23}
Mat.1	181.0	10.3	10.3	2.87	7.17	7.17	0.28	0.28	0.33
Mat.2*	137.9	14.48	14.48	5.86	5.86	5.86	0.21	0.21	0.21
PZT-G1195N‡	63.0	63.0	63.0	24.2	24.2	24.2	0.3	0.3	0.3
PZT-4†	81.23938	81.23938	64.07299	25.6	25.6	30.6	0.32744	0.34271	0.34271
PFRC-2$^\$$	38.87	13.68	13.20	3.0148	4.3541	4.3699	0.31080	0.41796	0.20079
Material	d_{31}	d_{32}	d_{33}	d_{24}	d_{15}	η_{11}	η_{22}	η_{33}	
PZT-G1195N	-145.1	-145.1	145.1	523.55	523.55	15.3	15.3	15.0	
PZT-4	-123.816	-123.816	291.296	496.093	496.093	13.06	13.06	11.51	
PFRC-2	-263	-224	485	0	0	29.769	29.769	24.403	

Units: Young's moduli Y_i and shear moduli G_{ij} in GPa; piezoelectric strain coefficients d_{ij} in pm/V; electric permittivities η_{ij} in nF/m; * [266]; ‡ [267]; † [141]; $^\$$[91]

The elastic layers are made up of Mat.1 and the piezoelectricity layers are made up of PZT-

G1195N and their electro-mechanical properties are listed in the Table 5.1. The laminate scheme

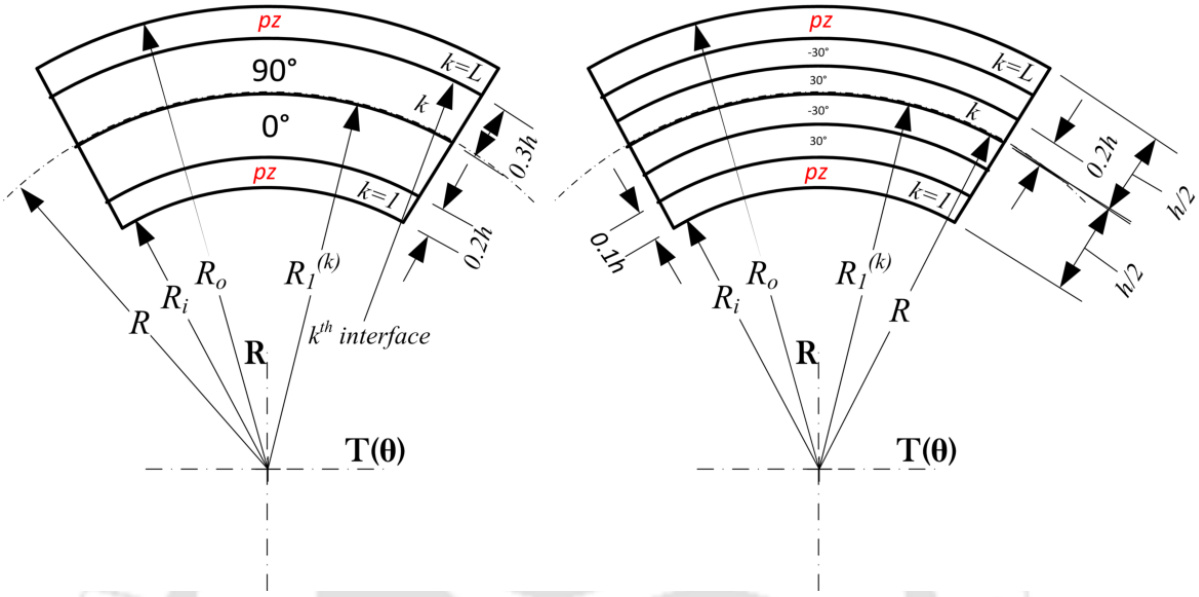

Fig. 5.2: Through-the-thickness laminate scheme of the cylindrical shell panels. Named as shell panel 5a (left) and 5b (right)

considered is that of the shell panel ($5a$) as shown in the Fig. 5.2. The piezoelectricity layers are denoted as pz in the figure of shell panel ($5a$). The elastic plies are of equal thickness $0.3h$, as well as the two surface mounted piezoelectricity layers are of $0.2h$ each. Under an applied uniform pressure loading (UDL), the electro-mechanical response of the hybrid cylindrical shell panels are obtained from the 3D solution. The loading is of magnitude $p_2 = 1\ N/m^2$ subjected over the outer surface, whereas there is no consideration of pressure loading on the inner surface ($p_1 = 0$) for all the following cases. Geometrically, 60^0 is taken as the circumferential span angle (ψ) and a substantially thick shell panel with $S = R/h = 4$ is considered. The shell panel is called SS, synonymous with simply-supported boundary conditions at both its circumferential edges coinciding with $\xi = 0,\ 1$, respectively.

The reported results have been nondimensionalized according to the following relations:

$(\bar{u}, \bar{v}) = (10u,\ v)Y_0/p_0hS^3, \quad (\bar{\sigma}_\theta,\ \bar{\tau}_{r\theta}) = (\sigma_\theta,\ \tau_{r\theta}S^3)/p_0S^2, \quad (\bar{D}_r) = (10D_r)d_0/Sp_0,$

$(\bar{D}_\theta) = (D_\theta)/Sd_0, \quad (\bar{\phi}) = 10^4\phi \quad$ Where $Y_0 = Y_2$ of pz, $d_0 = d_{32}$ and $p_0 = p_2$

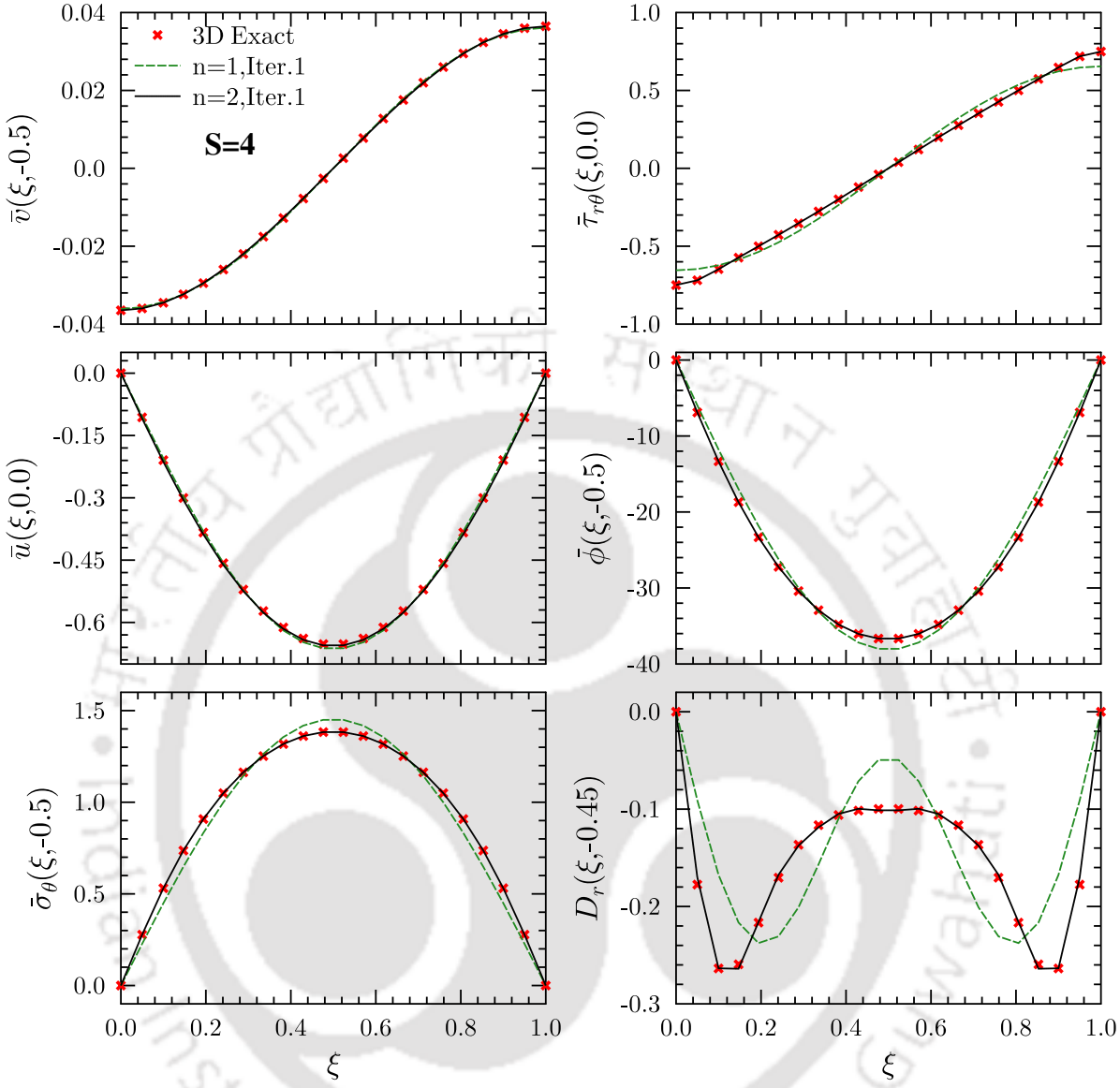

Fig. 5.3: Circumferential variation of field variables in the shell panel (5a) of S=4 with SS and CC-CC circumferential boundary conditions and OC-OC on its outer and inner surfaces.

The circumferential variation of the displacements, stresses and electrical field variables can be analysed from the Fig. 5.3 when the SS cylindrical shell panel has no applied electric potential on its outer and inner surfaces, i.e., open circuited (OC). In the figure, the variations are plotted for the field variables where they attain the highest value. The variations of the field variables appear to be symmetric about the circumferential midspan and are found to be in excellent agreement with the other results obtained from 3D exact solution [83]. Although, the displacement could be predicted with consideration of just a single (n=1) term in the EKM, an extra term (n=2) is

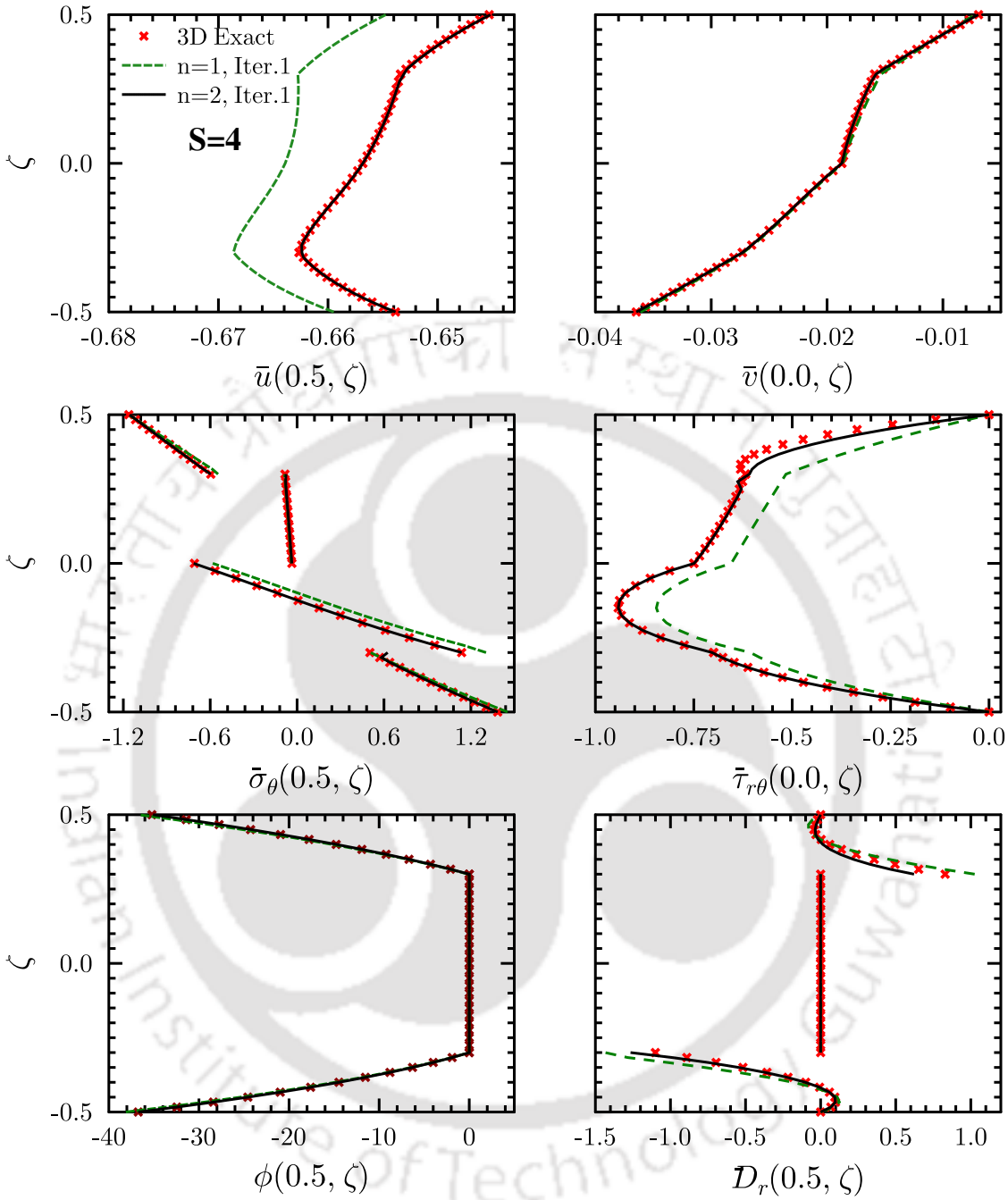

Fig. 5.4: Through-the-thickness variation of field variables in the shell panel (5a) of S=4 with SS and CC-CC circumferential boundary conditions and OC-OC on its outer and inner surfaces.

enough for accurate behaviour of other field variables while achieving convergence within a single (*Iter.* = 1) iteration. It should be noted that, requirement of such lesser number of terms and only a single iteration step, demonstrates the computational power of the MMEKM in the present case as compared to the 3D exact solution by Dumir et al. [83] where solution converged after

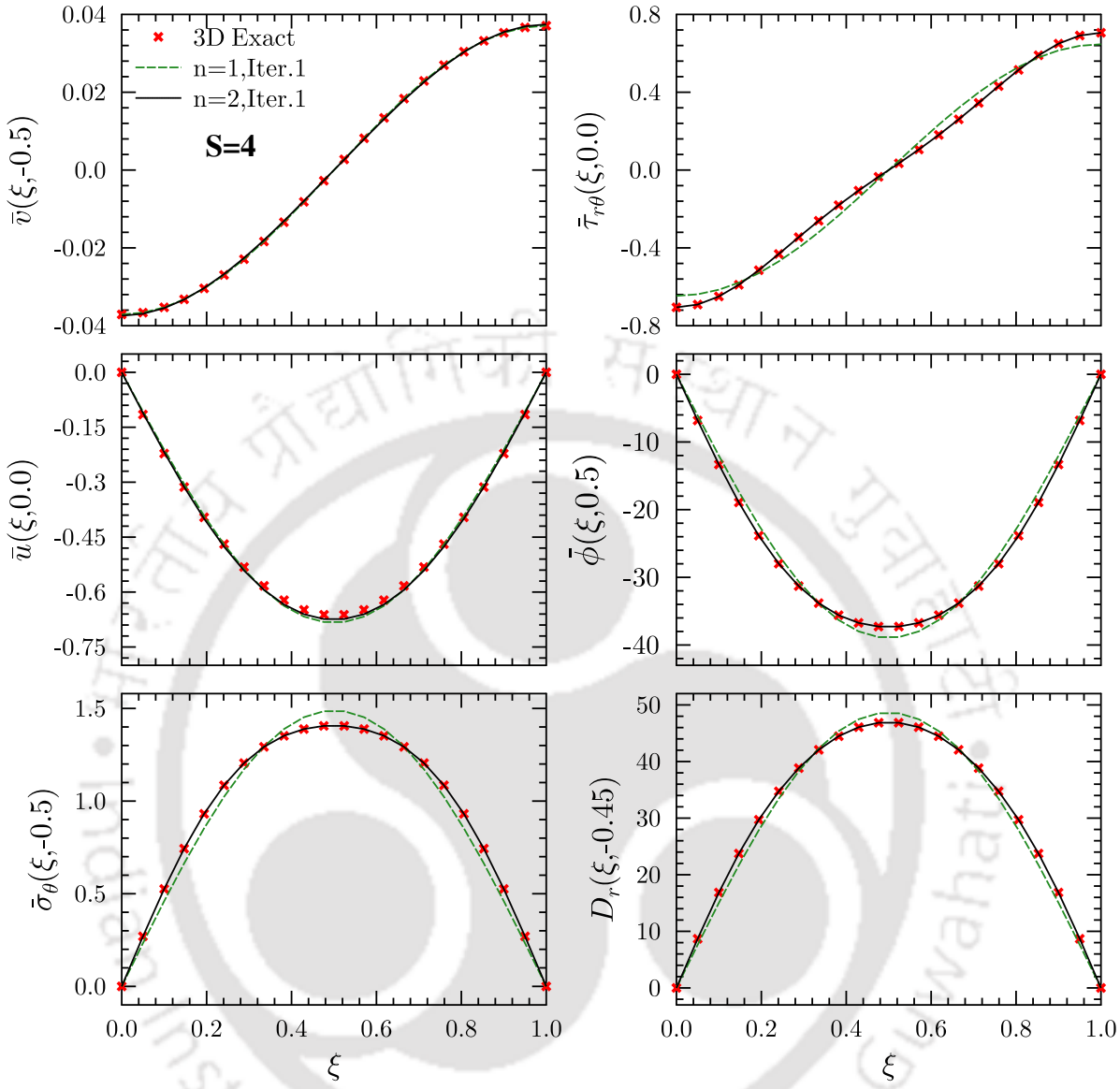

Fig. 5.5: Circumferential variation of field variables in the shell panel (5a) of S=4 with SS and CC-CC circumferential boundary conditions and OC-CC on its outer and inner surfaces, respectively.

49 non-zero Fourier terms in the single Fourier series expansion along the circumference θ of the cylindrical shell loaded with UDL. Moreover, even for the anti-symmetric cross-ply laminate where comparatively more layerwise inhomogeneity exists, the present solution gives accurate through-thickness variations with no extra term or iteration step. Through-the-thickness variation has been presented in the Fig. 5.4, for all the field variables. The nature of the transverse displacement can be inferred to not necessarily follow any predefined curve as customarily assumed in the two-

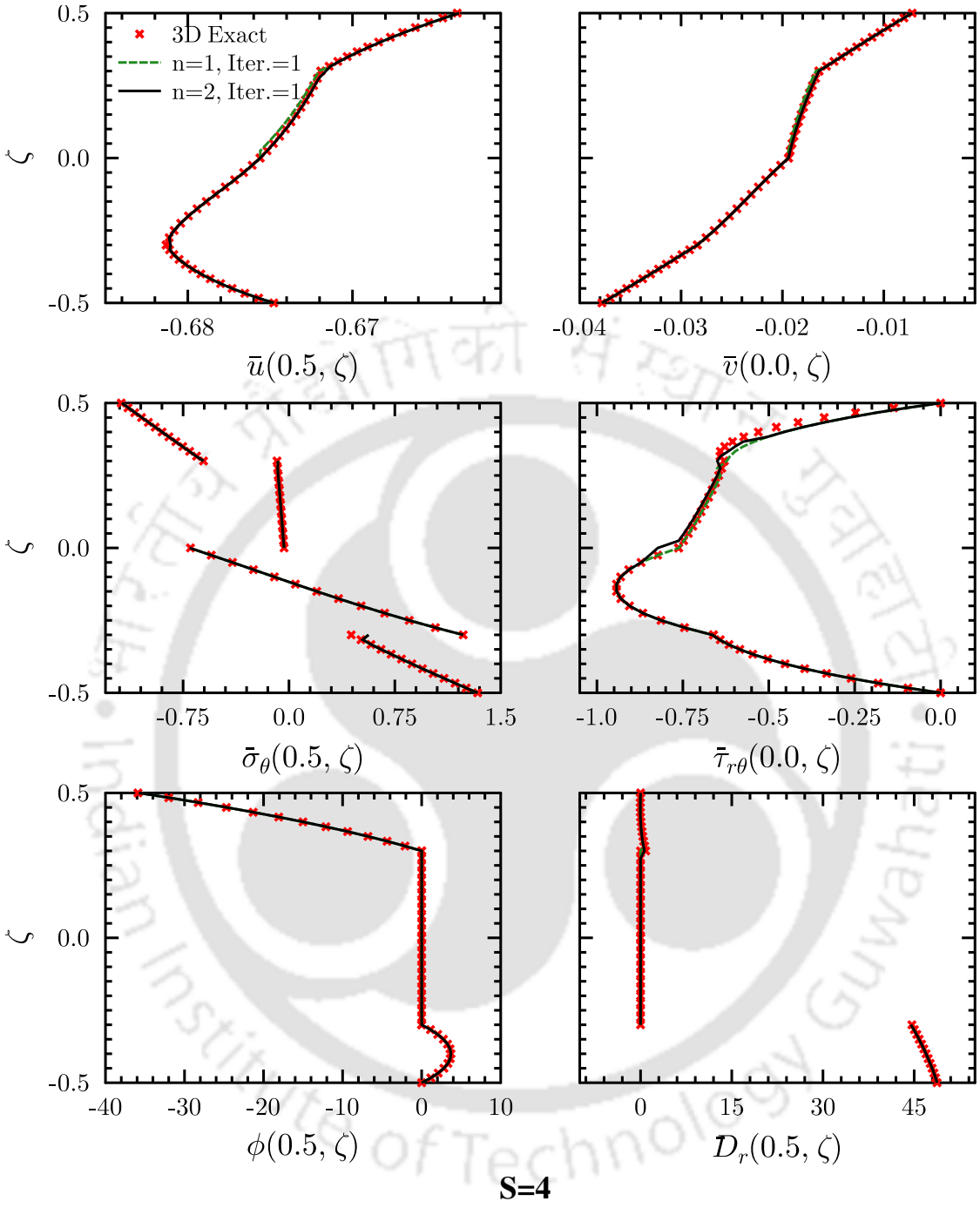

Fig. 5.6: Through-the-thickness variation of field variables in the shell panel (5a) of S=4 with SS and CC-CC circumferential boundary conditions and OC-CC on its outer and inner surfaces.

dimensional (2D) theories. The discontinuous and spontaneous variations across the interfaces are also predicted for the stresses and electric displacement components near exactly.

Analysis of the circumferential and through-thickness distributions of the field variables can be observed from the Figs. 5.5 and 5.6 for a SS cylindrical shell panel. The shell panel has similar

circumferential end electro-mechanical conditions but with closed circuited inner surface.

In such an CC condition, physically the inner surface is grounded where an electric potential ($\phi = 0$) is maintained due to which there occurs an electric charge displacement along the radial direction of the inner piezoelectricity layer (pz). As, for the concerned circumferential electro-mechanical boundary conditions results of the same 3D exact solution could be obtained, the comparison has been done with it. Computationally, the MMEKM demonstarted similar power and accuracy consistent with the interfacial and inner or outer surface boundary conditions. The nature of the variables follow a similar fashion as that of the previously discussed OC-OC condition at the outer-inner surface boundaries. Although, slight changes in the peak values of the displacements and stresses could be observed. But, it can be observed that, there is abrupt change in the nature of D_r along its circumference with alternating maxima and minima values in case of OC-OC condition. Also, in that condition the through-thickness value of the radial electric charge displacement (D_r) undergoes alternating negative and positive charges in the piezoelectricity layers which is again of different magnitude in different pz layers, as can be observed in the Fig. 5.4. The charge displacement is highest at the piezo-elastic layer interface due to which residual charge may be developed at the interface which demands an efficient charge disposal mechanism. Similarly charge discontinuity can be seen in the Fig. 5.6 for OC-CC case. From these variations in the mechanical displacement and electric potential, appropriate electric boundary condition can be employed for actuation and sensing applications.

Further, a benchmark result has been presented for a very thick ($S = 2$) cylindrical hybrid angle-ply shell panel with fully close circuited electrical boundary condition. The circumferential variation of its field variables are shown in the Fig. 5.7. The laminate scheme is as shown for the shell panel (5b) in the Fig. 5.2. The pz is of PFRC-2 and elastic layers are constituted of mat.2 from Table 5.1. Moreover, the span ψ is also taken to be 120^o corresponding to that of a deep shell. As previous procedure, the 3D exact results are obtained to compare all the displacements, stresses and electric entities. A convergence study of the present EKM solution for different iterations

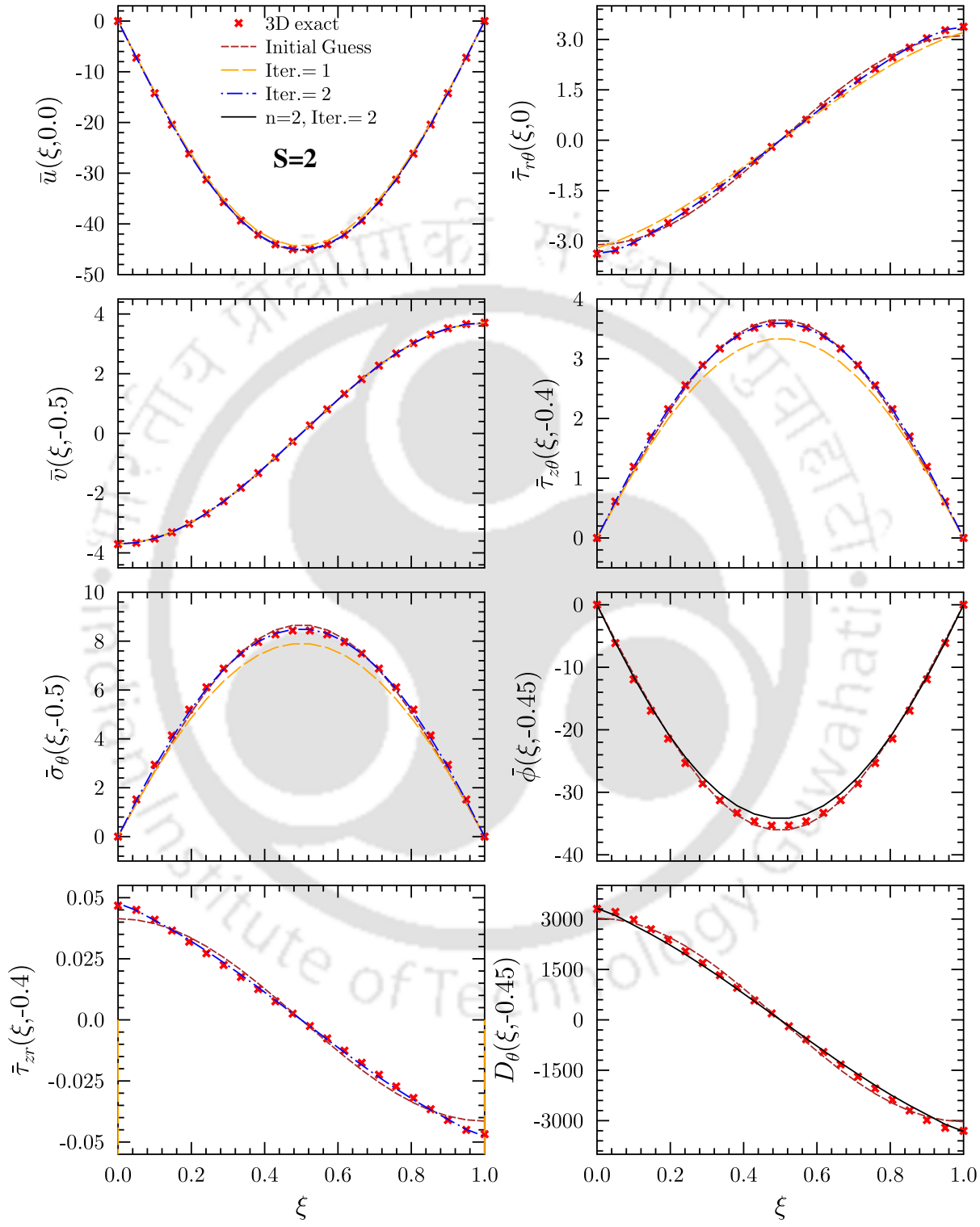

Fig. 5.7: Circumferential variation of field variables in the shell panel (5b) of S=2 with SS and CC-CC circumferential boundary conditions and CC-CC on its outer and inner surfaces, respectively.

(*Iter.*) from an initially guessed function can be inferred from the Fig. 5.7. Again, by the use of just a single term, the results converged after two number of iterations (*Iter.*=2) for most of the mechanical entities. Although, n=2 terms are necessary to undergo two number of iterations for obtaining the electrical entities. The transverse stresses inherent to an angle-ply laminate are presented at the piezo-elastic layer interface and the circumferential charge displacement due to CC-CC circumferential end conditions is also plotted in the figure.

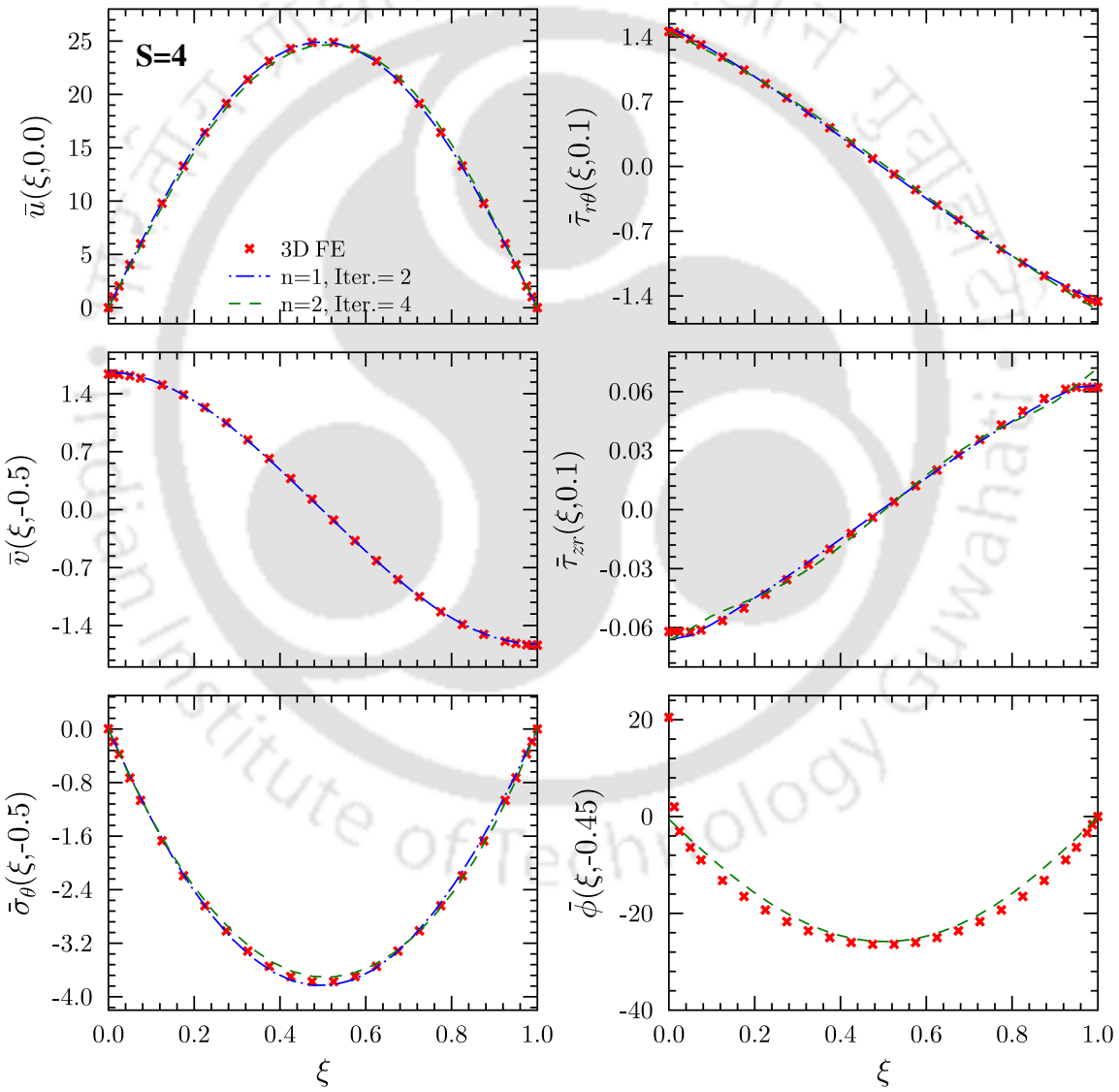

Fig. 5.8: Circumferential variation of field variables in the shell panel (5b) of S=4 and $\psi = 90^o$ with SS and OC-CC circumferential boundary conditions and CC-CC on its outer and inner surfaces, respectively.

5.7.2 Arbitrary boundary conditions along ξ

The feature of the present EKM solution, which is its ability to solve the problem for cases where arbitrary boundary conditions along its circumference (ξ ends) might arise is presented here. This is unlike the 3D exact solution used above which could not solve the cases with different combination of mechanical and electrical edge conditions. The hybrid angle-ply laminate scheme of shell panel (5b) from the Fig. 5.2 with different electrical boundary conditions (OC-CC) at the circumferential opposite ends is taken for the numerical study.

The geometrical configuration comprises of the thickness ratio S=4 and circumferential span ψ of 90^o. The shell panel is subjected to SS boundary conditions, mechanically and its radial surfaces are close circuited (CC). The elastic layers are made up of Mat.2 and PZT-4 material properties are considered for pz from the Table 5.1. Henceforth, for nondimensionalization, $Y_0 = Y_2$ of Mat.2 is considered in the relations expressed above.

The 3D EKM results are compared with 3D finite element (FE) results for this case. The 3D FE results are obtained from FE software ABAQUS [256]. The cylindrical shell is modelled as a very long panel along z-axis having axial length $(l)(\frac{l}{R} = 10)$. The FE solution is obtained using the 20 noded quadratic brick piezoelectric element (C3D20RE) with reduced integration for piezoelectric

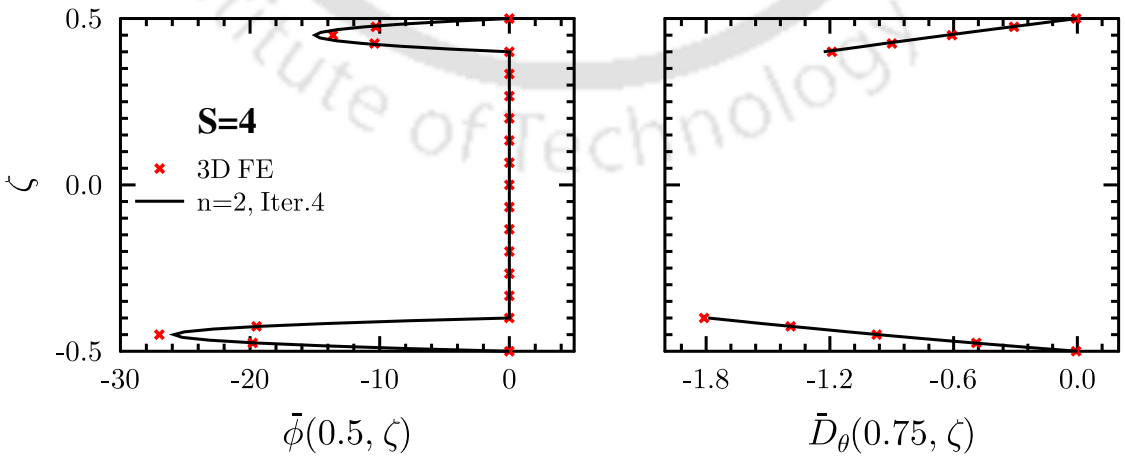

Fig. 5.9: Through-thickness variation of electrical entities in the shell panel (5b) of S=4 and $\psi = 90^o$ with SS and OC-CC circumferential boundary conditions and CC-CC on its outer and inner surfaces, respectively.

layer and a 20 noded quadratic serendipity hexahedral element with reduced integration (C3D20R) is used for elastic layer with mesh size of (16 × 80 × 40) along r, θ and z directions. Through-the-thickness, each elastic ply consists of three elements and the piezoelectricity plies are divided into two elements, each. It is observed from the circumferential plot shown in the Fig. 5.8, that

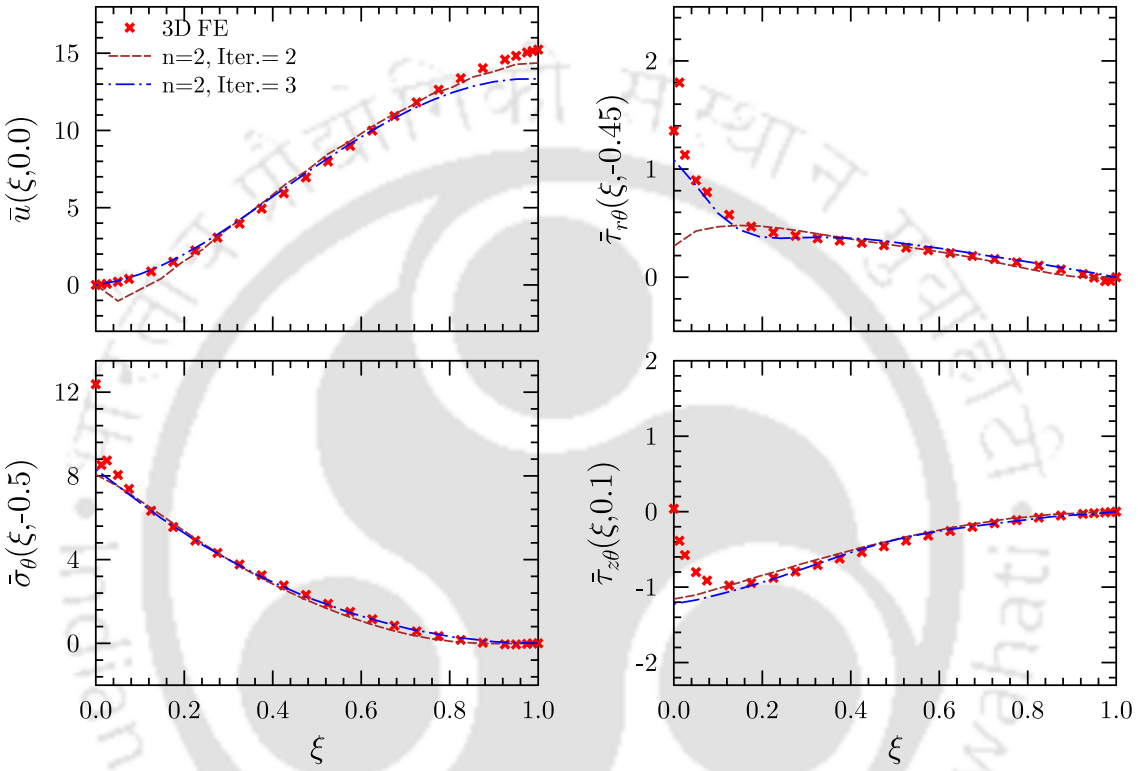

Fig. 5.10: Circumferential variation of field variables in the shell panel (5b) of S=4 and $\psi = 90^o$ with CF and CC-CC circumferential boundary conditions and OC-OC on its outer and inner surfaces, respectively.

only a single n=1 term in the EKM solution could predict the results for the present case for the displacement $(\bar{u}, \bar{v})$, normal and transverse stresses $(\bar{\sigma}, \bar{\tau}_{rz}, \bar{\tau}_{r\theta})$. However, for attaining convergence of the electric potential value along its circumference, two (n=2) number of terms and higher number of iterations ($Iter.$=4) are required. There is an induced potential at the ξ=0 location corresponding to the existence of an OC electrical end there.

The through-thickness plot of the same panel has been shown in the Fig. 5.9 which represents the nature of variation for the electrical entities $(\bar{\phi}, \bar{D}_{\theta})$ across the plies. As per intuition, there is

no charge density in the elastic layers where no value exists for $\bar{D}_\theta$ and are at zero electric potential (ϕ=0). The through-thickness variations obtained using n=2 and $Iter.$=4 match with that of the 3D FE, being consistent with the piezo-elastic layer interfacial (i.e., electrically grounded) and electric conditions at the radial surfaces (CC).

Further, the response of a similar hybrid cylindrical shell panel with CF boundary conditions at ξ=0,1 is considered. The shell panel has laminate configuration as represented by the shell panel (5b) in the Fig.5.2 and a span of $\psi = 90^o$. The elastic plies are made up of Mat 2. of Table 5.1 and the piezoelectricity layers (pz) are of PZT-G1195N. The circumferential variation of the field variables $\bar{u}, \bar{\sigma}_\theta, \bar{\tau}_{r\theta}$, and $\bar{\tau}_{z\theta}$ are plotted in the Fig. 5.10 which are obtained from the present solution in comparison with the 3D FE results.

There is edge effect in the vicinity of the clamped edge can be observed from the Fig. 5.10 which has been obtained in good agreement with the 3D FE results. However, such situation had been discussed in the previous chapters where the mismatch of 3D FE results at the clamped edge was reasoned due to failure of 3D FE in satisfying the outer and inner boundary conditions. However, the present results converged in three iterations and with just two number of terms in the MMEKM, the stress concentration zones could be predicted for an anti-symmetric hybridd laminate.

5.8 SUMMARY

For the first time, an accurate 3D solution for hybrid cylindrical shell panel has been developed based on piezoelasticity using the MMEKM. The coupled electromechanical responses are predicted precisely with very fast converging results as compared to available 3D exact solution for SS cylindrical shell panels. The present solution could also solve cases of arbitrarily supported shell panels under different electrical boundary conditions which provided reliable results at the boundary layer region and other stress concentration zones, as compared to the 3D FE solution. The numerical study for cross-ply SS hybrid laminates validated the present 3D solution as compared to 3D exact solution. The MMEKM solution converged with just a single term and 2 iterations. The nature of

variation for the electrical field variables were also studied. Further, a relatively inhomogeneous hybrid laminate made up of anti-symmetric angle-ply elastic plies with surface mounted piezoelectric layers under pressure loading was numerically studied. The sharp through-thickness variation of the induced electric field variables was yielded accurately with two terms in the multi-term EKM in case of electrically dissimilar circumferential edges of a SS shell panel. However, all the mechanical responses including the transverse shear stresses were predicted by using n=1 term. The generation of electric potential occurring due to difference in applied potential at the circumferential edges could be predicted for the same shell panel by the present solution. Similar to the earlier studied elastic laminates, only n=2 term solution provided converging results for CS and CF hybrid laminates. The stress concentrations near the clamped edge or interfaces could be predicted reliably, consistent with the stress-free boundary and/ or interlaminar continuity conditions. This novel development can be used to develop other piezoelasticity based 2D/ 3D solutions and the semi-analytical scheme can be extended to hybrid laminates under tension, bending and twisting loads.

Chapter 6

3D piezoelasticity solution for free vibration analysis of angle-ply piezolaminated cylindrical shell panel

6.1 INTRODUCTION

The free vibration of elastic/ piezoelasticity laminated composite cylindrical shells has been studied in this chapter. From the mixed-type extended Hamilton's principle, the weak form of the governing equations are obtained for development of the proposed 3D solution. As a result, the present solution achieves similar degree of accuracy for all the field variables at every point in the domain. By considering the coupled 3D constitutive relation, the electromechanical coupling is incorporated in the governing equations. These governing equations obtained from the variational principle, are partitioned into two systems of ordinary differential equations (ODE)s through the application of the extended Kantorovich method (EKM). The coupled field is addressed by the present technique due to which it is also termed as multi-field. The first-order ODEs are homogeneous and contain the frequency ω- term in the variable coefficients obtained for the r- radial coordinates. The system of ODEs corresponding to θ direction have constant coefficients. The ω is obtained through bracketing the roots and bisection method. Further, through the previously discussed modified power series method, the closed-form expressions for radial function is obtained by solving the variable coefficient ODE and by exactly solving the constant coefficient system of ODEs, the closed-form expression is attained for θ functions. The generalised piezoelasticity based 3D dynamic solution is applicable to laminated composites, sandwich and piezoelectric cylindrical

shell panels with any ply orientation scheme, arbitrary boundary conditions and material properties. The numerical study has been done for the piezoelectricity laminated composite shell panel and an elastic shell panel, where just single term in the EKM could predict the natural frequencies accurately. This solution can be referred to revisit other 1D/2D based theories or numerically obtained solutions.

6.2 CONFIGURATION OF HYBRID CYLINDRICAL SHELL PANEL

The laminate scheme for the hybrid composite may consist of surface mounted or embedded piezoelectric layers along with the elastic plies which are perfectly bonded to each other. All the piles are generally made up of orthotropic material and additionally, for the orthotropic piezoelectricity layer, the poling direction is along the radial r coordinate. As shown in Fig. 6.1, directions r, θ & z frames the cylindrical coordinate system for an L-layered angle-ply hybrid cylindrical shell of infinite axial length and circumferential span ψ. The principal material axes are x_1, x_2 and x_3 with respect to which material effective properties are oriented for any class mm2 symmetric orthorhombic or PFRC materials. Again, the material x_3 axis is considered to be aligned along the r-coordinate.

The local thickness $t^{(k)}$ of each kth layer along radial direction and global circumferential coordinates are introduced as dimensionless entities ξ & ζ defined in the range $\theta = 0, \psi$ and $r = R_1^{(k)}, R_1^{(k)} + t^{(k)}$, respectively as:

$$\xi = \theta/\psi, \qquad \zeta^{(k)} = (r - R_1^{(k)})/t^{(k)} \quad \text{with} \quad R_1^{(k)} = R - h/2 + \sum_{i=1}^{k-1} t^{(i)} \tag{6.1}$$

Where k is the layer number indexed from the inner surface of the cylindrical shell panel. The radius of inner surface of a kth layer is $R_1^{(k)}$. Geometrically, the cylindrical shell has its mid-surface radius at R and its total thickness along the radial direction is h. So, the inner surface of the shell panel is at a radius of $R_i = R - h/2$ and its outer surface is at $R_o = R + h/2$. Fiber direction of an individual ply lie in the θz which is oriented at an angle of $\beta^{(k)}$ with respect to the θ-axis. In the following sections, superscript 'k' for the layers is omitted unless needed for clarity. Arbitrary boundary conditions of the shell panel on its opposite circumferential edges (i.e., at $\theta = 0, \psi$) can

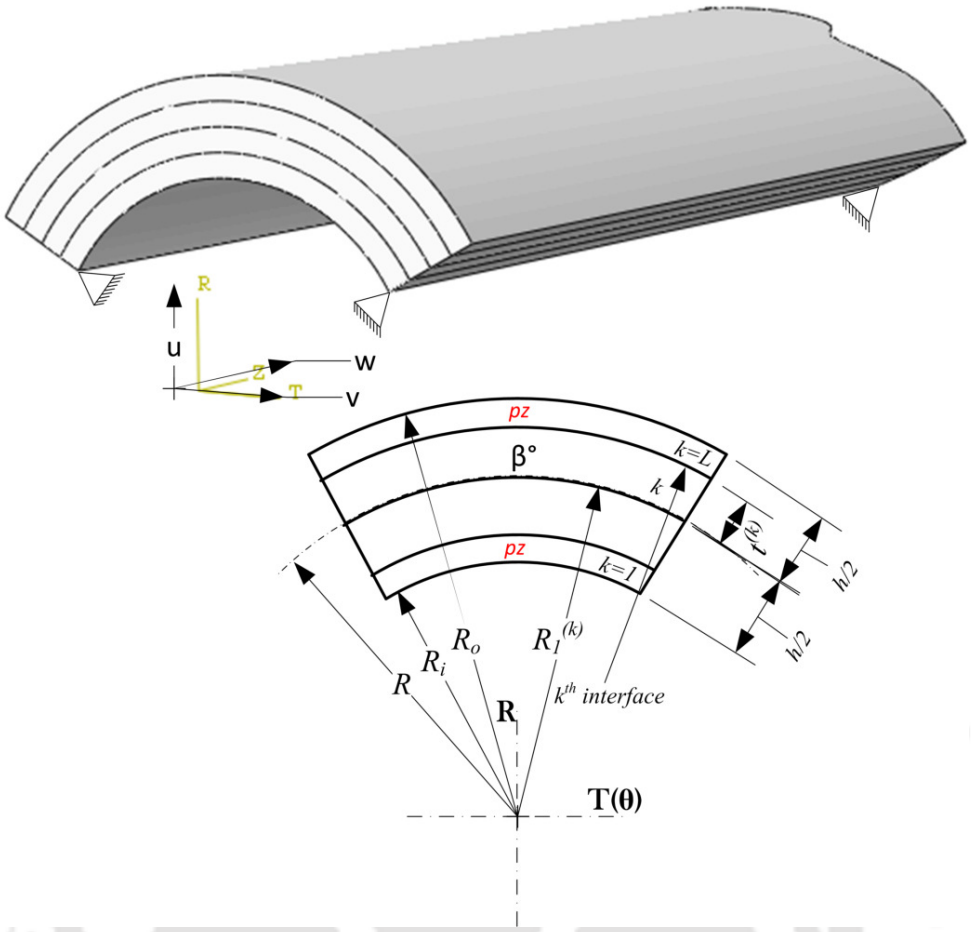

Fig. 6.1: Geometry of a Piezoelectric Shell panel

be clamped (C), free (F) or simply-supported (S). The electrical boundary conditions can also be changed with or without the application of electric potential (ϕ) called respectively as closed circuit (CC) and open circuit (OC) conditions.

6.3 GOVERNING EQUATIONS

The Young's moduli Y_i, major Poisson's ratios ν_{ij}, shear moduli G_{ij} are the engineering elastic material constants, along with the coupling piezoelectric terms, namely, piezoelectric coefficients d_{ij} and constant strain dielectric permittivities η_{ij} are used to obtain the expressions of the transformed constants as detailed in Eqs. (A.2)-(A.7) of Appendix A. According to a linear 3D piezoelasticity and using the transformation derived in Appendix A, the coupled material constitutive relations

has been shown below in cylindrical coordinate system as following relation:

$$\begin{bmatrix} \varepsilon_\theta \\ \varepsilon_z \\ \varepsilon_r \\ \gamma_{zr} \\ \gamma_{r\theta} \\ \gamma_{\theta z} \\ D_\theta \\ D_z \\ D_r \end{bmatrix} = \begin{bmatrix} \bar{s}_{11} & \bar{s}_{12} & \bar{s}_{13} & 0 & 0 & \bar{s}_{16} & 0 & 0 & \bar{d}_{31} \\ \bar{s}_{12} & \bar{s}_{22} & \bar{s}_{23} & 0 & 0 & \bar{s}_{26} & 0 & 0 & \bar{d}_{32} \\ \bar{s}_{13} & \bar{s}_{23} & \bar{s}_{33} & 0 & 0 & \bar{s}_{36} & 0 & 0 & \bar{d}_{33} \\ 0 & 0 & 0 & \bar{s}_{44} & \bar{s}_{45} & 0 & \bar{d}_{14} & \bar{d}_{24} & 0 \\ 0 & 0 & 0 & \bar{s}_{54} & \bar{s}_{55} & 0 & \bar{d}_{15} & \bar{d}_{25} & 0 \\ \bar{s}_{16} & \bar{s}_{26} & \bar{s}_{36} & 0 & 0 & \bar{s}_{66} & 0 & 0 & \bar{d}_{36} \\ 0 & 0 & 0 & \bar{d}_{14} & \bar{d}_{15} & 0 & \bar{\epsilon}_{11} & \bar{\epsilon}_{12} & 0 \\ 0 & 0 & 0 & \bar{d}_{24} & \bar{d}_{25} & 0 & \bar{\epsilon}_{21} & \bar{\epsilon}_{22} & 0 \\ \bar{d}_{31} & \bar{d}_{32} & \bar{d}_{33} & 0 & 0 & \bar{d}_{36} & 0 & 0 & \bar{\epsilon}_{33} \end{bmatrix} \begin{bmatrix} \sigma_\theta \\ \sigma_z \\ \sigma_r \\ \tau_{zr} \\ \tau_{r\theta} \\ \tau_{\theta z} \\ E_\theta \\ E_z \\ E_r \end{bmatrix} \tag{6.2}$$

Where, σ_i and τ_{ij} are the stress components, D_i are electric displacement components which are related to corresponding strain components ε_i and γ_{ij} along with electric field components E_i. These are related through the transformed elastic compliances ($\bar{s}_{ij}$), piezoelectric strain constants ($\bar{d}_{ij}$) and dielectric permittivities ($\bar{\epsilon}_{ij}$) at constant stress field, respectively. Furthermore, identical governing equations to those of the original ones are used with dimensionless forms of all the entities. The dimensionless entities for the mechanical variables have been defined in Eq. (3.14) of Chapter 3. The remaining electrical variables are nondimensionalized as

$$\begin{aligned} &(D_\theta^*, D_z^*, D_r^*) = (D_\theta, D_z, D_r)S/Y_0 d_0, \quad && \epsilon_{ij}^* = \epsilon_{ij}/Y_0 d_0^2 \\ &(\phi^*) = (\phi)d_0/h, && \rho^* = \rho/\rho_0, \quad (E_\theta^*, E_z^*, E_r^*) = (E_\theta, E_z, E_r)d_0 S \end{aligned} \tag{6.3}$$

Where d_0 and Y_0 used for nondimensionalisation, correspond to the values of the material piezoelectric constant and Young's modulus, respectively. However, for simplicity, the superscript * is removed from the dimensionless entities and the equations with dimensionless entities are used henceforth.

When the nature of all the field variables is independent of z, cylindrical bending occurs which is a case of generalised plane strain condition. Corresponding to which the mechanical strain-displacement and electric field-potential relations are in the following form:

$$\begin{aligned} &\varepsilon_\theta = (u + v_{,\theta})/r, && \gamma_{zr} = w_{,r}, && E_\theta = -\phi_{,\theta}/r, \\ &\varepsilon_z = 0, && \gamma_{r\theta} = (u_{,\theta} - v)/r + v_{,r}, && E_z = 0, \\ &\varepsilon_r = u_{,r}, && \gamma_{\theta z} = w_{,\theta}/r, && E_r = -\phi_{,r} \end{aligned} \tag{6.4}$$

where a comma in the subscript denotes differentiation. Using Eq. $(6.2)_9$, the expression for E_r in terms of D_r can be obtained as:

$$E_r = \frac{1}{\bar{\epsilon}_{33}} D_r - \bar{d}'_{31}\sigma_\theta - \bar{d}'_{32}\sigma_z - \bar{d}'_{33}\sigma_r - \bar{d}'_{36}\tau_{\theta z} \tag{6.5}$$

where $\bar{d}'_{ij} = \bar{d}_{ij}/\bar{\epsilon}_{33}$. Substituting E_r from Eq. (6.5) and ε_z from Eq. $(6.4)_2$ in Eq. $(6.2)_2$, σ_z is obtained as

$$\sigma_z = -(\bar{s}'_{12}/\bar{s}'_{22})\sigma_\theta - (\bar{s}'_{26}/\bar{s}'_{22})\tau_{z\theta} - (\bar{s}'_{23}/\bar{s}'_{22})\sigma_r - (\bar{d}'_{32}/\bar{s}'_{22})D_r \tag{6.6}$$

where $\bar{s}'_{ij} = \bar{s}_{ij} - \bar{d}_{3i}\bar{d}_{3j}/\bar{\epsilon}_{33}$. Using Eqs. (6.5) and (6.6), σ_z and E_r are eliminated from Eqs. $(6.2)_1$, $(6.2)_3$, $(6.2)_6$ and Eq. (6.5) to yield

$$\begin{aligned}
\varepsilon_\theta &= p_{11}\sigma_\theta + p_{16}\tau_{\theta z} + p_{13}\sigma_r + p_{18}D_r \\
\varepsilon_r &= p_{31}\sigma_\theta + p_{36}\tau_{\theta z} + p_{33}\sigma_r + p_{38}D_r \\
\gamma_{\theta z} &= p_{61}\sigma_\theta + p_{66}\tau_{\theta z} + p_{63}\sigma_r + p_{68}D_r \\
E_r &= -(p_{81}\sigma_\theta + p_{86}\tau_{\theta z} + p_{83}\sigma_r + p_{88}D_r)
\end{aligned} \tag{6.7}$$

where

$$\begin{aligned}
p_{ij} &= \bar{s}'_{ij} - \bar{s}'_{2i}\bar{s}'_{2j}/\bar{s}'_{22}, \qquad & p_{88} &= -1/\bar{\epsilon}_{33} - \bar{d}'^2_{32}/\bar{s}'_{22} \\
p_{i8} &= p_{8i} = \bar{d}'_{3i} - \bar{s}'_{2i}\bar{d}'_{32}/\bar{s}'_{22}, \quad \text{for} \quad (i,j) = 1,3,6 &&
\end{aligned} \tag{6.8}$$

Further, using the Eq. $(6.2)_2$ in Eq. $(6.4)_2$, σ_z can be differently expressed as

$$\sigma_z = -(\bar{s}_{12}/\bar{s}_{22})\sigma_\theta - (\bar{s}_{26}/\bar{s}_{22})\tau_{\theta z} - (\bar{s}_{23}/\bar{s}_{22})\sigma_r - (\bar{d}_{32}/\bar{s}_{22})E_r \tag{6.9}$$

Substituting σ_z from Eq. (6.9) into Eqs. $(6.2)_1$, $(6.2)_3$, $(6.2)_6$ and $(6.2)_9$, ε_θ, ε_r, $\gamma_{\theta z}$ and E_r can be expressed in terms of σ_θ, $\tau_{\theta z}$, σ_r and E_r as

$$\begin{aligned}
\varepsilon_\theta &= \bar{p}_{11}\sigma_\theta + \bar{p}_{16}\tau_{\theta z} + \bar{p}_{13}\sigma_r + \bar{p}_{18}E_r \\
\varepsilon_r &= \bar{p}_{31}\sigma_\theta + \bar{p}_{36}\tau_{\theta z} + \bar{p}_{33}\sigma_r + \bar{p}_{38}E_r \\
\gamma_{\theta z} &= \bar{p}_{61}\sigma_\theta + \bar{p}_{66}\tau_{\theta z} + \bar{p}_{63}\sigma_r + \bar{p}_{68}E_r \\
E_r &= -(\bar{p}_{81}\sigma_\theta + \bar{p}_{86}\tau_{\theta z} + \bar{p}_{83}\sigma_r + \bar{p}_{88}D_r)
\end{aligned} \tag{6.10}$$

where

$$\bar{p}_{ij} = \bar{s}_{ij} - \bar{s}_{2i}\bar{s}_{2j}/\bar{s}_{22}, \qquad \bar{p}_{8i} = (\bar{d}_{3i} - \bar{s}_{2i}\bar{d}_{32}/\bar{s}_{22})/[\bar{\epsilon}_{33} - (\bar{d}_{32})^2/\bar{s}_{22}]$$

$$\bar{p}_{i8} = \bar{d}_{3i} - \bar{s}_{2i}\bar{d}_{32}/\bar{s}_{22}, \qquad \text{for} \quad (i,j) = 1,3,6, \qquad \bar{p}_{88} = -1/[\bar{\epsilon}_{33} - (\bar{d}_{32})^2/\bar{s}_{22}]$$

Using Eqs. $(6.2)_4$, $(6.2)_5$ and $(6.2)_7$, γ_{zr}, $\gamma_{r\theta}$ and E_θ can be expressed in terms of τ_{zr}, $\tau_{r\theta}$ and D_θ as

$$\gamma_{zr} = p_{44}\tau_{zr} + p_{45}\tau_{r\theta} + p_{47}D_\theta \tag{6.11}$$

$$\gamma_{r\theta} = p_{54}\tau_{zr} + p_{55}\tau_{r\theta} + p_{57}D_\theta \tag{6.12}$$

$$E_\theta = -p_{74}\tau_{zr} - p_{75}\tau_{r\theta} + p_{77}D_\theta \tag{6.13}$$

where

$$p_{ij} = \bar{s}_{ij} - \bar{d}_{1i}\bar{d}_{1j}/\bar{\epsilon}_{11}, \quad \text{for} \quad (i,j) = (4,5), \qquad p_{47} = \bar{d}_{14}/\bar{\epsilon}_{11}$$

$$p_{74} = p_{47}, \qquad p_{77} = 1/\bar{\epsilon}_{11}, \qquad p_{57} = p_{75} = \bar{d}_{15}/\bar{\epsilon}_{11}$$

In case of cylindrical bending without consideration of any body forces or internal charge sources, the mixed variational form of extended Hamilton principle gives the following expression for the piezoelectric medium:

$$\begin{aligned}
&\int_{\mathbf{t}}\int_V [\delta u\left(\sigma_{r,r} + \frac{\tau_{r\theta,\theta}}{r} + \frac{(\sigma_r - \sigma_\theta)}{r} - \rho\ddot{u}\right) + \delta v\left(\tau_{r\theta,r} + \frac{\sigma_{\theta,\theta}}{r} + \frac{2\tau_{r\theta}}{r} - \rho\ddot{v}\right)\\
&+\delta w\left(\tau_{zr,r} + \frac{\tau_{\theta z,\theta}}{r} + \frac{\tau_{zr}}{r} - \rho\ddot{w}\right) + \delta\sigma_\theta\left(\varepsilon_\theta - \frac{(u + v_{,\theta})}{r}\right) + \delta\sigma_r(\varepsilon_r - u_{,r}) + \delta\tau_{\theta z}\left(\gamma_{\theta z} - \frac{w_{,\theta}}{r}\right)\\
&+\delta\tau_{zr}\left(\gamma_{zr} - w_{,r}\right) + \delta\tau_{r\theta}\left(\gamma_{r\theta} - \frac{(u_{,\theta} - v)}{r} - v_{,r}\right) - \delta\phi\left(D_{r,r} + \frac{D_r}{r} + \frac{D_{\theta,\theta}}{r}\right)\\
&+\delta D_\theta\left(E_\theta + \frac{\phi_{,\theta}}{r}\right) + \delta D_r\left(E_r - \phi_{,r}\right)]dV d\mathbf{t} = 0, \forall\ \delta u_i,\ \delta\sigma_i,\ \delta\tau_{ij},\ \delta\phi,\ \delta D_i
\end{aligned} \tag{6.14}$$

Where V denotes the volume of the panel per unit width in the z direction. Also, $\mathbf{t}$ is the time variable and $\ddot{u}_{ij}$ denotes the double time derivative.

Substituting the expressions from Eqs. (6.7) and (6.11)-(6.13) for ε_θ, ε_r, $\gamma_{z\theta}$, γ_{zr}, $\gamma_{r\theta}$, E_r and E_θ corresponding to the strain and electric field components, into Eq. (6.14) yields

$$\begin{aligned}
\int_{\mathbf{t}}\int_r\int_\theta\ [\ &\delta v(\rho\ddot{v} - \tau_{r\theta,r} - \sigma_{\theta,\theta}/r - 2\tau_{r\theta}/r)\\
&+ \delta w(\rho\ddot{w} - \tau_{zr,r} - \tau_{z\theta,\theta}/r - \tau_{zr}/r)\\
&+ \delta u(\rho\ddot{u} - \sigma_{r,r} - \tau_{r\theta,\theta}/r - (\sigma_r - \sigma_\theta)/r)
\end{aligned}$$

$$
\begin{aligned}
&+ \delta\sigma_\theta(p_{11}\sigma_\theta + p_{13}\sigma_r + p_{16}\tau_{z\theta} + p_{18}D_r - (u + v_{,\theta})/r) \\
&+ \delta\sigma_r(p_{13}\sigma_\theta + p_{33}\sigma_r + p_{36}\tau_{z\theta} + p_{38}D_r - u_{,r}) \\
&+ \delta\tau_{z\theta}(p_{16}\sigma_\theta + p_{36}\sigma_r + p_{66}\tau_{\theta z} + p_{68}D_r - (w_{,\theta}/r)) \\
&+ \delta\tau_{zr}(p_{44}\tau_{zr} + p_{45}\tau_{r\theta} + p_{47}D_\theta - (w_{,r})) \\
&+ \delta\tau_{r\theta}(p_{45}\tau_{zr} + p_{55}\tau_{r\theta} + p_{57}D_\theta - (u_{,\theta} - v)/r - v_{,r}) \\
&- \delta\phi(D_{r,r} + D_r/r + D_{\theta,\theta}/r) \\
&+ \delta D_\theta(p_{77}D_\theta - p_{74}\tau_{zr} - p_{75}\tau_{r\theta} + \phi_{,\theta}/r) \\
&+ \delta D_r(p_{81}\sigma_\theta + p_{83}\sigma_r + p_{86}\tau_{z\theta} + p_{88}D_r - \phi_{,r})]rd\theta drd\mathbf{t} = 0
\end{aligned} \tag{6.15}
$$

For the instance when the solution in θ direction is considered to be known and for the r direction the corresponding ODEs are to be formed, above Eq. (6.16) is employed. Whereas, for forming the ODEs corresponding to θ direction when r direction solutions are known, the alternative expressions for ε_θ, ε_r, $\gamma_{\theta z}$ and E_r from Eq. (6.10) are substituted in Eq. (6.14) to yield

$$
\begin{aligned}
\int_{\mathbf{t}}\int_r\int_\theta\ [\ &\delta v(\rho\ddot{v} - \tau_{r\theta,r} - \sigma_{\theta,\theta}/r - 2\tau_{r\theta}/r) \\
&+ \delta w(\rho\ddot{w} - \tau_{zr,r} - \tau_{z\theta,\theta}/r - \tau_{zr}/r) \\
&+ \delta u(\rho\ddot{u} - \sigma_{r,r} - \tau_{r\theta,\theta}/r - (\sigma_r - \sigma_\theta)/r) \\
&+ \delta\sigma_\theta(\bar{p}_{11}\sigma_\theta + \bar{p}_{13}\sigma_r + \bar{p}_{16}\tau_{z\theta} + \bar{p}_{18}E_r - (u + v_{,\theta})/r) \\
&+ \delta\sigma_r(\bar{p}_{13}\sigma_\theta + \bar{p}_{33}\sigma_r + \bar{p}_{36}\tau_{z\theta} + \bar{p}_{38}E_r - u_{,r}) \\
&+ \delta\tau_{z\theta}(\bar{p}_{16}\sigma_\theta + \bar{p}_{36}\sigma_r + \bar{p}_{66}\tau_{\theta z} + \bar{p}_{68}E_r - (w_{,\theta}/r)) \\
&+ \delta\tau_{zr}(p_{44}\tau_{zr} + p_{45}\tau_{r\theta} + p_{47}D_\theta - (w_{,r})) \\
&+ \delta\tau_{r\theta}(p_{45}\tau_{zr} + p_{55}\tau_{r\theta} + p_{57}D_\theta - (u_{,\theta} - v)/r - v_{,r}) \\
&- \delta\phi(D_{r,r} + D_r/r + D_{\theta,\theta}/r) \\
&+ \delta D_\theta(p_{77}D_\theta - p_{74}\tau_{zr} - p_{75}\tau_{r\theta} - E_\theta) \\
&+ \delta D_r(\bar{p}_{81}\sigma_\theta + \bar{p}_{83}\sigma_r + \bar{p}_{86}\tau_{z\theta} + \bar{p}_{88}D_r + E_r)]rd\theta drd\mathbf{t} = 0
\end{aligned} \tag{6.16}
$$

However, for the elastic case, the Eqs. (6.15) and (6.16) are not different as only the σ_z reduces corresponding to generalised plane strain.

6.4 BOUNDARY AND INTERFACE CONDITIONS

As the shell panel is undergoing a free vibration, the boundary conditions at the inner and outer surfaces of the shell panel are:

$$\begin{aligned} &\text{at } r = -\frac{h}{2} \qquad \sigma_r = 0,\ \tau_{r\theta} = \tau_{rz} = 0, \quad \phi = 0 \ \text{ or } \ D_r = 0 \\ &\text{at } r = +\frac{h}{2} \qquad \sigma_r = 0,\ \tau_{r\theta} = \tau_{rz} = 0, \quad \phi = 0 \ \text{ or } \ D_r = 0 \end{aligned} \tag{6.17}$$

For the considered piezoelastic laminates, in order to have effective actuation/ sensing the interfaces between the piezoelectric layers and the elastic layers are always taken as grounded. For such n_q $(q = 1, ..., L_a)$ number of interfaces, the electric potential is mathematically given as

$$[\phi|_{\zeta=1}]^{(n_q)} = 0, \qquad q = 1, \ldots, L_a \tag{6.18}$$

The equilibrium and the compatibility conditions at the kth interface between adjacent layers are:

$$[(v,\ w,\ u,\ \sigma_r,\ \tau_{zr},\ \tau_{z\theta},\ \phi,\ D_r)|_{\zeta=1}]^{(k)} = [(v,\ w,\ u,\ \sigma_r,\ \tau_{zr},\ \tau_{z\theta},\ \phi,\ D_r)|_{\zeta=0}]^{(k+1)} \tag{6.19}$$

for $k = 1, \ldots, L-1$, except for D_r for the interfaces $k = n_q,\ q = 1, \ldots, L_a$. The D_r is discontinuous for the interfaces n_q. For such surfaces, the continuity condition for D_r is to replaced by Eq. (6.18). The circumferential edges at $\xi = 0$ and 1 can be arbitrarily chosen among the following cases for numerical study, where the field variables are physically 0.

$$\begin{aligned} &\text{Simply Supported (S)}: \quad u = 0, \quad \sigma_\theta = 0, \quad \tau_{z\theta} = 0 \\ &\text{Clamped (C)}: \quad u = 0, \quad v = 0, \quad w = 0 \\ &\text{Free (F)}: \quad \tau_{r\theta} = 0, \quad \sigma_\theta = 0, \quad \tau_{z\theta} = 0 \end{aligned} \tag{6.20}$$

The electric condition at such edges can have a prescribed potential ($\phi = 0$) to be closed circuited or under an open circuit condition quantified to be $D_\theta = 0$.

6.5 GENERALIZED EKM SOLUTION

The field variables are simultaneously considered in the $\mathbf{X}$ vector as $\mathbf{X} = \begin{bmatrix} v & w & u & \sigma_\theta & \sigma_r & \tau_{\theta z} & \tau_{zr} & \tau_{r\theta} & \phi & D_\theta & D_r \end{bmatrix}^{\mathrm{T}}$. According to EKM, the solution of each component $X_l(\xi, \zeta)$ can be assumed as the product of separable univariate functions $f_l(\xi)$ and $g_l(\zeta)$, in the form of:

$$X_l(\xi, \zeta) = f_l(\xi) g_l(\zeta) \ \cos \omega \mathbf{t} \qquad \text{for} \qquad l = 1, 2, \ldots 11 \tag{6.21}$$

It can be realised that $g_l(\zeta)$ and $f_l(\xi)$ functions are valid for the kth layer and whole laminate, respectively. Satisfying all homogenous boundary conditions, the functions $g_l(\zeta)$ and $f_l(\xi)$ are iteratively obtained. In Eq. (6.21) no summation is meant for the repeated index l.

6.5.1 First Iteration Step

Assuming the $f_l(\xi)$ functions in this step, the variation δX for it is obtained as

$$\delta X_l = f_l(\xi) \delta g_l \ \cos \omega \mathbf{t}, \qquad l = 1, 2, \ldots 11 \tag{6.22}$$

Referring back to the through-the-thickness boundary conditions in Eqs. (6.17) and (6.18), the $g_l(\zeta)$ functions corresponding to those eight field variables are taken in a $\bar{\mathbf{G}}$ vector, while the remaining three $g_l(\zeta)$ functions appear in another vector $\hat{\mathbf{G}}$ as shown below:

$$\begin{aligned} \bar{\mathbf{G}} &= \begin{bmatrix} g_3 & g_1 & g_2 & g_5 & g_7 & g_8 & g_9 & g_{11} \end{bmatrix}^{\mathrm{T}} \\ \hat{\mathbf{G}} &= \begin{bmatrix} g_4 & g_6 & g_{10} \end{bmatrix}^{\mathrm{T}} \end{aligned} \tag{6.23}$$

Substituting X_l and δX_l from the Eqs. (6.21) and (6.22) in Eq. (6.16), results in a set of following 11 differential-algebraic equations.

$$\mathbf{M} \bar{\mathbf{G}}_{,\zeta} = t[\bar{\mathbf{A}}_\mathbf{m}(\omega) \bar{\mathbf{G}} + \hat{\mathbf{A}}_\mathbf{m} \hat{\mathbf{G}}] \tag{6.24}$$

$$\mathbf{K} \hat{\mathbf{G}} = \tilde{\mathbf{A}}_\mathbf{m} \bar{\mathbf{G}} \tag{6.25}$$

$$\text{where, } \bar{\mathbf{A}}_\mathbf{m} = \bar{\mathbf{A}}_\mathbf{0}(\omega) + \left(\frac{\bar{\mathbf{A}}_\mathbf{1}}{(\zeta t + R_1)}\right), \ \hat{\mathbf{A}}_\mathbf{m} = \hat{\mathbf{A}}_\mathbf{0} + \left(\frac{\hat{\mathbf{A}}_\mathbf{1}}{(\zeta t + R_1)}\right),$$
$$\tilde{\mathbf{A}}_\mathbf{m} = \tilde{\mathbf{A}}_\mathbf{0} + \left(\frac{\tilde{\mathbf{A}}_\mathbf{1}}{(\zeta t + R_1)}\right) \tag{6.26}$$

where, Eq. (6.24) is the set of 8 ODE and 3 algebraic equations are expressed in Eq. (6.25). These are obtained by equating the coefficients of the arbitrary variations $\delta g_l \, (l = 1, \ldots, 11)$ individually to zero and performing the integrations over ξ direction. The elements of the matrices $\bar{\mathbf{A}}_\mathbf{0}$, $\bar{\mathbf{A}}_\mathbf{1}$, $\hat{\mathbf{A}}_\mathbf{0}$, $\hat{\mathbf{A}}_\mathbf{1}$, $\tilde{\mathbf{A}}_\mathbf{0}$, $\tilde{\mathbf{A}}_\mathbf{1}$, $\mathbf{K}$ and $\mathbf{M}$ which are non-zero are listed below.

$$\begin{aligned}
&M_{11} = M_{44} = \langle f_5 f_3 \rangle_\psi, \quad M_{22} = M_{66} = \langle f_8 f_1 \rangle_\psi, \quad M_{33} = M_{55} = \langle f_7 f_2 \rangle_\psi, \\
&M_{77} = M_{88} = \langle f_{11} f_9 \rangle_\psi \\
&\bar{A}_{0_{41}} = \rho\omega^2 \langle f_3 f_3 \rangle_\psi, \quad \bar{A}_{0_{53}} = \rho\omega^2 \langle f_2 f_2 \rangle_\psi, \quad \bar{A}_{0_{62}} = \rho\omega^2 \langle f_1 f_1 \rangle_\psi, \\
&\bar{A}_{0_{14}} = p_{33} \langle f_5 f_5 \rangle_\psi, \quad \bar{A}_{0_{18}} = p_{38} \langle f_5 f_{11} \rangle_\psi, \quad \bar{A}_{0_{25}} = p_{45} \langle f_8 f_7 \rangle_\psi, \\
&\bar{A}_{0_{26}} = p_{55} \langle f_8 f_8 \rangle_\psi, \quad \bar{A}_{0_{35}} = p_{44} \langle f_7 f_7 \rangle_\psi, \quad \bar{A}_{0_{36}} = p_{45} \langle f_7 f_8 \rangle_\psi, \\
&\bar{A}_{0_{74}} = p_{38} \langle f_{11} f_5 \rangle_\psi, \quad \bar{A}_{0_{78}} = p_{88} \langle f_{11} f_{11} \rangle_\psi, \quad \bar{A}_{1_{21}} = -\tfrac{1}{\psi} \langle f_8 f_{3,\xi} \rangle_\psi \\
&\bar{A}_{1_{22}} = \langle f_8 f_1 \rangle_\psi, \quad \bar{A}_{1_{44}} = -\langle f_3 f_5 \rangle_\psi, \quad \bar{A}_{1_{46}} = -\tfrac{1}{\psi} \langle f_3 f_{8,\xi} \rangle_\psi \\
&\bar{A}_{1_{55}} = -\langle f_2 f_7 \rangle_\psi, \quad \bar{A}_{1_{66}} = -2\langle f_1 f_8 \rangle_\psi, \quad \bar{A}_{1_{88}} = -\langle f_9 f_{11} \rangle_\psi, \\
&\hat{A}_{0_{11}} = p_{31} \langle f_5 f_4 \rangle_\psi, \quad \hat{A}_{0_{12}} = p_{36} \langle f_5 f_6 \rangle_\psi, \quad \hat{A}_{0_{23}} = p_{57} \langle f_8 f_{10} \rangle_\psi, \\
&\hat{A}_{0_{71}} = p_{81} \langle f_{11} f_4 \rangle_\psi, \quad \hat{A}_{0_{72}} = p_{86} \langle f_{11} f_6 \rangle_\psi, \quad \hat{A}_{1_{41}} = \langle f_3 f_4 \rangle_\psi, \\
&\hat{A}_{1_{52}} = -\tfrac{1}{\psi} \langle f_2 f_{6,\xi} \rangle_\psi, \quad \hat{A}_{1_{61}} = -\tfrac{1}{\psi} \langle f_1 f_{4,\xi} \rangle_\psi, \quad \hat{A}_{1_{61}} = -\tfrac{1}{\psi} \langle f_1 f_{4,\xi} \rangle_\psi, \\
&\tilde{A}_{0_{14}} = p_{13} \langle f_4 f_5 \rangle_\psi, \quad \tilde{A}_{0_{18}} = p_{18} \langle f_4 f_{11} \rangle_\psi, \quad \tilde{A}_{0_{24}} = p_{36} \langle f_6 f_5 \rangle_\psi, \\
&\tilde{A}_{0_{28}} = p_{68} \langle f_6 f_{11} \rangle_\psi, \quad \tilde{A}_{0_{35}} = -p_{47} \langle f_{10} f_7 \rangle_\psi, \quad \tilde{A}_{0_{36}} = -p_{57} \langle f_{10} f_8 \rangle_\psi, \\
&\tilde{A}_{1_{11}} = -\langle f_4 f_3 \rangle_\psi, \quad \tilde{A}_{1_{12}} = -\tfrac{1}{\psi} \langle f_4 f_{1,\xi} \rangle_\psi, \quad \tilde{A}_{1_{23}} = -\tfrac{1}{\psi} \langle f_6 f_{2,\xi} \rangle_\psi, \\
&\tilde{A}_{1_{37}} = -\tfrac{1}{\psi} \langle f_{10} f_{9,\xi} \rangle_\psi, \quad K_{11} = -p_{11} \langle f_4 f_4 \rangle_\psi, \quad K_{12} = -p_{16} \langle f_4 f_6 \rangle_\psi, \\
&K_{21} = -p_{16} \langle f_6 f_4 \rangle_\psi, \quad K_{22} = -p_{66} \langle f_6 f_6 \rangle_\psi, \quad K_{33} = -p_{77} \langle f_{10} f_{10} \rangle_\psi
\end{aligned} \tag{6.27}$$

where for integration over the circumferential span ψ, a notation $\langle \ldots \rangle_\psi = \psi \int_0^1 (\ldots) d\xi$ has been used. The matrices, $\mathbf{M}$, $\bar{\mathbf{A}}_\mathbf{0}$, $\bar{\mathbf{A}}_\mathbf{1}$ are 8×8, $\hat{\mathbf{A}}_\mathbf{0}$, $\hat{\mathbf{A}}_\mathbf{1}$ are 8×3, $\tilde{\mathbf{A}}_\mathbf{0}$, $\tilde{\mathbf{A}}_\mathbf{1}$ are 3×8 and $\mathbf{K}$ is 3×3 matrix.

Since the functions f_l are known analytical functions, elements of the matrices defined in Eq. (6.27) are evaluated in close form, as described in Sec. 3.6 of Chapter 3. Solving the system of algebraic equations (6.25) for $\hat{\mathbf{G}}$ and substituting it back into the Eq. (6.24) yields the following first-order ODE after using a shell geometric constant $s = R_1/t$.

$$(\zeta + s)^2 \bar{\mathbf{G}}_{,\zeta} = [s^2\mathbf{A} + \zeta\mathbf{A_3} + \zeta^2\mathbf{A_4}](\omega)\bar{\mathbf{G}} \tag{6.28}$$

where

$$\begin{aligned}
\mathbf{A_4} &= \left(\frac{R_1}{s}\right)\mathbf{M}^{-1}\bar{\mathbf{A}}_\mathbf{0} + \left(\frac{R_1}{s}\right)\mathbf{M}^{-1}\hat{\mathbf{A}}_\mathbf{0}\mathbf{K}^{-1}\tilde{\mathbf{A}}_\mathbf{0} \\
\mathbf{A_3} &= 2R_1\mathbf{M}^{-1}\bar{\mathbf{A}}_\mathbf{0} + \mathbf{M}^{-1}\bar{\mathbf{A}}_\mathbf{1} + 2R_1\mathbf{M}^{-1}\hat{\mathbf{A}}_\mathbf{0}\mathbf{K}^{-1}\tilde{\mathbf{A}}_\mathbf{0} + \mathbf{M}^{-1}\hat{\mathbf{A}}_\mathbf{0}\mathbf{K}^{-1}\tilde{\mathbf{A}}_\mathbf{1} + \mathbf{M}^{-1}\hat{\mathbf{A}}_\mathbf{1}\mathbf{K}^{-1}\tilde{\mathbf{A}}_\mathbf{0} \\
\mathbf{A} &= \frac{R_1}{s}\mathbf{M}^{-1}\bar{\mathbf{A}}_\mathbf{0} + \frac{1}{s}\mathbf{M}^{-1}\bar{\mathbf{A}}_\mathbf{1} + \frac{R_1}{s}\mathbf{M}^{-1}\hat{\mathbf{A}}_\mathbf{0}\mathbf{K}^{-1}\tilde{\mathbf{A}}_\mathbf{0} + \frac{1}{s}\mathbf{M}^{-1}\hat{\mathbf{A}}_\mathbf{0}\mathbf{K}^{-1}\tilde{\mathbf{A}}_\mathbf{1} + \frac{1}{s}\mathbf{M}^{-1}\hat{\mathbf{A}}_\mathbf{1}\mathbf{K}^{-1}\tilde{\mathbf{A}}_\mathbf{0} \\
&\quad + \left(\frac{1}{sR_1}\right)\mathbf{M}^{-1}\hat{\mathbf{A}}_\mathbf{1}\mathbf{K}^{-1}\tilde{\mathbf{A}}_\mathbf{1}
\end{aligned} \tag{6.29}$$

Equation (6.28) represents a system of homogeneous first-order ODEs with variable coefficients. By using the method of modified power series expansion, a closed form solution for the system of equations (6.28) is obtained. Hence, a general solution is acquired in the following form for the variable coefficient ODE in Eq. (6.28) as:

$$[\bar{\mathbf{G}}(\zeta)] = \left[\sum_{i=0}^{\infty}\left(\frac{\hat{\mathbf{H}}_i\zeta^i}{i!}\right)\right][C_o^i] \tag{6.30}$$

The power series is terminated with ample number of terms such that inclusion of any more terms has negligible contribution in the order of η $(= 10^{-10})$. The boundary and interface conditions in Eqs. (6.17)-(6.19) can be written in terms of functions $g_l(\zeta)$ as

$$\begin{aligned}
&\text{for } k = 1, \quad \text{at } \zeta = 0: \quad g_5 = 0, \quad g_7 = 0, \quad g_8 = 0, \quad g_9 \quad \text{or} \quad g_{11} = 0 \\
&\text{for } k = L, \quad \text{at } \zeta = 1: \quad g_5 = 0, \quad g_7 = 0, \quad g_8 = 0, \quad g_9 \quad \text{or} \quad g_{11} = 0
\end{aligned} \tag{6.31}$$

$$[(g_1,\, g_2,\, g_3,\, g_5,\, g_7,\, g_8,\, g_9,\, g_{11})|_{\zeta=1}]^{(k)} = [(g_1,\, g_2,\, g_3,\, g_5,\, g_7,\, g_8,\, g_9,\, g_{11})|_{\zeta=0}]^{(k+1)} \tag{6.32}$$

At the $k = n_q$ $(q = 1, \ldots L_a)$ interfaces for $k = 1, 2, \ldots, L-1$ except for g_{11} where ϕ is prescribed,

the following condition is replaced instead of the continuity condition on g_{11}

$$g_9|_{\zeta=1} = 0; \qquad q = 1, ..., L_a \tag{6.33}$$

After applying them, the Eq. (6.30) yields

$$\sum_{i=1}^{8} \mathbf{K_d}_i(\zeta) C_o^i = \mathbf{0} \tag{6.34}$$

where, $\mathbf{K_d}$ is the coefficient matrix and is dependent on $\omega = \omega_n$. The determinant of the matrix $\mathbf{K_d}$ is zero for obtaining its non-trivial solution. The natural frequencies ω_n are determined from the $\mathbf{K_d}$ matrix by the bisection method where its determinant is zero. This procedure is similar to the one earlier taken by Kapuria et al. [90] in order to handle those roots which did not satisfy the inner and outer transverse stress boundary condition.

Equations (6.31)-(6.33) give the 8 boundary conditions and $8\times(L-1)$ interface continuity conditions which are used to obtain the $8\times L$ constants $C_o^{i(k)}$s for L layers. Once the natural frequencies are known then the mode shapes are obtained using the Eq. (6.30). Further, from the algebraic equation Eq. (6.25), functions $\hat{\mathbf{G}}$ can be determined. Hence, the first solution step is completed.

6.5.2 Second Iteration Step

In this step, the solution of the previous step is taken as the known approximate solution for $g_l(\zeta)$, while functions f_l are considered unknown. The variation δX for this case is given by

$$\delta X_l = g_l(\zeta)\delta f_l \quad \text{for} \quad l = 1, 2, \ldots, 11 \tag{6.35}$$

According to Eq. (6.20) $f_l(\xi)$ functions are partitioned into

$$\begin{aligned} \bar{\mathbf{F}} &= \begin{bmatrix} f_3 & f_1 & f_2 & f_4 & f_6 & f_8 & f_9 & f_{10} \end{bmatrix}^{\mathrm{T}} \\ \hat{\mathbf{F}} &= \begin{bmatrix} f_5 & f_7 & f_{11} \end{bmatrix}^{\mathrm{T}} \end{aligned} \tag{6.36}$$

Substituting Eqs. (6.35) and (6.21) in Eq. (6.16) this time, and the arbitrary coefficients of δf_l are individually equated to zero to yield the 8 system of differential equations and 3 simultaneous

algebraic equations for f_l which are in the form of

$$\mathbf{N}\bar{\mathbf{F}}_{,\xi} = \bar{\mathbf{B}}\bar{\mathbf{F}} + \hat{\mathbf{B}}\hat{\mathbf{F}} \tag{6.37}$$

$$\mathbf{L}\hat{\mathbf{F}} = \tilde{\mathbf{B}}\bar{\mathbf{F}} \tag{6.38}$$

The non-zero elements of the matrices are listed below

$$N_{11} = N_{66} = \tfrac{1}{\psi}\langle\tfrac{g_8 g_3}{\zeta t+R_1}\rangle_h, \quad N_{22} = N_{44} = \tfrac{1}{\psi}\langle\tfrac{g_4 g_1}{\zeta t+R_1}\rangle_h,$$

$$N_{33} = N_{55} = \tfrac{1}{\psi}\langle\tfrac{g_6 g_2}{\zeta t+R_1}\rangle_h, \quad N_{77} = N_{88} = \tfrac{1}{\psi}\langle\tfrac{g_{10} g_9}{\zeta t+R_1}\rangle_h,$$

$$\bar{B}_{42} = \rho\omega^2\langle g_1 g_1\rangle_h, \quad \bar{B}_{53} = \rho\omega^2\langle g_2 g_2\rangle_h, \quad \bar{B}_{61} = \rho\omega^2\langle g_3 g_3\rangle_h,$$

$$\bar{B}_{12} = \langle\tfrac{g_8 g_1}{\zeta t+R_1}\rangle_h - \tfrac{1}{t}\langle g_8 g_{1,\zeta}\rangle_h, \quad \bar{B}_{16} = \bar{p}_{55}\langle g_8 g_8\rangle_h, \quad \bar{B}_{18} = p_{57}\langle g_8 g_{10}\rangle_h,$$

$$\bar{B}_{21} = \langle\tfrac{g_4 g_3}{\zeta t+R_1}\rangle_h, \quad \bar{B}_{24} = \bar{p}_{11}\langle g_4 g_4\rangle_h, \quad \bar{B}_{25} = \bar{p}_{16}\langle g_4 g_6\rangle_h,$$

$$\bar{B}_{27} = -\tfrac{\bar{p}_{18}}{t}\langle g_4 g_{9,\zeta}\rangle_h, \quad \bar{B}_{34} = \bar{p}_{16}\langle g_6 g_4\rangle_h, \quad \bar{B}_{35} = \bar{p}_{66}\langle g_6 g_6\rangle_h,$$

$$\bar{B}_{37} = -\tfrac{\bar{p}_{68}}{t}\langle g_6 g_{9,\zeta}\rangle_h, \quad \bar{B}_{46} = -2\langle\tfrac{g_1 g_8}{\zeta t+R_1}\rangle_h - \tfrac{1}{t}\langle g_1 g_{8,\zeta}\rangle_h, \quad \bar{B}_{64} = \langle\tfrac{g_3 g_4}{\zeta t+R_1}\rangle_h,$$

$$\bar{B}_{76} = p_{75}\langle g_{10} g_8\rangle_h, \quad \bar{B}_{34} = -\bar{p}_{77}\langle g_{10} g_{10}\rangle_h,$$

$$\hat{B}_{12} = \bar{p}_{45}\langle g_8 g_7\rangle_h, \quad \hat{B}_{21} = \bar{p}_{13}\langle g_4 g_5\rangle_h, \quad \hat{B}_{31} = \bar{p}_{36}\langle g_6 g_5\rangle_h,$$

$$\hat{B}_{52} = -\langle\tfrac{g_2 g_7}{\zeta t+R_1}\rangle_h - \tfrac{1}{t}\langle g_2 g_{7,\zeta}\rangle_h, \quad \hat{B}_{61} = -\langle\tfrac{g_3 g_5}{\zeta t+R_1}\rangle_h - \tfrac{1}{t}\langle g_3 g_{5,\zeta}\rangle_h,$$

$$\hat{B}_{72} = p_{74}\langle g_{10} g_7\rangle_h, \quad \hat{B}_{83} = -\langle\tfrac{g_9 g_{11}}{\zeta t+R_1}\rangle_h - \tfrac{1}{t}\langle g_9 g_{11,\zeta}\rangle_h,$$

$$\tilde{B}_{11} = -\tfrac{1}{t}\langle g_5 g_{3,\zeta}\rangle_h, \quad \tilde{B}_{14} = \bar{p}_{13}\langle g_5 g_4\rangle_h, \quad \tilde{B}_{15} = \bar{p}_{36}\langle g_5 g_6\rangle_h,$$

$$\tilde{B}_{17} = -\tfrac{\bar{p}_{38}}{t}\langle g_5 g_{9,\zeta}\rangle_h, \quad \tilde{B}_{23} = -\tfrac{1}{t}\langle g_7 g_{2,\zeta}\rangle_h, \quad \tilde{B}_{26} = \bar{p}_{45}\langle g_7 g_8\rangle_h,$$

$$\tilde{B}_{28} = \bar{p}_{47}\langle g_7 g_{10}\rangle_h, \quad \tilde{B}_{34} = \bar{p}_{81}\langle g_{11} g_4\rangle_h, \quad \tilde{B}_{35} = \bar{p}_{86}\langle g_{11} g_6\rangle_h,$$

$$\tilde{B}_{37} = -\tfrac{1}{t}\langle g_{11} g_{9,\zeta}\rangle_h, \quad L_{11} = -\bar{p}_{33}\langle g_5 g_5\rangle_h, \quad L_{22} = -\bar{p}_{44}\langle g_7 g_7\rangle_h,$$

$$L_{31} = -\bar{p}_{83}\langle g_{11} g_5\rangle_h, \quad L_{33} = -\bar{p}_{88}\langle g_{11} g_{11}\rangle_h$$

where $\langle\ldots\rangle_h = \sum_{k=1}^{L} t^{(k)} \int_0^1 (\ldots)^{(k)}\, d\zeta$ denotes integration across the thickness. Above integrations are performed over the ζ direction on the known functions of ζ and by applying integration by parts wherever necessary. Thus size of the obtained matrices, $\mathbf{N}$, $\bar{\mathbf{B}}$, $\hat{\mathbf{B}}$, $\mathbf{L}$ and $\tilde{\mathbf{B}}$ are 8×8, 8×8, 8×3, 3×3 and 3×8, respectively. Referring back to the Sec. 3.6 of Chapter 3 as discussed, all the above integrations are evaluated in closed form because the general solution obtained in Eq. (6.30)

gives close form $g_l(\zeta)$ functions.

Substituting $\hat{\mathbf{F}}$ which is algebraically solved in Eq. (6.38) back into Eq. (6.37) yields the following set of first order ODEs for $\bar{\mathbf{F}}$:

$$\bar{\mathbf{F}}_{,\xi} = \mathbf{B}(\omega)\bar{\mathbf{F}} \tag{6.39}$$

with $\mathbf{B} = \mathbf{N}^{-1}[\bar{\mathbf{B}} + \hat{\mathbf{B}}\mathbf{L}^{-1}\tilde{\mathbf{B}}]$. Equation (6.39) represents a system of homogeneous first-order ODEs with constant coefficients. Its complementary solution is of the form $\bar{\mathbf{F}}_{\mathbf{c}}(\xi) = e^{\lambda\xi}\mathbf{Y}$, which on substitution in the Eq. (6.39) yields

$$\mathbf{BY} = \lambda\mathbf{Y} \tag{6.40}$$

Hence, the exponent λ and $\mathbf{Y}$ are the 8 eigenvalue and eigenvector pairs of matrix $\mathbf{B}$. Thus, the complete complementary solution $\bar{\mathbf{F}}_{\mathbf{c}}(\xi)$ can be expressed in terms of 8 real constants C_i as

$$\bar{\mathbf{F}}_{\mathbf{c}} = \sum_{i=1}^{8} \mathbf{F}_i(\zeta)C_i \tag{6.41}$$

where $\mathbf{F}_i(\xi)$ are column vectors of functions corresponding to the eigen pair λ_i and Y_i, whose functional forms depend on the nature of λ_i (real or complex), details of which can be found in Sec. 3.4.2 of Chapter 3. The prescribed circumferential edge boundary conditions in Eq. (6.20) are expressed in terms of $\bar{\mathbf{F}}$ to be satisfied by the general solution in Eq. (6.41) for obtaining the constants C_i

$$\begin{aligned}
&\text{Simply Supported (S) :} && f_3 = 0, \quad f_4 = 0, \quad f_6 = 0 \\
&\text{Clamped (C) :} && f_3 = 0, \quad f_1 = 0, \quad f_2 = 0 \\
&\text{Free (F) :} && f_8 = 0, \quad f_4 = 0, \quad f_6 = 0, \qquad (i = 1, 2, \ldots, n)
\end{aligned} \tag{6.42}$$

The electric boundary condition is given by

$$f_9 \quad \text{or} \quad f_{10} = 0 \tag{6.43}$$

After applying them, the Eq. (6.20) yields

$$\sum_{i=1}^{8} \mathbf{K}_{\mathbf{d}i}(\zeta)C_i = \mathbf{0} \tag{6.44}$$

Similarly, ω can be obtained by finding roots of the equation $|det(\mathbf{K_d})|$=0 by using bisection method. Now, the undamped natural frequencies $\omega_{11} = \omega_m$ are known and further, the mode shapes are determine using the Eq. (6.41). Further, from the algebraic equation Eq. (6.38), functions $\hat{\mathbf{F}}$ can be determined. Hence, the second solution step is completed. These two steps of solution in (Secs. 6.5.1 and 6.5.2) comprises one iteration of alternating directions for approximate and analytical solutions, which are repeated until a prescribed level of convergence is achieved. The similar treatment for handling the large positive eigenvalues is adopted here as used in Ref. [200].

6.6 NUMERICAL RESULTS

The natural frequencies are presented as obtained from the present solution and are compared with the available literature results. The lowest frequencies are tabulated for a piezolaminated shell panel in Table 6.1 composed of a single layer of [PZT-5A]. This is similar to the panel analysed previously by Kapuria et al. [90] which had the following material properties:

Cylindrical shell configuration: S=5, 10, 20, ψ=60^o;

Young's, shear moduli & Poisson's ratios: $Y_1 = 61.0$ GPa, $Y_2 = 61.0$ GPa, $Y_3 = 53.2$ GPa, $G_{23} = 21.1$ GPa, $G_{13} = 21.1$ GPa, $G_{12} = 22.6$ GPa; $\nu_{12} = 0.35$, $\nu_{13} = 0.38$, $\nu_{23} = 0.38$; $d_{31} = -171\times10^{-12}$ m/V, $d_{32} = -171\times10^{-12}$ m/V, $d_{33} = 374\times10^{-12}$ m/V, $d_{24} = 584\times10^{-12}$ m/V, $d_{15} = 584\times10^{-12}$ m/V; $\eta_{11} = 1.53\times10^{-8}$ F/m, $\eta_{22} = 1.53\times10^{-8}$ F/m, $\eta_{33} = 1.50\times10^{-8}$ F/m; $\rho = 7600\ kg/m^3$;

Non-dim.: Natural frequency $\bar{\omega}_n = \omega_n R S_1(\rho_0/Y_0)^{1/2}$ with $Y_0 = 61.9$ GPa, $\rho_0 = 7600\ kg/m^3$, $S_1 = S$ and $S = R/h$ ([90]).

The mentioned shell panel has simply-supported boundary conditions (SS) and electrically, those circumferential ends are both close circuited (CC). However, its inner and outer radial surfaces are open circuited (OC).

The natural frequencies are tabulated in Table 6.1 for the piezoelectric shell panels of different thickness ratios S. The presented lowest three frequencies are for the spatial modes n and corresponding flexural modes $m = 1$.

Table 6.1: Lowest natural frequencies $\bar{\omega}_n$ for piezoelectricity laminated shell panels corresponding to m=1

	Mode(n, m)	$S = 5$	$S = 10$	$S = 20$
Present	$n = 1$	2.4301	2.5213	2.5459
Ref. [90]		2.4313	2.5210	2.5456
Present	$n = 2$	9.6597	10.9893	11.4498
Ref. [90]		9.6614	10.992	11.449
Present	$n = 3$	19.2094	23.8013	25.8971
Ref. [90]		19.016	23.800	25.890

Similarly, first three lowest frequencies are also presented in Table 6.2 for the elastic shell panel of lamination scheme [0/90/90/0] with the following properties of orthotropic material:

Young's, shear moduli & Poisson's ratios: $Y_1 = 137.9$ GPa, $Y_2 = 14.48$ GPa, $Y_3 = 14.48$ GPa, $G_{23} = 5.86$ GPa, $G_{13} = 5.86$ GPa, $G_{12} = 5.86$ GPa; $\nu_{12} = 0.21$, $\nu_{13} = 0.21$, $\nu_{23} = 0.21$; and $\rho = 1578\ kg/m^3$;

Non-dim.: Natural frequency $\bar{\omega}_n = \omega_n R S_1 (\rho_0/Y_0)^{1/2}$ with $Y_0 = 14.48$ GPa, $\rho_0 = 1578\ kg/m^3$, $S_1 = S$ and $S = R/h$.

Table 6.2: Lowest natural frequencies $\bar{\omega}_n$ for elastic laminated shell panels corresponding to m=1

	Mode(n, m)	$S = 5$	$S = 10$	$S = 20$
Present	$n = 1$	4.84461	5.88209	6.28434
3D FE		4.845802	5.882043	6.28452
Present	$n = 2$	14.7525	22.0148	26.6822
3D FE		14.75628	22.01557	26.68278
Present	$n = 3$	26.6791	41.1347	56.1760
3D FE		26.68278	41.13601	56.17684

The cylindrical shell panels of S=5, 10, 20 are simply-supported and for all panels $\psi = 60^o$ and each ply is assumed to have the same thickness. The present results shows excellent agreement with 3D FE. The 3D FE model is done in a similar fashion as discussed in the previous chapters to mimic the cylindrical shell panel exactly. However, mesh size of $60 \times 16 \times 50$ in (θ, r, z) is taken

with 3D elements (C3D20R) in the ABAQUS.

In general, the frequencies increased for thinner shell panels. And, from the computational efficiency point of view, the present EKM results converged by including a single term showing very good agreement with the 3D FE results.

6.7 SUMMARY

A novel 3D semi-analytical solution for the free vibration analysis of the hybrid cylindrical shell panels has been developed by considering full electro-mechanically coupled piezo-elasticity. The present solution is valid for different cross-ply, angle-ply laminate schemes and the dynamic solution for elastic laminates can also be deduced out of the present robust algorithm. Typical numerical study for elastic and hybrid cylindrical shell laminates under free vibration revealed that just a single term is enough for extracting the natural frequencies for thick cylindrical shell panels with SS boundary condition for both elastic and piezoelastic cases. The fundamental frequencies are tabulated for ready reference.

Chapter 7

CONCLUSIONS

Shell structures are extensively used in structural engineering applications for their ability of carrying higher loads, high degree of reserved strength and structural integrity, high stiffness, containment of space, high strength : weight ratio and adds aesthetics. Further, incorporating smart materials such as conforming PFRCs on the shell structures widen its applications to structronic structures such as containers for food processing, sports accessories, modern manufacturing, aircraft wings and engine design, medical wearable instruments, etc. Complexity in prediction of electromechanical response during such applications asks for 3D stress analysis. By assuming certain displacement fields, 1D/2D analytical solutions have been presented but exact through-thickness variations of the displacements are not extracted. Approximate 3D solutions have been developed mostly by employing the numerical techniques as developing analytical solution for such cases is faced with mathematical singularities where its challenging to derive a closed-form solution. Further, there is loss of accuracy in determination of the stresses obtained from displacement based variational equations.

A novel semi-analytical solution approach has been developed in the present work. First time, elasticity based accurate 3D solutions are presented for the static cylindrical bending of laminated orthotropic composite cylindrical shell supported on arbitrary boundary conditions. Subsequently, a 3D solution has been presented for more realistic case of elastic laminated composites with imperfect interlaminar bonding between the plies of such arbitrarily supported cylindrical shell

panels. Further effort has been directed towards developing a 3D solution based on piezoelasticity where electro-mechanical coupling was considered. Lastly, the formulation has been extended to obtain the 3D results for the cylindrical panel undergoing free vibration.

The formulation of the problem is based on the Reissner's type mixed variational principle where it is considered that all the displacement, stress, electric potential and electric displacement variables are the primary variables. As a result, the boundary and interface conditions are satisfied in exact pointwise manner, and it is ensured that all the field variables acquire same order of accuracy. Similarly, for the dynamic analysis of the mentioned cylindrical shell panels a modified Hamilton's principle with the inertia terms has been employed. After obtaining the weak form, the multi-field multi-term extended Kantorovich method (EKM) has facilitated its reduction to separate systems of non-homogeneous first-order ordinary differential equations (ODEs) as it assumes the functions as the product of separate coordinate variable functions. This recently developed iterative method includes multiple number of such product terms and can integrate coupled loading field through the Kronecker delta property. For the cylindrical shell, the system of ODEs corresponding to the radial variable r has variable coefficients whose solution is obtained in form of a novel power series and a solution based on Pagano's approach has been obtained for the constant coefficient system of ODE along the coordinate direction θ. As, the ODEs give closed-from solutions, these are iteratively employed for solving analytically and get fast converging results. Apart from the computational advantage, this is the essence of accurate prediction of boundary effects.

During numerical study, the present results excellently agreed on comparing with those taken from the literature and modelled 3D FE results. Results have been reported for static response of thin, moderately thick and thick cylindrical shell panels made up of different laminate scheme (cross-ply, angle-ply and sandwich schemes), arbitrary boundary conditions and circumferential span angles in the second chapter. Further, for the imperfectly bonded cylindrical laminates by varying the stiffness of the cohesive zone, interlaminar behavior of the field variables are presented and its physical effects has been inferred in addition to study of previously mentioned parameters.

Subsequently, the circumferential and through-the-thickness variations of the electrical and mechanical field variables have been analysed for the cylindrical bending of piezolaminated cylidrical shells. Boundary effects and results at the other stress concentration zones which are inherent to such structural laminates are accurately predicted and some new benchmark results are also computed. Finally, the frequencies obtained from the present solution exactly match with reference 3D results from the dynamic analysis along with presentation of few new results. Following are the observations and inferences drawn from the numerical studies, regarding the physical implications and efficiency aspects of the proposed 3D solutions for different cases

7.1 CHAPTERWISE SYNOPTIC CONCLUSIONS FROM THE PRESENT WORK

(1) The multi-term EKM along with mixed formulation based on displacements and stresses has been used to obtain 3D closed form solution for static bending of thick, moderately thick and thin cylindrical shell panels. Linear constitutive model for the orthotropic material is considered in the elasticity based formulation. Through the generalized solution, nature of response for cylindrical shell panels with arbitrary boundary conditions has also been investigated. An extensive numerical study is conducted by taking single layer and multi-layer cross-ply, angle-ply and sandwich composite panels. The effect of shallowness of the cylindrical shell panels has also been investigated. Specific points from the computed results and study are as follows:

- The present 3D technique gives accurate results with better computational efficiency. It is efficient as just one or two terms and two or three iteration steps give excellently matching results with 3D FE for arbitrary boundary conditions. Moreover, just single term with 2 iteration steps give excellent results for SS boundary condition when compared to 3D exact solution where 21 terms in Fourier expansion had to be used.
- Apart from accurate results throughout the circumferential and thickness span, boundary

layer effects are also obtained with convincing accuracy which are developed in the arbitrarily supported panels.

- Such boundary effects are not that accurately predicted by the single-term EKM solution. However, there is drastic improvement in the accuracy of the results with addition of just one or two more terms in the trial functions as compared to the single-term results. This is one of the notable feature of the method for which it is powerful.
- It is noted that the present stress distribution matched well with the 3D FE solution beyond boundary layer region in the interior, but 3D FE fails completely in predicting them in the vicinity of the edges as it is unable to satisfy the conditions of applied normal and shear traction at the top and bottom surfaces, and the conditions of continuity at the layer interfaces.
- The variation in the direction of developed stresses while moving along ξ direction has been shown for arbitrarily supported panels. The extent of boundary effects in the shell panels are dependent on geometric thickness ratio S which increases with their thickness. Deformations in deep shells are higher than those in shallow shells, thus developed stresses and boundary effects are also higher in the deep shells.
- A single layer angle-ply thick shell panel is studied. Other transverse stresses along with the corresponding boundary effects are also accurately predicted which are inherent to angle-ply laminates. The boundary effects in the developed stresses is significantly more in the sandwich laminates. These analysis can be readily considered as design guidelines.

This novel development would be beneficial for obtaining computationally faster and accurate results for arbitrarily supported cylindrical shell panels which can act as benchmark for assessing other theories.

(2) In this work, the shear-slip phenomena between the lamina is incorporated with multi-term EKM to propose a generalized analytical solution for static analysis of an arbitrarily supported

cylindrical shell panel having uniform bonding imperfection at the interfaces. The linear spring-layer model is considered to include the shear-slip between the lamina. The shear-slip is quantified in terms of imperfection compliance. Ideally, for very first time results for an arbitrarily supported thick cylindrical panel with weak interfaces has been reported. Further, the effect of varying amount of imperfection compliance has been investigated and the combined effect of span angle and boundary conditions on the weakly bonded panel has also been demonstrated. Hence, following major observations are drawn from the numerical study of the cross-ply laminate:

- Results for CS and CF panels converged by using just two terms in the multi-term expansion of EKM. Moreover, for SS panel even one term predict the results accurately. Higher number of iterations are required for CF panel but only two iterations provided converged results in case of CS and SS panels.
- The displacements and stresses increased substantially as compared to those for a perfectly bonded cylindrical panel. Thus, the field variables are highly sensitive to bonding imperfection which is further higher for thick panel. Due to the interlaminar shear-slip, there is a discontinuous jump in the in-plane displacements across the interface which also creates large stress difference in the two differently oriented adjacent plies.
- The stress difference is observed to be very high at the clamped edge than at any other midspan locations. This necessitates the need of accurate prediction of the edge effects which has been efficiently computed by the presently developed solution.
- There is non-linear increase of the field variable entities with increase in imperfection compliance ($\mathbf{R}$). This increment is very sensitive at lower values of $\mathbf{R}$ which later tends to remain constant at higher range of $\mathbf{R}$. This gives the hint of debonding between the plies.
- Cylindrical panels with larger span angle undergo high deformation and stress variation.

In addition, edge boundary conditions also significantly affect the behavior of such panels. For example, SS and CS panels are more sensitive than CF panel.

The theory can be readily extended to study of delamination. Structural health monitoring can be performed using this study as the response of the shell panel changes with the onset of imperfect bonding between the plies.

(3) The powerful multi-term EKM is generalised to solve 3D piezoelasticity problems of hybrid laminated shell panels for the first time. The numerical study reveals that

- The multi-term EKM predicts the coupled electromechanical response of hybrid elastic-piezoelectric laminated panels accurately which may be loaded under pressure loading condition and with different applied surface potentials.
- The electric charge density generated at the piezo-elastic interface could be inferred from the through-thickness plots which can direct the necessity of its grounding or appropriate circuit design for effective sensing and actuating applications.
- A higher number of terms (up to n=4) is usually required to predict the sharp variations of electric variables in the case of unsymmetrical surface potential even for SS shell panels. Though the convergence is achieved with two n=2 terms even for higher thickness ratio.
- Similar to the case of elastic laminate, for pressure loading, a two-term solution is able to yield accurate results for all variables in case of an arbitrarily supported cylindrical shell panel.
- The 3D FE solution fails to satisfy the stress free conditions at the clamped edge. Consequently, it yields inaccurate results for stresses in close vicinity of such supports. The present solution could accurately predict all the electro-mechanical field variables reliably, which are consistent with the boundary conditions.

The present study will facilitate development of accurate semi-analytical solutions of many other unresolved problems in 3D piezoelasticity such as the free edge stresses in hybrid piezoelectric laminates under bending, tension and twisting.

(4) A novel 3D semi-analytical solution for the free vibration analysis of the hybrid cylindrical shell panels has been developed by considering full electro-mechanically coupled piezoelasticity. The present solution is valid for different cross-ply, angle-ply laminate schemes and the dynamic solution for elastic laminates can also be deduced out of the present robust algorithm. Typical numerical study for elastic and hybrid cylindrical shell laminates under free vibration revealed that just a single term is enough for extracting the natural frequencies even for thick cylindrical shell panels with SS support conditions.

7.2 SOME GUIDELINES FOR THE PRACTICAL DESIGN OF SMART SHELL STRUCTURES

From the present work specific non-intuitive guidelines which needs to be realised while practically designing smart shell structures are based on the following outcomes:

1. The state of stress is truely three-dimensional (3D) in nature throughout the domain of the shell structure. Further, the magnitude of boundary effects depends on the geometric mid-surface radius to thickness ratio of the cylindrical shell. Therefore, thick structures should be designed with additional reinforcements and novel adhesive/ bonding design (e.g. stepped, etc.), as the displacement/ stress field follows a non-linear trend through-the-thickness and in order to smoothly transfer the stresses across the interfaces. Moreover, this necessitates the development of 3D theory where no kinematic assumptions exist unlike 1D/2D theories. Material with higher modulus should also be employed for thicker structures as the generated stresses are larger.

2. The stresses are comparatively large at certain boundary conditions. There its sense changes abruptly from compressive to tensile or vice-versa through-the-thickness which is dependent

on the laminate scheme and boundary conditions. Hence, the stacking sequence should be designed in order to balance the laminate and minimize the stress alterations. Similarly, by reducing the ply-angle in the angle-ply laminates such peak stresses can be reduced.

3. In case of imperfect bonding between the plies, the design should consider factor of safety as there is sudden failure of the bonding after certain stiffness value of the cohesive zone. The selected adhesives should have comparable material properties with those of the parent plies for smoother interlaminar stress transfer.

4. Furthermore, the cohesive zone is subjected to stress singularity at the clamped boundary which is also computed from the present 3D solution. Use of functionally graded adhesive material with higher strength at the clamped boundaries and/or varying the thickness of the adhesive layer can be proposed.

5. The piezoelectric smart composites are also subjected to similar stress behavior as previously discussed. The piezoelectricity lamina should be designed to sustain minimal load when integrated with other material substrate. Practically, they are usually accompanied with various control system which should be efficiently insulated yet rigidly locked with the elastic plies for efficient actuation and sensing.

6. Further, in case of distributed sensing or actuation applications, the piezoceramics should be accordingly chosen which possess required strength and their location should be optimally designed whenever they are employed over the shell surfaces with variation in magnitude and nature of strain. Hence, very recently impetus has been directed towards PFRCs which has functional advantages.

7. The geometry of the structures has significant effect on its natural frequencies. The location of deflection extremities also differ with change in geometry. These should be carefully considered for a stable design so that appropriate control mechanisms can be employed.

7.3 CONTRIBUTIONS OF PRESENT THESIS

The salient contributions of the present thesis to alleviate the hindering issues related to computational mechanics of shell structures is of significant engineering interest. Computational mechanics of shell structures has faced hindrances owing to their geometry, mathematical complexity, lack of efficient computational methods, etc. The significant and novel contributions of the thesis are as follows:

1. The response of a structure depends on the existing boundary conditions and its geometry such as shape, thickness ratio, shallowness, etc. Therefore, design of structures predominantly depends on the choice of 3D or other refined 2D theories. The choice should be made within the constraints of accuracy, applicability and computational cost. The present work has contributed in these aspects.

2. Geometric complexity and new material development has intrigued the development of a generalized and accurate multi-physics theory to cater the corresponding challenges such as curvature, imperfect bonding, material inhomogeneity, boundary effects and obtaining accurate frequencies. The present formulation has incorporated these physical aspects which are realistic.

3. A unique semi-analytical solution has been developed which is reliable, powerful and favourably reduces the computational cost.

4. It is noteworthy, that the developed solution is very efficient for the thick and deeper shell geometries.

5. Development of these solutions might be integral in spontaneously generating multi variable dependent data for further statistical analysis to predict various physical phenomena.

6. This thesis provides benchmark results for the arbitrarily supported cylindrical shell structures under static and dynamic conditions.

7. It can be utilized to assess other 2D theories and revisit the packages based on numerical solutions.

8. The present study can form the basis of developing 2D theories which are able to predict stresses at the boundary layer near the supports, more accurately.

7.4 FUTURE SCOPE OF WORK

Based on the present work, the future studies can be directed in the following aspects:

1. Since the last decade, multi-term EKM has been extended to a wide range of problems concerning plate structures. The present extension of the solution opens its feasibility study for similar problems of shell structures. Following 3D solutions can be readily developed:

   (i) Static and free vibration study of finite length cylindrical shells with Levy-type boundary conditions based on the 3D elasticity/piezoelasticity solution.

   (ii) 3D elasticity/ piezoelasticity based solutions can be developed for the curved beams and circular plates.

   (iii) Similar 3D solution can be obtained for cylindrical shells made up of functionally graded materials.

2. As the physical connection/ adhesion between the piezo element and elastic substrate plays a significant role in effective sensing and actuation, the effect of interlaminar cohesive zone needs to be addressed through development of 3D solution. This can be employed for accurate prediction of onset of the interlaminar failure/ delamination at the edges.

3. An experimental study on the delamination failure in hybrid laminates will validate the developed theoretical model, which will immensely help in establishing the integrity of laminated smart structures.

4. Further, thermal/hygrothermal effects can be incorporated in the formulation to obtain thermo-electro-mechanical based 3D solution for smart cylindrical shell structures. This area has been sparsely explored.

5. Development of a 3D solution for buckling analysis of the smart cylindrical shells and their dynamic characteristics under forced vibration can be explored.

6. Developing a generalized 3D solution based on the multi-field multi-term EKM for spherical shells can be attempted.

7. The present approach and solution method can further be used to develop elasticity/ piezoelasticity based solutions for static and dynamic analysis of cylindrical shells with cutouts or ribs.

8. Analytical solutions for static and dynamic (free vibration) analysis of laminated composite, piezoelectric laminates and functionally graded cylindrical shells with variable radius of curvature/ thickness can be presented.

Bibliography

[1] Kebadze, E. M., Guest, S. D. and Pellegrino, S. (2004), 'Bistable prestressed shell structures', *Thin Walled Structures* **41**, 2801–2820.

[2] Yang, B. and Yun, K. S. (2012), 'Piezoelectric shell structures as wearable energy harvesters for effective power generation at low-frequency movement', *Sensors and Actuators A: Physical* **188**, 427–433.

[3] Calladine, C. R. (1989), *Theory of shell structures*, Cambridge university press.

[4] Tzou, H. S. (2018), *Piezoelectric shells: Sensing, Energy Harvesting, and Distributed Control—Second Edition*, Springer.

[5] Sinapius, J. M. (2021), *Adaptronics-Smart Structures and Materials*, Springer, Berlin, Germany.

[6] Janocha, H. (1999), *Adaptronics and smart structures*, Springer-Verlag Berlin Heidelberg.

[7] García-Pérez, J. V., Cárcel, J. A., De la Fuente-Blanco, S. and De Sarabia, E. R-F. (2006), 'Ultrasonic drying of foodstuff in a fluidized bed: Parametric study', *Ultrasonics* **44**, e539–e543.

[8] Bastaits, R., Rodrigues, G., Jetteur, P., Hagedorn, P. and Preumont, A. (2012), 'Multi-layer adaptive thin shells for future space telescopes', *Smart materials and structures* **21**, 064004.

[9] Scott, R. C. and Weisshaar, T. A. (1994), 'Panel flutter suppression using adaptive material actuators', *Journal of aircraft* **31**, 213–222.

[10] Bernhard, A. PF. and Chopra, I. (2001), 'Analysis of a bending-torsion coupled actuator for a smart rotor with active blade tips', *Smart Materials and Structures* **10**, 35.

[11] Schiller, N. H., Saunders, W. R., Chishty, W. A., Vandsburger, U. and Baumann, W. T. (2006), 'Development of a piezoelectric-actuated fuel modulation system for active combustion control', *Journal of intelligent material systems and structures* **17**, 403–410.

[12] Liao, W. H., Wang, D. H. and Huang, S. L. (2001), 'Wireless monitoring of cable tension of cable-stayed bridges using PVDF piezoelectric films', *Journal of Intelligent Material Systems and Structures* **12**, 331–339.

[13] O'neal, G. P., Min, B. K., Pasek Z. J. and Koren, Y. (2001), 'Integrated structural/control design of micro-positioner for boring bar tool insert', *Journal of Intelligent Material Systems and Structures* **12**, 617–627.

[14] Uchino, K. (1998), 'Piezoelectric ultrasonic motors: overview', *Smart materials and structures* **7**, 273.

[15] Uchino, K. (2017), *Piezoelectric actuators and ultrasonic motors*, Springer Science & Business Media.

[16] Altenbach, H. and Victor, E. (2017), *Shell-like structures*, Springer, New York.

[17] Love, A. E. H. (1888), 'The small free vibrations and deformation of a thin elastic shell', *Philosophical Transactions of the Royal Society of London. A* **179**, 491–546.

[18] Jiashi, Y. (2006), *Mechanics of piezoelectric structures*, World Scientific.

[19] Khan'Chau, L. (1986), 'The theory of piezoelectric shells', *Journal of Applied Mathematics and Mechanics* **50**, 98–105.

[20] Timoshenko, S. and Woinowsky-Krieger, S. (1959), *Theory of plates and shells*, McGraw-Hill, New York, United States.

[21] Sanders, Jr. and Lyell, J. (1959), *An improved first-approximation theory for thin shells*, NASA Rep.

[22] Flügge, W. (1973) , *Thin elastic shells*, Springer, Berlin.

[23] Kraus, H. (1967) , *Thin elastic shells*, John Wiley & Sons.

[24] Leissa, A. W. (1973), 'The free vibration of rectangular plates', *Journal of Sound and vibration* **31**, 257–293.

[25] Tiersten, H. F. (1969) , *Linear Piezoelectric Plate Vibrations*, Plenum Press, New York.

[26] Tzou, H. S. (1993), *Piezoelectric shells: Distributed Sensing and Control of Continua*, Kluwer Academic Publishers, Dordrecht.

[27] Rogacheva, N. N. (1994), *The theory of piezoelectric shells and plates*, CRC press.

[28] Noor, A. K. and Burton, W. S. (1992), 'Computational models for high-temperature multilayered composite plates and shells', *Applied Mechanics Reviews* **45**, 419–446.

[29] Soldatos, K. P. (1994), 'Review of three dimensional dynamic analyses of circular cylinders and cylindrical shells', *Applied Mechanics Reviews* **47**, 501–516.

[30] Saravanos, D. A. and Heyliger, P. R. (1999), 'Mechanics and computational models for laminated piezoelectric beams, plates and shells', *Applied Mechanics Reviews* **52**, 305–320.

[31] Piskunov, V. G. and Rasskazov, A. O. (2002), 'Evolution of the theory of laminated plates and shells', *International applied mechanics* **38**, 135–166.

[32] Carrera, E. (2002), 'Theories and finite elements for multilayered, anisotropic, composite plates and shells', *Archives of Computational Methods in Engineering* **9**, 87–140.

[33] Moussaoui, F. and Benamar, R. (2002), 'Non-linear vibrations of shell-type structures: a review with bibliography', *Journal of sound and vibration* **255**, 161–184.

[34] Qatu, M. S. (2002), 'Recent research advances in the dynamic behavior of shells: 1989-2000, Part 2: Homogeneous shells', *Applied Mechanics Reviews* **55**, 415–434.

[35] Qatu, M. S., Sullivan, R. W. and Wang, W. (2010), 'Recent research advances on the dynamic analysis of composite shells: 2000–2009', *Composite Structures* **93**, 14–31.

[36] Qatu, M. S., Asadi, E. and Wang, W. (2012), 'Review of recent literature on static analyses of composite shells: 2000-2010', *Scientific Research Publishing* **2**, 61–86.

[37] Caliri, M. F., Ferreira, A. J. M. and Tita, V. (2016), 'A review on plate and shell theories for laminated and sandwich structures highlighting the Finite Element Method', *Composite Structures* **156**, 63–77.

[38] Kant, T. (1993), 'A critical review and some results of recently developed refined theories of fiber-reinforced laminated composites and sandwiches', *Composite Structures* **23**, 293–312.

[39] Benjeddou, A. (2000), 'Advances in piezoelectric finite element modeling of adaptive structural elements: a survey', *Computers & Structures* **76**, 347–363.

[40] Wu, C-P., Chiu, K-H. and Wang, Y-M. (2008), 'A review on the three-dimensional analytical approaches of multilayered and functionally graded piezoelectric plates and shells', *Computers, Materials and Continua* **8**, 93–132.

[41] Liew, K. M., Zhao, X. and Ferreira, A. J. M. (2011), 'A review of meshless methods for laminated and functionally graded plates and shells', *Composite Structures* **93**, 2031–2041.

[42] Thai, H-T. and Kim, S-E. (2015), 'A review of theories for the modeling and analysis of functionally graded plates and shells', *Composite Structures* **128**, 70–86.

[43] Wu, C-P. and Liu, Y-C. (2016), 'A review of semi-analytical numerical methods for laminated composite and multilayered functionally graded elastic/piezoelectric plates and shells', *Composite Structures* **147**, 1–15.

[44] Sarvestani, H. Y. and Hojjati, M. (2016), 'Three-dimensional stress analysis of orthotropic curved tubes-part 2: laminate solution.', *European Journal of Mechanics-A/Solids* **60**, 339–358.

[45] Bert, C. W. and Malik, M. (1996), 'Free vibration analysis of thin cylindrical shells by the differential quadrature method.', *Journal of Pressure Vessel Technology* **118**, 1–12.

[46] Das, R. R., Singla, A. and Srivastava, S. (2016), 'Thermo-mechanical Interlaminar Stress and Dynamic Stability Analysis of Composite Spherical Shells', *Procedia Engineering* **144**, 1060–1066.

[47] Pochhammer, Lt. (1876), 'Ueber die Fortpflanzungsgeschwindigkeiten kleiner Schwingungen in einem unbegrenzten isotropen Kreiscylinder.', *Journal für die reine und angewandte Mathematik* **81**, 324–336.

[48] Chree, C. (1886), 'Longitudinal vibrations of a circular bar', *Quarterly Journal of Pure and Applied Mathematics* **21**, 287–298.

[49] Barton, M. V.. (1941), 'The circular cylinder with a band of uniform pressure on a finite length of the surface', *Journal of Applied Mechanics* **8**, A97–A104.

[50] Rankin, A. W. and Schenectady, N. Y. (1944), 'Shrink-fit stresses and deformations', *Journal of Applied Mechanics* **11**, A77–A85.

[51] Kasano, H., Matsumoto, H. and Nakahara, I. (1978), 'An infinite solid cylinder subjected to two diametrically opposite concentrated loads', *Bulletin of JSME* **21**, 7–12.

[52] Ren, J. G. (1987), 'Exact solutions for laminated cylindrical shells in cylindrical bending', *Composites Science and Technology* **29**, 169–187.

[53] Kapania, R. K. (1989), 'A review on the analysis of laminated shells', *Journal of Pressure Vessel Technology* **111**, 88–96.

[54] Soldatos, K. P. and Hadjigeorgiou, V. P. (1990), 'Three-dimensional solution of the free vibration problem of homogeneous isotropic cylindrical shells and panels', *Journal of Sound and Vibration* **137**, 369–384.

[55] Noor, A. K. and Burton, W. S. (1990), 'Assessment of computational models for multilayered composite shells', *Applied Mechanics Reviews* **43**, 67–97.

[56] Chandrashekhara, K. and Kumar, D. P. (1995), 'Assessment of shell theories for the static analysis of cross-ply laminated circular cylindrical shells', *Thin-walled Structures* **22**, 291–318.

[57] Jaunky, N. and Knight Jr, N. F. (1999), 'An assessment of shell theories for buckling of circular cylindrical laminated composite panels loaded inaxial compression', *International journal of solids and structures* **36**, 3799–3820.

[58] Liew, K. M. and Lim, C. W. (1995), 'A Ritz vibration analysis of doubly-curved rectangular shallow shells using a refined first-order theory', *Computer Methods in Applied Mechanics and Engineering* **127**, 145–162.

[59] Liew, K. M. and Lim, C. W. (1995), 'Vibratory behavior of doubly curved shallow shells of curvilinear planform', *Journal of engineering mechanics* **121**, 1277–1283.

[60] Mizusawa, T. and Kato, T. (1996), 'Application of the spline prism method to analyse vibration of thick circular cylindrical panels', *International journal of solids and structures* **33**, 967–976.

[61] Lepik, Ülo. (1996), 'Axisymmetric vibrations of elastic-plastic cylindrical shells by Galerkin's method', *International journal of impact engineering* **18**, 489–504.

[62] Ding, H. J. and Chen, W. Q. (1996), 'Natural frequencies of an elastic spherically isotropic hollow sphere submerged in a compressible fluid medium', *Journal of Sound and Vibration* **192**, 173–198.

[63] Wu, C-P. and Lo, J-Y. (2000), 'Three-dimensional elasticity solutions of laminated annular spherical shells', *Journal of engineering mechanics* **126**, 882–885.

[64] Wang, X. and Zhong, Z. (2003), 'Three-dimensional solution of smart laminated anisotropic circular cylindrical shells with imperfect bonding', *International journal of solids and structures* **40**, 5901–5921.

[65] Toupin, R. A. and Gürdal, Z. (1959), 'Piezoelectric relations and the radial deformation of a polarized spherical shell', *The Journal of the Acoustical Society of America* **31**, 315–318.

[66] Paul, H. S. and Venkatesan, M. (1986), 'Axisymmetric vibration of a piezoelectric solid cylinder guided by a thin film', *The Journal of the Acoustical Society of America* **80**, 1091–1096.

[67] Drumheller, D. S. and Kalnins, A. (1970), 'Dynamic shell theory for ferroelectric ceramics', *The Journal of the Acoustical Society of America* **47**, 1343–1353.

[68] Dökmeci, M. C. (1978), 'Theory of vibrations of coated, thermopiezoelectric laminae', *Journal of Mathematical Physics* **19**, 109–126.

[69] Tzou, H. S. and Gadre, M. (1989), 'Theoretical analysis of a multi-layered thin shell coupled with piezoelectric shell actuators for distributed vibration controls', *Journal of Sound and Vibration* **132**, 433–450.

[70] Tzou, H. S. and Zhong, J. P. (1993), 'Electromechanics and vibrations of piezoelectric shell distributed systems', *Transactions-American Society of Mechanical Engineers Journal of Dynamic Systems Measurement and Control* **115**, 506–506.

[71] Saravanos, D. A. (1997), 'Mixed laminate theory and finite element for smart piezoelectric composite shell structures', *AIAA journal* **35**, 1327–1333.

[72] Mitchell, J. A. and Reddy, J. N. (1995), 'A study of embedded piezoelectric layers in composite cylinders', *Journal of Applied Mechanics* **62**, 166-173.

[73] Heyliger, P. (1997), 'A note on the static behavior of simply supported laminated piezoelectric cylinders', *International Journal of Solids and Structures* **34**, 3781–3794.

[74] Nosier, A. and Ruhi, M. (2006), 'Three dimensional analysis of laminated cylindrical panels with piezoelectric layers', *International Journal of Engineering Transactions B Applications* **19**, 61.

[75] Santos, H., Soares C. M. M., Soares C. A. M. and Reddy, J. N. (2006), 'A finite element model for the analysis of 3D axisymmetric laminated shells with piezoelectric sensors and actuators', *Composite structures* **75**, 170–178.

[76] Wu, C-P. and Tsai, T-C. (2012), 'Exact solutions of functionally graded piezoelectric material sandwich cylinders by a modified Pagano method', *Applied Mathematical Modelling* **36**, 1910–1930.

[77] Xu, K. and Noor, A. K. (1996), 'Three-dimensional analytical solutions for coupled thermoelectroelastic response of multilayered cylindrical shells', *AIAA journal* **34**, 802–812.

[78] Chen, W. Q., Ding, H. J. and Xu, R. Q. (2001), 'Three-dimensional free vibration analysis of a fluid-filled piezoceramic hollow sphere', *Computers & Structures* **79**, 653–663.

[79] Chen, W. Q., Wang, L. Z. and Lu, Y. (2002), 'Free vibrations of functionally graded piezoceramic hollow spheres with radial polarization', *Journal of Sound and Vibration* **251**, 103–114.

[80] Chen, W. Q., Bian, Z. G., Lv, C. F. and Ding, H. J. (2004), '3D free vibration analysis of a functionally graded piezoelectric hollow cylinder filled with compressible fluid', *International Journal of Solids and Structures* **41**, 947–964.

[81] Larbi, W. and Deü, J-F. (2011), 'A 3D state-space solution for free-vibration analysis of a radially polarized laminated piezoelectric cylinder filled with fluid', *Journal of Sound and Vibration* **330**, 162–181.

[82] Chen, C-Q., Shen, Y-P., and Wang, X-M. (1996), 'Exact solution of orthotropic cylindrical shell with piezoelectric layers under cylindrical bending', *International Journal of Solids and Structures* **33**, 4481–4494.

[83] Dumir, P. C., Dube, G. P. and Kapuria, S. (1997), 'Exact piezoelastic solution of simply-supported orthotropic circular cylindrical panel in cylindrical bending', *International Journal of Solids and Structures* **34**, 685–702.

[84] Kapuria, S., Sengupta, S. and Dumir, G. P. (1997), 'Three-dimensional solution for a hybrid cylindrical shell under axisymmetric thermoelectric load', *Archive of Applied Mechanics* **67**, 320–330.

[85] Kapuria, S., Dumir, P. C. and Sengupta, S. (1997), 'Nonaxisymmetric exact piezothermoelastic solution for laminated cylindrical shell', *AIAA journal* **35**, 1792–1795.

[86] Chen, C-Q. and Shen, Y-P. (1998), 'Three-dimensional analysis for the free vibration of finite-length orthotropic piezoelectric circular cylindrical shells', *Transactions-American Society of Mechanical Engineers Journal of Vibration and Acoustics* **120**, 194–198.

[87] Hussein, M. and Heyliger, P. (1998), 'Three-dimensional vibrations of layered piezoelectric cylinders', *Journal of engineering mechanics* **124**, 1294–1298.

[88] Chen, W. Q., Ding, H. J. and Liang, J. (2001), 'The exact elasto-electric field of a rotating piezoceramic spherical shell with a functionally graded property', *International journal of solids and structures* **38**, 7015–7027.

[89] Wu, X-H., Shen, Y-P. and Chen, C. (2003), 'An exact solution for functionally graded piezothermoelastic cylindrical shell as sensors or actuators', *Materials Letters* **57**, 3532–3542.

[90] Kapuria, S., Kumari, P. and Nath, J. K. (2009), 'Analytical piezoelasticity solution for vibration of piezoelectric laminated angle-ply circular cylindrical panels', *Journal of Sound and Vibration* **325**, 832–849.

[91] Kapuria, S. and Kumari, P. (2010), 'Three-dimensional piezoelasticity solution for dynamics of cross-ply cylindrical shells integrated with piezoelectric fiber reinforced composite actuators and sensors', *Composite Structures* **92**, 2431–2444.

[92] Cheng, Z-Q. and Reddy, J. N. (2002), 'Asymptotic theory for laminated piezoelectric circular cylindrical shells', *AIAA journal* **40**, 553–558.

[93] Wu, C-P., Lo, J-Y. and Chao, J-K. (2005), 'A three-dimensional asymptotic theory of laminated piezoelectric shells', *Computers, Materials and Continua* **2**, 119–137.

[94] Wu, C-P., Syu, Y-S. and Lo, J-Y. (2007), 'Three-dimensional solutions of multilayered piezoelectric hollow cylinders by an asymptotic approach', *International journal of mechanical sciences* **49**, 669–689.

[95] Wu, C-P. and Syu, Y-S. (2007), 'Exact solutions of functionally graded piezoelectric shells under cylindrical bending', *International Journal of Solids and Structures* **44**, 6450–6472.

[96] Wu, C-P. and Lo, J-Y. (2006), 'An asymptotic theory for dynamic response of laminated piezoelectric shells', *Acta mechanica* **183**, 177–208.

[97] Wu, C-P. and Tsai, Y-H. (2009), 'Cylindrical bending vibration of functionally graded piezoelectric shells using the method of perturbation', *Journal of Engineering Mathematics* **63**, 95–119.

[98] Wu, C-P. and Kuo, C-H. (2013), 'A unified formulation of PVD-based finite cylindrical layer methods for functionally graded material sandwich cylinders', *Applied Mathematical Modelling* **37**, 916–938.

[99] Wu, C-P. and Chang, Y-T. (2012), 'A unified formulation of RMVT-based finite cylindrical layer methods for sandwich circular hollow cylinders with an embedded FGM layer', *Composites Part B: Engineering* **43**, 3318–3333.

[100] Wu, C-P., Chen, Y-C. and Peng, S-T. (2013), 'Buckling analysis of functionally graded material circular hollow cylinders under combined axial compression and external pressure', *Thin-Walled Structures* **69**, 54–66.

[101] Wu, C-P., Fan, T-Y. and Li, H-Y. (2014), 'Reissner's mixed variational theorem-based finite cylindrical layer methods for the three-dimensional free vibration analysis of sandwich circular hollow cylinders with an embedded functionally graded material layer', *Journal of Vibration and Control* **20**, 1199–1223.

[102] Wu, C-P., Peng, S-T. and Chen, Y-C. (2014), 'RMVT-and PVD-based finite cylindrical layer methods for the three-dimensional buckling analysis of multilayered FGM cylinders under axial compression', *Applied Mathematical Modelling* **38**, 233–252.

[103] Wu, C-P. and Yang, S-W. (2011), 'RMVT-based meshless collocation and element-free Galerkin methods for the approximate 3D analysis of multilayered composite and FGM circular hollow cylinders', *Composites Part B: Engineering* **42**, 1683–1700.

[104] Wu, C-P., Wang, J-S. and Yang, Y-M. (2009), 'A DRK interpolation-based collocation method for the analysis of functionally graded piezoelectric hollow cylinders under electro-mechanical loads', *Computer Modeling in Engineering and Sciences* **52**, 1–37.

[105] Wu, C-P. and Yang, S-W. (2011), 'A semi-analytical element-free Galerkin method for the 3D free vibration analysis of multilayered FGM circular hollow cylinders', *Journal of Intelligent Material Systems and Structures* **22**, 1993–2007.

[106] Wu, C-P., Chiu, K-H. and Jiang, R-Y. (2012), 'A meshless collocation method for the coupled analysis of functionally graded piezo-thermo-elastic shells and plates under thermal loads', *Journal of Intelligent Material Systems and Structures* **56**, 29–48.

[107] Chen, W. Q., Lv, C. F. and Bian, Z. G. (2003), 'Elasticity solution for free vibration of laminated beams', *Composite Structures* **62**, 75–82.

[108] Akgün, Gö. kçe. and Kurtara, H. (2018), 'Geometrically nonlinear transient analysis of laminated composite super-elliptic shell structures with generalized differential quadrature method', *International Journal of Non-Linear Mechanics* **105**, 221–241.

[109] Alibeigloo, A. and Nouri, V. (2010), 'Static analysis of functionally graded cylindrical shell with piezoelectric layers using differential quadrature method', *Composite Structures* **92**, 1775–1785.

[110] Tong, B., Li, Y., Zhu, X. and Zhang, Y. (2019), 'Three-dimensional vibration analysis of arbitrary angle-ply laminated cylindrical shells using differential quadrature method', *Applied Acoustics* **146**, 390–397.

[111] Monge, J. C., Mantari, J. L. and Arciniega, R. A. (2020), 'Computational semi-analytical method for the 3D elasticity bending solution of laminated composite and sandwich doubly-curved shells', *Engineering Structures* **221**, 110938.

[112] Monge, J. C. and Mantari, J. L. (2020), '3D elasticity numerical solution for the static behavior of FGM shells', *Engineering Structures* **208**, 110159.

[113] Monge, J. C., and Mantari, J. L. (2021), 'A quasi-exact solution for the analysis of smart multilayered simply supported shallow shell panels', *Composite Structures* **265**, 113710.

[114] Liang, X., Zha, X., Jiang, X., Wang, L., Leng, J. and Cao, Z. (2018), 'Semi-analytical solution for dynamic behavior of a fluid-conveying pipe with different boundary conditions', *Ocean Engineering* **163**, 183–190.

[115] Kulikov, G. M. and Plotnikova, S. V. (2013), 'A sampling surfaces method and its application to three-dimensional exact solutions for piezoelectric laminated shells', *International Journal of Solids and Structures* **50**, 1930–1943.

[116] Kulikov, G. M. and Plotnikova, S. V. (2014), '3D exact thermoelastic analysis of laminated composite shells via sampling surfaces method', *Composite Structures* **115**, 120–130.

[117] Kulikov, G. M. and Plotnikova, S. V. (2014), 'Analytical method for solving three-dimensional thermoelasticity problems for composite shells', *Journal of Machinery Manufacture and Reliability* **43**, 132–139.

[118] Kulikov, G. M. and Plotnikova, S. V. (2013), 'Advanced formulation for laminated composite shells: 3D stress analysis and rigid-body motions', *Composite Structures* **95**, 236–246.

[119] Kulikov, G. M. and Plotnikova, S. V. (2017), 'Strong sampling surfaces formulation for layered shells', *International Journal of Solids and Structures* **121**, 75–85.

[120] Kulikov, G. M. and Kulikov, M. G. (2021), 'High-precision stress calculations for composite cylindrical shells with general boundary conditions using strong SaS formulation and extended DQ method', *Mechanics of Advanced Materials and Structures* , 1–21.

[121] Wu, C-P. and Li, H-Y. (2013), 'An RMVT-based finite rectangular prism method for the 3D analysis of sandwich FGM plates with various boundary conditions', *Computers, Materials, & Continua* **34**, 27–62.

[122] Alibeigloo, A. and Shakeri, M. (2007), 'Elasticity solution for the free vibration analysis of laminated cylindrical panels using the differential quadrature method', *Composite structures* **81**, 105–113.

[123] Alibeigloo, A. and Shakeri, M. (2009), 'Elasticity solution for static analysis of laminated cylindrical panel using differential quadrature method', *Engineering Structures* **31**, 260–267.

[124] Alibeigloo, A. (2009), 'Static and vibration analysis of axi-symmetric angle-ply laminated cylindrical shell using state space differential quadrature method', *International Journal of Pressure Vessels and Piping* **86**, 738–747.

[125] Alibeigloo, A. and Kani, A. M. (2010), '3D free vibration analysis of laminated cylindrical shell integrated piezoelectric layers using the differential quadrature method', *Applied Mathematical Modelling* **34**, 4123–4137.

[126] Jodaei, A. and Yas, M. H. (2012), 'Three-dimensional free vibration analysis of functionally graded annular plates on elastic foundations via state-space based differential quadrature method', *Journal of Pressure Vessel Technology* **134**, 031208.

[127] Jodaei, A., Jalal, M. and Yas, M. H. (2012), 'Free vibration analysis of functionally graded annular plates by state-space based differential quadrature method and comparative modeling by ANN', *Composites Part B: Engineering* **43**, 340–353.

[128] Alibeigloo, A. (2012), 'Three-dimensional semi-analytical thermo-elasticity solution for a functionally graded solid and an annular circular plate', *Journal of Thermal Stresses* **35**, 653–676.

[129] Liang, X., Kou, H-L., Liu, G-H., Wang, L-Z., Wang, Z-Y. and Wu, Z-J. (2015), 'A semi-analytical state-space approach for 3D transient analysis of functionally graded material cylindrical shells', *Journal of Zhejiang University SCIENCE A* **16**, 525–540.

[130] Alibeigloo, A., Kani, A. M. and Pashaei, M. H. (2012), 'Elasticity solution for the free vibration analysis of functionally graded cylindrical shell bonded to thin piezoelectric layers', *International Journal of Pressure Vessels and Piping* **89**, 98–111.

[131] Wu, C-P. and Jiang, R-Y. (2012), 'A state space differential reproducing kernel method for the 3D analysis of FGM sandwich circular hollow cylinders with combinations of simply-supported and clamped edges', *Composite Structures* **94**, 3401–3420.

[132] Wu, C-P. and Jiang, R-Y. (2014), 'A state space differential reproducing kernel method for the buckling analysis of carbon nanotube-reinforced composite circular hollow cylinders', *Computer Modeling in Engineering and Sciences* **97**, 239–279.

[133] Sheng, H. Y. and Ye, J. Q. (2003), 'A three-dimensional state space finite element solution for laminated composite cylindrical shells', *Computer methods in applied mechanics and engineering* **192**, 2441–2459.

[134] Wu, C-P. and Chen, C-W. (2001), 'Elastic buckling of multilayered anisotropic conical shells', *Journal of Aerospace Engineering* **14**, 29–36.

[135] Wu, C-P. and Chiu, S-J. (2001), 'Thermoelastic buckling of laminated composite conical shells', *Journal of Thermal Stresses* **24**, 881–901.

[136] Wu, C-P. and Tsai, Y-H. (2004), 'Asymptotic DQ solutions of functionally graded annular spherical shells', *European Journal of Mechanics-A/Solids* **23**, 283–299.

[137] Wu, C-P. and Jiang, R-Y. (2015), 'An asymptotic meshless method for sandwich functionally graded circular hollow cylinders with various boundary conditions', *Journal of Sandwich Structures & Materials* **17**, 469–510.

[138] Wu, C-P. and Jiang, R-Y. (2015), 'Three-Dimensional Free Vibration Analysis of Sandwich FGM Cylinders with Combinations of Simply-Supported and Clamped Edges and Using the Multiple Time Scale and Meshless Methods', *Computers Materials & Continua* **46**, 17–56.

[139] Wu, C-P., Wang, Y-M. and Hung, Y-C. (2001), 'Asymptotic finite strip analysis of doubly curved laminated shells', *Computational mechanics* **27**, 107–118.

[140] Ye, W., Liu, J., Zang, Q. and Lin, G. (2020), 'Magneto-electro-elastic semi-analytical models for free vibration and transient dynamic responses of composite cylindrical shell structures', *Mechanics of Materials* **148**, 103495.

[141] Liu, J., Ye, W., Zang, Q. and Lin, G. (2020), Semianalytical piezoelastic solution of orthotropic circular cylindrical panel using SBFEM: Bending and free vibrations', *Mechanics of Advanced Materials and Structures* **148**, 1–18.

[142] Wang, X. and Zhong, Z. (2003), 'Three-dimensional solution of smart laminated anisotropic circular cylindrical shells with imperfect bonding', *International Journal of Solids and Structures* **40**, 5901–5921.

[143] Librescu, L. and Schmidt, R. (2001), 'A general linear theory of laminated composite shells featuring interlaminar bonding imperfections', *International Journal of Solids and Structures* **38**, 3355–3375.

[144] Kweon, J. H., Jung, J. W., Kim, T. H., Choi, J. H. and Kim, D. H. (2006), 'Failure of carbon composite-to-aluminum joints with combined mechanical fastening and adhesive bonding', *Composite Structures* **75**, 192–198.

[145] Abouhamze, M., Aghdam, M. and Alijani, F. (2007), 'Bending analysis of symmetrically laminated cylindrical panels using the extended kantorovich method', *Mechanics of Advanced Materials and Structures* **14**, 523–530.

[146] Wang, X., Yuan, Z. and Deng, J. (2019), 'A Review on the Discrete Singular Convolution Algorithm and Its Applications in Structural Mechanics and Engineering', *Archives of Computational Methods in Engineering* **2**, 1–28.

[147] Ye, T., Jin, G., Su, Z. and Jia, X. (2014), 'A unified Chebyshev–Ritz formulation for vibration analysis of composite laminated deep open shells with arbitrary boundary conditions', *Archive of Applied Mechanics* **84**, 441–471.

[148] Lin, H., Cao, D. and Shao, C. (2018), 'An admissible function for vibration and flutter studies of FG cylindrical shells with arbitrary edge conditions using characteristic orthogonal polynomials', *Composite Structures* **185**, 748–763.

[149] Civalek, O. (2005), 'Geometrically nonlinear dynamic analysis of doubly curved isotropic shells resting on elastic foundation by a combination of harmonic differential quadrature-finite difference methods', *International Journal of Pressure Vessels and Piping* **82**, 470–479.

[150] Civalek, O. (2007), 'Linear vibration analysis of isotropic conical shells by discrete singular convolution (DSC)', *Structural Engineering and Mechanics* **25**, 127–130.

[151] Civalek, O. (2008), 'Vibration analysis of conical panels using the method of discrete singular convolution', *Communications in Numerical Methods in Engineering* **24**, 169–181.

[152] Civalek, O. and Acar, M. H. (2007), 'Discrete singular convolution method for the analysis of Mindlin plates on elastic foundations', *International Journal of Pressure Vessels and Piping* **84**, 527–535.

[153] Akgoz, B. and Civalek, O. (2011), 'Nonlinear vibration analysis of laminated plates resting on nonlinear two-parameters elastic foundations', *Steel & Composite Structures* **11**, 403–421.

[154] Lü, C. F., Lim, C. W. and Xu, F. (2007), 'Stress analysis of anisotropic thick laminates in cylindrical bending using a semi-analytical approach', *Composite Structures* **8**, 1740–1745.

[155] Alibeigloo, A., and Shakeri, M. (2009), 'Elasticity solution for static analysis of laminated cylindrical panel using differential quadrature method', *Engineering Structures* **31**, 260–267.

[156] Alibeigloo, A. (2009), 'Static and vibration analysis of axi-symmetric angle-ply laminated cylindrical shell using state space differential quadrature method', *International Journal of Pressure Vessels and Piping* **86**, 738–747.

[157] Asadi, E. and Qatu, M. S. (2012), 'Static analysis of thick laminated shells with different boundary conditions using GDQ', *Thin-Walled Structures* **51**, 76–81.

[158] Maleki, S., Tahani, M. and Andakhshideh, A. (2012), 'Static and transient analysis of laminated cylindrical shell panels with various boundary conditions and general lay-ups', *Zeitschrift für Angewandte Mathematik und Mechanik* **92**, 124–140.

[159] Liang, X., Deng, Y., Cao, Z., Jiang, X., Wang, T., Ruan, Y. and Zha, X. (2012), 'Three-dimensional dynamics of functionally graded piezoelectric cylindrical panels by a semi-analytical approach', *Composite Structures* **226**, 111176.

[160] Lene, F. and Leguillon, D. (1982), 'Homogenized constitutive law for a partially cohesive composite material', *International Journal of Solids and Structures* **18**, 443–458.

[161] Benveniste, Y. (1984), 'On the effect of debonding on the overall behavior of composite materials', *Mechanics of Materials* **3**, 349–358.

[162] Yan, W., Ying, J. and Chen, W. (2007), 'The behavior of angle-ply laminated cylindrical shells with viscoelastic interfaces in cylindrical bending', *Composite Structures* **78**, 551–559.

[163] Saeb, S., Firooz, S., Steinmann, P. and Javili, A. (2021), 'Generalized interfaces via weighted averages for application to graded interphases at large deformations.', *Journal of the Mechanics and Physics of Solids* **149**, 104234.

[164] Kapuria, S. and Agrahari, J. K. (2016), 'Two dimensional shear lag solution for stress transfer between rectangular piezoelectric wafer transducer and orthotropic host plate.', *European Journal of Mechanics-A/Solids* **55**, 181-191.

[165] Chen, W., Wang, Y., Cai, J. and Ye, G. (2004), 'Three-dimensional analysis of cross-ply laminated cylindrical panels with weak interfaces', *International Journal of Solids and Structures* **41**, 2429–2446.

[166] Cai, J., Chen, W. and Ye, G. (2004), 'Effect of interlaminar bonding imperfections on the behavior of angle-ply laminated cylindrical panels', *Composites Science and Technology* **64**, 1753–1762.

[167] Chen, W. and Lee, K. Y. (2005), 'Benchmark solution of angle-ply piezoelectric-laminated cylindrical panels in cylindrical bending with weak interfaces', *Archive of Applied Mechanics* **74**, 466–476.

[168] Chen, W., Jung, J. P. and Lee, K. Y. (2006), 'Static and dynamic behavior of simply-supported cross-ply laminated piezoelectric cylindrical panels with imperfect bonding', *Archive of Applied Mechanics* **74**, 265–276.

[169] Chen, W., Jung, J. P., Kim, G. W. and Lee, K. Y. (2005), 'Cross-ply laminated cylindrical panels with viscous interfaces subjected to static loading', *European Journal of Mechanics - A/Solids* **24**, 728–739.

[170] Yan, W., Wang, J. and Chen, W. (2014), 'Cylindrical bending responses of angle-ply piezoelectric laminates with viscoelastic interfaces', *Applied Mathematical Modelling* **38**, 6018–6030.

[171] Alibeigloo, A. (2015), 'Three-dimensional static and free vibration analysis of laminated cylindrical panel with viscoelastic interfaces', *Journal of Composite Materials* **49**, 2415–2430.

[172] Parand, A. A., Alibeigloo, A. and Lee, K. Y. (2017), 'Static and vibration analysis of sandwich cylindrical shell with functionally graded core and viscoelastic interface using DQM', *Composites Part B: Engineering* **126**, 1–16.

[173] Kantorovich, L. V. and Krylov, V. I. (1958), 'Approximate Methods of Higher Analysis', *Interscience Publishers*, New York.

[174] Kerr, A. D. (1968), 'An extension of the Kantorovich method', *Quarterly of Applied Mathematics* **26**, 219–229.

[175] Kerr, A. D. and Alexander, H. (1968), 'An application of the extended Kantorovich method to the stress analysis of a clamped rectangular plate', *Acta Mechanica* **6**, 180–196.

[176] Dalaei, M. and Kerr, A. D. (1996), 'Natural vibration analysis of clamped rectangular orthotropic plates', *Journal of Sound and Vibration* **189**, 399–406.

[177] Naumenko, K., Altenbach, J., Altenbach, H. and Naumenko, V. K. (2001), 'Closed and approximate analytical solutions for rectangular Mindlin plates', *Acta Mechanica* **147**, 153–172.

[178] Ungbhakorn, V. and Wattanasakulpong, N. (2006), 'Bending analysis of symmetrically laminated rectangular plates with arbitrary edge supports by the extended Kantorovich method', *Science & Technology Asia* , 33–44.

[179] Shufrin, I., Rabinovitch, O. and Eisenberger, M. (2008), 'A semi-analytical approach for the non-linear large deflection analysis of laminated rectangular plates under general out-of-plane loading', *International Journal of Non-Linear Mechanics* **43**, 328–340.

[180] Aghdam, M. M. and Mohammadi, M. (2009), 'Bending analysis of thick orthotropic sector plates with various loading and boundary conditions', *Composite structures* **88**, 212–218.

[181] Nik, A. MN. and Tahani, M. (2009), 'Analytical solutions for bending analysis of rectangular laminated plates with arbitrary lamination and boundary conditions', *Journal of mechanical science and technology* **23**, 2253–2267.

[182] Alijani, F. and Aghdam, M. M. (2009), 'A semi-analytical solution for stress analysis of moderately thick laminated cylindrical panels with various boundary conditions', *Composite Structures* **89**, 543–550.

[183] Fereidoon, A., Mohyeddin, A., Sheikhi, M. and Rahmani, H. (2012), 'Bending analysis of functionally graded annular sector plates by extended Kantorovich method', *Composites Part B: Engineering* **43**, 2172–2179.

[184] Singhatanadgid, P. and Singhanart, T. (2019), 'The Kantorovich method applied to bending, buckling, vibration, and 3D stress analyses of plates: A literature review', *Mechanics of advanced materials and structures* **26**, 170–188.

[185] Bigdeli, K. and Aghdam, M. (2011), 'A semianalytical solution for the bending of clamped laminated doubly curved or spherical panels', *Journal of Mechanics of Materials and Structures* **5**, 855–873.

[186] Ranji, A. R. and Hoseynabadi, H. R. (2012), 'A semi-analytical technique for bending analysis of cylindrical panels with general loading and boundary conditions', *Journal of Mechanical Science and Technology* **26**, 1711–1718.

[187] Lee, L. HN. (1974), 'Dynamic behavior of inelastic cylindrical shells at finite deformation', *International Journal of Non-Linear Mechanics* **9**, 193–207.

[188] Grigorenko, Y. M. and Tumashova, O. V. (1989), 'Stress-strain state of flexible cylindrical panels with variable geometric parameters', *International Applied Mechanics* **25**, 454–462.

[189] Eslami, M. R., Shakeri, M. and Sedaghati, R. (1994), 'Coupled thermoelasticity of an axially symmetric cylindrical shell', *Journal of thermal stresses* **17**, 115–135.

[190] Shariyat, M. and Eslami, M. R. (2000), 'On thermal dynamic buckling analysis of imperfect laminated cylindrical shells', *ZAMM-Journal of Applied Mathematics and Mechanics/Zeitschrift für Angewandte Mathematik und Mechanik* **80**, 171–182.

[191] Wang, Y-G. and Song, H. F. (2010), 'On the nonlinear vibration of heated bimetallic shallow shells of revolution', *International Journal of Mechanical Sciences* **52**, 464–470.

[192] Ruocco, E. and Fraldi, M. (2012), 'Critical behavior of flat and stiffened shell structures through different kinematical models: a comparative investigation', *Thin-Walled Structures* **60**, 205–215.

[193] Moeenfard, H. and Maleki, S. (2017), 'Characterization of the static behavior of electrically actuated micro-plates using extended Kantorovich method', *Proceedings of the Institution of Mechanical Engineers, Part C: Journal of Mechanical Engineering Science* **231**, 2327–2339.

[194] Andakhshideh, A., Rafiee, R. and Maleki, S. (2019), '3D stress analysis of generally laminated piezoelectric plates with electromechanical coupling effects', *Applied Mathematical Modelling* **74**, 258–279.

[195] Aghdam, M. M., Bigdeli, K. and Shahmansouri, N. (2010), 'A semi-analytical solution for bending of moderately thick doubly curved functionally graded panels', *Mechanics of Advanced Materials and Structures* **17**, 320–327.

[196] Obodan, N. I. and Gromov, V. A. (2013), 'Nonlinear behavior and buckling of cylindrical shells subjected to localized external pressure', *Journal of Engineering Mathematics* **78**, 239–248.

[197] Edalat, P., Khedmati, M. R. and Soares, C. G. (2015), 'Free vibration of stiffened open shells with variable radii of curvature using extended Kantorovich–Ritz method', *Ships and Offshore Structures* **10**, 94–106.

[198] Tahani, M., Andakhshideh, A. and Maleki, S. (2016), 'Interlaminar stresses in thick cylindrical shell with arbitrary laminations and boundary conditions under transverse loads', *Composites Part B: Engineering* **98**, 151–165.

[199] Kapuria, S. and Kumari, P. (2011), 'Extended Kantorovich method for three-dimensional elasticity solution of laminated composite structures in cylindrical bending', *Journal of Applied Mechanics* **78**, 061004.

[200] Kapuria, S. and Kumari, P. (2012), 'Multiterm extended Kantorovich method for three-dimensional elasticity solution of laminated plates', *Journal of Applied Mechanics, Transactions ASME* **79**, 061018.

[201] Kumari, P., Kapuria, S. and Rajapakse, RKND. (2014), 'Three-dimensional extended Kantorovich solution for Levy-type rectangular laminated plates with edge effects', *Composite Structures* **107**, 167–176.

[202] Kapuria, S. and Kumari, P. (2013), 'Extended Kantorovich method for coupled piezoelasticity solution of piezolaminated plates showing edge effects', *Proceedings of the Royal Society A: Mathematical, Physical and Engineering Sciences* **469**, 20120565.

[203] Kumari, P., Behera, S. and Kapuria, S. (2016), 'Coupled three-dimensional piezoelasticity solution for edge effects in Levy-type rectangular piezolaminated plates using mixed field extended Kantorovich method', *Composite Structures* **140**, 491–505.

[204] Kumari, P. and Behera, S. (2017), 'Three-dimensional free vibration analysis of levy-type laminated plates using multi-term extended Kantorovich method', *Composites Part B: Engineering* **116**, 224–238.

[205] Behera, S. and Kumari, P. (2019), 'Analytical piezoelasticity solution for natural frequencies of levy-type piezolaminated plates', *International Journal of Applied Mechanics* **11**, 1950023.

[206] Kumari, P., Singh, A., Rajapakse, RKND. and Kapuria, S. (2017), 'Three-dimensional static analysis of Levy-type functionally graded plate with in-plane stiffness variation', *Composite Structures* **168**, 780–791.

[207] Kar, S. and Kumari, P. (2020), 'A 3D solution for angle-ply cylindrical shell panel supported arbitrarily on its boundaries using extended Kantorovich method', *International Journal of Advances in Engineering Sciences and Applied Mathematics* **12**, 51–64.

[208] Kar, S. and Kumari, P. (2020), 'Three-dimensional analytical solution of arbitrarily supported cylindrical panels with weak interfaces using the extended Kantorovich method', *Composite structures* **236**, 111802.

[209] Clausen, W. E., Hopper, A. T., Hulbert, L. E. and Leissa, A. W. (1969), 'A comparison of approximate methods for the solution of plate bending problems.', *AIAA Journal* **7**, 920–928.

[210] Laura, P. A., Grossi, R. O. and Soni, S. R. (1979), 'Free vibrations of a rectangular plate of variable thickness elastically restrained against rotation along three edges and free on the fourth edge', *Journal of Sound and Vibration* **62**, 493-503.

[211] Chang, S. H. and Tung, Y. C. (1999), 'Electro-elastic characteristics of asymmetric rectangular piezoelectric laminae', *IEEE Transactions on Ultrasonics, Ferroelectrics, and Frequency Control* **46**, 950-960.

[212] Wang, G., Wereley, N. M. and Chang, D. C. (2003), 'Analysis of bending vibration of rectangular plates using 2D plate modes', *Collection of Technical Papers - AIAA/ASME/ASCE/AHS/ASC Structures, Structural Dynamics and Materials Conference* **5**, 3406-3416.

[213] Shufrin, I. and Eisenberger, M. (2005), 'Stability and vibration of shear deformable plates - First order and higher order analyses', *International Journal of Solids and Structures* **42**, 1225-1251.

[214] Shufrin, I. and Eisenberger, M. (2006), 'In-plane vibrations of rectangular plates with rectangular cutouts', *Proceedings of the EPMESC X*

[215] Shufrin, I. and Eisenberger, M. (2006), 'Vibration of shear deformable plates with variable thickness - First-order and higher-order analyses', *Journal of Sound and Vibration* **290**, 465-489.

[216] Ranji, A. R. and Hoseynabadi, H. R. (2010), 'A semi-analytical solution for forced vibrations response of rectangular orthotropic plates with various boundary conditions', *Journal of Mechanical Science and Technology* **24**, 357-364.

[217] Phongsrisuk, K., Ingsuwan, P., Rangsri, W., Klongpanich, W., Juangjandee, P., Sucharitakul, T., Kamonpet, P. and Yimpong, R. (2010), 'Free vibration analysis of symmetrically laminated composite rectangular plates using extended Kantorovich method', *Maejo International Journal of Science and Technology* **4**, 512–532.

[218] Naserian-Nik, A. M. and Tahani, M. (2010), 'Free vibration analysis of symmetrically laminated composite rectangular plates using extended Kantorovich method', *Structural Engineering and Mechanics* **35**, 217-240.

[219] Fallah, A., Kargarnovin, M. H. and Aghdam, M. M. (2011), 'Free vibration analysis of symmetrically laminated fully clamped skew plates using extended Kantorovich method', *Key Engineering Materials* **471-472**, 739-744.

[220] Wang, J., Liu, B., Du, J. and Ma, T. (2012), 'Approximate frequencies of rectangular quartz plates vibrating at thickness-shear modes with free edges', *IEEE International Frequency Control Symposium, IFCS 2012, Proceedings* **6243624**, 717-720.

[221] Fallah, A., Aghdam, M. M. and Kargarnovin, M. H. (2013), 'Free vibration analysis of moderately thick functionally graded plates on elastic foundation using the extended Kantorovich method', *Archive of Applied Mechanics* **83**, 177-191.

[222] Liu, B., Xing, Y. F., Eisenberger, M. and Ferreira, A. J. M. (2014), 'Thickness-shear vibration analysis of rectangular quartz plates by a numerical extended Kantorovich method', *Composite Structures* **107**, 429-435.

[223] Shufrin, I. and Eisenberger, M. (2016), 'Semi-analytical modeling of cutouts in rectangular plates with variable thickness–Free vibration analysis', *Applied Mathematical Modelling* **40**, 6983–7000.

[224] Fariborz, S. J. and Pourbohloul, A. (1989), 'Application of the extended Kantorovich method to the bending of variable thickness plates', *Computers & structures* **31**, 957–965.

[225] Aghdam, M. M. and Falahatgar, S. R. (2003), 'Bending analysis of thick laminated plates using extended Kantorovich method', *Composite structures* **62**, 279–283.

[226] Kargarnovin, M. H. and Joodaky, A. (2010), 'Bending analysis of thin skew plates using extended Kantorovich method', *10th Biennial Conference on Engineering Systems Design and Analysis, ESDA2010* **2**, 39-44.

[227] Aghdam, M. M., Shahmansouri, N. and Bigdeli, K. (2011), 'Bending analysis of moderately thick functionally graded conical panels', *Composite Structures* **93**, 1376-1384.

[228] Aghdam, M. M., Shahmansouri, N. and Bigdeli, K. (2012), 'Extended Kantorovich method for static analysis of moderately thick functionally graded sector plates', *Mathematics and Computers in Simulation* **86**, 118-130.

[229] Mousavi, S. M. and Tahani, M. (2012), 'Analytical solution for bending of moderately thick radially functionally graded sector plates with general boundary conditions using multi-term extended Kantorovich method', *Composites Part B: Engineering* **43**, 1405-1416.

[230] Fereidoon, A., Mohyeddin, A., Sheikhi, M. and Rahmani, H. (2012), 'Bending analysis of functionally graded annular sector plates by extended Kantorovich method', *Composites Part B: Engineering* **43**, 2172-2179.

[231] Tahani, M. and Mousavi, S. M. (2013), 'Analytical solution for bending problem of moderately thick composite annular sector plates with general boundary conditions and loadings using multi-term extended Kantorovich method', *Archive of Applied Mechanics* **83**, 969-985.

[232] Joodaky, A., Joodaky, I., Hedayati, M., Masoomi, R. and Farahani, E. B. (2013), 'Deflection and stress analysis of thin FGM skew plates on Winkler foundation with various boundary conditions using extended Kantorovich method', *Composites Part B: Engineering* **51**, 191-196.

[233] Mousavi, S. M. and Tahani, M. (2015), 'Bending of Moderately Thick Annular Sector Plates with Variable Thickness and General Boundary Conditions Using Extended Knatorovich Method', *Journal of Engineering Mechanics* **141**, 04015021.

[234] Huang, B. and Kim, H. S. (2015), 'Interlaminar stress analysis of piezo-bonded composite laminates using the extended Kantorovich method', *International Journal of Mechanical Sciences* **90**, 16–24.

[235] Huang, B., Wang, J., Du, J., Guo, Y., Ma, T. and Yi, L. (2016), 'Extended Kantorovich method for local stresses in composite laminates upon polynomial stress functions', *Acta Mechanica Sinica* **32**, 854–865.

[236] Hassan, A. H. A. and Kurgan, N. (2020), 'Bending analysis of thin fgm skew plate resting on Winkler elastic foundation using multi-term extended Kantorovich method', *Engineering Science and Technology* **23**, 788–800.

[237] Rabinovitch, O. and Vinson, J. R. (2003), 'Smart fins: Analytical modeling and basic design concepts', *Mechanics of Advanced Materials and Structures* **10**, 249–269.

[238] Movassagh, A. A. and Mahmoodi, M. J. (2013), 'A micro-scale modeling of Kirchhoff plate based on modified strain-gradient elasticity theory', *European Journal of Mechanics-A/Solids* **40**, 50–59.

[239] Moeenfard, H., Ahmadian, M. T. and Farshidianfar, A. (2013), 'Modeling squeezed film air damping in torsional micromirrors using extended Kantorovich method', *Meccanica* **48**, 791-805.

[240] Park, I. and Lee, U. (2015), 'Spectral element modeling and analysis of the transverse vibration of a laminated composite plate', *Composite Structures* **134**, 905–917.

[241] Wang, M., Li, Z. M. and Qiao, P. (2016), 'Semi-analytical solutions to buckling and free vibration analysis of carbon nanotube-reinforced composite thin plates', *Composite Structures* **144**, 33–43.

[242] Mamandi, A. and Ghasemipour Masooleh, S. (2020), 'Bending Analysis of a Thin Annular Sector Plate Resting on a Nonlinear Winkler Foundation under Uniform and Nonuniform Loadings using Extended Kantorovich Method', *Journal of Mechanical Engineering* **50**, 205–213.

[243] Alijani, F., Bakhtiari-Nejad, F., Arvin, H. and Mohammadi, M. (2016), 'Free vibration analysis of symmetrically laminated cylindrical panels via extended Kantorovich method', *16th International Congress on Sound and Vibration 2009, ICSV 2009* **5**, 2886-2893.

[244] Abouhamze, M., Aghdam, M. M. and Alijani, F. (2007), 'Bending analysis of symmetrically laminated cylindrical panels using the extended Kantorovich method', *Mechanics of Advanced Materials and Structures* **14**, 523–530.

[245] Alijani, F., Aghdam, M. M. and Abouhamze, M. (2008), 'Application of the extended Kantorovich method to the bending of clamped cylindrical panels', *European Journal of Mechanics-A/Solids* **27**, 378–388.

[246] Jam, J. E., Maleki, S. and Andakhshideh, A. (2013), 'Static Analysis of Laminated Piezoelectric Cylindrical Panels', *International Journal of Aerospace Sciences* **2**, 16–28.

[247] Ali, M. S. and Tahani, M. (2015), 'Thermal bending analysis of doubly curved composite laminated shell panels with general boundary conditions and laminations', *Journal of Thermal Stresses* **38**, 250–270.

[248] Mirzavand, B., Rezapour, P. and Bohlooly, M. (2016), 'Thermal buckling of shallow/nonshallow piezoelectric-composite cylindrical shells', *Mechanics of Advanced Materials and Structures* **23**, 1236–1243.

[249] Obodan, N. I. and Gromov, V. A. (2016), 'The complete bifurcation structure of nonlinear boundary problem for cylindrical panel subjected to uniform external pressure', *Thin-Walled Structures* **107**, 612–619.

[250] Zafarabadi, M. M. and Aghdam, M. M. (2021), 'Semi-analytical solutions for buckling and free vibration of composite anisogrid lattice cylindrical panels', *Composite Structures* **275**, 114422.

[251] Ebrahimi, N. and Beni, Y. T. (2016), 'Electro-mechanical vibration of nanoshells using consistent size-dependent piezoelectric theory', *Steel and Composite Structures* **22**, 1301–1336.

[252] Shames, I. and Dym, C. (1985), *Energy and Finite Element Methods in Structural Mechanics*, Hemisphere, NY.

[253] Averill, R. C. and Yip, Y. C. (1996), 'Thick beam theory and finite element model with zig-zag sublaminate approximations', *AIAA journal* **34**, 1627–1632.

[254] Xu, K., Noor, A. K. and Tang, Y. Y. (1996), 'Three-dimensional solutions for coupled thermoelectroelastic response of multilayered plates', *Computer Methods in Applied Mechanics and Engineering* **126**, 355–371.

[255] Vel, S. S. and Batra, R. C. (2000), 'Three-dimensional analytical solution for hybrid multilayered piezoelectric plates', *Journal of Applied Mechanics* **67**, 558–567.

[256] ABAQUS (2009), *ABAQUS/STANDARD User's Manual*, Version 6.9-1.

[257] Pagano, N. J. (1970), 'Influence of shear coupling in cylindrical bending of anisotropic laminates', *Journal of composite materials* **4**, 330–343.

[258] Kumari, P. and Kar, S. (2019), 'Static behavior of arbitrarily supported composite laminated cylindrical shell panels: An analytical 3d elasticity approach', *Composite Structures* **207**, 949–965.

[259] Kapuria, S. and Dhanesh, N. (2014), 'Three-dimensional extended kantorovich solution for accurate prediction of interlaminar stresses in composite laminated panels with interfacial imperfections', *Journal of Engineering Mechanics* **141**, 04014140.

[260] Jones, R. M. (2014), *Mechanics of composite materials*, CRC press.

[261] Cheng, Z. Q., Jemah, A. and Williams, F. (1996), 'Theory for multilayered anisotropic plates with weakened interfaces', *Journal of Applied Mechanics* **63**, 1019–1026.

[262] Lu, X. and Liu, D. (1992), 'Interlayer shear slip theory for cross-ply laminates with nonrigid interfaces', *AIAA J* **30**, 1063–1073.

[263] Kapuria, S. and Dhanesh, N. (2016), 'Free edge stresses in composite laminates with imperfect interfaces under extension, bending and twisting loading', *International Journal of Mechanical Sciences* **113**, 148–161.

[264] Pipes, R. B. and Pagano, N. (1994), 'Interlaminar stresses in composite laminates under uniform axial extension', *Mech. Compos. Mater.*, 234–245.

[265] Kapuria, S. and Achary, G. G.S. (2016), 'Exact 3D piezoelasticity solution of hybrid cross–ply plates with damping under harmonic electro-mechanical loads', *Journal of sound and vibration* **282**, 617–634.

[266] Stango, R. J. and Wang, S. S. (1984), 'Process-induced residual thermal stresses in advanced fiber-reinforced composite laminates', *Journal of Manufacturing Science and Engineering* **106**, 48–54.

[267] Rao, M. N., Tarun, S., Schmidt, R. and Schröder, K. U. (2016), 'Finite element modeling and analysis of piezo-integrated composite structures under large applied electric fields', *Smart Materials and Structures* **25**, 055044.

[268] Auld, B. A. (1973), *Acoustic fields and waves in solids. Vol I*, John Wiley & Sons, New York.

[269] Achary, G. (2005), *Coupled exact 3D solutions and 2D zigzag theory for thermo-electromechanical analysis of hybrid piezoelectric plates*, Ph.D Thesis, Department of Applied Mechanics, IIT Delhi, India.

[270] Massachusetts Institute of Technology. (2014), *Twenty-node brick element with reduced integration (C3D20R and F3D20R)*, 16 September 2021, *http* : $//web.mit.edu/calculix_v2.7/CalculiX/ccx_2.7/doc/ccx/node30.html$.

[271] Lapidus, L. and Pinder, G. F. (1982), *Numerical solution of partial differential equations in science and engineering*, John Wiley & Sons, New York.

[272] González, E. V., Maimí, P., Turon, A, Camanho, P. P. and Renart, J. (2016), 'Simulation of delamination by means of cohesive elements using an explicit finite element code', *Computers, Materials & Continua (CMC)* **9**, 51.

Appendix A

A.1 CONSTITUTIVE EQUATIONS

The commonly applied piezoelectricity materials PZT and PVDF belong to the class of crystals which has mm2 symmetry with respect to the principal material axes x_1, x_2, x_3 [268]. Considering polarization to be along the x_3, i.e, the thickness direction of the crystal, then 3D linear piezoelectricity constitutive relation without any material non-linearity and temperature or hygrothermal effects on the material constants, is given as:

$$\begin{bmatrix} \varepsilon_1 \\ \varepsilon_2 \\ \varepsilon_3 \\ \gamma_{23} \\ \gamma_{31} \\ \gamma_{12} \\ D_1 \\ D_2 \\ D_3 \end{bmatrix} = \begin{bmatrix} s_{11} & s_{12} & s_{13} & 0 & 0 & 0 & 0 & 0 & d_{31} \\ s_{12} & s_{22} & s_{23} & 0 & 0 & 0 & 0 & 0 & d_{32} \\ s_{13} & s_{23} & s_{33} & 0 & 0 & 0 & 0 & 0 & d_{33} \\ 0 & 0 & 0 & s_{44} & 0 & 0 & 0 & d_{24} & 0 \\ 0 & 0 & 0 & 0 & s_{55} & 0 & d_{15} & 0 & 0 \\ 0 & 0 & 0 & 0 & 0 & s_{66} & 0 & 0 & 0 \\ 0 & 0 & 0 & 0 & d_{15} & 0 & \epsilon_{11} & 0 & 0 \\ 0 & 0 & 0 & d_{24} & 0 & 0 & 0 & \epsilon_{22} & 0 \\ d_{31} & d_{32} & d_{33} & 0 & 0 & 0 & 0 & 0 & \epsilon_{33} \end{bmatrix} \begin{bmatrix} \sigma_1 \\ \sigma_2 \\ \sigma_3 \\ \tau_{23} \\ \tau_{31} \\ \tau_{12} \\ E_1 \\ E_2 \\ E_3 \end{bmatrix} \tag{A.1}$$

where ε_i and γ_{ij} denote the normal and shearing strain components, σ_i and τ_{ij} denote the normal and shear stress components, D_i denotes the electric displacements, E_i denotes the electric field components in the principal material axis system. Constants s_{ij}, d_{ij}, and ϵ_{ij} are the elastic compliances, piezoelectric strain constants and dielectric constants, respectively. The macromechanical material properties are used to build the elements of the compliance matrix for the orthotropic material through the following relations:

$$\begin{aligned} &s_{11} = 1/Y_1, && s_{44} = 1/G_{23}, && s_{12} = -\nu_{21}/Y_2 = -\nu_{12}/Y_1 \\ &s_{22} = 1/Y_2, && s_{55} = 1/G_{31}, && s_{13} = -\nu_{31}/Y_3 = -\nu_{13}/Y_1 \\ &s_{33} = 1/Y_3, && s_{66} = 1/G_{12}, && s_{23} = -\nu_{32}/Y_3 = -\nu_{23}/Y_2 \end{aligned} \tag{A.2}$$

$$\epsilon_{11} = \eta_{11} + e_{15}d_{15}, \qquad \epsilon_{22} = \eta_{22} + e_{24}d_{24}$$
$$\epsilon_{33} = \eta_{33} + e_{31}d_{31} + e_{32}d_{32} + e_{33}d_{33}, \qquad q_3 = p_3 + e_{31}\alpha_1 + e_{32}\alpha_2 + e_{33}\alpha_3 \tag{A.3}$$

where

$$\begin{bmatrix} e_{31} & e_{32} & e_{33} \end{bmatrix} = \begin{bmatrix} d_{31} & d_{32} & d_{33} \end{bmatrix} \begin{bmatrix} s_{11} & s_{12} & s_{13} \\ s_{12} & s_{22} & s_{23} \\ s_{13} & s_{23} & s_{33} \end{bmatrix}^{-1}$$
$$e_{24} = d_{24}/s_{44}, \qquad e_{15} = d_{15}/s_{55} \tag{A.4}$$

where Young's modulus are Y_i, shear modulus are G_{ij}, Poisson's ratio are ν_{ij} and constant strain electric permittivities are η_{ij}.

Consider the reference axes θ, z, r such that $r = x_3$ and the material principal axes x_1, x_2 are at angle ψ to the inplane reference axes θ, z. Using transformations, the 3D constitutive equations w.r.t. axes θ, z, r are obtained as [269]:

$$\begin{bmatrix} \varepsilon_\theta \\ \varepsilon_z \\ \varepsilon_r \\ \gamma_{zr} \\ \gamma_{r\theta} \\ \gamma_{\theta z} \\ D_\theta \\ D_z \\ D_r \end{bmatrix} = \begin{bmatrix} \bar{s}_{11} & \bar{s}_{12} & \bar{s}_{13} & 0 & 0 & \bar{s}_{16} & 0 & 0 & \bar{d}_{31} \\ \bar{s}_{12} & \bar{s}_{22} & \bar{s}_{23} & 0 & 0 & \bar{s}_{26} & 0 & 0 & \bar{d}_{32} \\ \bar{s}_{13} & \bar{s}_{23} & \bar{s}_{33} & 0 & 0 & \bar{s}_{36} & 0 & 0 & \bar{d}_{33} \\ 0 & 0 & 0 & \bar{s}_{44} & \bar{s}_{45} & 0 & \bar{d}_{14} & \bar{d}_{24} & 0 \\ 0 & 0 & 0 & \bar{s}_{54} & \bar{s}_{55} & 0 & \bar{d}_{15} & \bar{d}_{25} & 0 \\ \bar{s}_{16} & \bar{s}_{26} & \bar{s}_{36} & 0 & 0 & \bar{s}_{66} & 0 & 0 & \bar{d}_{36} \\ 0 & 0 & 0 & \bar{d}_{14} & \bar{d}_{15} & 0 & \bar{\epsilon}_{11} & \bar{\epsilon}_{12} & 0 \\ 0 & 0 & 0 & \bar{d}_{24} & \bar{d}_{25} & 0 & \bar{\epsilon}_{21} & \bar{\epsilon}_{22} & 0 \\ \bar{d}_{31} & \bar{d}_{32} & \bar{d}_{33} & 0 & 0 & \bar{d}_{36} & 0 & 0 & \bar{\epsilon}_{33} \end{bmatrix} \begin{bmatrix} \sigma_\theta \\ \sigma_z \\ \sigma_r \\ \tau_{zr} \\ \tau_{r\theta} \\ \tau_{\theta z} \\ E_\theta \\ E_z \\ E_r \end{bmatrix} \tag{A.5}$$

where with $c = \cos\psi$, $s = \sin\psi$:

$$\begin{aligned}
\bar{s}_{11} &= c^4 s_{11} + c^2 s^2 (2s_{12} + s_{66}) + s^4 s_{22}, & \bar{d}_{31} &= c^2 d_{31} + s^2 d_{32} \\
\bar{s}_{12} &= c^2 s^2 (s_{11} + s_{22} - s_{66}) + (c^4 + s^4) s_{12}, & \bar{d}_{32} &= s^2 d_{31} + c^2 d_{32} \\
\bar{s}_{16} &= c^3 s (2s_{11} - 2s_{12} - s_{66}) + cs^3 (2s_{12} - 2s_{22} + s_{66}), & \bar{d}_{33} &= d_{33} \\
\bar{s}_{22} &= s^4 s_{11} + c^2 s^2 (2s_{12} + s_{66}) + c^4 s_{22}, & \bar{d}_{36} &= 2cs(d_{31} - d_{32}) \\
\bar{s}_{26} &= c^3 s (2s_{12} - 2s_{22} + s_{66}) + cs^3 (2s_{11} - 2s_{12} - s_{66}), & \bar{d}_{14} &= \bar{d}_{25} = cs(d_{15} - d_{24}) \\
\bar{s}_{66} &= 4c^2 s^2 (s_{11} - 2s_{12} + s_{22}) + (c^2 - s^2)^2 s_{66}, & \bar{d}_{15} &= c^2 d_{15} + s^2 d_{24}
\end{aligned} \tag{A.6}$$

$$
\begin{aligned}
\bar{s}_{13} &= c^2 s_{13} + s^2 s_{23}, \\
\bar{s}_{23} &= s^2 s_{13} + c^2 s_{23}, \\
\bar{s}_{36} &= 2cs(s_{13} - s_{23}), \\
\bar{s}_{33} &= s_{33}, \\
\bar{s}_{44} &= c^2 s_{44} + s^2 s_{55}, \\
\bar{s}_{45} &= cs(s_{55} - s_{44}), \\
\bar{s}_{55} &= s^2 s_{44} + c^2 s_{55};
\end{aligned}
\qquad
\begin{aligned}
\bar{d}_{24} &= s^2 d_{15} + c^2 d_{24} \\
\bar{\epsilon}_{11} &= c^2 \epsilon_{11} + s^2 \epsilon_{22} \\
\bar{\epsilon}_{22} &= s^2 \epsilon_{11} + c^2 \epsilon_{22} \\
\bar{\epsilon}_{12} &= cs(\epsilon_{11} - \epsilon_{22}) \\
\bar{\epsilon}_{33} &= \epsilon_{33}
\end{aligned}
\tag{A.7}
$$

The constitutive equations for the elastic plates are obtained as a special case of Eq. (A.5) with the piezoelectric constants being zero.

Appendix B

B.1 THREE-DIMENSIONAL ELEMENTS IN FE PACKAGE ABAQUS

ABAQUS is the package used to solve the structural problems through finite element methods (FE). There, numerical integrations are performed to obtain the element matrices. Computations in the plane of the lamina is done through Gauss quadrature, and Simpson's rule is used in the stacking direction for a laminated structure [256]. For the FE analysis of the problems, the following

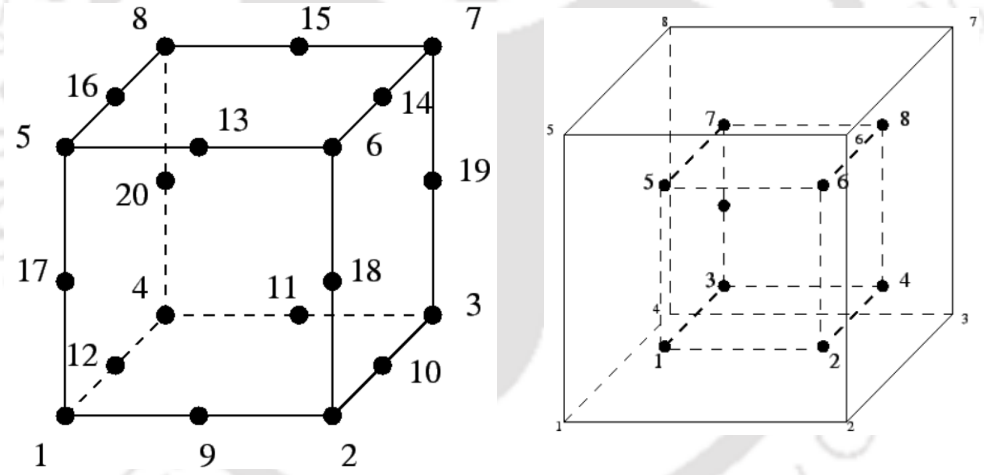

Fig. B.1: (a) Brick element and position of the nodes (b)2x2x2 integration point scheme in hexahedral elements.

3D elements are chosen such as a 20 noded quadratic serendipity hexahedral elements with reduced integration (C3D20R) are used for elastic plies, a C3D20RE element for the piezoelectricity plies and the cohesive zone consists of the COH3D8 elements. The quadratic brick element C3D20R has 2x2x2 reduced integration points which can be visualised in the Fig. B.1b. The position of the nodes are also shown there in Fig. B.1a. These elements perform well for bending analysis, as it is not stiff unlike the C3D20 elements. Further, even through reduced number of integration points are

considered, there is no observed hourglassing effect. According to ABAQUS documentation [256], C3D20R (8 integration points) is approximately 3.5 times cheaper than C3D20 (27 integration points) during the assembly of the elements. It also suggests that in ABAQUS/Standard, the results are more accurate from second-order (quadratic) reduced-integration elements as compared to fully integrated ones. The reduced integration is adopted to avoid shear locking, and hourglassing for the same will be inconsequential for the quadratic element specially in presence of multiple elements in the thickness direction while modeling a structure. However, it has been reported that, the high surface stress concentrations are not captured with coarse meshing as the distance of the integration points from boundary of the element is about one quarter of the C3D20R element size and the trilinear values are extrapolated from the integration points to the nodes [270]. The basis functions for a serendipity type C^0 hexahedral element are given in the following form [271]:

$$\begin{aligned}
\phi_i &= \frac{1}{8}(1+\xi\xi_i)(1+\eta\eta_i)(1+\zeta\zeta_i)(\xi\xi_i+\eta\eta_i+\zeta\zeta_i-2) \quad (i=1,3,5,7,9,11,13,15,17,19)\\
\phi_i &= \frac{1}{4}(1-\zeta^2)(1+\xi\xi_i)(1+\eta\eta_i) \quad (i=9,10,11,12)\\
\phi_i &= \frac{1}{4}(1-\xi^2)(1+\eta\eta_i)(1+\zeta\zeta_i) \quad (i=8,4,16,20)\\
\phi_i &= \frac{1}{4}(1-\eta^2)(1+\xi\xi_i)(1+\zeta\zeta_i) \quad (i=2,6,18,14)
\end{aligned} \tag{B.1}$$

where ξ_i, ζ_i and η_i are the local coordinates of the ith point and ξ, ζ and η are the global non-dimensionalised coordinates. C3D20RE is a similar 3D solid continuum element in ABAQUS with electric (E) variables corresponding to the piezoelectricity effect.

The interfaces between the imperfectly bonded plies is modelled using the zero-thickness type elements COH3D8 in ABAQUS/Standard. Its is a 8 noded three-dimensional element which has 4 integration points. The element can be thought of consisting of elements in its top face and corresponding elements in the bottom face separated through cohesive zone thickness. These elements employ linear shape functions. Traction-separation response is used to obtain the governing equations of the cohesive zone. In this model based on the interpolated separation displacements, the nodal forces are generated and the tractions are obtained from these displacements [272]. The

authors had also indicated that the value of thickness of the cohesive zone should be normally small between 0.001 and 0.1 mm.

Brief Biodata of the Author

The author, Shranish Kar, was born in the year 1989 in the town Balasore situated in Odisha State, India. He graduated with B.Tech in Mechanical Engineering in the year 2011 from Institute of Technical Education and Research (ITER), Siksha O Anusandhan University, Bhubaneswar, Odisha. Then, he worked at the Godrej & Boyce Mfg. Co. Ltd., Vikhroli (Mumbai) in the engineering design department for a year in 2011. Further, on the basis of GATE (All India Graduate Aptitude Test in Engineering) score in mechanical engineering paper, in 2012 he got the opportunity to pursue his M.Tech degree in Petroleum Engineering from the Indian School of Mines IIT(ISM), Dhanbad. Again after qualifying the GATE in 2015, he joined the Ph.D. program in the same year at the Department of Mechanical Engineering, IIT Guwahati and this research work is carried out during this period.

List of Publications from the Thesis

List of Publications in International Journals

List of Publications

Peer reviewed Journal Publications

1. Kumari, P., **Kar, S.**, 2019. Static behavior of arbitrarily supported composite laminated cylindrical shell panels: An analytical 3D elasticity approach. Composite Structures 207, 949–965.

2. Kar, S., Kumari, P., 2020. Three-Dimensional analytical solution of arbitrarily supported cylindrical panels with weak interfaces using the extended Kantorovich Method. Composite Structures 236, 111802.

3. Kar, S., Kumari, P., 2020. A 3D solution for angle-ply cylindrical shell panel supported arbitrarily on its boundaries using extended Kantorovich Method. International Journal of Advances in Engineering Sciences and Applied Mathematics, 1-14.

4. Kar, S., Kumari, P. (*Accepted*). Static behavior of arbitrarily supported piezolaminated cylindrical shell panels: An analytical 3D piezoelasticity approach. Journal of Structural Engineering-SERC Madras.

5. Kar, S., Kumari, P. (*Under preparation*). Three-Dimensional analytical free vibration solution for piezolaminated cylindrical shell panel.

6. Kar, S., Kumari, P. (*Under preparation*). Three-dimensional solution approaches for bending and dynamic analysis of piezolaminated cylindrical shell structures: A review.

International Conference Publication

1. Kar, S., Kumari, P., 2022 (*Abstract Accepted*). Effect of adhesive thickness on the cylindrical bending of arbitrarily supported piezolaminated shells. *ICC25 - 25th International Conference on Composite Structures & MECHCOMP8 - 8th International Conference on Mechanics of Composites*, 19-22 July, 2022, Porto, Portugal.

2. Kar, S., Kumari, P., Potkar, AS., 2021. Solution for three-dimensional stresses and displacements of a piezoelectric cylindrical shell panel using the extended Kantorovich method. *The 7th Asian Conference on Mechanics of Functional Materials and Structures (ACMFMS2020 +1)*, March 13-15, 2021 Virtually at Tohoku University, Japan.

3. Kar, S., Kumari, P., 2020. An analytical three-dimensional piezoelectricity solution for arbitrarily supported cylindrical shell using the extended Kantorovich method. *ICCS23 - 23rd International Conference on Composite Structures & MECHCOMP6 - 6th International Conference on Mechanics of Composites*, 1-4 September, 2020, Porto, Portugal.

4. Kar, S., Kumari, P., 2019. A 3D solution for angle-ply cylindrical shell panel supported arbitrarily on its boundaries using extended Kantorovich method. *4th Indian Conference on Applied Mechanics (INCAM-2019)*, July 3-5, 2019 at IISc Bangalore, India.

5. Kar, S., Kumari, P., 2019. Three dimensional bending solution of cylindrical shell panel having arbitrary edge support conditions using extended Kantorovich method. *10th International*

Conference on Material for Advanced Technologies, 23-28 June, 2019, Marina Bay Sands, Singapore.

6. Kumari, P., **Kar, S.**, 2017. Three-dimensional elasticity solution for a simply supported cylindrical composite shell panel using the extended Kantorovich method. *International Conference on Composite Materials and Structures (ICCMS)*, 27-29th December 2017, IIT Hyderabad, India.

7. Kar, S., Kumari, P., 2017. A review on three-dimensional solution approaches for bending and dynamic analysis of piezolaminated cylindrical shell structures. *13th International Conference on Vibration Problems (ICOVP-2017)*, 29th November-2nd December 2017, IIT Guwahati, India.

National Conference Publication

1. Kar, S., Kumari, P., 2020. An analytical three-dimensional coupled piezoelectricity solution for a smart cylindrical thick shell panel using the extended Kantorovich method. *International Conference on Advances in Smart Materials and Emerging Technologies (ASMET 2020)*, 23-24th January 2020, IGDTU New Delhi, India.

2. Kar, S., Kumari, P., 2019. A three-dimensional extended Kantorovich solution for accurate static analysis of an arbitrarily edge supported sandwich cylindrical shell panel. *National Conference on Advances in Mechanical Engineering (AME 2019)*, 25-26th February 2019, Government college of Engineering, Keonjhar, India.